

Journal of Communications

ISSN 1796-2021

Volume 6, Number 4, July 2011

Special Issue: Practical Physical Layer Techniques for 4G Systems & Beyond

Guest Editors: Sudhanshu Gaur, Geoffrey Ye Li, Li-Chun Wang, and Neelesh B. Mehta

Contents

Guest Editorial <i>Sudhanshu Gaur, Geoffrey Ye Li, Li-Chun Wang, and Neelesh B. Mehta</i>	271
<hr/>	
SPECIAL ISSUE PAPERS	
System-Level Impact of Multi-User Diversity in SISO and MIMO-based Cellular Systems <i>Rahul N. Pupala, Larry J. Greenstein, and David G. Daut</i>	274
Downlink System Throughput Statistics for Various MEA Configurations <i>Rahul N. Pupala, Yifei Yuan, Qi Bi, and Larry J. Greenstein</i>	285
Coverage Analysis for Multiuser MIMO Broadcast Systems <i>Li-Chun Wang and Chu-Jung Yeh</i>	293
A Practical Resource Allocation Approach for Interference Management in LTE Uplink Transmission <i>Liyang Li, Gang Wu, Hongbing Xu, Geoffrey Ye Li, and Xin Feng</i>	301
Impact of CSI on Radio Resource Management Techniques for the OFDMA Downlink <i>Leonidas Sivrdis, Xinheng Wang, and Jinho Choi</i>	306
Understanding Static Inter-Cell Interference Coordination Mechanisms in LTE <i>Ashley Mills, David Lister, and Marina De Vos</i>	312
Power-efficient Irregular Repeat-Accumulate Encoded BICM-ID for 16-ary Signal Constellations <i>Wei Kwang Han, Stephane Le Goff, Bayan Sharif, and Arafat Al-Dweik</i>	319
Dedicated-Relay vs. User Cooperation in Time-Duplexed Multiaccess Networks <i>Lalitha Sankar, Gerhard Kramer, and Narayan B. Mandayam</i>	330
Green Communications: A Call for Power Efficient Wireless Systems <i>An He, Ashwin Amanna, Thomas Tsou, Xuetao Chen, Dinesh Datla, Joseph Gaeddert, Timothy R. Newman, S.M. Shajedul Hasan, Haris I. Volos, Jeffery H. Reed, and Tamal Bose</i>	340

Special Issue on Practical Physical Layer Techniques for 4G Systems & Beyond

Guest Editorial

If one looks at the last thirty years and measures the rate at which technological innovation is impacting human life, then it can be safely concluded that we are living in extremely exciting times. Wide-spread adoption of Internet triggered an information revolution that has changed the human society in fundamental ways. Subsequent development of cellular communication systems and the resulting ubiquity of cellphones enabled people to communicate while on the go, and within a decade, “anytime-anywhere” communications has become a normal service for majority of people in both developed and developing nations. Ever increasing penetration of smart phones, tablets etc. in mass markets has given users a taste of “anywhere-ubiquitous” access to information & entertainment, and this too will soon become a must have, commodity service for everyone.

Meeting these growing user demands requires next generation cellular networks to have vastly improved spectral efficiencies and coverage. Thus there is a constant need for fundamental as well as applied research on the components and algorithms for forthcoming 4G systems and beyond. The aim of this special issue is to collect and present a set of cutting edge research contributions that would hopefully be representative of the wide spectrum of on-going activities on the Physical layer front for these next generation cellular systems.

To this end, we have identified nine high-quality publications after a thorough peer-review process. The papers can broadly be divided into three categories. The first category groups contributions that present system level performance analysis of PHY techniques that have been recently proposed in the research literature. This category is quite important from a practical point of view because it tries to vet theoretically promising techniques by quantifying their real impact on a deployed system through simulations. Any research idea that aspires to be part of a 4G standard has to pass through such system level evaluations. The second category focuses on resource management algorithms and mechanisms for LTE/OFDMA systems. The selected papers either present algorithms extending state of the art, or provide a better understanding of existing interference coordination mechanisms in LTE. The third category consists of papers aiming to improve the power efficiency of cellular networks. The accepted contributions range from a paper proposing new power efficient PHY coding techniques, to a forward looking article comparing the efficiency of relay assisted networks versus user cooperation, and culminate with an invited survey article on green communications. In the paragraphs that follow, we will briefly summarize the basic ideas presented in each paper from this issue.

The first three papers evaluate multi-user (MU) multiple-input multiple-output (MIMO) technique in the context of cellular networks. The first paper, “System-Level Impact of Multi-User Diversity in SISO and MIMO-based Cellular Systems” by R. Pupala, L.J. Greenstein, and D.G. Daut, considers several parameters in wireless multi-cell systems and evaluate their impacts on aggregate throughputs with different schedulers. This work attempts to quantify the benefits of multiuser diversity and excess degrees of freedom from multiple receive antennas. The second paper “Downlink System Throughput Statistics for Various MEA Configurations” by R. Pupala, Y. Yuan, Q. Bi, and L.J. Greenstein, investigates the merit in modifying a SISO link with added antenna elements at one or both ends. Practical considerations such as channel estimation overhead are considered to evaluate relative merits of various multi-antenna configurations. The third paper “Coverage Analysis for Multiuser MIMO Broadcast Systems” by L.C. Wang and C.J. Yeh, investigates the diversity gain and coverage of zero-forcing beamforming (ZFB) and zero-forcing dirty paper coding (ZF-DPC) techniques with/without the consideration of multiuser scheduling for multiuser MIMO broadcast channels. The proposed work shows that the use of multiuser scheduling can act as soft coverage enhancement technique without requiring additional transmit power.

Next three papers focus on resource management algorithms and mechanisms for LTE/OFDMA systems. In the fourth paper, “A Practical Resource Allocation Approach for Interference Management in LTE Uplink Transmission” by L. Li, G. Wu, H. Xu, G. Li and X. Feng, the authors propose a novel resource allocation method for LTE uplink to reduce inter-cell interference. This paper investigates joint power control and resource allocation techniques for LTE uplink and proposes an efficient way to improve system performance, especially for cell edge users. In the next paper “Impact of CSI on Radio Resource Management Techniques for the OFDMA Downlink” by L. Sivridis, X. Wang and J. Choi, the authors propose sub-carrier allocation algorithm for OFDMA downlink. This work improves upon a previously known algorithm by reallocating the subcarriers of users who will not be able to meet their quality of service (QoS) requirements. The sixth paper “Understanding Static Inter-Cell Interference Coordination Mechanisms in LTE” by A. Mills, D.R. Lister, and M.D. Vos, considers modulation and coding scheme (MCS) based soft frequency reuse issue in cellular systems. Based on this metric the paper challenges the idea that cell edge users should have a high reuse factor.

The remaining three papers focus on power-efficient system architectures and PHY techniques for cellular systems. The paper “Power-efficient Irregular Repeat-Accumulate Encoded BICM-ID for 16-ary Signal Constellations” by W.K. Han, S. Y. L. Goff, B. Sharif, and A. J. Al-Dweik presents novel results on the application of bit-interleaved coded modulation (BICM) along with irregular repeat accumulate and low-density parity-check codes to improve bit error rate

(BER) performance over Rayleigh fading channels. The next paper “Dedicated-Relay vs. User Cooperation in Time-Duplexed Multiaccess Networks” by L. Shankar, G. Kramer, and N. Mandayam, investigates the performance trade-offs of cooperation in a multi-user uplink network. Two basic modes of cooperation are considered: user cooperation, in which users forward each other's messages, and dedicated relaying, in which a single dedicated relay forwards users' messages. This work explores whether user cooperation or dedicated relaying is more energy efficient, as measured by outage probability versus total transmit and processing power. Environmental impact and power usage are major concerns for next generation networks. An He et al., provide a survey of energy efficient advances in renewable and alternative energy resources for base stations in the ninth paper “Green Communications: A Call for Power Efficient Wireless Systems”. This paper is of tutorial nature and presents an interesting overview of technology and economics that could affect green communication systems.

We feel that this special issue succeeds in its attempt to give readers an insight into on-going activities on fundamental as well as applied research on the Physical layer algorithms and system level design for forthcoming 4G systems and beyond. We would like to thank all the authors who submitted their work for consideration for this issue, and the reviewers for their timely and constructive feedback. We also thank the staff at the JCM Academy Publisher for their help in handling the manuscripts. Lastly, we would like to extend our sincere appreciation to Dr. Linda Xie, Editor of the Journal of Communications, for her great support, and Dr. Haohong Wang, Editor-in-Chief of the Journal of Communications for providing us the opportunity to organize this special issue.

Guest Editors

Sudhanshu Gaur, Hitachi America R&D, USA (sudhanshu.gaur@hal.hitachi.com)

Geoffrey Ye Li, Georgia Institute of Technology, USA (lye@ece.gatech.edu)

Li-Chun Wang, National Chiao Tung University, Taiwan (lichun@g2.nctu.edu.tw)

Neelesh B. Mehta, Indian Institute of Science, India (nbmehta@ece.iisc.ernet.in)



Sudhanshu Gaur (M'02 – SM'10) received his Bachelor of Technology degree in Instrumentation Engineering from the Indian Institute of Technology (IIT), Kharagpur in 2000. He obtained his Master's degree from Virginia Tech in 2003 and PhD from Georgia Institute of Technology in 2008, both in Electrical & Computer Engineering.

From 2005 onwards, he has been working at Hitachi's wireless research lab in Santa Clara and is currently a Principal Research Engineer. He leads physical layer research and system design targeting LTE-Advanced standardization and is actively involved in RAN1 activities in 3GPP. Earlier he led a project on HD video transmission over WiFi and was also involved with IEEE 802.11aa standardization. Previously, he had also worked in GPRS MAC design at Sasken Communication Technologies, Bangalore. His research activities span MIMO signal processing, interference management, multiple access protocols, and performance analysis of cellular systems. He holds several US patents, and has authored several peer-reviewed publications in wireless communications.



Geoffrey Ye Li received his B.S.E. and M.S.E. degrees in 1983 and 1986, respectively, from the Department of Wireless Engineering, Nanjing Institute of Technology, Nanjing, China, and his Ph.D. degree in 1994 from the Department of Electrical Engineering, Auburn University, Alabama.

He was a Teaching Assistant and then a Lecturer with Southeast University, Nanjing, China, from 1986 to 1991, a Research and Teaching Assistant with Auburn University, Alabama, from 1991 to 1994, and a Post-Doctoral Research Associate with the University of Maryland at College Park, Maryland, from 1994 to 1996. He was with AT&T Labs - Research at Red Bank, New Jersey, as a Senior and then a Principal Technical Staff Member from 1996 to 2000. Since 2000, he has been with the School of Electrical and Computer Engineering at Georgia Institute of Technology as an Associate and then a Full Professor. He is also holding the Cheung Kong Scholar title at the University of Electronic Science and Technology of China since March 2006.

His general research interests include statistical signal processing and telecommunications, with emphasis on OFDM and MIMO techniques, cross-layer optimization, and signal processing issues in cognitive radios. In these areas, he has published over 200 papers in refereed journals or conferences and two books, 20 of which are with over 100 Google citations. He has over 20 patents granted or filed. He once served or is currently serving as an editor, a member of editorial board, and a guest editor for over 10 technical journals. He organized and chaired many international conferences, including technical program vice-chair of *IEEE ICC'03* and co-chair of *IEEE SPARC'11*. He has been awarded an IEEE Fellow for his contributions to *signal processing for wireless communications* since 2006, selected as a *Distinguished Lecturer* for 2009 - 2010 by *IEEE Communications Society*, and won 2010 *IEEE Communications Society* Stephen O. Rice Prize Paper Award in the field of communications theory.



Li-Chun Wang (M'96 – SM'06 – F'11) received the B.S. degree from National Chiao Tung University, Taiwan, R. O. C. in 1986, the M.S. degree from National Taiwan University in 1988, and the Ms. Sci. and Ph. D. degrees from the Georgia Institute of Technology, Atlanta, in 1995, and 1996, respectively, all in electrical engineering.

From 1990 to 1992, he was with the Telecommunications Laboratories of the Ministry of Transportations and Communications in Taiwan (currently the Telecom Labs of Chunghwa Telecom Co.). In 1995, he was affiliated with Bell Northern Research of Northern Telecom, Inc., Richardson, TX. From 1996 to 2000, he was with AT&T Laboratories, where he was a Senior Technical Staff Member in the Wireless Communications Research Department. In August 2000, he has joined the Department of Electrical Engineering of National Chiao Tung University in Taiwan and has been promoted to the full professor since 2005. His current research

interests are in the areas of radio resource management and cross-layer optimization techniques for wireless systems, heterogeneous wireless network design, and cloud computing for mobile applications.

He was elected to the IEEE Fellow grade in 2011 for his contributions in cellular architectures and radio resource management in wireless networks. Dr. Wang was a co-recipient (with Gordon L. Stüber and Chin-Tau Lea) of the 1997 IEEE Jack Neubauer Best Paper Award for his paper "Architecture Design, Frequency Planning, and Performance Analysis for a Microcell/Macrocell Overlaying System," IEEE Transactions on Vehicular Technology, vol. 46, no. 4, pp. 836-848, 1997. He has published over 180 journal and international conference papers. He served as an Associate Editor for the IEEE Trans. on Wireless Communications from 2001 to 2005, the Guest Editor of Special Issue on "Mobile Computing and Networking" for IEEE Journal on Selected Areas in Communications in 2005 and on "Radio Resource Management and Protocol Engineering in Future IEEE Broadband Networks" for IEEE Wireless Communications Magazine in 2006. He is holding nine US patents.



Neelesh B. Mehta received his Bachelor of Technology degree in Electronics and Communications Engineering from the Indian Institute of Technology (IIT), Madras in 1996, and his M.S. and PhD degrees in Electrical Engineering from the California Institute of Technology, Pasadena, CA, USA in 1997 and 2001, respectively. He is now an Assistant Professor at the Dept. of Electrical Communication Engineering, Indian Institute of Science (IISc), Bangalore, India. Before joining IISc, he has held research scientist positions in the Wireless Systems Research group in AT&T Laboratories, NJ, USA, Broadcom Corp., NJ, USA and Mitsubishi Electric Research Laboratories (MERL), MA, USA.

His research includes work on link adaptation, multiple access protocols, system-level performance analysis of cellular systems, MIMO and antenna selection, and cooperative communications. He was also actively involved in radio access network physical layer (RAN1) standardization activities in 3GPP. He has served on several TPCs. He was a TPC co-chair for WISARD 2010 and 2011 workshops, National Conference on Communications (NCC) 2011, the Transmission technologies track of VTC 2009 (Fall), the Frontiers of Networking and Communications symposium of Chinacom 2008, and the tutorials co-chair for SPCOM 2010. He is an Editor of the IEEE Transactions on Wireless Communications and an executive committee member of the IEEE Bangalore Section and the Bangalore chapter of the IEEE Signal Processing Society.

System-Level Impact of Multi-User Diversity in SISO and MIMO-based Cellular Systems

Rahul N. Pupala

Alcatel-Lucent/Bell Labs, Murray Hill, NJ 07974, USA
Email: rahul.pupala@alcatel-lucent.com

Larry J. Greenstein (*Life Fellow, IEEE*)

ECE (WINLAB), Rutgers – The State University of New Jersey, North Brunswick, NJ 08902, USA
Email: ljg@winlab.rutgers.edu

David G. Daut (*Senior Member, IEEE*)

ECE, Rutgers – The State University of New Jersey, Piscataway, NJ 08854, USA
Email: daut@ece.rutgers.edu

Abstract— We quantify cell-wide mean throughputs of single-input-single-output (SISO) and multiple-input-multiple-output (MIMO)-based cellular systems which employ multi-user diversity (MuD). Our study considers several practical and useful system-level design dimensions, including: number of transmit/receive antennas; antenna-pattern (omni-directional or sectorized); degree of error-protection (Shannon coding, no coding or intermediate coding strategies); allowable constellation size; Rician κ -factor; number of users and scheduling algorithm (Greedy (i.e. MAX C/I), Proportional Fair, or Equal Grade of Service) in single-cell (noise-limited) and multi-cell (co-channel-interference-limited) environments.

We also provide a comparison between single-user systems having excess receive antennas and multi-user diversity systems with no excess receive antennas. Both strategies improve signal quality. Since economic costs of RF chains, mobile size and form factor limit the number of antennas a mobile receiver can have, multi-user diversity can be a more practical option. We observe that MuD with only a few scheduled users leads to comparable throughputs as receivers with excess receive antennas. By quantifying the average throughput gains that accrue from using multi-user SISO and MIMO-based cellular systems, this study serves the needs of operators to assess these promising technologies.

Index Terms— MIMO, MMSE, multipath fading, shadow fading, co-channel interference, cross-stream interference, interference cancellers, multi-user diversity, MAX, PF, EGoS

I. INTRODUCTION

Since the publication of seminal papers [1], [2] a decade ago, multi-element antenna (MEA) systems has been an area of considerable interest to the wireless communications community. Commercial interest in multiple-input-multiple-output (MIMO) systems, which employ multiple antennas at both ends of the link, grew after the successful laboratory implementation of the well-known vertical Bell-Labs layered space-time architecture

(VBLAST) [3]. VBLAST demonstrated the feasibility of the MIMO concept, delivering spectral efficiencies of 20–40 bps/Hz under indoor conditions. Later research demonstrated the different ‘modes’ of MIMO systems, notably, Diversity and Spatial Multiplexing. The diversity mode improves signal quality using the spatial resources [4]–[6]; the multiplexing mode, a chief reason for the industry’s interest in MIMO systems, increases the data rate that can be pumped through a given bandwidth. By appropriate signal processing at the transmitter and/or the receiver, several de-coupled parallel single-input-single-output (SISO) channels can be created, which greatly enhances link capacity of the MIMO channel [1], [2], [7]–[13]. A tradeoff between these modes has been established [14], and linear codes that use a combination of both modes have been discovered [15]. Relevant definitions pertaining to MIMO/MEA¹ systems appear in the Appendix A.

In much of previous MEA/MIMO research, a *link-level* view, that of point-to-point communication, is taken. More recently, a *network-level* view of a cellular system has been adopted, which permits a new form of diversity — Multi-user Diversity (MuD) [16]–[20]. MuD can be viewed as a form of selection diversity (SD), in which the base station (BS) transmits to (or receives from) a mobile station (MS) with a good channel. Diversity is possible since all users are subject to independent fading, and in a system with sufficient number of users, a ‘good’ user exists with high probability. MuD is suitable for *delay-elastic* applications, i.e., those applications that can tolerate reasonable delays, such as data (but not voice). The implication of the network view was a paradigm shift in exploiting MEA/MIMO techniques: the multi-antenna link could now be used in multiplexing mode to extract maximal rate benefit, while diversity would come from

Manuscript received February 15, 2011; revised May 15, 2011; accepted June 15, 2011.

¹MEA links are assumed to have n transmitters and m receivers. They are denoted as MEA (n, m) or simply (n, m).

the network itself [18], [21].

Most MuD performance studies (e.g., [18], [21]–[25]) focus only on a particular link between the transmitter and the receiver. Performance measures such as bit error rate (BER) or throughput (TP) are determined with signal-to-noise ratio (SNR) treated as a parameter, with external factors such as co-channel interference (CCI) ignored or indirectly treated using the signal-to-interference-plus-noise ratio (SINR) in place of the SNR. Some work on SISO/MEA (but not MuD) systems has been reported, however, that takes a broader view (e.g., [8]–[13]). This work determines the *distribution* of performance over a coverage area, e.g., the cumulative distributive function (CDF) of TP over the randomness of user location and shadow fading, which jointly specify the SNR value. Furthermore, in the case of multi-cell environments, it also means taking into account the CCI produced by co-channel users in other cells.

In this study, we extend the latter work to the multi-user scenario with scheduling. We quantify cell-wide mean throughputs of SISO and MIMO-based cellular systems which employ multi-user diversity, and we do so over several useful system-level design dimensions: number of transmit/receive antennas; antenna-pattern (omni-directional or sectorized); degree of error-protection (Shannon coding, no coding or intermediate coding strategies); allowable constellation size; Rician κ -factor²; number of users and scheduling algorithm (Greedy, Proportional Fair or Equal Grade of Service) in single-cell (noise-limited) and multi-cell (CCI-limited) environments. In this connection, we note that the greedy (also popularly known as MAX C/I) and the equal grade-of-service scheduling algorithms define upper and lower bounds on throughput that any useful scheduler can offer; the proportional fair scheduler is considered owing to its popularity both in industry and in academic communities.

We also provide a comparison between single-user systems having excess degrees of freedom (SU-EDoF) and multi-user diversity systems having no excess degrees of freedom (MuD-wo-EDoF). Both mechanisms attempt to improve received signal quality, as measured by the post-processing SINR. In SU-EDoF, a receiver does so by using excess receive antennas to obtain diversity and/or null one or more interfering co-channel streams on an optimal basis [26]. By contrast, MuD-wo-EDoF improves signal quality by scheduling the user with the best signal (and weakest interference), i.e., interference avoidance is an inherent feature. Since costs of RF chains, mobile size, device form factor and other practical considerations limit the number of antennas a receiver can have, multi-user diversity may be a more practical and cost-effective option. Studying the tradeoffs between SU-EDoF and MuD-wo-EDoF enriches our ability to make engineering value-judgements, while designing practical systems that use these promising technologies.

For single-user scenarios, cell-wide average throughput

²Normally, K is used instead of κ , but, we use K here for the number of users sharing the channel.

per-user is typically used as a performance metric. For multi-user scenarios, wherein a channel is shared over many simultaneous users, a more appropriate metric is cell-wide average throughput *per-channel*. For the single-user case, ‘channel’ and ‘user’ are synonymous, and the metric continues to remain relevant³. We do not consider specific and precise metrics for fairness and stability. Even so, these considerations do enter our discussion, since they are prevalent in the literature. Essentially, when the throughput per-channel differences between the various scheduling algorithms are small, a sub-optimal scheduler may be used, trading a small throughput loss for greater ‘fairness’ or ‘stability’.

This paper is organized as follows. The system model and simulation platform are discussed in Section II, and numerical results are presented in Section III. Section IV offers a comparison between excess receive antennas and multi-user diversity, while Section V summarizes our work and presents some key conclusions.

II. SYSTEM MODEL AND SIMULATION PLATFORM

We have developed a system-level simulation platform for computing the throughputs of multi-user SISO/MEA cellular systems which employ network scheduling. The test-bed is sufficiently general to allow us to work with the several key system-level parameters noted earlier.

A. Network-level Description: Base Station Viewpoint (MAC-layer)

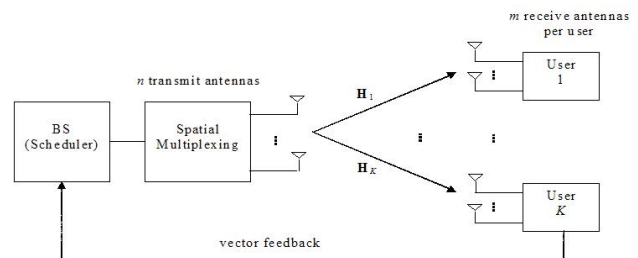


Figure 1. A multiuser scheduling system with n transmit antennas at the BS and m receive antennas at each MS. The scheduler can employ any user selection algorithm. In this study, the Greedy (MAX), Proportional Fair (PF) and the Equal Grade of Service (EGoS) schedulers are considered.

Fig. 1 shows a wireless system with a base station serving K downlink mobile stations. Each user MS tracks its individual channel from the BS, and sends a measure of the channel quality index (CQI) to the BS. The BS schedules any one user in a given time slot depending

³The reader is cautioned against attempting conversion from the per-channel metric to an ‘equivalent’ per-user metric (e.g., by dividing the per-channel metric by the number of users). MuD leads to gains that are logarithmically proportional to the number of users. Since, the per-user metric normalizes this figure by the number of users, it will cast multi-user diversity in poor light. We take the view that such a conversion is inappropriate, since multi-user diversity applies only for *delay-elastic* applications. Users are willing to wait, and are scheduled only when a channel becomes available.

on the present CQI, past transmissions to all users, and fairness/latency requirements.

In this study, perfect and instantaneous feedback of the CQI from each MS to the BS is assumed. The full-buffer traffic model is used; i.e. users always have data to receive, and all transmissions are initiated at the start of the simulation (i.e., users cannot ‘enter’ or ‘leave’ a set of users being serviced by the BS).

Three scheduling algorithms are considered — Greedy (MAX), Proportional Fair (PF) and Equal Grade of Service (EGoS). By evaluating the performance of two extreme schedulers (MAX, EGoS), we attempt to obtain a perspective on the performances realized by a range of useful schedulers. The PF scheduler is considered as a representative and widely popular example. In what follows,

- $CQI(k, t)$ denotes the vector CQI for user k at time instant t . Achievable substream-throughput vector (if k is scheduled at time t) is used for CQI ⁴.
- $SCQI(k, t)$ denotes the user’s sum-CQI (the summation is over all sub-streams), and is a scalar quantity.
- $TP(k, t)$ denotes the throughput of user k at time instant t . Note that $TP(k, t)$ differs from $SCQI(k, t)$, since only 1 of K users is scheduled at every time instant.

1) *MAX*: Schedules the user with maximum SCQI. Thus,

$$k^*(t) = \arg \max_k SCQI(k, t) \quad k = 1, 2, \dots, K \tag{1}$$

where $k^*(t)$ denotes the user selected at time t . MAX is optimum from a throughput standpoint, in that no other algorithm can achieve more throughput. However, it ignores the past transmission history of all users, and hence, is unfair and biased in that aspect.

2) *EGoS*: Schedules that user who has been relatively starved throughput-wise over a time-window that extends to the indefinite past. Thus,

$$k^*(t) = \arg \min_k \sum_t TP(k, t) \quad k = 1, 2, \dots, K \tag{2}$$

EGoS can be considered to be the ultimate *throughput-fair* scheduler, since it allows each user to catch-up with other users, regardless of their channel conditions.

3) *PF*: All other schedulers will lead to performances that will be bracketed by the above two schedulers. We use the well-known PF scheduler [17], [20] as an example of one that attempts a better balance between throughput performance and fairness. Thus,

⁴We note that, although a single scalar quantity such as the total link-capacity would suffice as CQI information for user scheduling, a vector CQI is needed for adaptive transmission reasons. See Appendix B.

$$k^*(t) = \arg \max_k \frac{SCQI(k, t)}{TP(k, t)} \quad k = 1, 2, \dots, K \tag{3}$$

where $\overline{TP}(k, t)$ is a measure of the mean throughput of link k over a window extending from t back to the indefinite past⁵. $\overline{TP}(k, t)$ is updated using an exponentially weighted Infinite Impulse Response (IIR) filter as

$$\overline{TP}(k, t + 1) = \beta * \overline{TP}(k, t) + \delta(k^*, k) * SCQI(k, t) \tag{4a}$$

$$\delta(k^*, k) = \begin{cases} 1 & k^* = k \\ 0 & else \end{cases} \tag{4b}$$

where, δ is the Kronecker delta (sifting) operator, and β is the decay rate (or forgetting factor). We use $\beta = 0.98$ in the simulations, corresponding to an effective averaging window of 50 transmissions. This is a reasonable number for getting an accurate running mean.

We add that Round-Robin (RR) is another plausible scheduler. RR is a fair scheduler from a service-time perspective. However, it is known that for users with independent and identically distributed (i.i.d.) fades, the benefit of multi-user diversity is lost when RR is employed [21]. On the other hand, it is also known that PF best balances between the conflicting tradeoffs — offering service-time fairness to all users (in the asymptotic sense), while optimizing user performance at the same time [20], [27].

B. Link-level Description: Mobile Station Viewpoint (PHY-layer)

While the simulation platform developed in this study is quite general with respect to system and channel parameters, most numerical results were obtained using the parameters detailed in Table I. The various assumptions invoked in developing the platform are outlined here.

1) *Channel Model*: We consider three cases for Rician κ -factor, namely, $\kappa = 0$ (Rayleigh fading, i.e., only the scatter component); $\kappa = 10$ (dominant specular component); and κ a function of distance. The κ -factor typically decreases as the MS moves farther away from the BS, and the variation of κ with distance assumed here for the third case is given in Table II.

The complex baseband channel gain between the j th transmit antenna of a given base station and the i th receive antenna of a given user-terminal is modeled by

$$h_{ij} = \sqrt{A \left(\frac{d_0}{d}\right)^\Gamma} s \left[\sqrt{\frac{\kappa}{\kappa + 1}} e^{j\phi} + \sqrt{\frac{1}{\kappa + 1}} z_{ij} \right] \tag{5}$$

where,

⁵Our averaging formula for $\overline{TP}(k, t)$ is slightly different from the formula introduced in [17], [20].

TABLE I.
PARAMETER VALUES USED IN THE SYSTEM SIMULATIONS.

Cell Geometry	Hexagonal Array with side $R = 1000$ m
Carrier Frequency	$f_c = 2$ GHz
System Bandwidth	$W = 5$ MHz
Path Loss Exponent	$\Gamma = \begin{cases} 2 & 30 \leq d \leq 100\text{m} \\ 3.7 & \text{else} \end{cases}$
Shadow Fading	Lognormal, with Standard Deviation $\sigma = 8$ dB
Multipath Fading	Rician, with κ -factor = 0 (Rayleigh), 10, or a function of Transmit-Receive (T-R) distance (see Table II)
Antenna Pattern	Omnidirectional, or Uniform over 120°
Thermal Noise Density	$N_0 = -174$ dBm/Hz
Mobile Terminal's Noise Figure	$N_F = 8$ dB
Transmit Power	$P_T = 5$ W
Median cell-boundary SNR	$\rho = 20$ dB

TABLE II.
VARIATION OF RICIAN κ -FACTOR AS A FUNCTION OF BS-MS SEPARATION DISTANCE (PERCENTAGES SPECIFY THE DISTANCES RELATIVE TO THE CELL RADIUS).

Distance %	0-5	5-15	15-25	25-35	35-45	45-55	55-65	65-75	75-85	85-100
Rician κ	10	9	8	7	6	5	4	3	2	0

- d is the link length, Γ is the path loss exponent, and A is the median of the path gain at reference distance d_0 ($d_0 = 100$ m in the simulations).
- $s = 10^{S/10}$ is a log-normal shadow fading variable, where S is a zero-mean Gaussian random variable with standard deviation σ dB.
- κ is the Rician κ -factor for the given base-to-mobile path.
- $\phi = 2\pi d/\lambda$ is the phase shift of a line-of-sight (LOS) plane wave from the transmitter to the receiver. $\lambda = c/f_c$ is the wavelength. We assume that for a given transmit-receive pair, all LOS paths have the same length.
- z_{ij} represents the phasor sum of scattering components for the (i, j) path which are assumed to be zero-mean, unit-variance, i.i.d. complex Gaussian random variables.

We assume a base station height of $h = 30$ m above ground. For receivers located close to the ground, the direct path has a length $d = [r^2 + h^2]^{1/2}$, where r is the distance along the ground from the receiver to the base station. This implies that all Transmitter-Receiver (T-R) distances are 30 m or greater. We use a loss exponent of 2.0 (free space loss) for distances close to the base station (30 – 100 m), and 3.7 for distances beyond 100 m. We also apply shadow fading regardless of the T-R distance. This has been shown to be an empirically reasonable model [28]. For antenna sectoring, perfect beams are assumed instead of shaped antenna patterns.

2) *Simplifying System Assumptions:* We invoke assumptions often made in conjunction with MEA systems [1], [2]: (i) narrowband signaling, (ii) quasi-static (block) fading, (iii) long burst interval, and (iv) independently faded complex Gaussian path gains. This permits

a mathematical representation for the SISO/MEA cellular system⁶ as follows

$$\mathbf{Y} = \mathbf{H}\mathbf{X} + \mathbf{Z}, \tag{6}$$

where $\mathbf{X} \in \mathbb{C}^{7n}$, $\mathbf{Y} \in \mathbb{C}^m$, are transmit (serving and interfering) and receive signal vectors, $\mathbf{H} \in \mathbb{C}^{m \times 7n}$ is the channel gain matrix, and $\mathbf{Z} \in \mathbb{C}^m$ is a thermal noise vector, that is Gaussian distributed with zero-mean and one-sided power spectral density (PSD) N_0 . Since the noises corrupting the different receive antennas are independent, \mathbf{Z} has an autocorrelation matrix $N_0 \mathbf{I}_{m \times m}$, with $\mathbf{I}_{m \times m}$ being the identity matrix.

We assume only one tier of interferers around the serving BS (Fig. 2). This assumption is made to simplify the simulations and is slightly optimistic. However, the rapid decay of signal power with distance makes this assumption reasonable. Moreover, we offset it with the pessimistic assumption that all co-channel interferers are transmitting all the time. (In the single-cell case co-channel interferers are not present, and $\mathbf{H} \in \mathbb{C}^{m \times n}$).

We assume an adaptive transmission algorithm that perfectly adapts the transmission on each transmit antenna (via the constellation size) according to the instantaneous radio channel and interference conditions. It is possible for different transmit antennas to choose different bit rates (constellation sizes), although all transmissions operate at the same symbol rate. The procedure to compute the optimum size of the transmit constellations appears in the Appendix B.

Since cell-site (macro) diversity has been shown to have minimal impact on mean throughput calculations

⁶Following explanation offered in the Introduction, configurations employing Transmit Diversity are not considered. Hence, configurations that have more transmit than receive antennas ($n > m$) are excluded from this study.

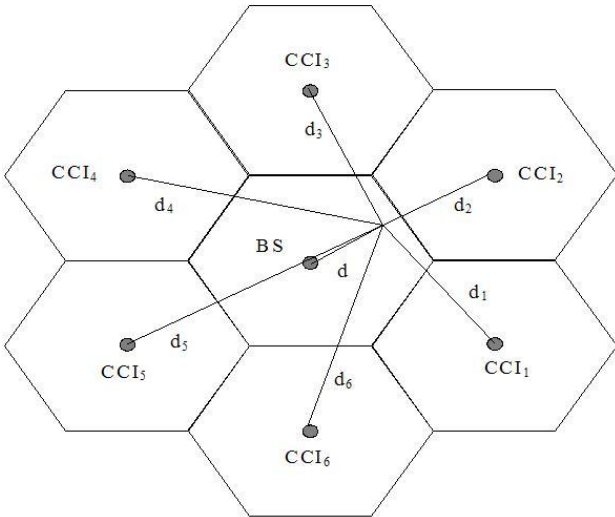


Figure 2. Plot of an interference-limited system, showing the serving and co-channel base stations. Regular hexagonal geometry with side $R = 1000$ m is assumed.

[9], [10], it is not used in the simulations, i.e., for simplicity, we assume that users communicate with the base station that is the nearest, not necessarily the strongest. Finally, perfect channel estimation, perfect T-R synchronization, and perfect instantaneous feedback are also assumed. These simplifications focus the problem on the essential issues we wish to investigate.

3) *Array Processing:* Depending on the availability of channel state information (CSI) at the transmitter, it is possible to design transmit-adaptation (e.g. eigen-beamforming) and receive-adaptation (e.g., minimum mean-square error) array processing strategies. Since we assume CQI but not CSI feedback to the transmitter, only the receive-adaptation scheme is discussed here. The minimum mean-square error (MMSE) scheme uses uniform power allocation among the n transmit antennas. To analyze MMSE reception, the analyst takes into account the path gains from all BSs — serving and interfering — in the channel gain matrix ($\mathbf{H} \in \mathbb{C}^{m \times 7n}$). Received data streams are separated by computing a linear combination of the received signals using a set of weights that achieves the minimum mean-square error between the output estimate and the true signal sample. Thus, we have that

$$\hat{\mathbf{X}} = \mathbf{W}^H \mathbf{Y}. \tag{7}$$

The performance index for a given weight matrix is

$$\zeta(\mathbf{W}^H) \triangleq E \left[\sum_{j=1}^n |\epsilon_j|^2 \right] = E \left[\sum_{j=1}^n |x_j - \hat{x}_j|^2 \right] \tag{8}$$

where x_j is the j th transmitted signal. The expectation in (8) is taken with respect to the noise and the statistics of the data sequences. The weight matrix \mathbf{W} that yields the

minimum mean-square error is [10]

$$\mathbf{W} = \mathbf{A}^{-1} \mathbf{H}, \tag{9a}$$

$$\mathbf{A} = \mathbf{H} \mathbf{H}^H + \frac{\sigma^2}{P_T/n} \mathbf{I}_{m \times m}. \tag{9b}$$

The post-processing SINR on the j th decoded stream can be shown to be [8], [10]

$$\gamma_j = (\mathbf{H}_j^H \mathbf{R}_j^{-1} \mathbf{H}_j), \quad j = 1, 2, \dots, n \tag{10}$$

where

$$\mathbf{R}_j = \sum_{l=1, l \neq j}^{7n} (\mathbf{H})_l (\mathbf{H})_l^H + \frac{\sigma^2}{P_T/n} \mathbf{I}_{m \times m} \tag{11}$$

and $(\mathbf{H})_j$ is the j th column of \mathbf{H} . (For the noise-only (single-cell) case, the summation will have n terms, instead of $7n$).

4) *Link Throughput Bounds:* The per-user data throughput is the sum of the throughputs of the sub-streams. We determine the throughput T_j of sub-stream j for two extreme cases:

- Ideally Coded Signals – The throughput is upper-bounded by the Shannon capacity,

$$T_j = \log_2 (1 + \gamma_j). \tag{12}$$

- Uncoded Signals – Assuming error detection in each block, the throughput is

$$\begin{aligned} T_j(M_j) &= (1 - BLER_j) \log_2(M_j) \\ &= (1 - BER_j)^L \log_2(M_j) \end{aligned} \tag{13}$$

where $\log_2(M_j)$ is the number of bits per symbol in stream j , BER_j is the bit error rate for stream j , and $BLER_j$ is the corresponding block error rate for L -bit blocks. In this study $L = 500$ bits is assumed, though the results are robust for values of L over a wide practical range [10].

We wish to simplify (13) to the form of (12) for convenience of calculation. Under the simplifying assumption that the channel undergoes quasi-static block fading, it is possible to regard the channel as *AWGN conditioned on the instantaneous gains*. For QAM modulation, we can then use the procedure in [9]–[11] to bring this to the form

$$T_j = \max T_j(M_j) \approx \log_2 \left(1 + \frac{\gamma_j}{6.4} \right). \tag{14}$$

Thus, the curve for uncoded transmission is 8 dB ($= 10 \log_{10}(6.4)$) shifted from the curve for perfectly-coded (Shannon) transmission. A variety of practical coding strategies can then be modeled by using other shifts less than 8 dB.

5) *Simulation Trials*: For the purpose of averaging throughput over a cell, we conduct 500 trials in a simulation. In any given trial, K users are distributed at random locations uniformly over the cell/sector. A given trial assigns a location, shadow-fade combination to each user, and user locations are uncorrelated. In each trial, users experience 1000 different multipath fades⁷. Thus, there are 500,000 quasi-static-block-fade transmission intervals in all. In this study, we consider both limited and unlimited constellation sizes. For the limited constellation case, modulations up to 16-QAM (leading to a symbol rate of up to 4 bits/symbol) are considered. This maximum is practical for present-day cellular implementations⁸.

III. NUMERICAL RESULTS

Figs. 3–6 show the cell-wide average throughputs that are offered by MMSE systems for the many dimensions we considered. We show only a sample listing, instead of presenting throughputs over all dimensions, to keep the discussion useful and concise. Our initial discussion refers to the case of a Rician κ -factor of $\kappa = 0$ and omnidirectional antennas. Any deviations we make from this baseline case in subsequent paragraphs will be so noted.

We have organized our figures as follows: Figures 3 and 4 consider the single- and multi-cell cases respectively for the (1, 1) configuration; while figures 5 and 6 do the same for the (3, 3). Figures 7 and 8 refer to (3, 3) with sectorized antenna patterns.

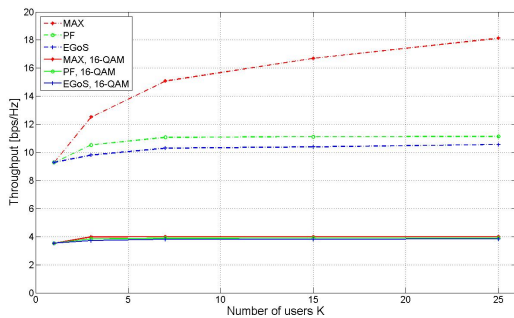


Figure 3. Mean throughput as a function of number of users for the (1, 1) system, single-cell environment, $\kappa = 0$, and omnidirectional antennas. Throughputs are plotted for all three scheduling algorithms, for both unlimited constellation (with ideal coding) and limited constellation size (16-QAM).

Effect of Number of Users and Scheduling Algorithm:

It is known that at the link-level, multi-user diversity with network scheduling leads to gains that grow as $O(\log K)$. Referring to Figs. 3–6, we see that this is also the case for system-level simulations for unlimited constellation sizes (although the scalar multipliers, and lower order terms, are different for different scheduling algorithms).

⁷Since Rayleigh fading has significant density at the tail, 1000 realizations are needed for statistical stability.

⁸The state-of-art is 16-QAM for mobile wireless systems, and 64-QAM for fixed wireless systems.

It is clear that MAX leads to higher gains with increasing K , while EGoS leads to limited gains. In some cases (the multicell scenarios), EGoS leads to throughput loss rather than gain. This is readily explained by the fact that EGoS is a “poor man’s” scheduling algorithm. It penalizes users with better channels to allow users with poor channels to catch up. This leads to a situation in which users with weak channels determine the overall scheduler performance.

The PF scheduler, in contrast to the EGoS scheduler, always leads to gains with increasing number of users. It is also evident from the figures that PF with $\beta = 0.98$ leads to curves parallel to those for EGoS in the mid-to-high region of K . Different values of β can lead to a range of ‘tunable’ PF schedulers, although, $0.90 \leq \beta < 1.00$ is a practical range⁹.

As explained earlier, MAX leads to very good gains as compared to EGoS and PF. However, it is a biased/greedy algorithm, which may not serve well for environments having quality of service (QoS) requirements. EGoS attempts throughput fairness, while PF attempts to strike a balance between cell-wide throughput and fairness. However, as will be seen shortly, EGoS can also be useful under practical circumstances.

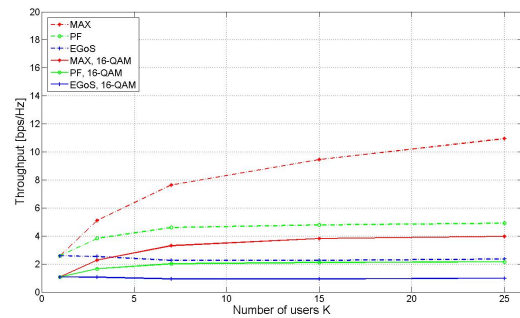


Figure 4. Mean throughput as a function of number of users for the (1, 1) system, multi-cell environment, $\kappa = 0$, and omnidirectional antennas. Throughputs are plotted for all three scheduling algorithms, for both unlimited constellation (with ideal coding) and limited constellation size (16-QAM).

Effect of Co-Channel Interference: In the single-cell scenario, multi-user diversity improves the signal (channel) quality, while in the multi-cell case, it has room to perform an additional function: that of interference avoidance [20]. This means that we can expect better gains with increasing K for the multi-cell case. This is indeed so, as evidenced by a comparison between Fig’s. 3 and 4 or 5 and 6; i.e.,

$$\frac{TP_{single-cell, K=25}}{TP_{single-cell, K=1}} < \frac{TP_{multi-cell, K=25}}{TP_{multi-cell, K=1}}.$$

SINRs in the single-cell case (20 dB to 60 dB) are much higher than those in the multi-cell case (–5 dB to

⁹With $0.90 \leq \beta < 1.00$, the effective averaging window is 10 transmissions or greater, which is sufficient for averaging purposes. For $\beta < 0.90$, exponential averaging will have an extremely short memory.

25 dB), leading to correspondingly lower throughputs for the latter. MAX and EGoS curves display more or less similar trends for the single and multi-cell cases, whereas PF yields better gains (the PF curve moves away from EGoS, closer to the MAX curve) for the multi-cell case.

Effect of Degrees of Freedom: In a (1, 1) system, multi-user diversity improves the operating SINR. In a (3, 3) system, multi-user diversity improves both the operating SINR, as well as the available degrees of freedom of the system. In other words, the entire channel subspace structure (the number, as well as values of the eigen-space) is improved [18].

Note that neither the SISO (1, 1), nor the MIMO (3, 3) system have excess degrees of freedom. It is clear that, although we see a substantial increase in mean throughput for the MIMO (3, 3) system as compared to the SISO (1, 1) system, we cannot expect the increase to be three-fold, despite the creation of three parallel decoupled streams at the receiver. This is because the available degrees of freedom (receive antennas) are used to combat cross-stream interference (XSI), even at the cost of noise enhancement. Also, each transmit antenna in the (3, 3) system now uses only 1/3 the total transmit power as compared to the SISO system.

Similar trends are seen for both single and multi-cell cases. Note the change in scale of the y-axis for the (3, 3) configuration (Figs. 5, 6) as compared to the (1, 1) configuration (Figs. 3, 4).

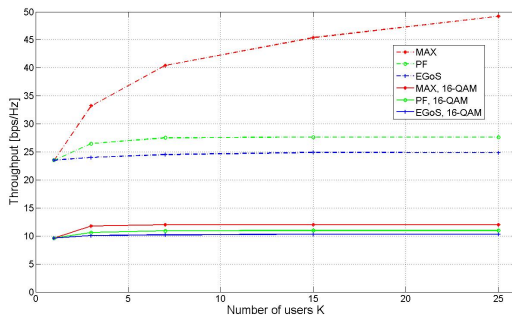


Figure 5. Mean throughput as a function of number of users for the (3, 3) system, single-cell environment, $\kappa = 0$, and omni-directional antennas. Throughputs are plotted for all three scheduling algorithms, for both unlimited constellation (with ideal coding) and limited constellation size (16-QAM). (Note the change in the vertical scale relative to Figures 3 and 4).

Effect of Antenna Sectorization: Antenna sectorization is an interference suppression technique. Co-channel interference is reduced by using antenna beam patterns and frequency coloring [29], [30]. By contrast, multi-user diversity is an interference avoidance technique, which also improves channel subspace structure (by avoiding ill-conditioned channels). Since antenna sectorization cannot improve channel structure, it is clear that multi-user diversity is the superior technique, particularly for a system with many users. Antenna sectorization and multi-user

diversity can be used in conjunction, since their goals are not necessarily conflicting. It stands to reason that as the number of users increases, the combined gain will have diminishing benefit, with multi-user diversity playing an increasingly major role.

From Figs. 6 and 7, for a reuse factor of 1, using sectorized antennas leads to about a two-fold improvement in throughput over omni-directional antennas for the single-user case¹⁰.

As the number of users is increased, the benefit due to antenna sectorization gradually decreases for all three schedulers, as was expected. As a percentage, sectorization leads to far more improvement in EGoS performance as compared to MAX and PF.

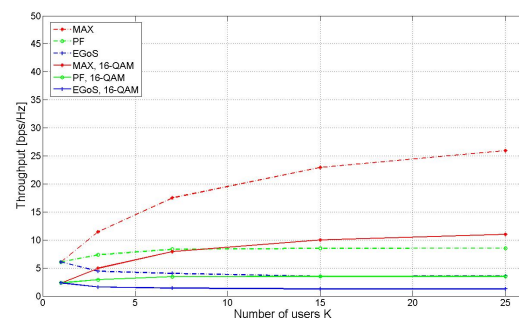


Figure 6. Mean throughput as a function of number of users for the (3, 3) system, multi-cell environment, $\kappa = 0$, and omni-directional antennas. Throughputs are plotted for all three scheduling algorithms, for both unlimited constellation (with ideal coding) and limited constellation size (16-QAM). (Note the change in the vertical scale relative to Figures 3 and 4).

Effect of Rician κ -Factor: It is known that, in the presence of a strong specular component ($\kappa \sim 10$) the mean throughput of SISO (1, 1) systems increases [1], [9], [11], [22]. Adding users and scheduling algorithms results in the following changes: mean throughput increases slightly ($\sim 3\%$) for the MAX scheduler, decreases slightly ($\sim 5\%$) for PF, and decreases moderately ($\sim 9\%$) for EGoS, over all K . Similar trends hold for the single- and multi-cell cases.

For the MIMO (3, 3) system, going from $\kappa = 0$ to $\kappa = 10$ leads to a substantial decrease in capacity [1], [9], [11], [22]. However, as the number of users is increased, the losses are reduced. This can be explained by the inherent property of multi-user diversity to choose the relatively best channel. Loss reduction with increasing number of system users is the highest in MAX, followed in order by PF and EGoS.

Mean throughput values for Rician fading with κ -factor a function of distance (Table II) are bracketed those obtained for $\kappa = 0$ and $\kappa = 10$, closer to those obtained using $\kappa = 10$.

¹⁰This is consistent with results from conventional systems (using three-sector antennas enables cellular system planners to bring down the reuse factor from 12 to 7, which amounts to a similar throughput increase [30, Ch. 3]).

Effect of Coding: For the single-cell case, for both (1, 1) and (3, 3) systems, the reduction in throughput at $K = 1$, for uncoded signals relative to Shannon coded signals is about 20% [11], [31]. As the number of users is increased, we experience a decrease in the throughput loss for uncoded transmission. Throughput loss at $K = 25$ is about 15% for the MAX scheduler, 22% for PF and 25% for EGoS.

For the multi-cell case, the coding loss at $K = 1$ for both (1, 1) and (3, 3) systems is about 40–50% [11], [31]. At $K = 25$, the losses are about 25%, 45% and 50%, for MAX, PF and EGoS respectively.

Thus, at higher K , there is improvement for MAX, but not for PF and EGoS in both the single- and multi-cell cases.

This can be explained as follows: Loss due to uncoded transmission depends on the operating SINR. For the single-cell case, the operating SINR is high, hence the throughput loss is comparatively low, and comparable percentage losses are recorded by all three schedulers. On the other hand, operating SINRs are significantly lower for the multi-cell case, hence throughput losses are higher. Multi-user diversity has the inherent property of seeking users with good SINRs; however, this applies to the MAX scheduler more than to the PF and EGoS schedulers. Depending on past transmission history, PF and EGoS schedulers may not be able to choose the best user. Hence, they lead to correspondingly less improvement.

For sectorization, SINRs, and hence coding losses observed, will be bracketed by the single-cell and multi-cell cases above.

Effect of Limited Constellation Sizes: Whereas unlimited constellation size provides insight to the potentially achievable throughputs the system can offer, it is also necessary to look into throughputs that practical systems can actually realize. Figs. 3–6 give some illustrative results. Limiting the transmit alphabet size to 16-QAM amounts to capping throughput at $4n$ bps/Hz. The effect is to reduce the potential benefit from increasing number of users in the system, particular choice of scheduling algorithm, and antenna sectorization.

Compared to the case of unlimited constellation sizes, we notice a substantial throughput loss for both (1, 1) [Fig. 3 for single-cell, Fig. 4 for multi-cell] and (3, 3) systems [Fig. 5 for single-cell, Fig. 6 for multi-cell]. Throughput saturation (due to constellation size capping) is almost immediate ($K = 3$) for the single-cell case. For the multi-cell case, throughput leveling occurs at $K = 7$ for PF and EGoS, and the differences between the throughputs offered by the scheduling algorithms are substantially reduced.

Since throughput per-cell differences between the various schedulers are negligible for the single-cell case, and significantly reduced even for the multi-cell case, it becomes reasonable to view these findings through the prism of other metrics. In this context, we note the following: EGoS can be more suitable than MAX

and PF for the single-cell case [Figs. 3 and 5] since it is the ultimate throughput-fair scheduler; MAX may be unsuitable since it is biased, while PF may be unsuitable since it is *not* stable¹¹ [32]. For the multi-cell case, PF may be more suitable than MAX, depending on QoS requirements [Figs. 4 and 6]. This observation has important implications for current state-of-the-art systems that can support signal constellations up to 16-QAM.

IV. MULTI-USER DIVERSITY SYSTEMS WITH NO EXCESS DEGREES OF FREEDOM VS. SINGLE-USER SYSTEMS WITH EXCESS DEGREES OF FREEDOM

We now provide a brief comparison between single-user systems employing excess degrees of freedom (SU-EDoF), and multi-user diversity systems having no excess degrees of freedom (MuD-wo-EDoF). Both mechanisms attempt to improve received signal quality, as measured by the post-processing SINR, and use of one technique does not preclude using the other (i.e., it is possible to combine multi-user diversity with excess degrees of freedom (MuD-EDoF)).

In SU-EDoF, a receiver uses excess antennas achieving diversity to combat fading, or to suppress one or more co-channel interference streams, or a combination of both [26]. SU-EDoF is a *radio-layer* technique, and can be used for all application types (delay-elastic, as in data applications, or delay-intolerant as in voice applications). By contrast, multi-user diversity schedules the user with the best signal quality, i.e., interference avoidance is inherently achieved. However, multi-user diversity (both MuD-EDoF and MuD-wo-EDoF) is applicable only to delay-elastic applications, wherein the scheduler selects one user for transmission. Viewed from this perspective, multi-user diversity may be considered as a *cross-layer technique* in which the radio (PHY)-layer continually educates the medium access control (MAC)-layer. Since multi-user diversity is able to improve the channel subspace structure (by avoiding ill-conditioned channels), a capability which SU-EDoF does not have, it can be the superior technique, particularly in a system having many users.

We now discuss how MuD-wo-EDoF may be used in lieu of SU-EDoF, thereby leading to a reduction in the number of receive antennas, while offering comparable or greater throughput¹². We have seen previously that, EGoS leads to small gains for the single-cell scenario, and moderate loss for the multi-cell scenario, as a function of number of users K . Hence, EGoS cannot be used as a scheduler in MuD-wo-EDoF to compete against SU-EDoF. Similarly, we have seen that the PF scheduler has curves that are nearly parallel to those of EGoS with higher multi-user diversity gains. This implies that the PF scheduler can be used with MuD-wo-EDoF to compete against SU-EDoF wherein the excess degrees of freedom in SU-EDoF are few (e.g. one). When excess degrees of

¹¹A stable algorithm always results in bounded queue lengths under any conceivable traffic scenario.

¹²Since there is a reduction in the number of receive antennas, there is considerable impact, since it affects all mobiles.

freedom in SU-EDoF are many, e.g. MIMO (3, 6), the MAX scheduler should be used.

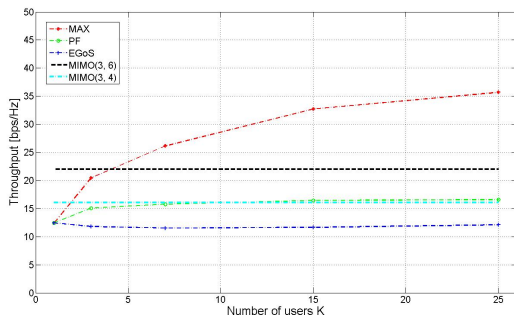


Figure 7. Mean throughput as a function of number of users for the (3, 3) system, with unlimited constellation sizes and ideal coding, multi-cell environment, $\kappa = 0$, and sectorized antennas. Throughputs for all three scheduling algorithms are plotted. The upper horizontal line is for the single-user MIMO (3, 6) system (no multi-user diversity), while the lower horizontal line is for the single-user MIMO (3, 4) system.

Fig. 7 illustrates a representative example, where the upper horizontal line indicates the performance of the single-user MIMO (3, 6) system, and the lower horizontal line indicates the performance of the single-user MIMO (3, 4) system. These systems are able to suppress up to 3 and 1 interfering streams, respectively. We see that a MuD-wo-EDoF system incorporating the MAX scheduler, with 2 or more users can offer equal or better performance than the single-user MIMO (3, 4) system, while 4 or more users are needed to achieve performance equal to or better than that for single-user MIMO (3, 6). With a MuD-wo-EDoF system incorporating a PF scheduler, 10 or more users are needed to compete with a single-user MIMO (3, 4) system. A PF-based MuD-wo-EDoF system cannot compete with a single-user MIMO (3, 6) system, no matter how large K is.

The above comparisons hold even for the case of limited constellation sizes, as seen in Fig. 8. In this case, however, the differences, in terms of design choices and their consequences, are markedly reduced.

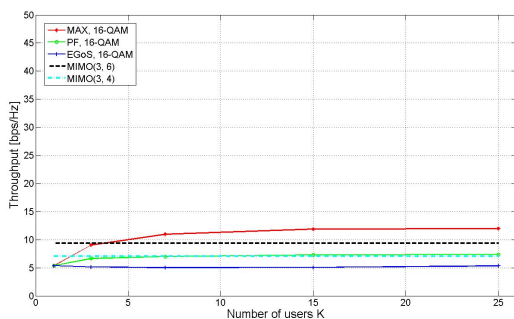


Figure 8. Mean throughput as a function of number of users for the (3, 3) system, with limited constellation size (16-QAM), multi-cell environment, $\kappa = 0$, and sectorized antennas. Throughputs for all three scheduling algorithms are plotted. The upper horizontal line is for the single-user MIMO (3, 6) system (no multi-user diversity), while the lower horizontal line is for the single-user MIMO (3, 4) system.

V. SUMMARY AND CONCLUSIONS

We have evaluated the throughput performance of SISO and MIMO-based cellular systems which employ multi-user diversity over several useful system-level design dimensions. By evaluating the performance of two extreme schedulers (MAX, EGoS), we have been able to obtain a perspective on the performances realized by a variety of useful schedulers. The PF scheduler was also considered as a representative and widely popular example. Our chief observation is that, although the various dimensions are important considerations for SISO and MEA systems, the potential benefits need to be weighed in the context of limited signal constellations that are prevalent in present day practical systems. Since per-channel throughput differences were negligible for the single-cell case, and dramatically reduced for the multi-cell case, other metrics (fairness and stability) were employed to get another perspective on the findings. There, EGoS seemed a reasonable choice for the single-cell case, and PF seemed reasonable in multi-cell scenarios when delay tolerance was allowed.

We also compared single-user MIMO systems that use excess degrees of freedom (SU-EDoF) and those that use multi-user diversity without excess degrees of freedom (MuD-wo-EDoF). Here, among scheduler choices, it is clear that EGoS is not a viable candidate; that PF has limitations in the number of excess receive antennas it can compete against in SU-EDoF based systems; and, that MAX is the best option in terms of cell-wide throughput.

In general, for applications that are delay-tolerant, a MuD-wo-EDoF system with a large number of users can deliver substantially higher throughputs than SU-EDoF links. This is especially when using SU-EDoF with only one extra antenna, but applies even to the case of up to three. Finally, the amount of improvement using MuD-wo-EDoF instead of SU-EDoF decreases with increasing limits on constellation size.

APPENDIX A DEFINITIONS

- 1) Array processor: the unit at the receiver, which attempts to separate the received streams in the face of cross-stream interference (XSI) and co-channel interference (CCI) as optimally as possible.
- 2) Degrees of Freedom: the number of decomposable parallel SISO channels that can be created after array processing. It equals the rank of the channel gain matrix \mathbf{H} , and is upper-bounded by $\min(n, m)$.
- 3) Excess Degrees of Freedom: the excess number of receive elements over transmit elements, i.e., $m - n$. When the receive array has at least as many antenna elements as the transmit array, we can receive all of the transmitted streams at the receiver after array processing.

APPENDIX B SIMULATION APPROACH

The intention in this study is to compute throughput statistics of several SISO/MIMO configurations in a multi-user scenario (employing network diversity scheduling) for various design options. Highlights of the steps involved are as follows:

- 1) Distribute K MSs in cell (uniform random uncorrelated locations), and generate channel matrices $\mathbf{H}_1, \dots, \mathbf{H}_K$ as given by (5).
- 2) $\forall k$, compute post-processing SINR for each substream j , assuming MMSE reception ((10)-(11)).
- 3) $\forall k$, compute the throughput for each substream j ((12), (14)). This is the vector CQI for user k .
- 4) $\forall k$, compute $SCQI = \sum_{\text{substreams}} CQI$.
- 5) Schedule user $k^*(t)$ (Equations (1), (2), (3)), and update his cumulative throughput ($\sum_t TP(k^*, t)$).
- 6) Update the averages ((4)) of all users.
- 7) Compute the average cell-wide multi-user throughput over 500 locations (each with lognormal shadow fading) and 1000 multipath fades per location.

At the beginning of each block-fade interval, pilot signals are transmitted to estimate the receiver array weights. The receiver then determines the constellation size (M) from the substream post-processing SINRs, and communicates this information to the transmitter. Based on CQI, past transmission history, delay/latency constraints and the particular scheduling algorithm in use, a particular user is selected for transmission. Adaptive modulations at each transmit antenna then quickly select the corresponding optimal QAM constellation. The channel remains known throughout, since estimation-feedback-adaptation occurs within the block fade interval. By assumption, we exclude all overheads (pilot signaling, channel estimation at receiver, feedback and signal-adaptation) from our throughput computation procedure.

ACKNOWLEDGEMENT

We greatly appreciate valuable comments from Professor Li-Chun Wang, Chandrasekharan Raman, Joydeep Acharya and Jasvinder Singh.

REFERENCES

- [1] I. Telatar, "Capacity of multi-antenna gaussian channels," *Euro. Trans. Telecommun.*, vol. 10, no. 6, pp. 585–595, November 1999.
- [2] G. Foschini and M. Gans, "On limits of wireless communications in a fading environment when using multiple antennas," *IEEE Wireless Personal Communications*, vol. 6, no. 3, pp. 311–335, March 1998.
- [3] P. Wolniansky, G. Foschini, G. Golden, and R. Valenzuela, "V-BLAST: an architecture for achieving very high data rates over the rich-scattering wireless channel," in *Proc. Int. Symp. Signals, Systems, and Electronics (ISSSE '98)*, Pisa, Italy, pp. 295–300, October 1998.
- [4] S. Alamouti, "A simple transmit diversity technique for wireless communications," *IEEE J. Sel. Areas Commun.*, vol. 16, no. 8, pp. 1451–1458, October 1998.
- [5] V. Tarokh, H. Jafarkhani, and A. Calderbank, "Space-time block codes from orthogonal designs," *IEEE Trans. Inf. Theory*, vol. 45, no. 5, pp. 1456–1467, July 1999.
- [6] V. Tarokh, N. Seshadri, and A. Calderbank, "Space-time block codes for high data rate wireless communication: Performance, criterion and code construction," *IEEE Trans. Inf. Theory*, vol. 44, no. 2, pp. 744–765, March 1998.
- [7] G. Foschini, "Layered space-time architecture for wireless communication in a fading environment when using multiple antennas," *Bell-Labs Tech. J. (BLTJ)*, vol. 1, no. 2, pp. 41–59, 1996.
- [8] S. Catreux, P. Driessen, and L. Greenstein, "Data throughputs using multiple-input-multiple-output (MIMO) techniques in a noise-limited cellular environment," *IEEE Trans. Wireless Commun.*, vol. 1, no. 2, pp. 226–235, April 2002.
- [9] —, "Attainable throughput of an interference-limited multiple-input multiple-output (MIMO) cellular system," *IEEE Trans. Commun.*, vol. 49, no. 8, pp. 1307–1311, August 2001.
- [10] S. Catreux, "Techniques d'antennes multi-entrees multi-sorties dans un systeme de type cellulaire," Ph.D. dissertation, INSA, Paris, France, April 2000.
- [11] R. Pupala, L. Greenstein, and D. Daut, "Downlink throughput statistics in interference-limited cellular systems with multi-element antennas," *IEEE Trans. Commun.*, vol. 58, no. 1, pp. 311–317, January 2010.
- [12] —, "Effects of channel dispersion and path correlations on system-wide throughput in MIMO-based cellular systems," *IEEE Trans. Wireless Commun.*, vol. 8, no. 11, pp. 5477–5482, November 2009.
- [13] —, "Throughput analysis of interference-limited MIMO-based cellular systems," *IEEE Trans. Wireless Commun.*, vol. 9, no. 6, pp. 1946–1951, June 2010.
- [14] L. Zheng and D. Tse, "Diversity and multiplexing: a fundamental tradeoff in multiple-antenna channels," *IEEE Trans. Inf. Theory*, vol. 49, no. 5, pp. 1073–1096, May 2003.
- [15] B. Hassibi and B. Hochwald, "High rate codes that are linear in space and time," *IEEE Trans. Inf. Theory*, vol. 48, no. 7, pp. 1804–1824, July 2002.
- [16] R. Knopp and P. Humblet, "Information capacity and power control in single cell multiuser communications," *IEEE Proc. ICC*, vol. 1, pp. 331–335, June 1995.
- [17] A. Jalali, R. Padovani, and R. Pankaj, "Data throughput of CDMA-HDR a high efficiency-high data rate personal communication wireless system," *IEEE Proc. VTC*, vol. 3, pp. 1854–1858, Spring 2000.
- [18] R. Heath, M. Airy, and A. Paulraj, "Multiuser diversity for MIMO wireless systems with linear receivers," *IEEE Proc. Asilomar Conf. Signals, Systems and Computers*, vol. 2, pp. 1194–1199, November 2001.
- [19] M. Airy, R. Heath, and S. Shakkottai, "Multiuser diversity for the multiple antenna broadcast channel with linear receivers: asymptotic analysis," *IEEE Proc. Asilomar Conf. Signals, Systems and Computers*, vol. 1, pp. 886–890, November 2004.
- [20] P. Viswanath, D. Tse, and R. Laroia, "Opportunistic beamforming using dumb antennas," *IEEE Trans. Inf. Theory*, vol. 48, no. 6, pp. 1277–1294, June 2002.
- [21] C. Chen and L. Wang, "Performance analysis of scheduling in multiuser MIMO systems with zero-forcing receivers," *IEEE J. Sel. Areas Commun.*, vol. 25, no. 7, pp. 1435–1445, July 2007.
- [22] A. Paulraj, R. Nabar, and D. Gore, *Introduction to Space-Time Wireless Communications*. Cambridge University Press, 2003.
- [23] D. Tse and P. Vishwanath, *Fundamentals of Wireless Communication*. Cambridge University Press, 2005.
- [24] C. Chen and L. Wang, "Enhancing coverage and capacity for multiuser MIMO systems by utilizing scheduling,"

- IEEE Trans. Wireless Commun.*, vol. 5, no. 5, pp. 1148–1157, May 2006.
- [25] —, “A unified capacity analysis for wireless systems with joint multiuser scheduling and antenna diversity in nakagami fading channels,” *IEEE Trans. Commun.*, vol. 54, no. 3, pp. 469–478, March 2006.
- [26] J. Winters, “Optimum combining in digital mobile radio with cochannel interference,” *IEEE J. Sel. Areas Commun.*, vol. 2, no. 4, pp. 528–539, July 1984.
- [27] J. Holtzman, “Asymptotic analysis of proportional fair algorithm,” *Proc. IEEE Symp. PIMRC*, vol. 2, pp. F33–F37, October 2001.
- [28] V. Erceg, L. Greenstein, S. Tjandra, S. Parkoff, A. Gupta, B. Kulic, A. Julius, and R. Bianchi, “An empirically based path loss model for wireless channels in suburban environments,” *IEEE J. Sel. Areas Commun.*, vol. 17, no. 7, pp. 1205–1211, July 1999.
- [29] G. Stuber, *Principles of Mobile Communications*. Kluwer Academic Publishers, 2001.
- [30] T. Rappaport, *Wireless Communications — principles and practice*. Prentice Hall, 2002.
- [31] R. Pupala, “Investigation of co-channel interference, channel dispersion & multiuser diversity in mimo-based cellular systems,” Ph.D. dissertation, Rutgers - The State University of New Jersey, US, February 2008.
- [32] M. Andrews, “Instability of the proportional fair scheduling algorithm for HDR,” *IEEE Trans. Wireless Commun.*, vol. 3, no. 5, pp. 1422–1426, September 2004.



Rahul N. Pupala received the B.E. degree in Computer Engineering from Victoria Jubilee Technical Institute (VJTI), Bombay in 1994, the M.S. degree in Computer Science in 2003, and the Ph.D. in Electrical Engineering in 2008 both from Rutgers - The State University of New Jersey. From 1994 to 1999, he worked in the software industry. He is currently at Alcatel-Lucent/Bell Labs, Murray Hill, NJ, responsible for PHY & MAC layer innovations for LTE-Advanced.

His research interests include Distributed Computing, Computer Networks, Signal Processing and Wireless Communications.



Larry J. Greenstein received the BS, MS and PhD degrees in electrical engineering from Illinois Institute of Technology in 1958, 1961 and 1967, respectively. From 1958 to 1970, he was at IIT Research Institute, where he worked on radio frequency interference and anti-clutter airborne radar. He joined Bell Laboratories in Holmdel, NJ in 1970. Over a 32-year career, he conducted research in digital satellites, point-to-point digital radio, optical transmission techniques and wireless communications.

For 21 years during that period (1979-2000), he led a research department renowned for its contributions in these fields. Since 2002, he has been a research professor at Rutgers University's WINLAB, working on PHY-based security techniques, MIMO-based cellular systems, broadband power line systems, cognitive radio and channel modeling.

Dr. Greenstein is an IEEE Life Fellow, an AT&T Fellow, a recipient of the IEEE Communications Society's Edwin Howard Armstrong and Joseph LoCicero Awards, and co-author of several award-winning papers, including the IEEE Donald G. Fink Prize Paper Award. He has served on numerous editorial boards and technical program committees and was, and is now again, the IEEE Communications Society's Director of Journals.



David G. Daut (S76-M80-SM88) received the B.S.E.E. from the New Jersey Institute of Technology (1976) and the M.S.E.E. and Ph.D. degrees from Rensselaer Polytechnic Institute (1977, 1981). He joined Rutgers University in 1980. He has served as Director, ECE Graduate Program (1991-1999) and as Director, Engineering Computer Center (1989-1998). He had served as Chairman of the Electrical and Computer Engineering Department from 1986 to 1988 and again from 1997 to

2006. Currently, a Professor of Electrical and Computer Engineering, his teaching and research activities are in the areas of communications and information systems.

His present research activities are focused on data/bandwidth compression techniques in the context of image coding and transmission, including: combined source and channel encoding of image data; digital communication system performance evaluation using different modulation and channel coding strategies in conjunction with both Gaussian and fading channel characterizations; wireless communication systems; the application of rate-distortion theoretic principles to the design of data and image transmission systems; and, optical communications systems employing Dense Wavelength Division Multiplexing in the presence of fiber nonlinearities. He has authored numerous journal and conference papers and was a co-recipient of the IEEE Communications Society Rice Prize Paper Award (1984).

Dr. Daut is an IEEE Senior Member and a member of Sigma Xi, Tau Beta Pi, Eta Kappa Nu as well as the Association for Computing Machinery, Optical Society of America, and the Society of Photo-Optical Instrumentation Engineers. He served as an elected member of the IEEE Board of Directors (Division III) during 1998 and 1999. In 2009 he served as General Co-Chair for the IEEE Sarnoff Symposium, Princeton, NJ.

Downlink System Throughput Statistics for Various MEA Configurations

Rahul N. Pupala

Alcatel-Lucent/Bell Labs, Murray Hill, NJ 07974, USA

Email: rahul.pupala@alcatel-lucent.com

Yifei Yuan (*Senior Member, IEEE*)

ZTE Corporation, Morristown, NJ 07960, USA

Email: yifei.yuan@zteusa.com

Qi Bi (*Fellow, IEEE*)

China Telecom - Beijing Research Institute, Beijing, China

Email: qibi@ctbri.com.cn

Larry J. Greenstein (*Life Fellow, IEEE*)

ECE (WINLAB), Rutgers – The State University of New Jersey, North Brunswick, NJ 08902, USA

Email: ljg@winlab.rutgers.edu

Abstract—The advent of applications that need higher throughputs motivates wireless service providers and cellular operators to embrace newer technologies that can meet these demands. Multiple-input-multiple-output (MIMO) systems have shown promise in their ability to deliver high throughput per bandwidth with reasonable constellation sizes. Adding antennas at the base station (BS) is practical due to reasons of size and cost amortization over users. However, adding antennas at the mobile station (MS), which does not have similar advantages, needs to be carefully evaluated. We therefore consider the more general class of techniques involving a multiple-element antenna (MEA) at one or both ends of the link (MIMO corresponding to the case of both).

From a commercial standpoint, one needs to address the following questions: (i) What is the benefit of a second antenna at the BS or the MS relative to the single-input-single-output (SISO) case? (ii) What is the added value of a second antenna at both ends? (iii) If a second antenna is indeed used at both ends, which mode of operation — spatial multiplexing (SM) or diversity (Div) — is the preferred one? Using (n, m) to denote a link with n BS transmit elements and m MS receive elements, we compare the downlink throughput performance of the SISO link with that of four MEA configurations: $(1, 2)$, $(2, 1)$, $(2, 2)$ with Div and $(2, 2)$ with SM. Our results indicate that, in the context of adaptive modulation with practical limits on constellation size, $(1, 2)$ is the preferred configuration. We also show this finding to be robust to assumptions used in the study.

Index Terms—SISO, MIMO, MEA, MMSE, multipath fading, shadow fading, co-channel interference, cross-stream interference, interference cancellers

I. INTRODUCTION

MULTIPLE-INPUT-MULTIPLE-OUTPUT (MIMO) systems have been accepted as a significant break-

through in modern digital communications, due to their ability to deliver higher spectral efficiencies with reasonable constellation sizes, as compared to single-input-single-output (SISO) systems [1]–[3]. A laboratory implementation of the so-called vertical Bell Labs layered space time architecture (VBLAST) demonstrated the feasibility of the MIMO concept, delivering spectral efficiencies of 20–40 bps/Hz under indoor conditions [4]. Not surprisingly, MIMO's potential is being tapped for commercial wireless products and networks such as wireless local area networks (WLANS), third-generation (3G) cellular networks, WiMAX, and future Internet-intensive wireless networks (including 4G networks).

A multi-element antenna (MEA) link (of which MIMO is a special case) employs a multi-element array at one or both ends. When only one end of the link uses an MEA, diversity can be achieved; this improves quality and thus enables higher throughput via larger signal constellations. When *both* ends use an MEA — the MIMO case — it is possible to enhance throughput via either diversity (Div), as above; spatial multiplexing (SM), whereby the receiver can de-couple multiple parallel streams sent by the transmitter; or a combination of both [5].

We will study and compare the performance of SISO links and several kinds of MEA links. Application type determines which aspect of performance matters most. For some applications (e.g., data), higher throughput, even if over intermittent connections or over smaller separation distances will be deemed as “good”, while other applications (e.g., voice, streaming) may prefer to trade throughput for sustained connections and/or a wider coverage area. It is thus clear that no single performance metric will suffice. Accordingly, we study the following metrics: (i) the mean, over the cell, of the per-link

Manuscript received February 15, 2011; revised May 15, 2011; accepted June 15, 2011.

TABLE I.
3GPP2 SIMULATION PARAMETER SUMMARY

1	Cell Geometry	Regular array of hexagonal cells, with site-to-site distance 2.5 km (i.e., cell radius of 1.4434 km).
2	Number of Cells	1 tier-ring, 3 sector system (21 sectors total).
3	Antenna Horizontal Pattern (sectoring)	70° (-3 dB), with 20-dB front-to-back ratio (see Note 1 below).
4	Antenna Orientation	0° azimuth is North (main lobe). No loss is assumed on the vertical dimension.
5	Propagation Model	28.6 + 35 log ₁₀ (<i>d</i>) dB, <i>d</i> in meters. Modified Hata Urban Propagation Model @ 1.9 GHz (COST 231). Min. separation of 35 m between MS and BS.
6	Lognormal Shadowing	Standard Deviation $\sigma = 8.9$ dB (see Note 2 below).
7	Base Station Correlation	0.5 (see Note 2 below).
8	Mobile Noise Figure	10 dB.
9	Thermal Noise Density	-174 dBm/Hz.
10	Carrier Frequency	2 GHz.
11	System Bandwidth	5 MHz.
12	BS Antenna Gain	15 dB total from 17 dB BS gain; 2-dB cable loss.
13	Other Losses	10 dB.
14	Fast Fading Model	Rician (see Table 2).
15	BS maximum PA Power	20 W.
16	Maximum C/I achievable	13 dB for typical IS-95 and cdma2000 1x systems and 18 dB for 1xEV-DV and 1xEV-DO systems.

throughput and (ii) 30th percentile of the link throughput.

Mean throughput provides a measure of the *data volume* an operator can deliver, in that this quantity times the number of channels per cell is a good approximation to the total throughput per cell. The 30th percentile of throughput is a useful measure of *user perception*, in that the vast majority of users (70%) will experience this throughput or more. Each metric thus has value from one perspective or another.

The essential aim of this study is to decide the merit in modifying a SISO link with added antenna elements at one or both ends. We denote a general downlink configuration by (*n*, *m*), where *n* is the number of base station (BS) transmit elements and *m* is the number of mobile station (MS) receive elements. Considering present-day technology and economics, we limit our study to the possibility of at most two antenna elements at each end. Thus, we investigate five configurations in all: (1, 1), which is SISO; (2, 1), MISO with transmit diversity; (1, 2), SIMO with minimum-mean-square-error (MMSE) receiver; (2, 2) with Div; and (2, 2) with SM. Computing the performances of these configurations, based on the metrics cited above, the differences can be used to decide whether (and where) addition of antenna elements is justified. By studying the performance of particular MEA configurations¹ for a specific standard (3GPP2), we are augmenting our knowledgebase in [6]–[9].

Systems engineers from several commercial companies have performed similar studies, for both High Speed Packet Access (HSPA) and Long Term Evolution (LTE)

¹For configuration (1, 2), we can employ either the maximal ratio combiner (MRC) or the minimum mean square error (MMSE) receiver structure. Of the two, MMSE is higher performing, as it offers an optimal balance between diversity and co-channel interference suppression, leading to higher throughput. MRC on the other hand offers only a diversity benefit.

networks. Their contributions feed into the knowledgebase maintained by the standards bodies (3GPP, 3GPP2), and can be found in [10]. A sampling of academic investigations for MIMO capacities is [11]–[13]. The rest of this paper is organized as follows. We discuss the simulation platform in Section II, and the results in Section III. Section IV summarizes our work, and presents some key conclusions.

II. SIMULATION PLATFORM

We developed a system-level simulation platform for computing the throughputs of MEA cellular systems. The test bed is sufficiently general to allow us to work with several key system-level parameters, namely, size of the transmit and receive MEAs; frequency reuse factor; antenna pattern (omni or sectorized); degree of error protection (perfect coding, no coding, or intermediate coding strategies); maximum constellation size; and, Rician *K*-factor.

A. MIMO System Model

In our MIMO cellular data environment, a given cell, consisting of a serving BS and a MS on every frequency channel, is surrounded by one contiguous tier of six cells. Our platform incorporates aspects of the 3GPP2 environment, as detailed in Table I.

NOTES

1. The base station antenna pattern used for each sector, is specified by

$$G(\theta) = -\min \left[12 \left(\frac{\theta}{\theta_{3\text{dB}}} \right)^2, A_m \right] \text{ dB}, \quad -180 \leq \theta \leq 180,$$

where $\theta_{3\text{dB}}$ is the 3-dB azimuth beamwidth and $A_m = 20$ dB is the maximum attenuation.

TABLE II.
 VARIATION OF RICIAN K -FACTOR AS A FUNCTION OF BS-MS SEPARATION DISTANCE (PERCENTAGES SPECIFY THE DISTANCES RELATIVE TO THE CELL RADIUS).

Distance %	0-5	5-15	15-25	25-35	35-45	45-55	55-65	65-75	75-85	85-100
Rician K	10	9	8	7	6	5	4	3	2	0

2. The random shadow fading x_k between a MS and a BS _{k} (whether serving or interfering) is the weighted sum of a component z common to all cell sites and a component z_k which is independent of z and from one cell site to the next. Both components are Gaussian distributed with zero mean and standard deviation σ . Thus, $x_k = az + bz_k$, $k = 0 \dots 6$, where $a^2 + b^2 = 1$. In this study, we assume $a^2 = b^2 = 1/2$, meaning that x_u and x_v , $u \neq v$, are 50% correlated.

The complex baseband channel gain between the j th transmit antenna and the i th receive antenna is modeled by

$$h_{ij} = \sqrt{G(\theta)} \sqrt{A \left(\frac{d_0}{d}\right)^\Gamma} s \left[\sqrt{\frac{K}{K+1}} e^{j\phi} + \sqrt{\frac{1}{K+1}} z_{ij} \right], \quad (1)$$

where

- θ is the angle between the 0° azimuth, and the BS-MS link.
- d is the link length, Γ is the path loss exponent, and A is the median path gain at reference distance d_0 .
- $s = 10^{S/10}$ is a log-normal shadow fading variable, where S is a zero-mean Gaussian random variable with standard deviation σ dB.
- $\phi = 2\pi d/\lambda$ is the phase shift of a plane wave from the transmitter to the receiver. We assume that for a given transmit-receive pair, all link-paths have the same length.
- z_{ij} represents the phasor sum of scattering components for the (i, j) path. These are assumed to be zero-mean, unit-variance, i.i.d. complex Gaussian random variables.
- K is the Rician K -factor.

Using appropriate parameter values in (1), the path-loss portion of the channel gain formula (first square root term outside the brackets) is made to follow the propagation model specified in Table I (Item 5). The Rician K -factor typically decreases as the MS moves farther away from the BS. The assumed variation of the K -factor with distance is given in Table II.

B. System Model Assumptions

We invoke the assumptions often made in conjunction with MIMO systems [1], [3]: (i) narrowband signaling, (ii) quasi-static (block) fading, (iii) long burst interval, and (iv) independently faded Rayleigh/Rician path gains. This permits a mathematical representation for the MIMO cellular system as follows:

$$\mathbf{Y} = \mathbf{H}\mathbf{X} + \mathbf{Z}, \quad (2)$$

where $\mathbf{X} \in \mathbb{C}^{7n}$, $\mathbf{Y} \in \mathbb{C}^m$, are transmit (serving and interfering) and receive signals, $\mathbf{H} \in \mathbb{C}^{m \times 7n}$ is the channel gain and $\mathbf{Z} \in \mathbb{C}^m$ is thermal noise, that is Gaussian distributed with zero mean and power spectral density (PSD) N_0 . Since the noises corrupting the different receive antennas are independent, \mathbf{Z} has an autocorrelation matrix $N_0 \mathbf{I}_{m \times m}$, with $\mathbf{I}_{m \times m}$ being the identity matrix.

We assume only one tier of interferers around the serving BS. This assumption is made to simplify the simulations and is slightly optimistic; however, the rapid decay of signal power with distance makes this assumption reasonable. Moreover, we offset it with the pessimistic assumption that all co-channel interferers are transmitting all the time.

We assume an algorithm that perfectly adapts the transmission (via the constellation size²) according to the instantaneous radio channel and interference conditions. For (2, 2) SM, it is possible for different transmit antennas to choose different constellation sizes.

The transmit power per antenna element is P/n so that the total power transmitted on each link is the same regardless of n . Additionally, since cell-site (macro) diversity has been shown to have minimal impact on mean throughput calculations [14], [15], we do not use this in our simulations, i.e., for simplicity, we assume that users communicate with the base station that is the nearest, not necessarily strongest.

C. Array Processing Schemes

1) *Transmit Diversity via Alamouti Coding:* The Alamouti scheme is an optimal transmit diversity scheme. It is optimal in the sense that it offers the maximum code rate ($r = 1$) and does not suffer from any loss of performance as compared to an MRC diversity scheme [16], [17]. Specific engineering aspects of this scheme are detailed in [18].

Under the assumption that noise plus co-channel interference (CCI) can be treated as complex Gaussian, the Alamouti scheme on a $(2, m)$ link has the same performance as the $(1, 2m)$ MRC receiver at half the transmit power of the $(2, m)$ MIMO configuration [18]. This enables an easy computation of the signal-to-interference-plus-noise-ratios (SINRs):

$$\gamma_i = \frac{|h_{i0}|^2 (P/2)}{\sigma^2 + \sum_k \text{CCI}_{ik}}, \quad i = 1, 2, \dots, 2m, \quad (3)$$

$$\gamma_{\text{alamouti}} = \sum_i \gamma_i, \quad i = 1, 2, \dots, 2m, \quad (4)$$

²The procedure to compute the optimum size of the transmit constellations for all five configurations will be made explicit later (see Appendix).

TABLE III.
OFFSETS FROM THE SHANNON CURVE FOR THE CONFIGURATIONS UNDER CONSIDERATION.

Configuration	(1, 1) SISO	(2, 1) Div	(1, 2) MMSE	(2, 2) Div	(2, 2) SM
Offset (dB)	3.5	4	4	5	6

where:

- h_{i0} is the instantaneous signal gain from the serving BS to the i th receive antenna.
- P is the total transmitter power.
- CCI_{ik} is the instantaneous power from the k th interfering BS at the i th receive antenna.
- γ_i is the input SINR at the i th branch of the MRC receiver.
- $\gamma_{alamouti}$ is the SINR at the receiver output.

Equation (4) is the well known result that the SINR of an MRC receiver is equal to the sum of SINRs of its individual branches.

2) *The Minimum Mean-Square Error (MMSE) Receiver:* MIMO permits the creation of several parallel transmission streams, i.e., spatial multiplexing. These streams interfere at each receive antenna, which the receiver array processor separates by using an appropriate set of weights. In this study, we assume use of the MMSE processor to implement spatial de-multiplexing. Other possible receiver array processors are zero-forcing (ZF), successive-interference-cancellation (SIC), ordered-SIC (OSIC) and OSIC-MMSE [14].

The MMSE array processing scheme separates the received signals by computing a linear combination of the received signals using a set of weights that achieves the minimum mean-square error between the output estimate and the true signal sample. Thus,

$$\hat{\mathbf{X}} = \mathbf{W}^H \mathbf{Y}. \tag{5}$$

The performance index is,

$$\zeta(\mathbf{W}^H) \triangleq E \left[\sum_{j=1}^n |\epsilon_j|^2 \right] = E \left[\sum_{j=1}^n |x_j - \hat{x}_j|^2 \right], \tag{6}$$

where x_j is the j th transmitted signal. The expectation in (6) is taken with respect to the noise and the statistics of the data sequences. The desired weight matrix that yields the minimum mean square error is given as [14]

$$\mathbf{W} = \mathbf{A}^{-1} \mathbf{H}, \tag{7}$$

where,

$$\mathbf{A} = \mathbf{H}\mathbf{H}^H + \frac{\sigma^2}{P/n} \mathbf{I}_{m \times m}. \tag{8}$$

The post-processing SINR on the j th decoded stream can be shown to be [14], [19],

$$\gamma_j = (\mathbf{H})_j^H \mathbf{R}_j^{-1} (\mathbf{H})_j, \quad j = 1, 2, \dots, n, \tag{9}$$

where

$$\mathbf{R}_j = \sum_{l=1, l \neq j}^n (\mathbf{H})_l (\mathbf{H})_l^H + \frac{\sigma^2}{P/n} \mathbf{I}_{m \times m}, \tag{10}$$

and $(\mathbf{H})_j$ is the j th column of \mathbf{H} .

D. Link Throughput

For AWGN channels, achievable throughput is upper-bounded by the Shannon limit

$$T_j = \log_2(1 + \gamma_j), \tag{11}$$

where T_j is the sub-channel throughput. The per-user data throughput is $\sum_j T_j$.

For practical systems, it is known that link throughput can be approximated by using curves shifted by SINR “offsets” from the Shannon curve [20]. The exact offset used depends on the link configuration (SISO, MEA), the receiver structure, etc. We can thus write

$$T_j = \log_2 \left(1 + \frac{\gamma_j}{10^{x/10}} \right). \tag{12}$$

The authors in [20] report that a 3-dB offset from the Shannon curve is needed to take into account finite alphabets and imperfect channel coding (especially when the block size is not very large), and overhead. For the SISO configuration, the channel estimation SINR penalty — from the overhead of the pilot signals and from non-ideal demodulation using the noisy channel estimate — is about 0.5 dB. This leads to an overall 3.5-dB offset for the SISO configuration.

When two transmit antennas are employed, the transmit power of the pilot has to be split evenly between them; and when two receive antennas are employed, the operating point of each receive antenna is lowered by 3 dB. In either case, the channel estimation penalty gets worse by about 0.5 dB as compared to SISO. When two transmit and two receive antennas are employed, the offset used is 1.5 dB — which is more than the cumulative effect of using either two transmit antennas or two receive antennas. Moreover, in (2, 2) SM, there is an additional 1-dB penalty in channel estimation, since the MMSE receiver needs to invert the channel gain matrix as part of the channel estimation procedure. This leads to the offsets from the Shannon curve, Table III.

We will use these SINR offsets in our computations. To confirm the robustness of our conclusions, however, we will also consider the case where all offsets are the same, as we discuss next.

III. SIMULATION RESULTS

We computed throughputs of all five configurations cited above, both where the SINR offsets are non-uniform, as given by Table III, and where they are all the same. In the latter case, we use a 6-dB offset.

TABLE IV.
MEAN THROUGHPUT OBTAINED FOR THE VARIOUS CONFIGURATIONS.

System	(1, 1) SISO	(2, 1) Div	(1, 2) MMSE	(2, 2) Div	(2, 2) SM
Diff. Est. Offsets (bps/Hz)	2.50	2.58	3.17	2.87	3.06
Unif. Est. Offsets (bps/Hz)	2.24	2.37	3.00	2.77	3.06

TABLE V.
30TH PERCENTILES OF THE MULTIPATH-AVERAGED THROUGHPUTS OBTAINED FOR THE VARIOUS CONFIGURATIONS.

System	(1, 1) SISO	(2, 1) Div	(1, 2) MMSE	(2, 2) Div	(2, 2) SM
Diff. Est. Offsets (bps/Hz)	0.64	0.66	1.60	0.97	0.52
Unif. Est. Offsets (bps/Hz)	0.43	0.47	1.26	0.83	0.52

Trying many possible combinations of offsets for the various configurations is too expensive an undertaking for gauging the sensitivity of conclusions to the chosen SINR-offsets. The search space is considerably reduced by investigating reasonable offsets that will likely “stress test” our conclusions. This is best brought about by using offset values that benefit the (2, 2) configurations or degrade the performance of the others. A uniform 6-dB offset for all configurations is one such example.

For the purpose of averaging, we distribute the MS with uniform randomness at 1000 locations over a given sector. To accommodate the fact that shadow fading and multipath fading are random, we allow each MS to experience 100 different shadow fades at a given location, and 1000 different multipath fades for each location-shadowing combination.

In this study, we permit only a small, discrete set of constellation sizes — BPSK and 4/8/16-QAM (corresponding, respectively, to symbol rates of 1/2/3/4 bits/symbol). These sizes are practical for present-day implementations. We now address the main questions motivating this study:

- (i) What is the benefit of a second antenna at the BS or MS relative to the SISO case?
- (ii) What is the added value of a second antenna at both ends?
- (iii) If a second antenna is indeed used at both ends, thereby creating a MIMO (2, 2) system, which mode of operation — SM or Div — is the preferred one?

We shall answer these questions by measuring how each configuration fares for each metric defined earlier. Our results are summarized next.

A. Metric 1: Mean Throughput

This metric gives the average of the link throughput, Table IV.

From this table, we conclude the following:

- (1, 2) MMSE is the best configuration for the case of differential SINR-offsets, and is very close to the best configuration for the case of uniform SINR-offsets. Hence neither (2, 2) configuration is attractive, considering receiver complexity and costs.
- (2, 1) Div is only slightly better than (1, 1), and is within approximately 0.6 bps/Hz of (1, 2) MMSE.

- (2, 2) SM is slightly better than (2, 2) Div.
- The performance gap among configurations narrows for the more realistic case of differential offsets as compared to the case of uniform offsets.

B. Metric 2: 30th Percentile of User Throughputs Cell-Wide

This metric gives the throughput achieved or exceeded on 70% of all links, taken over location and fading state, Table V. From this table, we draw conclusions similar to those above except that in this case (2, 2) Div fares slightly better than (2, 2) SM.

(2, 2) SM produces lower multipath-averaged throughputs for its 30th percentile users than (2, 2) Div (Table V), but produces higher mean throughput (Table IV). Since both configurations see the same set of users statistically, it is the receiver structure that results in the creation of these differences. The implication is that stream decoupling/cross-stream interference (XSI) in SM works against some set of users, while enhancing a favored set of users. Div, on the other hand, attempts throughput improvement over all users. These differences will likely further exaggerate for higher-order MEAs.

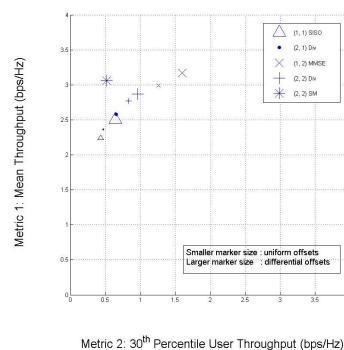


Figure 1. Scatter plot of the five configurations for Metrics 1 and 2. Both cases, uniform (smaller markers) and differential offsets (larger markers), are shown. For the (2, 2) SM case, the values overlap (See the last column in Tables IV and V).

Fig. 1 shows a scatter plot ranking all five configurations for both Metrics 1 and 2. The plot enables us to see

two perspectives simultaneously. From both perspectives, and for either offset case, (1, 2) MMSE is more attractive than the others, confirming previous conclusions.

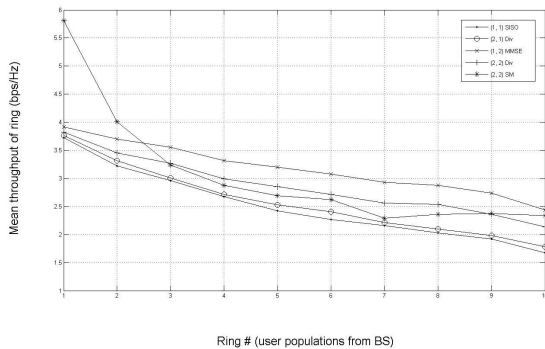


Figure 2. Mean throughputs of 10 rings of equal user population with differential SINR offsets.

Fig. 2 shows the mean throughputs of 10 concentric rings of equal user population. Ring 1 consists of the 10% of users closest to the BS. The throughput is averaged over multipath fading, shadowing, and location (the users in the ring). Examining Fig. 2, we see that:

- For users closest to the BS, (2, 2) SM offers a high average throughput.
- For other users, all configurations except (1, 2) MMSE provide comparable performance, with (2, 2) SM doing slightly better than (2, 2) Div for ring 10.

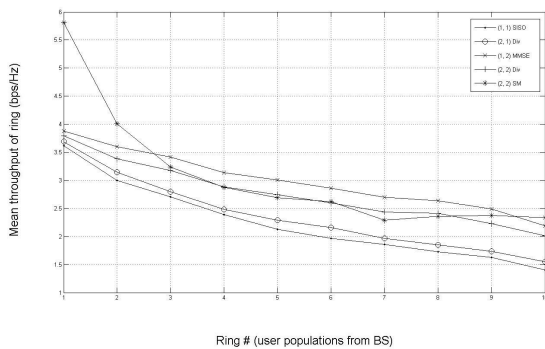


Figure 3. Mean throughputs of 10 rings of equal user population with uniform SINR offsets.

Fig. 3 shows the same plot for the case of uniform SINR-offsets. As expected, the curves diverge, since higher-order MEAs benefit from a lower relative offset penalty. However, the divergence is small. Moreover, except for populations closest to the BS, (1, 2) MMSE remains the most attractive configuration.

We have established that, although both SINR-offset cases result in minor differences in throughputs of the configurations, they do not change the overall conclusions. Therefore, we drop the case of uniform SINR-offsets from further consideration, opting to use the more realistic case of differential SINR-offsets from this point on.

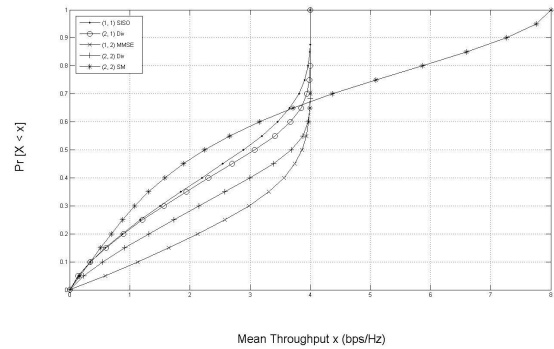


Figure 4. Fast-fading-averaged cell-wide distribution of throughput for all five configurations (differential offsets).

Fig. 4 shows another throughput statistic: the distribution of multipath-averaged user throughputs on a cell-wide basis. The following salient points should be noted:

- All configurations, with the exception of (2, 2) SM, operate with only one transmit stream and hence have a peak rate of 4 bps/Hz. (2, 2) SM operates with two streams, thus it can offer up to 8 bps/Hz.
- (2, 2) SM appears lucrative only for throughput requirements exceeding 4 bps/Hz. In fact, for throughputs less than 4 bps/Hz, it is the worst configuration.
- In the mid-region, the curves are about parallel to one another. It is for this reason that the value of the percentile chosen (lowest 30th) for Metric 2 is arbitrary.

IV. SUMMARY AND CONCLUSIONS

The objective of this study was to quantify and compare the throughput performance of five link configurations involving one or two antenna elements at each end.

Our results indicate that, in the context of a limited number of constellation sizes, and for the case of differential SINR-offsets, (1, 2) MMSE is the configuration of choice for both metrics considered. The other four are comparable in performance with each other. The main reasons why (1, 2) MMSE scores best are: relatively low channel estimation penalty, the absence of cross-stream interference at receive antennas, and an excess receive antenna to suppress CCI.

For the case of uniform offsets, the throughput results change by small amounts, but the main conclusions do not change from those for differential offsets. This reinforces our findings and shows them to be robust to assumptions used in the study.

The MMSE receiver assumed here for (2, 2) SM is one example of the many receivers that can decouple the SM streams; ZF, SIC, OSIC, and OSIC-MMSE receivers are some others. Since changing the particular receiver amounts to changing the SINR offset, against which our conclusions are found to be stable, we claim that (1, 2) MMSE is the preferred configuration regardless of the particular receiver chosen by (2, 2) SM to de-couple its streams.

APPENDIX A PROJECT DESCRIPTION SUMMARY

It is clear that we intend to compute throughput statistics of the five configurations. For the benefit of the reader, we list the steps involved:

- Distribute MSs in cell.
- Generate channel matrix \mathbf{H} as given by (1). The size of \mathbf{H} is given by (2).
- Compute post-processing SINR of substream j [(3) and (4) for Div, (9) and (10) for SISO, MMSE and SM].
- Compute throughputs for substream j [(12) and Table III].
- The “MEA throughput” is sum of the throughputs of the individual substreams.

At the beginning of each block-fade interval, pilot signals are transmitted to estimate the receiver array weights. The receiver then determines the constellation size (M) from the substream post-processing SINRs, and communicates this information to the transmitter. Adaptive modulations at each transmit antenna then quickly select the corresponding optimal QAM constellation. The channel remains known throughout, since estimation-feedback-adaptation occurs within the block fade interval.

ACKNOWLEDGEMENT

We greatly appreciate valuable comments from Dennis Morgan (Bell-Labs, Murray Hill, NJ), Chandrasekharan Raman, Joydeep Acharya, Jasvinder Singh and David Daut.

REFERENCES

[1] I. Telatar, “Capacity of multi-antenna gaussian channels,” *Euro. Trans. Telecommun.*, vol. 10, no. 6, pp. 585–595, November 1999.

[2] G. Foschini and M. Gans, “On limits of wireless communications in a fading environment when using multiple antennas,” *IEEE Wireless Personal Communications*, vol. 6, no. 3, pp. 311–335, March 1998.

[3] A. Paulraj, R. Nabar, and D. Gore, *Introduction to Space-Time Wireless Communications*. Cambridge University Press, 2003.

[4] P. Wolniansky, G. Foschini, G. Golden, and R. Valenzuela, “V-BLAST: an architecture for achieving very high data rates over the rich-scattering wireless channel,” in *Proc. Int. Symp. Signals, Systems, and Electronics (ISSSE '98)*, Pisa, Italy, pp. 295–300, October 1998.

[5] L. Zheng and D. Tse, “Diversity and multiplexing: a fundamental tradeoff in multiple-antenna channels,” *IEEE Trans. Inf. Theory*, vol. 49, no. 5, pp. 1073–1096, May 2003.

[6] R. Pupala, L. Greenstein, and D. Daut, “Downlink throughput statistics in interference-limited cellular systems with multi-element antennas,” *IEEE Trans. Commun.*, vol. 58, no. 1, pp. 311–317, January 2010.

[7] —, “Throughput analysis of interference-limited MIMO-based cellular systems,” *IEEE Trans. Wireless Commun.*, vol. 9, no. 6, pp. 1946–1951, June 2010.

[8] —, “Effects of channel dispersion and path correlations on system-wide throughput in MIMO-based cellular systems,” *IEEE Trans. Wireless Commun.*, vol. 8, no. 11, pp. 5477–5482, November 2009.

[9] R. Pupala, “Investigation of co-channel interference, channel dispersion & multiuser diversity in mimo-based cellular systems,” Ph.D. dissertation, Rutgers - The State University of New Jersey, US, February 2008.

[10] “3GPP Standards Methodology Document 36.814.”

[11] D. Gesbert, H. Bolcskei, D. Gore, and A. Paulraj, “MIMO wireless channels: capacity and performance prediction,” *IEEE Proc. Globecom.*, pp. 1083–1088, Nov 2000.

[12] H. Sampath, S. Talwar, J. Tellado, V. Erceg, and A. Paulraj, “A fourth generation MIMO-OFDM broadband wireless system: design, performance, and field trial results,” *IEEE Commun. Mag.*, vol. 40, no. 9, pp. 143–149, September 2002.

[13] F. Farrokhi, A. Lozano, G. Foschini, and R. Valenzuela, “Spectral efficiency of wireless systems with multiple transmit and receive antennas,” *Proc. IEEE Symp. PIMRC*, vol. 1, pp. 373–377, September 2000.

[14] S. Catreux, “Techniques d’antennes multi-entrees multi-sorties dans un systeme de type cellulaire,” Ph.D. dissertation, INSA, Paris, France, April 2000.

[15] S. Catreux, P. Driessen, and L. Greenstein, “Attainable throughput of an interference-limited multiple-input multiple-output (MIMO) cellular system,” *IEEE Trans. Commun.*, vol. 49, no. 8, pp. 1307–1311, August 2001.

[16] V. Tarokh, H. Jafarkhani, and A. Calderbank, “Space-time block codes from orthogonal designs,” *IEEE Trans. Inf. Theory*, vol. 45, no. 5, pp. 1456–1467, July 1999.

[17] V. Tarokh, N. Seshadri, and A. Calderbank, “Space-time block codes for high data rate wireless communication: Performance, criterion and code construction,” *IEEE Trans. Inf. Theory*, vol. 44, no. 2, pp. 744–765, March 1998.

[18] S. Alamouti, “A simple transmit diversity technique for wireless communications,” *IEEE J. Sel. Areas Commun.*, vol. 16, no. 8, pp. 1451–1458, October 1998.

[19] S. Catreux, L. Greenstein, and V. Erceg, “Some results and insights on the performance gains of MIMO systems,” *IEEE J. Sel. Areas Commun.*, vol. 21, no. 5, pp. 839–847, June 2003.

[20] Q. Bi, S. Vitebsky, Y. Yang, and Y. Yuan, “Broadcast-multicast in 1x EV-DO revision a systems and its application to enhanced mobile services,” *Bell-Labs Tech. J. (BLTJ)*, vol. 11, no. 4, pp. 237–252, December 2006.



Rahul N. Pupala received the B.E. degree in Computer Engineering from Victoria Jubilee Technical Institute (VJTI), Bombay in 1994, the M.S. degree in Computer Science in 2003, and the Ph.D. in Electrical Engineering in 2008 both from Rutgers - The State University of New Jersey. From 1994 to 1999, he worked in the software industry. He is currently at Alcatel-Lucent/Bell Labs, Murray Hill, NJ, responsible for PHY & MAC layer innovations for LTE-Advanced.

His research interests include Distributed Computing, Computer Networks, Signal Processing and Wireless Communications.



Yifei Yuan received Bachelor and Master degrees from Tsinghua University of China, and a Ph.D. from Carnegie Mellon University in 2000. He was with Alcatel-Lucent (formerly Lucent Technologies) from 2000 to 2008, working on intelligent antennas, advanced receiver, and channel element design for 3G and 4G wireless systems. Since 2008, he has been with ZTE, responsible for standards research on physical layer of LTE-Advanced. His research interests include multi-antenna

technology, turbo codes, radio resource management.



Qi Bi received his M.S. from Shanghai Jiao Tong University in 1981 and Ph.D. from Pennsylvania State University in 1986. He was with Bell Laboratories for 20 years as a member of technical staff, then distinguished member of technical staff, senior manager and director. Since 2010, he has been the president of China Telecom Technology Innovation Center.

Dr. Bi has been active in technical conferences. He organized the first and the second CDMA conferences at Lucent Technologies in 1999 and 2000 and served as the technical chair for IEEE Globecom wireless program from 2000 to 2002. He was the technical chair for the IEEE Wireless Communications and Network Conference in 2003. In 2005 and 2006, he serves as chair and organizer for the Wireless and Optical Communications Conference.

Dr. Bi was recognized in wireless areas. He received Awards of Excellence from the Advanced Technology Lab of AT&T in 1996 and 1997, and Bell Labs Presidents Gold Awards in 2000 and 2002. His team was awarded the Bell Labs Innovation Team Award in 2003 by the Bell Labs Basic Research Labs. In 2002, he became the first Chinese from the Peoples Republic of China to receive the prestigious Bell Laboratories Fellow Award. In 2005, he was recognized by the Chinese Institute of Engineers and was awarded the Asian American Engineer of the Year Award.

Dr. Bi has published extensively. He was also granted 35 US patents and 57 European patents. He is a Fellow of IEEE.



Larry J. Greenstein received the BS, MS and PhD degrees in electrical engineering from Illinois Institute of Technology in 1958, 1961 and 1967, respectively. From 1958 to 1970, he was at IIT Research Institute, where he worked on radio frequency interference and anti-clutter airborne radar. He joined Bell Laboratories in Holmdel, NJ in 1970. Over a 32-year career, he conducted research in digital satellites, point-to-point digital radio, optical transmission techniques and wireless communications.

For 21 years during that period (1979-2000), he led a research department renowned for its contributions in these fields. Since 2002, he has been a research professor at Rutgers University's WINLAB, working on PHY-based security techniques, MIMO-based cellular systems, broadband power line systems, cognitive radio and channel modeling.

Dr. Greenstein is an IEEE Life Fellow, an AT&T Fellow, a recipient of the IEEE Communications Society's Edwin Howard Armstrong and Joseph LoCicero Awards, and co-author of several award-winning papers, including the IEEE Donald G. Fink Prize Paper Award. He has served on numerous editorial boards and technical program committees and was, and is now again, the IEEE Communications Society's Director of Journals.

Coverage Analysis for Multiuser MIMO Broadcast Systems

Li-Chun Wang and Chu-Jung Yeh
National Chiao Tung University, Taiwan

Email : lichun@cc.nctu.edu.tw and teensky.cm93g@nctu.edu.tw

Abstract—In this paper, we present the closed-form expressions for the link outage and coverage of the zero-forcing beamforming (ZFB) and zero-forcing dirty-paper coding (ZF-DPC) multiuser multi-input multiple-output (MIMO) broadcast systems. We find that the ZF-DPC MIMO broadcast system has a larger diversity order and better coverage compared with the ZFB MIMO broadcast system. Furthermore, it is observed that the ZFB MIMO broadcast system with round-robin scheduling has only the diversity order of one and its cell coverage can only approach to that of the weakest link of the ZF-DPC MIMO broadcast system. By selecting the best group of users, multiuser scheduling can function as a *soft* coverage enhancement technique without increasing the extra transmission power in the physical layer. Our analytical formula can estimate to what extent the coverage performance of the ZF-DPC MIMO broadcast system can be improved as the number of users increases. Hence, the effect of increasing the number of antennas on the coverage performance of the ZF-DPC MIMO broadcast system can be quantitatively analyzed subject to the same transmission power from each base station.

Index Terms—MIMO systems, zero-forcing beamforming, zero-forcing dirty-paper coding, coverage, MIMO broadcast channels, outage probability, diversity order.

I. INTRODUCTION

Multiple-input multiple-output (MIMO) systems can significantly increase spectral efficiency by exploiting the degree of freedom in the spatial domain created by multiple antennas. In the point-to-multipoint multiuser MIMO broadcast channels, even with only one single receive antenna at the user end, the spatial multiplexing gain can be also achieved by sending precoded data across multiple transmit antennas to a group of users simultaneously [1]. With complete channel state information (CSI) available at the transmitter, the maximum sum rate of MIMO broadcast systems can be achieved by dirty paper coding (DPC) [1]. However, computational complexity and

the requirement of full CSI at the transmitter limit the applicability of DPC.

In the literature, the new lines of research from multiuser MIMO broadcast systems are classified into three categories:

- First, rather than using the optimal DPC, the suboptimal but more practical MIMO broadcast schemes were proposed [2]–[6], such as the zero-forcing dirty-paper coding (ZF-DPC), zero-forcing beamforming (ZFB), block-diagonalization (BD), orthogonal random beamforming, and receive ZF beamforming [7]–[10]. These suboptimal schemes can asymptotically achieve the same throughput of DPC when the number of users approaches to the infinity.
- Second, another important research direction for MIMO broadcast systems is to investigate the impacts of limited CSI due to the finite-rate or erroneous CSI feedback [11]–[17]. For example, [12] showed that the feedback load per user must be scaled together with both the number of transmit antennas as well as the system SNR to achieve the full multiplexing gain with the near-perfect CSI.
- Third, MIMO broadcast transmission strategies were also applied to the multi-cellular scenario to cancel the inter-cell interference for improving spectral efficiency [18]–[20]. For example, the network base station (BS) coordination conception is proposed based on ZFB and ZF-DPC schemes in [19], [20]. In This concept is also called the coordinated multipoint (CoMP) transmission in the third Generation Partnership Project (3GPP) Long-Term Evolution-Advanced (LTE-A) and the collaborative MIMO (Co-MIMO) transmission in the IEEE 802.16m Worldwide Interoperability for Microwave Access (WiMAX), respectively [21]–[23].

Although the capacity issues of MIMO broadcast systems have been extensively investigated, to our knowledge, the studies on the coverage performance of MIMO broadcast systems are rarely seen in the literature. From the perspective of tradeoff between multiplexing and diversity for a MIMO system [24], the transmit MIMO broadcast systems may be a diversity-deficient scheme due to it realizes spatial-multiplexing personalized transmissions. In this paper, we derive the analytical closed-form expressions for the link outage probability, link diversity order,

Manuscript received February 15, 2011; revised May 15, 2011; accepted June 15, 2011. Part of this paper was published in the 2008 IEEE 67th Vehicular Technology Conference (VTC2008-Spring), 11 – 14 May 2008, Marina Bay, Singapore. This work is sponsored by the National Science Council of Taiwan under grants NSC 99-2221-E-009-026-MY3, and by the Ministry of Education of Taiwan under the MoE ATU Program.

Li-Chun Wang is with the Department of Electrical Engineering, and the Institute of Communications Engineering, National Chiao Tung University, Taiwan (email: lichun@cc.nctu.edu.tw).

and the reliable coverage radius of a multiuser MIMO broadcast system. It is found that multiuser scheduling can function as a **link diversity compensation and soft coverage extension** technique for the MIMO broadcast systems. The concept of soft coverage extension by multiuser scheduling was suggested for point-to-point MIMO systems in [25] since multiuser scheduling can improve the coverage of MIMO broadcast systems without increasing transmission power in the physical layer. In [26], the authors derived the closed-form expressions for the outage and error rate performances in a single-user ZF-MIMO system with imperfect channel feedback. However, both [25], [26] only considered the single-user MIMO system that serves one single user at any time instant, rather than the MIMO broadcast systems that serves a group of users simultaneously. Our developed analytical framework can evaluate to what extent the multiuser scheduling can improve the coverage performance of the multiuser MIMO broadcast systems.

In this paper, we focus on two famous precoding schemes, ZF-DPC and ZFB, to address the link and coverage performance of a MIMO broadcast system. Different from the results in [27], we have further provided some other works to make the link performance issue of MIMO broadcast systems more complete. The additional works can be summarized as follows:

- We derived the link diversity order of MIMO broadcast systems with ZF-DPC and ZFB transmission precoding schemes. We find that the diversity order of the i -th link for an N_t -link ZF-DPC broadcast system without scheduling and ordering is $N_t - i + 1$ and that of the ZFB broadcast system without scheduling is one, where N_t is the number of transmit antennas. Taking the strongest link of ZF-DPC as an example. The diversity order becomes KN_t instead of N_t when combining with K -user greedy scheduling. In [27], we have observed this phenomenon via simulations but not provided theoretical proofs.
- We consider the coverage extension issue with different number of users K and antennas N_t when taking advantage of multiuser scheduling. We demonstrate a *soft* coverage enhancement technique for MIMO broadcast systems by taking advantage of multiuser scheduling.

The rest of this paper is organized as follows. Section II introduces the ZF-DPC and ZFB MIMO broadcast systems. In Section III, we define the link outage probability, diversity order, and reliable coverage radius in MIMO broadcast systems. In Sections IV and V, we derive the analytical expressions of these coverage related performance metrics for the ZF-DPC and ZFB MIMO broadcast systems. Numerical results are shown in Section VI. We give our concluding remarks in Section VII.

II. BACKGROUND

A. System Model

Consider a single-cell multiuser MIMO broadcast system with a BS and K users. The BS is equipped with

N_t transmit antennas, but each of K user terminals has only one receive antenna. Thus, N_t users are selected from K users for simultaneous transmission with different data streams. The subset of users' indices to which a BS intends to transmit different information is denoted by $\mathcal{S} \subset \{1, \dots, K\}$, $|\mathcal{S}| = N_t$.

The beamforming weight matrix at the transmitter is denoted by $\mathbf{W} = [\mathbf{w}_1 \dots \mathbf{w}_{N_t}]$, where $\mathbf{w}_i \in \mathbb{C}^{N_t \times 1}$ and the input signal vector is denoted by $\mathbf{u} = [\sqrt{P_1}u_1, \dots, \sqrt{P_{N_t}}u_{N_t}]^T$. Here u_i and P_i represent the uncorrelated unit-power signal symbol and the power of the symbol associated with user i , respectively. Then, the transmitted signal vector \mathbf{x} is written as $\mathbf{x} = \mathbf{W}\mathbf{u} = \sum_{i=1}^{N_t} \sqrt{P_i} \mathbf{w}_i u_i \in \mathbb{C}^{N_t \times 1}$. Let $\mathbf{y} \in \mathbb{C}^{N_t \times 1}$ be the received signal vector, and $\mathbf{G}(\mathcal{S})$ be the $N_t \times N_t$ channel matrix corresponding to \mathcal{S} . Denote $\mathbf{n} \in \mathbb{C}^{N_t \times 1}$ as the complex Gaussian noise vector with $E[\mathbf{n}\mathbf{n}^H] = \sigma^2 \mathbf{I}_{N_t}$, where $(\cdot)^H$ denotes conjugate transpose. Then, the received signal can be expressed as

$$\mathbf{y} = \mathbf{G}(\mathcal{S})\mathbf{x} + \mathbf{n} = \mathbf{g}\mathbf{H}(\mathcal{S})\mathbf{x} + \mathbf{n} \quad (1)$$

where \mathbf{g} is an $N_t \times N_t$ diagonal matrix with $\mathbf{g} = \text{diag}\{\sqrt{g_1}, \sqrt{g_2}, \dots, \sqrt{g_{N_t}}\}$ and g_i depicts the path loss between the BS and user i . For a user at a distance of R from the BS, g_i can be written as [28]

$$10 \log_{10} g_i = -10\mu \log_{10} R + g_0 \quad [\text{dB}] \quad (2)$$

where μ is the path loss exponent and g_0 is a constant subject to certain path loss models¹. Assume that all users experience independent flat Rayleigh fading and the transmission power is constrained by $E[\mathbf{x}^H \mathbf{x}] = P_T$.

B. Zero-Forcing Dirty-Paper Coding (ZF-DPC)

Based on QR-type decomposition, a suboptimal solution of \mathbf{W} was found in [1]. Let $\mathbf{H}(\mathcal{S}) = \mathbf{L}\mathbf{Q}$ be the QR-type decomposition of $\mathbf{H}(\mathcal{S})$, where \mathbf{L} is a lower triangular matrix and \mathbf{Q} is a unitary matrix. With $\mathbf{W} = \mathbf{Q}^H$, the corresponding system model in (1) can be written as

$$y_i = l_{i,i} \sqrt{g_i P_i} u_i + \sum_{j < i} l_{i,j} \sqrt{g_j P_j} u_j + n_i \quad , \quad i = 1, \dots, N_t. \quad (3)$$

Note that $\mathbf{W} = \mathbf{Q}^H$ can cancel the interference from users with indices $j > i$. The remaining interference terms with indices $j < i$ are taken care of by applying DPC successively. For simplicity, we consider the equal power allocation, that is, $P_i = P_T/N_t$, where $i = 1, \dots, N_t$. The rate of the i th link for ZF-DPC is $\log_2(1 + |l_{i,i}|^2 \rho_i/N_t) = \log_2(1 + \gamma_i)$, where ρ_i is the average received signal-to-noise ratio (SNR), γ_i is the effective received SNR, and the term

¹For example, in a macro-cell environment, the path loss model of modified COST-231 Hata urban and suburban models are respectively $-35 \log_{10} R - 31.5$ [dB] (i.e., $\mu = 3.5$ and $g_0 = -31.5$ dB) and $-35 \log_{10} R - 34.5$ [dB] (i.e., $\mu = 3.5$ and $g_0 = -34.5$ dB) [29], where the antenna height of the base station is 32 m, the antenna height of the user terminal is 1.5 m, and carrier frequency is 1.9 GHz.

$|l_{i,i}|^2$ can be viewed as the effective channel gain at the i th link. Specifically, ρ_i can be represented as

$$\rho_i = \frac{P_T g_i}{\sigma^2} = \frac{P_T 10^{g_0/10}}{\sigma^2 R_i^\mu} . \quad (4)$$

C. Zero-Forcing Beamforming (ZFB)

The ZFB scheme [1] aims at inverting the channel matrix to create orthogonal channels between the transmitter and the receiver. By choosing the weight matrix $\mathbf{W} = \mathbf{H}(\mathcal{S})^H (\mathbf{H}(\mathcal{S})\mathbf{H}(\mathcal{S})^H)^{-1}$, the corresponding system model in (1) can be written as

$$\mathbf{y} = \mathbf{g}\mathbf{H}(\mathcal{S})\mathbf{H}(\mathcal{S})^H (\mathbf{H}(\mathcal{S})\mathbf{H}(\mathcal{S})^H)^{-1} \mathbf{u} + \mathbf{n} = \mathbf{g}\mathbf{u} + \mathbf{n} , \quad (5)$$

and the i th received signal is given by $y_i = \sqrt{g_i P_i} u_i + n_i$. Due to the transmit power constraint $E[\mathbf{x}^H \mathbf{x}] \leq P_T$, we have the following relation:

$$\|\mathbf{w}_1\|^2 P_1 + \dots + \|\mathbf{w}_{N_t}\|^2 P_{N_t} \leq P_T , \quad (6)$$

where $\|\mathbf{w}_i\|^2 = [(\mathbf{H}(\mathcal{S})\mathbf{H}(\mathcal{S})^H)^{-1}]_{i,i}$. In (6), it implies that ZFB incurs an excess transmission power penalty due to the required interference cancellation power on \mathbf{W} . According to (6), power loading is $\|\mathbf{w}_i\|^2 P_i = P_T/N_t$, where $i = 1, \dots, N_t$. As a result, the data rate at the i th link of ZFB is

$$\log_2 \left(1 + \frac{g_i P_i}{\sigma^2} \right) = \log_2 \left(1 + \frac{b_i \rho_i}{N_t} \right) = \log_2 (1 + \gamma_i) , \quad (7)$$

where $b_i = 1/\|\mathbf{w}_i\|^2$ is the effective channel gain.

III. PERFORMANCE METRICS

A. Link Outage Probability

We first define the link outage probability to reflect what extent a MIMO broadcast system can reliably support the corresponding link quality. For a single-input single-output system (SISO), link outage [30] is usually defined as the probability of the effective received SNR is less than a predetermined value γ_{th} , i.e., $P_{out} = P_r\{\gamma < \gamma_{th}\}$. As for the MIMO broadcast systems, all the data links serve different individual users. Thus, we can define the link outage probability of the i th link the same as in the SISO case, i.e., $P_{out}^i = P_r\{\gamma_i < \gamma_{th}\}$.

B. Diversity Order

Let link outage probability $P_{out}(\cdot)$ be a function of SNR. Then, the link diversity order D_{order} is defined as [31]

$$D_{order} \triangleq - \lim_{\rho \rightarrow \infty} \frac{\log P_{out}(\rho)}{\log \rho} , \quad (8)$$

where ρ is the receive SNR. The metric can provide an intuitional observation on link performance.

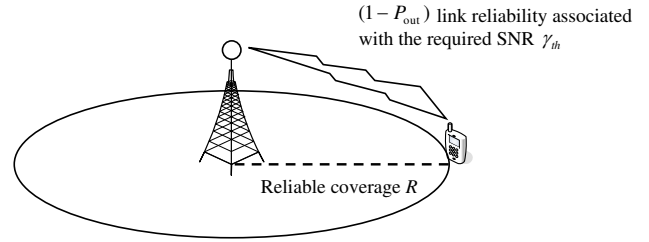


Fig. 1. Illustration of link reliability and reliable coverage.

C. Link Coverage Reliability

Referring to the link outage probability P_{out} , we further define $(1 - P_{out})$ as the link coverage reliability for its corresponding link radius associated with the required SNR as shown in Fig. 1. Specifically, the link coverage reliability $(1 - P_{out})$ represents the probability of the effective received SNR being higher than γ_{th} . Therefore, the link radius associated with the required SNR and $(1 - P_{out})$ reliability is defined as the **reliable coverage**. Typically, 90% link reliability is required for most wireless systems.

IV. ANALYSIS OF MIMO BROADCAST SYSTEMS WITHOUT SCHEDULING

A. ZF-DPC without Scheduling

At first we analyze the coverage performance of ZF-DPC MIMO broadcast systems without user selection, i.e., based on round-robin scheduling. Clearly, selecting users randomly cannot result in multiuser diversity gain. By Lemma 2 in [1], $d_i = |l_{i,i}|^2$ is independent central Chi-squared random variable $\mathcal{X}_{2(N_t-i+1)}^2$ with $2(N_t - i + 1)$ degrees of freedom. The probability density function (PDF) of a Chi-squared random variable \mathcal{X}_{2a}^2 is $f(z) = z^{a-1} e^{-z} / (a-1)!$ for $z > 0$. Thus, the PDF of the effective channel gain d_i can be written as

$$f_{d_i}(z) = \frac{z^{N_t-i} e^{-z}}{(N_t-i)!} \quad \text{for } i = 1, \dots, N_t , \quad (9)$$

where $i = 1$ and $i = N_t$ represent the strongest and the weakest links in the statistics, respectively. The corresponding cumulative distribution function (CDF) of d_i can be written as

$$F_{d_i}(z) = 1 - \frac{\Gamma(N_t - i + 1, z)}{\Gamma(N_t - i + 1)} = 1 - \Gamma_R(N_t - i + 1, z) , \quad (10)$$

where $\Gamma(a) = \int_0^\infty t^{a-1} e^{-t} dt$ is the complete gamma function, $\Gamma(a, x) = \int_x^\infty t^{a-1} e^{-t} dt$ is the upper incomplete gamma function, and $\Gamma_R(a, x) = \frac{\Gamma(a, x)}{\Gamma(a)}$ is the regularized gamma function. The CDF of the effective received SNR $\gamma_i = d_i \rho_i / N_t$ for the i th link is

$$F_{\gamma_i}(\gamma) = F_{d_i} \left(\frac{N_t \gamma}{\rho_i} \right) = 1 - \Gamma_R \left(N_t - i + 1, \frac{N_t \gamma}{\rho_i} \right) . \quad (11)$$

Thus, for a given threshold $\gamma_{th} > 0$, the link outage probability for the i th link of the ZF-DPC MIMO broadcast system is

$$P_{out}^i = F_{\gamma_i}(\gamma_{th}) = 1 - \Gamma_R \left(N_t - i + 1, \frac{N_t \gamma_{th}}{\rho_i} \right) . \quad (12)$$

The following shows the analysis of the link diversity order.

Theorem 1: The diversity order of the i th link for an N_t -link ZF-DPC MIMO broadcast system without scheduling and ordering is $N_t - i + 1$.

Proof: To ease analysis, we define a function $Z_i(s)$ as

$$Z_i(s) = \frac{\log(1 - \Gamma_R(N_t - i + 1, N_t s \gamma_{th}))}{\log s} = \frac{\text{Num}_i(s)}{\text{Den}_i(s)} , \quad (13)$$

where $s = \rho_i^{-1}$. When $\rho_i \rightarrow \infty$, $s \rightarrow 0$. Thus, we can have

$$\begin{aligned} D_{order}^i &= - \lim_{\rho_i \rightarrow \infty} \frac{\log P_{out}^i(\rho_i)}{\log \rho_i} \\ &= \lim_{s \rightarrow 0} Z_i(s) . \end{aligned} \quad (14)$$

Note that $\lim_{s \rightarrow 0} \text{Num}_i(s) = -\infty$ and $\lim_{s \rightarrow 0} \text{Den}_i(s) = -\infty$ and according to the L'Hôpital's rule, we can obtain

$$\begin{aligned} D_{order}^i &= \lim_{s \rightarrow 0} \frac{\text{Num}'_i(s)}{\text{Den}'_i(s)} \\ &= \lim_{s \rightarrow 0} \left[\frac{(N_t s \gamma_{th})^{N_t - i + 1} e^{-N_t s \gamma_{th}}}{\Upsilon(N_t - i + 1, N_t s \gamma_{th})} \right] , \end{aligned} \quad (15)$$

where $\Upsilon(a, x) = \int_0^x t^{a-1} e^{-t} dt$ is the lower incomplete gamma function. With the property $\Upsilon(a, x)/x^a \rightarrow 1/a$ as $x \rightarrow 0$, we can obtain the diversity order $D_{order}^i = N_t - i + 1$ for an N_t -link ZF-DPC MIMO broadcast system without scheduling and ordering. \square

This theorem provides a surprising result that the ZF-DPC MIMO broadcast system can support extra diversity gains for $N_t - i$ links instead of traditional diversity order of one in the spatial multiplexing based MIMO systems. For example, the link diversity orders are respectively order three for $i = 1$, order two for $i = 2$, and order three for $i = 3$ as $N_t = 3$. The first two links obtain extra diversity gains under the ZF-DPC MIMO broadcast transmissions.

To derive cell coverage R_{ZFDP}^i from (12), we first introduce the inverse of the regularized incomplete gamma function as follows:

$$x = \Gamma_R(a, z) \Rightarrow z = \Gamma_R^{-1}(a, x) . \quad (16)$$

By substituting (4) and (16) into (12), the link coverage can be written as

$$R_{ZFDP}^i = \left[\frac{P_T 10^{g_0/10}}{N_t \gamma_{th} \sigma^2} \Gamma_R^{-1} \left(N_t - i + 1, 1 - P_{out}^i \right) \right]^{\frac{1}{\mu}} , \quad i = 1, \dots, N_t . \quad (17)$$

B. ZFB without Scheduling

Alternately, we analyze the coverage performance of the ZFB MIMO broadcast system without user selection. In this case, all the elements in each channel vector are Rayleigh faded. Due to the same statistics, we can view the system as an point-to-point $N_t \times N_t$ (single user) MIMO system with a ZF receiver. The PDFs of the effective channel gain $\{b_i\}_{i=1}^{N_t}$ can be obtained through the PDFs of the ZF receiver's substream SNRs. According to [32], the distribution of the substream SNRs $\{\gamma_i\}_{i=1}^{N_t}$ for an $N_t \times N_r$ MIMO system with ZF receiver under equal power allocation are identically distributed $\mathcal{X}_{2(N_r - N_t + 1)}^2$. In the case of $N_t = N_r$, the PDF of unordered $\{b_i\}_{i=1}^{N_t}$ can be obtained from (9) by letting $i = N_t$, which result in exponentially distributed random variable with parameter one.

Therefore, the link outage probability and the coverage performance of the ZFB MIMO broadcast system can be obtained from (12) and (17) with $i = N_t$. Clearly, under the same link outage requirement, all ZFB substream links equal the ZF-DPC's weakest link and has the diversity order of one.

Corollary: The link diversity order of the ZFB MIMO broadcast system without scheduling is one.

V. ANALYSIS OF MIMO BROADCAST SYSTEMS WITH SCHEDULING

A. ZF-DPC with Greedy Scheduling

Now we consider the effects of multiuser scheduling in the MIMO broadcast systems. We focus on the strongest stream link which has the largest radius to determine the cell range. In [33], the authors proposed a greedy scheduling algorithm to *select* N_t users out of K users to form $\mathbf{H}(\mathcal{S})$ and *ordering* those selected channel row vectors in the Gram-Schmidt orthogonalization to maximize the system throughput.

The strongest link can be determined by the first selected user's channel row vector $\mathbf{h}_k \in \mathcal{C}^{1 \times N_t}$ for $k = 1, \dots, K$. According to the greedy selection algorithm, the selected user k^* is

$$k^* = \arg \max_{k \in \{1, \dots, K\}} d_{1,k} , \quad (18)$$

where $d_{1,k} = \mathbf{h}_k \mathbf{h}_k^*$. Note that $d_{1,k}$ is the sum of N_t squared magnitudes of circularly symmetric, zero-mean, unit-variance complex Gaussian random variables. Therefore, $d_{1,k} \sim \mathcal{X}_{2N_t}^2$ with PDF $f_{d_{1,k}}(z) = z^{N_t-1} e^{-z} / (N_t - 1)!$. The effective channel gain of the strongest link for the greedy scheduling algorithm is $\tilde{d}_1 = d_{1,k^*}$ of which PDF can be obtained by the order statistics analysis as follows:

$$f_{\tilde{d}_1}(z) = K [F_{d_{1,k}}(z)]^{K-1} f_{d_{1,k}}(z) . \quad (19)$$

Hence the link outage probability is

$$\begin{aligned} P_{out}^1 &= F_{\tilde{\gamma}_1}(\gamma_{th}) = F_{\tilde{d}_1} \left(\frac{N_t \gamma_{th}}{\rho_1} \right) \\ &= \left(1 - \Gamma_R \left(N_t, \frac{N_t \gamma_{th}}{\rho_1} \right) \right)^K . \end{aligned} \quad (20)$$

The following theorem gives the diversity order of the strongest link in the ZF-DPC MIMO broadcast system.

Theorem 2: The diversity order of the strongest link for the N_t -link ZF-DPC broadcast system with K -user greedy scheduling is KN_t .

Proof: Similar to the proof of Theorem 1, we define $\tilde{Z}_1(s)$ as

$$\tilde{Z}_1(s) = \frac{\log([1 - \Gamma_R(N_t, N_t s \gamma_{th})]^K)}{\log s} = \frac{\tilde{\text{Num}}_1(s)}{\tilde{\text{Den}}_1(s)}, \quad (21)$$

where $s = \rho_1^{-1}$. Thus, the diversity order is

$$\begin{aligned} \tilde{D}_{\text{order}}^1 &= - \lim_{\rho_1 \rightarrow \infty} \frac{\log P_{\text{out}}^1(\rho_1)}{\log \rho_1} \\ &= \lim_{s \rightarrow 0} \tilde{Z}_1(s) \\ &\stackrel{(a)}{=} \lim_{s \rightarrow 0} \frac{\tilde{\text{Num}}_1'(s)}{\tilde{\text{Den}}_1'(s)} \\ &= \lim_{s \rightarrow 0} \left[\frac{K(N_t s \gamma_{th})^{N_t} e^{-N_t s \gamma_{th}}}{\Upsilon(N_t, N_t s \gamma_{th})} \right] \\ &\stackrel{(b)}{=} KN_t, \end{aligned} \quad (22)$$

where (a) follows L'Hôpital's rule with $\lim_{s \rightarrow 0} \tilde{\text{Num}}_1(s) = -\infty$ and $\lim_{s \rightarrow 0} \tilde{\text{Den}}_1(s) = -\infty$ and (b) comes from the property $\Upsilon(a, x)/x^a \rightarrow 1/a$ as $x \rightarrow 0$. \square

To derive the link coverage $\tilde{R}_{\text{ZF-DPC}}^1$ of the strongest link from (20), we use the inverse of the regularized incomplete gamma function to obtain

$$\tilde{R}_{\text{ZF-DPC}}^1 = \left[\frac{P_T 10^{g_0/10}}{N_t \gamma_{th} \sigma^2} \Gamma_R^{-1} \left(N_t, 1 - \sqrt[\kappa]{P_{\text{out}}^1} \right) \right]^{\frac{1}{\mu}}. \quad (23)$$

1) *Effect of user ordering:* Even with random user selection, the ZF-DPC MIMO broadcast system can still take advantage of users ordering. This case is similar to the multiuser MIMO broadcast system with $K = N_t$ users. The benefit of pure user ordering (not combined with users selection) will be shown in the section of numerical results.

2) *Soft coverage extension by scheduling:* To examine the benefits of multiuser scheduling, we define the *coverage extension ratio* $\eta_{\text{ZF-DPC}}^1$ as

$$\eta_{\text{ZF-DPC}}^1 = \frac{\tilde{R}_{\text{ZF-DPC}}^1}{R_{\text{ZF-DPC}}^1} = \left[\frac{\Gamma_R^{-1} \left(N_t, 1 - \sqrt[\kappa]{P_{\text{out}}^1} \right)}{\Gamma_R^{-1} \left(N_t, 1 - P_{\text{out}}^1 \right)} \right]^{\frac{1}{\mu}}, \quad (24)$$

where $\eta_{\text{ZF-DPC}}^1$ is a function of $\{N_t, K, P_{\text{out}}^1, \mu\}$ and can be used to examine how N_t and K affect the reliable coverage range of the MIMO broadcast system. Here we take the strongest link of ZF-DPC MIMO broadcast system ($i = 1$) as an example to address the coverage extension issue. We will show that the reliable coverage increases as the number of users increases and decreases as the number of antennas increases in the numerical results.

For the other links ($i = 2, \dots, N_t$) of ZF-DPC MIMO broadcast system with greedy scheduling, per link analysis

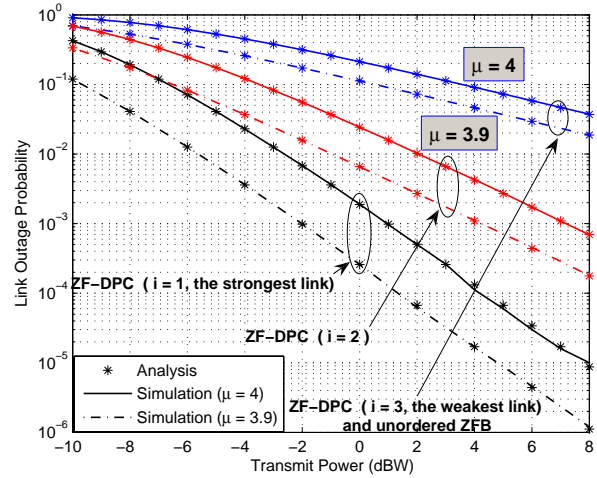


Fig. 2. Link outage probability performance against the transmit power P_T when path loss exponent $\mu = 3.9$ and 4 for both the ZF-DPC and ZFB MIMO broadcast systems, where $N_t = 3$, $\sigma^2 = -103$ dBm, $R = 1$ km and $\gamma_{th} = 2$ dB.

is more difficult than no scheduling case. Although, the equation (46) in [2] provides the PDF of effective channel gains of ZF-DPC with greedy scheduling for $i = 2, \dots, N_t$, this formula is complicated and intractable to derive its closed-form expression for link outage and coverage of ZF-DPC MIMO broadcast system with greedy scheduling so that the exact coverage extension gain can not be found easily.

B. ZFB with Scheduling

For the ZFB MIMO broadcast system with scheduling, some suboptimal user selection algorithms [2] [3] were proposed to reduce the complexity of the exhaustive search. However, it is difficult to find the exact per link closed-form expression for the ZFB MIMO broadcast system with scheduling. To compare with the ZF-DPC MIMO broadcast system, we will show the simulation results of the ZFB MIMO broadcast system based on exhaustive search in Section VI.

VI. NUMERICAL RESULTS

In this section, we illustrate the achievable link outage and link coverage performances of both the ZF-DPC and ZFB MIMO broadcast systems. Assume that the predetermined value $\gamma_{th} = 2$ dB, $\sigma^2 = -103$ dBm, $g_0 = -32$ dB, $\mu = 4$ and $N_t = 3$.

Figure 2 shows the simulative and analytical link outage performances of both the ZF-DPC and ZFB MIMO broadcast systems without scheduling when user terminals are at the distance of $R = 1$ km from BS and path loss exponents $\mu = 3.9$ or 4 . Clearly, the link outage probability becomes higher for a larger path loss exponent. Note that $\mu = 2$ is for free space, and $\mu = 3.5 \sim 4$ is for two-path model of an urban radio channel. The diversity orders of different links match our analytical results in Theorem 1.

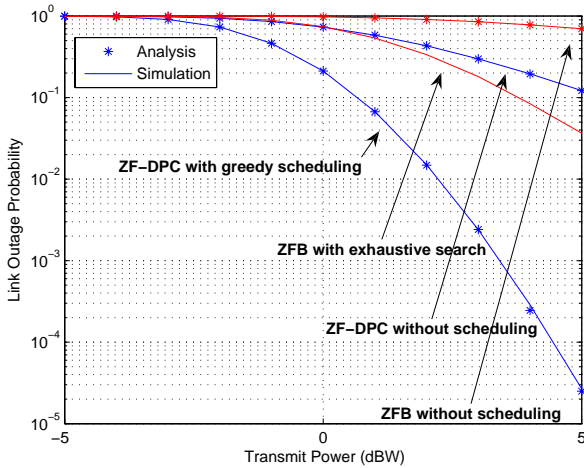


Fig. 3. Link outage probability performance against the transmit power P_T for the strongest links of both the ZF-DPC and ZFB MIMO broadcast systems with and without scheduling when $N_t = 3$, $\sigma^2 = -103$ dBm, $\mu = 4$, $R = 2$ km, $K = 5$ and $\gamma_{th} = 2$ dB.

For example, the strongest link $i = 1$ has the diversity order of three, the link $i = 2$ has the diversity order of two, but the weakest link $i = 3$ has only the diversity order of one. Clearly, the ZF-DPC MIMO broadcast system can support extra diversity gains for $N_t - 1$ links instead of traditional diversity order of one in a spatial multiplexing based MIMO system. However, the broadcast system with ZF precoding has merely diversity order of one.

Figure 3 shows the link outage for the strongest links of both the ZF-DPC and ZFB MIMO broadcast systems with and without scheduling for five users ($K = 5$) at the distance of $R = 2$ km from BS. In the figure, it is shown that the multiuser diversity gain is still significant even if the degree of freedom is merely $K = 5$. From this figure, the curve of ZF-DPC with greedy scheduling tends to have the diversity of order $KN_t = 15$. As a result, the deficient diversity of the spatial multiplexing based MIMO broadcast system can be compensated by taking advantage of multiuser scheduling.

Figure 4 shows the corresponding link coverage performance of Fig. 3 in which we set the link reliability as 0.9 under $\gamma_{th} = 2$ dB. Clearly, coverage is extended in both the ZF-DPC and ZFB MIMO broadcast systems with scheduling even with $K = 5$. For example, it can only maintain 90% link reliability as far as about 1.6 km radius without scheduling, but can extend to 2.1 km with scheduling for the ZF-DPC MIMO broadcast systems when $P_T = 0$ dBW, i.e. the achievable coverage increases 31.25% by the help of multiuser scheduling.

Figure 5 shows the coverage improvement for a different numbers of users in the ZF-DPC and ZFB MIMO broadcast systems when $P_T = 0$ dBW. The benefit of user ordering can be clearly observed from the coverage enhancement of ZF-DPC's strongest link at $K = N_t = 3$. Specifically, the cell radius is improved from 1.46 km to 1.8 km.

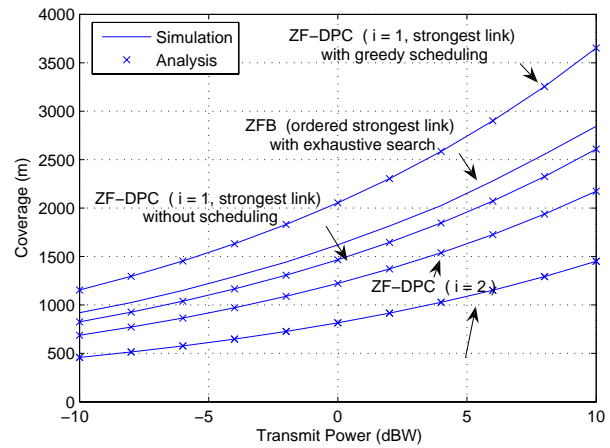


Fig. 4. Link coverage performance against the transmit power P_T for different stream links of both the ZF-DPC and ZFB MIMO broadcast systems when $N_t = 3$, $\sigma^2 = -103$ dBm, $\mu = 4$, $P_{out} = 0.1$, $K = 5$ and $\gamma_{th} = 2$ dB.

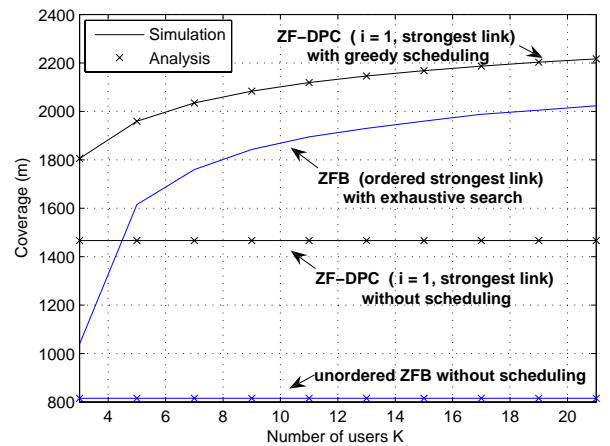


Fig. 5. Link coverage performance against the number of users K for different stream links of both the ZF-DPC and ZFB MIMO broadcast systems when $N_t = 3$, $\sigma^2 = -103$ dBm, $\mu = 4$, $P_{out} = 0.1$, $P_T = 0$ dBW and $\gamma_{th} = 2$ dB.

Figure 6 shows the coverage extension gain with different N_t and K according to (24). One can see that the benefit of multiuser scheduling is significant as K increases. However, the multiuser scheduling gain will reduce as more antennas are employed at the BS, i.e., for a larger N_t . From the above numerical results, we know that **soft coverage** enhancement can be achieved by applying multiuser scheduling techniques without increasing transmission power. That is, link quality is improved by multiuser diversity so that the reliable coverage can be extended. As the number of antennas equipped at a base station increases, transmit power allocated to each link will decrease under the same transmit power constraint. As a result, it will be hard for the MIMO broadcast system to maintain the same reliable coverage with a predetermined SNR requirement.

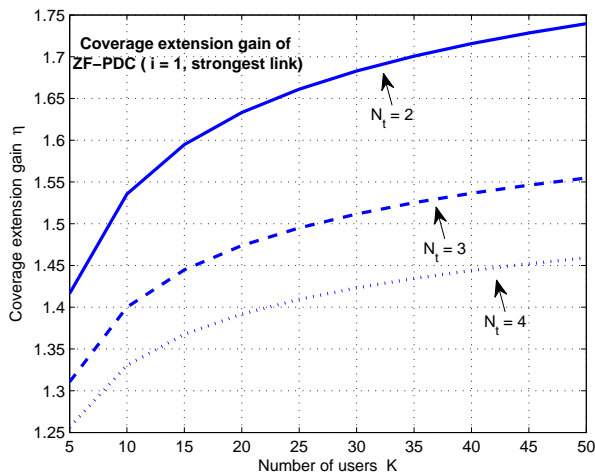


Fig. 6. Coverage extension gain against the number of users K for the strongest link of the ZF-DPC MIMO broadcast system with $N_t = 2, 3,$ and 4 .

VII. CONCLUSION

In this paper, we have analyzed the link outage, diversity order, and link coverage performance for the multiuser MIMO broadcast systems. We derive analytical closed-forms of the link outage probability, diversity order and reliable link coverage for both the ZF-DPC and ZFB MIMO broadcast systems. We define the coverage extension ratio to demonstrate how multiuser scheduling can improve the reliable coverage of the MIMO broadcast system without increasing BS transmission power. From our analysis, the reliable coverage can be extended significantly as the number of users increases, but the performance gain due to multiuser scheduling is reduced as the antennas installed at a BS increase.

REFERENCES

[1] G. Caire and S. Shamai, "On the achievable throughput of a multi-antenna Gaussian broadcast channel," *IEEE Trans. on Information Theory*, vol. 49, no. 7, pp. 1691 – 1706, Jul. 2003.

[2] G. Dimic and N. D. Sidiropoulos, "On downlink beamforming with greedy user selection: performance analysis and a simple new algorithm," *IEEE Trans. on Signal Processing*, vol. 53, no. 10, pp. 3857 – 3868, Oct. 2005.

[3] T. Yoo and A. Goldsmith, "On the optimality of multi-antenna broadcast scheduling using zero-forcing beamforming," *IEEE Journal on Selected Areas in Commun.*, vol. 24, no. 3, pp. 528 – 541, Mar. 2006.

[4] Q. H. Spencer, A. L. Swindlehurst, and M. Haardt, "Zero-forcing methods for downlink spatial multiplexing in multi-user MIMO channels," *IEEE Trans. on Signal Processing*, vol. 52, no. 2, pp. 461 – 471, Feb. 2004.

[5] M. Sharif and B. Hassibi, "On the capacity of MIMO broadcast channels with partial side information," *IEEE Trans. on Information Theory*, vol. 51, no. 2, pp. 506 – 522, Feb. 2005.

[6] M. Kountouris, D. Gesbert, and T. Salzer, "Enhanced multiuser random beamforming dealing with the not so large number of users case," *IEEE Journal on Selected Areas in Commun.*, vol. 26, no. 8, pp. 1536 – 1545, Oct. 2008.

[7] R. W. Heath, Jr., M. Airy, and A. J. Paulraj, "Multiuser diversity for MIMO wireless systems with linear receivers," *Proc. Asilomar Conf. Signals, Systems and Computers*, pp. 1194 – 1199, Nov. 2001.

[8] M. Airy, R. W. Heath, Jr., and S. Shakkottai, "Multi-user diversity for the multiple antenna broadcast channel with linear receivers: asymptotic analysis," *Proc. Asilomar Conf. Signals, Systems, and Computers*, pp. 886 – 890, Nov. 2004.

[9] C. J. Chen and L. C. Wang, "Performance analysis of scheduling in multiuser MIMO system with zero-forcing receivers," *IEEE Journal on Selected Areas in Commun.*, vol. 25, no. 7, pp. 1435 – 1445, Sep. 2007.

[10] L. C. Wang and C. J. Yeh, "Scheduling for multiuser MIMO broadcast systems: transmit or receive beamforming?" *IEEE Trans. on Wireless Commun.*, vol. 9, no. 9, pp. 2779 – 2791, Sep. 2010.

[11] D. J. Love and R. W. Heath, Jr., "What is the value of limited feedback for MIMO channels?" *IEEE Commun. Magazine*, vol. 42, no. 10, pp. 54 – 59, Oct. 2004.

[12] N. Jindal, "MIMO broadcast channels with finite rate feedback," *IEEE Trans. on Information Theory*, vol. 52, no. 11, pp. 5045 – 5059, Nov. 2006.

[13] T. Yoo, N. Jindal, and A. Goldsmith, "Multi-antenna downlink channels with limited feedback and user selection," *IEEE Journal on Selected Areas in Commun.*, vol. 25, no. 7, pp. 1478 – 1491, Sep. 2007.

[14] P. Ding, D. Love, and M. Zoltowski, "Multiple antenna broadcast channels with shape feedback and limited feedback," *IEEE Trans. on Signal Processing*, vol. 55, no. 7, pp. 3417 – 3428, Jul. 2007.

[15] K. Huang, J. G. Andrews, and R. W. Heath, Jr., "Performance of orthogonal beamforming with SDMA with limited feedback," *IEEE Trans. on Vehicular Technology*, vol. 58, no. 1, pp. 152 – 164, Jan. 2009.

[16] G. Caire, N. Jindal, M. Kobayashi, and N. Ravindran, "Multiuser MIMO achievable rates with downlink training and channel state feedback". [Online]. Available: <http://arxiv.org/abs/0711.2642>

[17] J. Zhang, R. W. Heath, Jr., M. Kountouris, and J. G. Andrews, "Mode switching for the multi-antenna broadcast channel based on delay and channel quantization," *EURASIP Journal on Advances in Signal Processing*, vol. 2009, article ID 802548.

[18] S. Shamai and B. M. Zaidel, "Enhancing the cellular downlink capacity via co-processing at the transmitting end," *IEEE Vehicular Technology Conf.*, vol. 3, pp. 1745 – 1749, May 2001.

[19] M. K. Karakayali, G. J. Foschini, and R. A. Valenzuela, "Network coordination for spectrally efficient communications in cellular systems," *IEEE Trans. on Wireless Commun.*, vol. 13, no. 4, pp. 56 – 61, Aug. 2006.

[20] G. J. Foschini, M. K. Karakayali, and R. A. Valenzuela, "Coordinating multiple antenna cellular networks to achieve enormous spectral efficiency," *IEE Proc. Commun.*, vol. 153, no. 4, pp. 548 – 555, Aug. 2006.

[21] 3GPP TSG RAN 1 R1-101695. (2010, Feb.) "Text proposal for 3GPP TR 36.814 on CoMP".

[22] 3GPP TR 36.814 v9.0.0. (2010, Mar.) "Evolved universal terrestrial radio access (E-UTRA); further advancements for E-UTRA physical layer aspects (Release 9)".

[23] *IEEE Standard 802.16. Part 16: air interface for fixed and mobile broadband wireless access systems – DRAFT amendment to IEEE standard for local and metropolitan area networks - advanced air interface*, IEEE P802.16m/D4, Feb. 2010.

[24] L. Zheng and D. N. C. Tse, "Diversity and multiplexing: A fundamental tradeoff in multiple antenna channels," *IEEE Trans. on Information Theory*, vol. 49, no. 5, pp. 1079 – 1296, May 2003.

[25] C. J. Chen and L. C. Wang, "Enhancing coverage and capacity for multiuser MIMO systems by utilizing scheduling," *IEEE Trans. on Wireless Commun.*, vol. 5, no. 5, pp. 1148 – 1157, May 2006.

[26] C. Wang, E. K. S. Au, R. D. Murch, W. H. Mow, R. S. Cheng, and V. Lau, "On the performance of the MIMO zero-forcing receiver in the presence of channel estimation error," *IEEE Trans. on Wireless Commun.*, vol. 6, no. 3, pp. 805 – 810, Mar. 2007.

[27] L. C. Wang, C. J. Yeh, and C. F. Li, "Coverage performance analysis of multiuser MIMO broadcast systems," *IEEE Vehicular Technology Conf.*, pp. 832 – 836, May 2008.

[28] G. L. Stuber, *Principles of Mobile Communication*, 2nd ed. Kluwer Academic Publishers, 2001.

- [29] COST Action 231, "Digital radio mobile towards future generation systems, final report," *Tech. Rep. European Communities, EUR 18957*, 1999.
- [30] M. K. Simon and M. S. Alouini, *Digital Communication over Fading Channels: A Unified Approach to Performance Analysis*, 1st ed. Wiley-Interscience, 2000.
- [31] D. Tse and P. Viswanath, *Fundamentals of Wireless Communication*. Cambridge University Press, 2005.
- [32] D. A. Gore, R. W. Heath, Jr., and A. J. Paulraj, "Transmit selection in spatial multiplexing systems," *IEEE Commun. Letter*, vol. 6, no. 11, pp. 491 – 493, Nov. 2002.
- [33] Z. Tu and R. S. Blum, "Multiuser diversity for a dirty paper approach," *IEEE Commun. Letter*, vol. 7, no. 8, pp. 370 – 372, Aug. 2003.



Li-Chun Wang (M'96 – SM'06 – F'11)

received the B.S. degree from National Chiao Tung University, Taiwan, R. O. C. in 1986, the M.S. degree from National Taiwan University in 1988, and the Ms. Sci. and Ph. D. degrees from the Georgia Institute of Technology, Atlanta, in 1995, and 1996, respectively, all in electrical engineering.

From 1990 to 1992, he was with the Telecommunications Laboratories of the Ministry of Transportations and Communications in Taiwan (currently the Telecom Labs of Chungwa Telecom Co.). In 1995, he was affiliated with Bell Northern Research of Northern Telecom, Inc., Richardson, TX. From 1996 to 2000, he was with AT&T Laboratories, where he was a Senior Technical Staff Member in the Wireless Communications Research Department. Since August 2000, he has been an Associate Professor in the Department of Communication Engineering of National Chiao Tung University in Taiwan. His recent research interests are in cognitive radio, energy-efficient and heterogeneous cross-network design, and cloud computing for mobile applications.

Dr. Wang was a co-recipient (with Gordon L. Stüber and Chin-Tau Lea) of the 1997 IEEE Jack Neubauer Best Paper Award for his paper "Architecture Design, Frequency Planning, and Performance Analysis for a Microcell/Macrocell Overlaying System," *IEEE Transactions on Vehicular Technology*, vol. 46, no. 4, pp. 836-848, 1997 (best systems paper published in 1997 by the IEEE Vehicular Technology Society). He has published over 150 journal and international conference papers and is holding eight US patents. He was elected to the IEEE Fellow grade in 2011 for his contributions in cellular architectures and radio resource management in wireless networks. He served as an Associate Editor for the *IEEE Trans. on Wireless Communications* from 2001 to 2005, the Guest Editor of Special Issue on "Mobile Computing and Networking" for *IEEE Journal on Selected Areas in Communications* in 2005 and on "Radio Resource Management and Protocol Engineering in Future IEEE Broadband Networks" for *IEEE Wireless Communications Magazine* in 2006.



Chu-Jung Yeh (S'08)

received the B.S. degree in electrical engineering from National Dong Hwa University, Hualien, Taiwan, in 2004, and the Ph. D. degree in the Institute of Communications Engineering, National Chiao Tung University, Hsinchu, Taiwan, in 2010. He was a post doctoral researcher in the Department of Electrical Engineering of National Chiao Tung University from September 2010 to February 2011. His research interests include MIMO systems with scheduling, network

MIMO systems, and resource management and performance analysis for cellular mobile networks.

A Practical Resource Allocation Approach for Interference Management in LTE Uplink Transmission[†]

Liyang Li*, Gang Wu, Hongbing Xu, Geoffrey Ye Li, and Xin Feng

Abstract—In this paper, we investigate power control and resource allocation for *long-term evolution* (LTE) uplink. We develop an efficient way to improve system performance, especially for those users at the edge of a cell, by taking interference to and from adjacent cells into consideration. Simulation results show that the spectrum efficiency for edge users is improved by about 20% over the independent resource allocation and by about 10% over the soft frequency reuse scheme.

I. INTRODUCTION

The aim of *long term evolution* (LTE) standardized for *3rd Generation Partnership Project* (3GPP) is to satisfy the requirements on high data rate, *quality-of-service* (QoS), and infrastructure [1]. LTE uses *single-carrier frequency division multiple access* (SC-FDMA) for the uplink transmission. SC-FDMA can be viewed as a *fast Fourier transform* (FFT)-precoded version of OFDMA, however, achieves lower *peak-to-average-power ratio* (PAPR) compared with OFDMA [3]. It transmits information symbols sequentially rather than in parallel as in OFDM while still keeping orthogonal transmission among intra-cell users. Therefore, there is no intra-cell interference in LTE uplink systems. Since all or part of the spectrum is reused in adjacent cells, inter-cell interference exists, especially when two or more edge users in adjacent cells use the same band. Inter-cell interference limits the performance of the system.

Inter-cell coordination allows the adjacent cells to manage the spectrum coordinately to minimize the inter-cell interference. To date, three schemes, *fixed-frequency reuse* (FFR), *soft-frequency reuse* (SFR), and adaptive SFR, have been proposed to reduce inter-cell interference. FFR allows each of the adjacent cells to use part

of the spectrum so that spectrum allocated to the users in the adjacent cells are orthogonal. SFR [4] divides the spectrum and users into two groups for the cell-edge users and cell-center users, respectively. In [5], an adaptive SFR has been developed to deal with inter-cell interference for different cell loads by allowing the edge users to borrow the center spectrum under certain situations.

In LTE, the minimum resource unit is a *physical resource block* (PRB), which consists of 12 subcarriers within one *transmission time interval* (TTI). SC-FDMA has two types of subcarrier mapping: *localized FDMA* (L-FDMA) and *interleaved FDMA* (I-FDMA). For L-FDMA, consecutive PRBs are assigned to the same user while PRBs are distributively allocated over the entire spectrum for I-FDMA. LTE adopts L-FDMA for uplink transmission. An optimal and a greedy algorithm for resource allocation in LTE uplink systems have been introduced [9]. Since resource allocation is performed independently in each cell and ignores inter-cell interference, the spectrum efficiency is not good. In this paper, we will develop a spectrum allocation scheme to improve both the average cell throughput and the cell edge throughput only at the expense of only limited signaling overhead between the coordinated base stations.

It has been shown in [8] that combining adaptive modulation and power control can lead to a significant throughput improvement compared with the case with power control only. In this paper, we will further consider the adaptive *modulation and coding scheme* (MCS) selection to improve the system performance.

In the rest of this paper, we will first describe the system model in Section II. In Section III, we will develop a novel resource allocation scheme to mitigate inter-cell interference and improve the throughput of those users at cell edge. We will present simulation results to demonstrate performance improvement in Section IV and conclude our paper in Section V.

Manuscript received February 15, 2011; revised May 15, 2011; accepted June 15, 2011.

[†] This work was supported in part by the Research Gift from Huawei Technologies Co., Ltd. and National Major Science and Technology Project under grant 2011ZX03003-001-04.

* The corresponding author: Ms Liyang Li. School of CAE, University of Electronic Science and Technology of China, Chengdu, China; Email: liyangli0815@gmail.com.

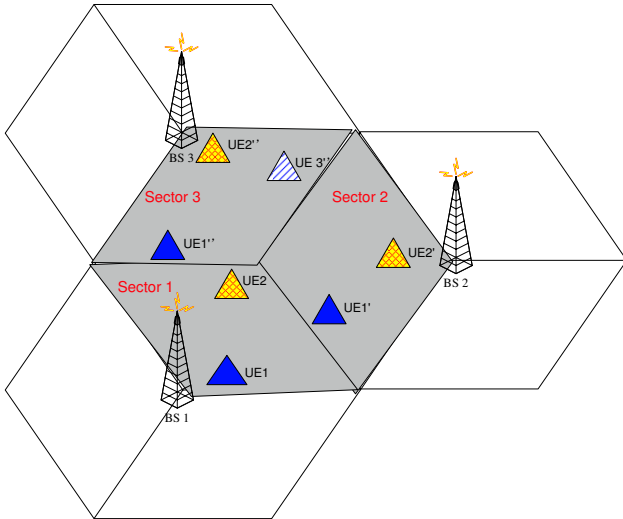


Fig. 1. The system model.

II. SYSTEM MODEL

Consider a system shown as in Figure 1, each cell is divided into three sectors and each sector is covered by a 120-degree directional antenna. Therefore, each sector has two adjacent ones. We assume that there are M users in a sector and they share L PRBs for data transmission. Each user can be only allocated to consecutive PRBs as required by L-FDMA in LTE uplink.

In LTE uplink, the overall transmission power is uniformly distributed among the subcarriers allocated to the same user. Denote P_m and \mathcal{K}_m to be the overall transmission power and the set of consecutive PRBs assigned to user m , respectively. Then the transmission power of each subcarrier for user m is $P_{m,i} = \frac{P_m}{12|\mathcal{K}_m|}$, where $|\mathcal{K}_m|$ is the number of PRBs in the set of \mathcal{K}_m . The SINR at the i th subcarrier of the n th PRB corresponding to user m will be

$$\gamma_{i,n}^{(m)} = \frac{P_{m,i}G_{m,i}G(\theta)}{I_{i,n}^{(m)} + P_N}, \tag{1}$$

where $G_{m,i}$ is the channel gain from user m to its base station, including pathloss, shadowing, and multipath fading, $G(\theta)$ is the antenna gain from user m to its service base station. $I_{i,n}^{(m)}$ is the power of interference from users in other sectors using the same PRB as user m , and P_N is the power of additive white Gaussian noise (AWGN).

The transmission data rate of user m can be expressed as

$$R(P_m, \mathcal{K}_m) = B|\mathcal{K}_m| \log_2 \left(1 + \frac{\gamma(P_m, \mathcal{K}_m)}{\Gamma} \right), \tag{2}$$

where B is the effective bandwidth of each PRB, Γ is the SINR gap to satisfy block-error rate (BLER)

requirement, $\gamma(P_m, \mathcal{K}_m)$ is the effective SINR for user m . From [7], the effective SINR can be expressed as

$$\gamma(P_m, \mathcal{K}_m) = -\beta \ln \left(\frac{1}{12|\mathcal{K}_m|} \sum_{n \in \mathcal{K}_m} \sum_{i=1}^{12} e^{-\gamma_{i,n}^{(m)}/\beta} \right), \tag{3}$$

where β depends on modulation order and coding rate.

If we consider independent proportional fairness resource allocation for each sector, then the objective can be expressed as

$$\{(P_1, \dots, P_M), (\mathcal{K}_1, \dots, \mathcal{K}_M)\} = \arg \max \sum_{m=1}^M \ln R(P_m, \mathcal{K}_m), \tag{4}$$

subject to

$$\mathcal{K}_i \cap \mathcal{K}_j = \emptyset \quad \forall i \neq j, \quad i, j \in \{1, 2, \dots, M\}, \tag{5}$$

$$P_m \leq P_{max}, \tag{6}$$

where P_{max} is the power threshold for each user. Constraint (5) indicates that each PRB can only be allocated to one user in a sector.

III. JOINT POWER CONTROL AND RESOURCE ALLOCATION

In this section, we will first introduce the fractional power control in LTE uplink and then present our proposed resource allocation scheme.

Fractional power control is suggested by LTE working groups, which can be expressed as [2]

$$P_m = \min\{P_{max}, P_0 + \alpha PL + 10 \log_{10} |\mathcal{K}_m| + \Delta_{mcs} + f(\Delta_i)\}, \tag{7}$$

where P_0 is a cell-specific parameter decided by the higher layers, α is a compensation parameter that is chosen from set $\{0, 0.4, 0.5, 0.6, 0.7, 0.8, 0.9, 1\}$ and decided by the base station of the serving cell, PL is the pathloss from user m to its base station, Δ_{mcs} is a transport format (TF) dependent offset used to consider different SINR requirements for various MCSs, and $f(\Delta_i)$ represents the correction value provided by close-loop power control. The objective of the power control in LTE uplink is to limit inter-cell interference and to maintain SINR requirements based on the QoS constraint, cell load, and user equipment power capabilities. In general, power control in uplink determines the average SINR range a user is operating at.

Using fractional power control to limit interference with other sectors can simplify the resource allocation for cellular systems. However, the inter-cell interference is still very strong since resource allocation is performed without considering adjacent sectors, especially when

two or more edge users in adjacent sectors are using the same PRBs. In this paper, we develop an adaptive PRB allocation method that will adjust the PRBs used by cell-edge users with the help of information on the allocated PRBs and users' positions in adjacent cells obtained through X2 interface.

Each sector first performs resource allocation independently based on proportional fairness introduced in Section II while fractional power control is used. PRBs for the adjacent edge users are jointly adjusted based on users' position and initial PRB allocation. Users' position can be obtained at the base station side. As the shadow area in Figure 1, we assume that there is a primary sector among every three adjacent sectors of different cells. The primary sector will collect information of resource allocation and users' position of the coordination sectors and perform PRB rescheduling. Since PRB adjustment may change interference environment of the center users, we will finally re-allocate the transmission power for center users.

There will be severe inter-cell interference if the same PRB is used by two or three edge users in adjacent sectors who have different closest adjacent base stations. For example, *user equipment* (UE) 1' in Sector 2 is close to Sector 1 and UE 3'' in Sector 3 is close to Sector 2 in Figure 1. If UEs 1' and 3'' use the same band, there will be severe interference. UE 3'' will cause severe interference to UE 1''. Therefore, PRBs in this case need to be re-allocated. We assume that two edge users at adjacent sectors with different base stations may use the same PRB simultaneously if there is no severe interference with each other, as UE 1'' and UE 1' in Figure 1.

After PRB reallocation and power control, we will further consider MCS adaption in each sector. Each sector will choose an MCS to maximize the throughput based on the SINR. The throughput is determined by the *initial BLER* (IBLER) for the UE with allocated PRBs and transmission power and can be expressed as,

$$\max_i T(i) = R(i)(1 - P(i, \gamma_{e,i})), \quad (8)$$

where i is the MCS index in LTE, $R(i)$ is the data rate achieved by using MCS i , $\gamma_{e,i}$ is the exponential effective SINR achieved by using MCS i as expressed in Equation (3), $P(i, \gamma_{e,i})$ is the IBLER for the used blocks. From [10], the IBLER for each block can be approximated by

$$P_b(i, \gamma_{e,i}) = \frac{1}{2} \operatorname{erfc} \left(\frac{\gamma_{e,i} - b_i}{\sqrt{2}c_i} \right), \quad (9)$$

where b_i and c_i are parameters obtained by curve-fitting corresponding to MCS i . Consequently, the IBLER for

the user with MCS i can be expressed as

$$P(i, \gamma_{e,i}) = 1 - (1 - P_b(i, \gamma_{e,i}))^{|\mathcal{K}_m|}.$$

The proposed scheme can be summarized as following.

- *Step 1:* Each sector performs independent power control and resource allocation. For example, three sectors in shadow area shown in Figure 1 perform independent power control and resource allocation based on proportional fairness introduced in Section II.
- *Step 2:* Exchange information on resource allocation and users' position of the sectors to the primary sector. For example, Sectors 2 and 3 send the information on PRB allocation and users' position to Sector 1.
- *Step 3:* The primary sector re-allocates the PRBs based on the information and sends back the final resource allocation information to the other two sectors. For example, Sector 1 re-allocates the PRBs based on the information received from Sectors 2 and 3 and sends the adjusted PRB allocation information to these two sectors. The detailed re-allocation algorithm is shown in Table 1. The PRB allocation matrix is the index of PRBs allocated to each user in the sectors. Users' position matrix is about the position of users in each sector. From this matrix we can know the closest interference sector of each user.
- *Step 4:* The coordinate sectors adjust the transmission power of their center users based on the information from the primary sector.
- *Step 5:* All sectors perform adaptive MCS allocation and the users transmit data based on the information from their base stations.

IV. SIMULATION RESULTS

In this section, we will compare performance of our scheme with independent resource allocation with fractional power control and SFR [4]. For SFR, the transmission power for the edge users is larger than that of the center users. We consider the system as shown in Figure 1, where a half of sector users are randomly distributed at the edge and the other half are randomly distributed in the center. The edge area is assumed to be the outer one third of the whole sector area. The major simulation parameters are summarized in Table 2.

Since each user can only use consecutive PRBs in LTE uplink, the optimal algorithm for resource allocation is an NP-hard problem [6]. There are several sub-optimal algorithms with only a little performance degradation but with much lower complexity. It has been shown in [6]

TABLE I
RE-ALLOCATION ALGORITHM

Algorithm Re-allocation

Input: PRB allocation matrix J and users' position matrix P

Output: PRB re-allocation matrix J_n

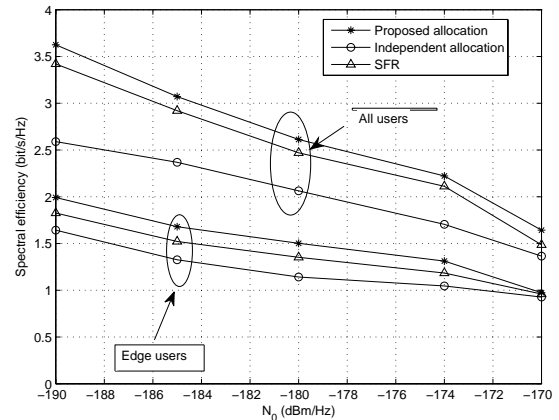
1. Get the matrix of closest adjacent sector number N for each user based on P (N_i for user i)
2. **for** sector=1 to 3 **do**
3. find PRBs used by two edge users i and j
4. **if** $N_i \neq N_j$
5. switch the PRB of user i with a PRB used by its center user
6. **end if**
7. **end for**
8. **return** J_n

TABLE II
MAIN SIMULATION PARAMETERS

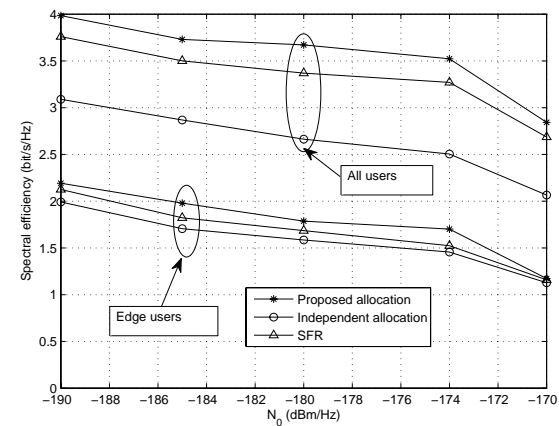
Parameter	Value
Bandwidth	10 MHz
Carrier frequency	2 GHz
Total number of PRBs	48 PRBs (PUSCH)
Cell radius	500 m
Ratio of cell edge area	1/3
Distance-dependent pathloss	$128.1+37.6\log_{10}(d)$ d in Km
Shadowing standard deviation	8 dB
PSD of thermal noise	-174 dBm/Hz
P_0	-80 dBm
α	0.7

that grouping algorithm, which allocates equal number of consecutive PRBs to each user, performs the best among these suboptimal ones. Hence, we will use it to allocate PRBs in our simulation. Fractional power control is used for independent resource scheduling. We assume the cell load is larger than 80%, and all the users in a sector are allocated the same number of PRBs, which is consistent with the grouping algorithm.

Figure 2 demonstrates spectrum efficiency of the three schemes versus the *power spectral density* (PSD) of channel noise when there are 6 users and 8 users, respectively. We assume that there are six users in a sector with three on the edge. From the figure, our scheme improves both the spectrum efficiency for the edge users and overall spectrum efficiency. It increases 20% over the independent resource allocation and about 10% over SFR for edge users' spectrum efficiency. We can also see that the proposed scheme performs better when the



(a) M=6



(b) M=8

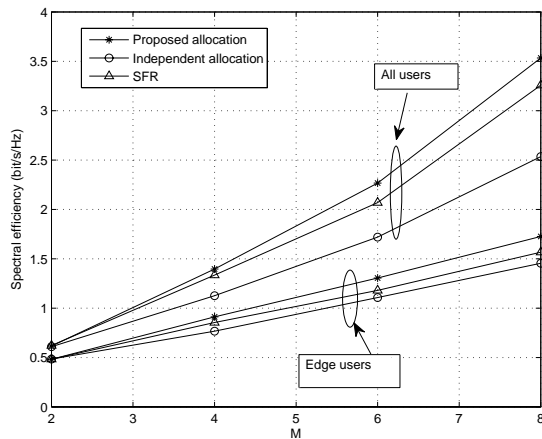
Fig. 2. Spectral efficiency of different schemes versus noisy density for different number of users.

system is interference dominant, which corresponds to the case with lower noise PSD in the figure.

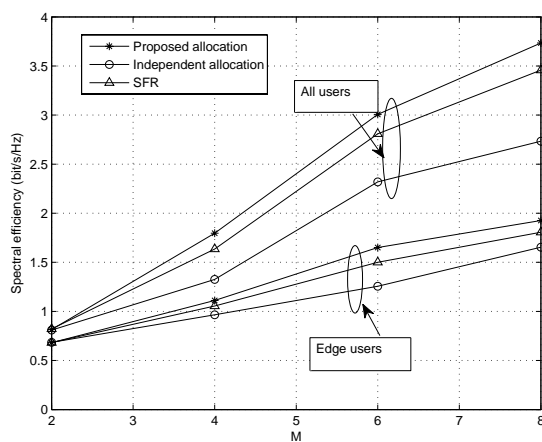
Figure 3 shows spectrum efficiency versus the number of users with noise PSD of -174 dBm and -185 dBm, respectively. From the figure, the performance gain of our scheme increases with the number of users. It can be easily seen that the information exchanged between sectors is pretty limited, only several hundred bits for 10 users in a sector. For example, if using 6 bits for user index, information exchanged for 48 PRBs will be 288 bits.

V. CONCLUSION

In this paper, we have introduced a resource allocation scheme for LTE uplink systems. The proposed scheme first allocates PRBs in each cell independently, then adjusts the PRBs and perform power control for the center users based on information on PRB allocation and users' position among adjacent cells. Simulation results have indicated that our scheme can improve spectrum efficiency for edge users and overall spectrum efficiency



(a) $N_0 = -174$ dBm/Hz



(b) $N_0 = -185$ dBm/Hz

Fig. 3. Spectral efficiency comparison of different schemes for different numbers of users.

compared with independent resource allocation and SFR. Since we have considered all constraints in LTE uplink, the proposed algorithm is ready to be used in real systems for performance improvement.

REFERENCES

[1] 3GPP TS 36.300 V9.0.0 “Evolved universal terrestrial radio access (E-UTRA) and evolved universal terrestrial radio access network (E-UTRAN); overall description; Release 9,” June 2009.
 [2] 3GPP TS 36.213 V9.0.0 “Evolved universal terrestrial radio access (E-UTRA); physical layer procedures; Release 9,” Dec. 2009.
 [3] H. G. Myung, J. Lim, and David J. Goodman, “Single carrier FDMA for uplink wireless transmission,” *IEEE Veh. Tech. Mag.*, vol.1, no.3, pp. 30–38, 2006.
 [4] R1-050507, “Soft frequency reuse scheme for UTRAN LTE,” Huawei. 3GPP TSG RAN WG1 Meeting, Athens, Greece, May 2005.
 [5] X. Mao, A. Maaref, and K. Teo, “Adaptive soft frequency reuse for inter-cell interference coordination in SC-FDMA based 3GPP LTE uplink,” in *Proc. of IEEE GLOBECOM 2008*, Nov. 2008, pp. 1–6.

[6] S. Lee, I. Pefkianakis, A. Meyerson, S. Xu, and S. Lu, “Proportional fair frequency-domain packet scheduling for 3GPP LTE uplink,” in *Proc. of IEEE INFOCOM*, Apr. 2009.
 [7] R. Giuliano and F. Mazzenga, “Exponential effective SINR approximations for OFDM/OFDMA-based cellular system planning,” *IEEE Trans. Wireless Commu.*, vol.8, no.9, pp. 4434–4439, 2009.
 [8] X. Qiu and K. Chawla, “On the Performance of Adaptive Modulation in Cellular Systems,” *IEEE Trans. Commu.*, vol. 47, no.6, pp. 884–895, June. 1999.
 [9] I. C. Wong, O. Oteri, and W. McCoy, “Optimal resource allocation in uplink SC-FDMA systems,” *IEEE Trans. Wireless Commu.*, vol.8, no.5, pp. 2161–2165, May 2009.
 [10] K. Sayana, J. Zhang, and K. Stewart, “Link performance abstraction based on mean mutual information per bit (MMIB) of the LLR channel,” *IEEE 802.16 Broadband Wireless Access Working Group*.

Impact of CSI on Radio Resource Management Techniques for the OFDMA Downlink

Leonidas Sivrdis, Xinheng Wang and Jinho Choi
 School of Engineering
 Swansea University, SA2 8PP, UK
 email: {392924, j.choi}@swansea.ac.uk

Abstract—Adaptive resource allocation can drastically increase the throughput of an Orthogonal Frequency Division Multiple Access (OFDMA) system when the Channel State Information (CSI) is accurately known. Unfortunately, in practice, perfect CSI is rarely possible. In this paper, we consider adaptive sub-carrier assignment for downlink multiuser OFDMA systems, where the transmitter has no knowledge of the instantaneous channel realizations. The problem we address is maximizing the sum-capacity of the system subject to user Quality of Service (QoS) requirements. A heuristic algorithm presented in [1] is modified in order to provide an enhanced sub-optimal solution. Numerical results show that resources can be adaptively allocated using statistical CSI (SCSI) and that such an approach allows for an important number of user QoS requirements to be met. Comparisons between the instantaneous CSI (ICSI) and SCSI based resource allocation schemes demonstrate that their performance difference is highly dependent on the number of active users present in the cell, the QoS constraint, and the transmit power.

I. INTRODUCTION

Orthogonal Frequency Division Multiple Access (OFDMA) is based on Orthogonal Frequency Division Multiplex (OFDM); and thus, inherits its key benefits while allowing for multiuser diversity to be exploited [2]. This leads to more efficient radio resource management (RRM) as spectrum can be allocated to users with better channel conditions. For these reasons, RRM solutions for OFDMA systems have attracted significant interest. The research in this area can be broadly divided into two categories, namely margin-adaptive and rate-adaptive. Margin adaptation is the minimization of the transmit power subject to minimum Quality of Service (QoS) requirements for each user [3]. Examples of such work are [4] and [5]. Rate adaptation is the maximization of the data-rates subject to QoS constraints [3]. An example of rate adaptation is presented in [1]. The solution to these problems depends on the availability of accurate Channel State Information (CSI) at the transmitter. There are a number of reasons that lead to unavailable user CSI at the transmitter. Under significant user mobility, the small coherence time makes channel estimation procedures less accurate. Other reasons that contribute towards unavailable instantaneous CSI are prediction errors as well as feedback/processing delays. Therefore, in some cases, it is more reasonable to send back channel distribution information. We refer to knowledge of the channel distribution at the transmitter as statistical CSI (SCSI). Under SCSI based resource allocation, users only need

to feed back the mean of the channel SNR distribution. This leads to fewer wireless resources such as transmit power and bandwidth being consumed for feedback purposes.

In this paper, we solve a rate-adaptation problem for users whose instantaneous channel realizations are unavailable at the transmitter but perfectly known by the receiver. The optimum data-rate with which each sub-carrier can be loaded is computed by using a relationship between the average user signal-to-noise ratio (SNR) and the Lambert-W function. To further enhance the performance of the system, a well-known heuristic algorithm presented in [1] is extended. Using this approach, it is shown that a significant number of user QoS constraints can be met. However, comparisons between the instantaneous CSI (ICSI) and SCSI based RRM schemes show that the lack of accurate CSI causes a significant degradation on the overall system performance. The incurred losses heavily depend on the number of active users present in the cell, the QoS constraint, and the transmit power.

II. SYSTEM MODEL

A downlink OFDM system with K users and N sub-carriers is considered. Each sub-carrier n has a total bandwidth equal to B . The k_{th} user's minimum bit-rate is denoted by R_k . Resource allocation is performed for each sub-carrier, and sub-carriers cannot be shared between users. An assignment indicator c_{kn} is defined for the k_{th} user and the n_{th} sub-carrier. Therefore, $c_{kn} = 1$ when carrier n is allocated to user k and 0 otherwise. When the instantaneous channel conditions are unknown by the transmitter but known at the receiver side, the capacity of each sub-carrier is viewed as a random variable and is

$$C(\nu) = B \log_2 \left(1 + \nu \frac{P_t}{N_o} \right), \quad (1)$$

where ν is exponentially distributed as Rayleigh fading is considered. Here, P_t is the transmit power and N_o is the noise spectral density. Under these conditions, there is a non-zero probability that the actual channel conditions cannot support an assigned rate ρ . This value is given as [6]

$$\begin{aligned} P_{out} &= \Pr \left(\frac{C(\nu)}{B} < \rho \right) \\ &= 1 - \exp[-(\bar{\gamma}^{-1})(2^\rho - 1)]. \end{aligned} \quad (2)$$

A useful measure for resource allocation purposes is the goodput which is defined [7] as the average successfully

transmitted rate. For user k and sub-carrier n it is expressed as

$$G_{k,n} = \rho_{k,n}(1 - P_{out}(k,n)), \quad (3)$$

Each sub-carrier can be optimally loaded by selecting the value of $\rho_{k,n}$ which maximizes $G_{k,n}$. This value is

$$\rho_{kn} = \frac{W(\bar{\gamma}_{kn})}{\ln(2)}, \quad (4)$$

where W denotes the Lambert- W function, the solution to the transcendental equation $W(x)e^{W(x)} = x$. A derivation of (4) is presented in Appendix A. Using (4), the maximum goodput user k can achieve on sub-carrier n is

$$G_{k,n} = \frac{W(\bar{\gamma}_{kn})}{\ln(2)} (\exp[-(\bar{\gamma}_{kn}^{-1})(2^{\frac{W(\bar{\gamma}_{kn})}{\ln(2)}} - 1)]). \quad (5)$$

When the transmitter knows the ICSI there are no outages, and each sub-carrier is loaded with a bit-rate equal to the Shannon capacity.

III. PROBLEM FORMULATION

The objective of this problem is to maximize the sum-goodput of the OFDMA downlink under minimum user data-rate requirement constraints. Equal power allocation across all sub-carriers is assumed as this reduces the complexity of the problems and minimally decreases the data throughput of a multiuser OFDM system [8]. This is due to the nature of OFDMA systems, where sub-carriers are commonly assigned to the users with the best channel gains. For the SCSi based scheme, the problem can be mathematically formulated as follows:

$$P1 : \quad \max_{c_{kn}} \sum_{k=1}^K \sum_{n=1}^N c_{kn} G_{k,n} B \quad (6)$$

Subject to :

$$C1 : \quad \sum_{n=1}^N c_{kn} G_{k,n} B \geq R_k, \forall k$$

$$C2 : \quad \text{If } c_{k'n} = 1, \text{ then } c_{kn} = 0 \forall k \neq k'.$$

Note that the first constraint, C1, ensures that the QoS requirement is met for all users k , while the second constraint ensures that a single carrier is not shared between different users. The equivalent problem can be formulated for the case of ICSI by replacing the goodput with the Shannon capacity in P1. That is:

$$P2 : \quad \max_{c_{kn}} \sum_{k=1}^K \sum_{n=1}^N c_{kn} \log_2(1 + \frac{\nu P_t}{N_o}) B \quad (7)$$

Subject to :

$$C1 : \quad \sum_{n=1}^N c_{kn} \log_2(1 + \frac{\nu P_t}{N_o}) B \geq r_k, \forall k$$

$$C2 : \quad \text{If } c_{k'n} = 1, \text{ then } c_{kn} = 0 \forall k \neq k'.$$

A. Complexity of the Problem

In P1, both the goodput and the Shannon capacity can be treated as constants. Therefore, P1 is converted into an integer linear programming problem which is one of the earliest members of the NP-hard class [9]. There are now KN integer variables and $K + N$ constraints, where the number of sub-carriers is high (i.e $N = 1024$ used in our simulations). As the complexity of the problem grows exponentially with KN and $K + N$ [10], it cannot be solved by using standard integer linear programming methods such as Branch and Bound. Thus, a heuristic needs to be developed. In [1], an algorithm which exhibited excellent sub-optimal properties was proposed to solve a problem of the same nature. However, its use may lead to carriers being allocated to users who are unable to meet their QoS constraints. In this paper, we use an extended version of that algorithm in order to mitigate this problem.

B. Heuristic Subcarrier-Bit Allocation Algorithm

The algorithm used in [1] first allocates sub-carriers to the users who can transmit the highest amount of data on them. As this process does not guarantee fairness, they are then re-allocated to the users whose constraints have not been met by using a cost function. This cost function ensures that any reallocations cause a small reduction in the overall sum-capacity of the system, and that the running time of the algorithm is minimized. Any remaining sub-carriers are then assigned to the users with the better channel gains. Here, we extend the algorithm as when carriers are allocated to users who do not meet C1, their requests will be rejected, and any carriers allocated to them will be wasted. Consider $X \subseteq \{1, 2, \dots, K\}$ to be the set of users who have not had their QoS constraints satisfied following the execution of the algorithm proposed in [1]. The cardinality of this set equals l . It is expected that a number of these users will still have been allocated some sub-carriers. The data-rates allocated to these l users by [1] are given in vector $\mathbf{y}=[y_1, \dots, y_l]$ whereas their associated QoS constraints are $\mathbf{z}=[t_1, \dots, t_l]$. Furthermore, it is assumed that $W \subseteq \{1, 2, \dots, N\}$ is the set of sub-carriers that have been allocated to these l users through [1]. In order to improve the overall performance, the following extension is proposed:

Algorithm 1 Proposed extension

- 1: Initialize : $W \subseteq \{1, 2, \dots, N\}$, $X \subseteq \{1, 2, \dots, K\}$, y, z
 - 2: \forall users $u \in X$
 - 3: Calculate $r(u) = z(u) - y(u)$
 - 4: $u^* = \arg \min_u r(u)$ //find the user u^* closest to meeting his QoS requirement
 - 5: $y_{u^*} = y_{u^*} + \rho_{u^*i} B$ // give sub-carrier $i \in W$ to u^*
 - 6: $W = W - i$ // remove sub-carrier i from W
 - 7: **if** $y_{u^*} > t_{u^*}$ **then**
 - 8: $X = X - \{u^*\}$ // remove u^* from X
 - 9: **end if**
-

In Algorithm 1, ρ_{u^*i} is the optimum goodput user u^* can achieve on carrier i . The use of this extension enables any

unused sub-carriers to be assigned to the users closest to meeting their data-rate requirements. Therefore, the number of utilized sub-carriers increases, and a higher overall system performance can be achieved. Moreover, the number of satisfied users grows.

C. Sub-Optimal Properties of Heuristic Algorithm

The sub-optimal properties of the heuristic algorithm are demonstrated in Fig. 1. The results of the algorithm are compared with the optimal results obtained through a brute-force search. The algorithm efficiency is defined as the ratio of the goodput achieved through the use of the sub-optimal algorithm to the goodput that can be achieved through a brute-force search.

Due to the long computational time, only eight sub-carriers and three users are considered. The QoS constraint is set to 4000 bits. Fig.1 shows that the algorithm exhibits excellent sub-optimal properties when SCSi is used to perform RRM.

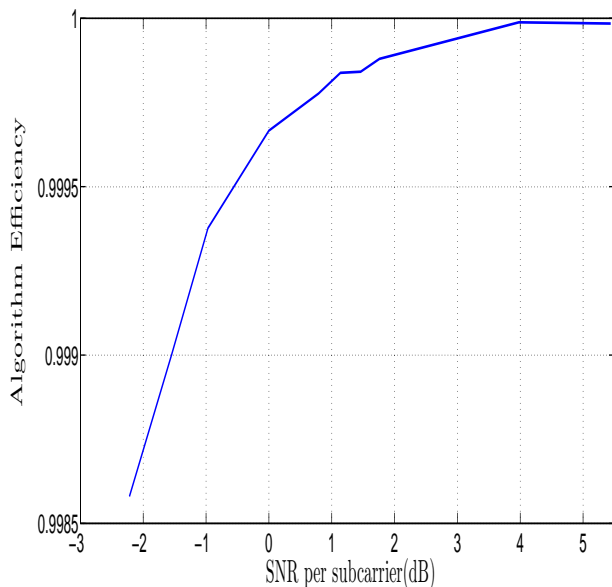


Fig. 1. Performance comparison between brute-force search and sub-optimal algorithm used to perform resource allocation

D. Impact of Extension to Original Algorithm

In order to present the importance of the final part of the algorithm, a throughput gain factor is defined as the ratio of the goodput achieved with the original version to the goodput that can be achieved using the extended version. Assume that there are 4 users in a cell and 8 sub-carriers that can be assigned to them. Fig.2 shows that when the QoS constraint is high and SCSi is used for resource allocation, an important increase in throughput occurs. As the user QoS requirements grow, it becomes increasingly difficult for the SCSi based scheme to meet these demands. Therefore, a higher number of unsatisfied users will be realized. With the original algorithm, any sub-carriers allocated to them would be discarded.

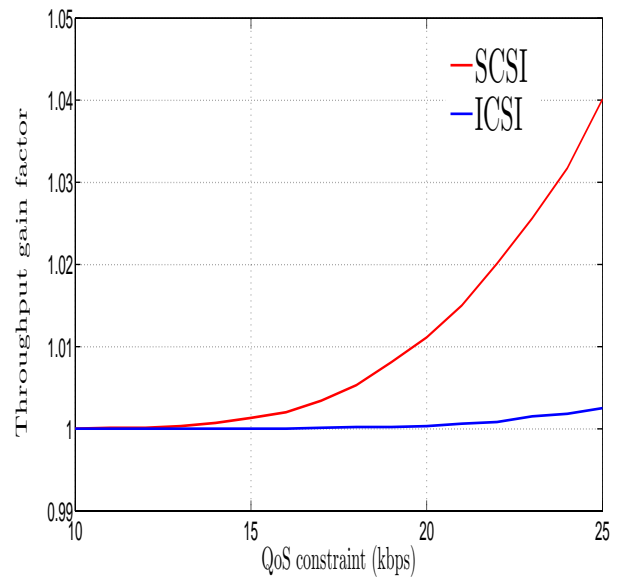


Fig. 2. Impact of the proposed extension to the original algorithm

IV. SIMULATION RESULTS

In this section, the significance of accurate CSI on RRM techniques for OFDMA systems is presented. In order to measure the impact of ICSI knowledge, a capacity gain factor is defined. This is the ratio of the optimum sum-capacity of a system where the user ICSI is known to the optimum sum-goodput of that same system when only the user SCSi is available. In the first subsection, the effect of a varying transmit power on the performance difference between SCSi and ICSI based adaptive RRM is presented. Then, the significance of a varying QoS constraint is analyzed. The simulation parameters used are listed in Table I. The environment is assumed to be variable, which is modeled by a fast fading with independently fading Rayleigh processes, whose power delay profile is described by the ITU Vehicular A model. The performances are evaluated using simulations over 10,000 instances of independent channel realizations. When averaging over a large number of channel realizations it is possible to accurately compare the ICSI and SCSi resource allocation schemes.

TABLE I
TABLE I: SIMULATION PARAMETERS USED

Parameter	Value
Number of sub-carriers	1024
Tx Power	8 → 35mW per sub-carrier
Noise power density	10^{-10} W/Hz
Channel Model	ITU Vehicular A
Bandwidth	10MHz
QoS constraint	1Mbps, 0 → 1.6Mbps

A. Impact of Transmit Power

It is worthwhile to investigate the significance ICSI knowledge has on the probability of satisfying the user QoS con-

straints. In Fig. 3, we notice that an important number of QoS constraints can be met by using SCSl. However, when the instantaneous channel realizations are known, nearly all of the user data-rate requirements are satisfied. A further comparison

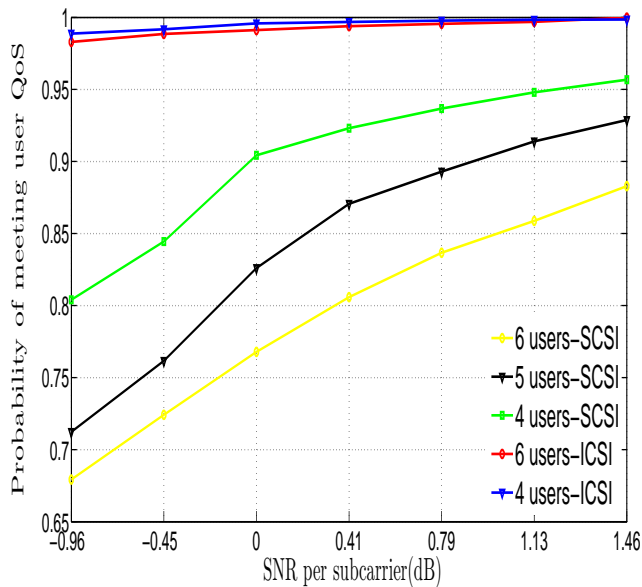


Fig. 3. Probability of user QoS requirements being met versus SNR per subcarrier for the SCSl and ICSl based resource allocation schemes

between the SCSl and ICSl based resource allocation schemes is made in Fig. 4. Here, it is observed that approximately 6dB more power per sub-carrier is required when the transmitter does not know the ICSl.

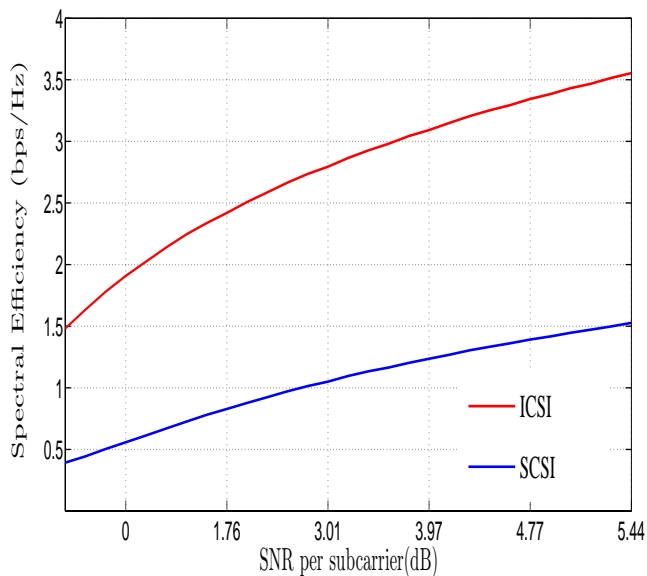


Fig. 4. Maximized sum-capacity versus average SNR per subcarrier

Fig. 5 presents the variation of the capacity gain factor

with SNR per subcarrier for 4 users without QoS constraints. For comparison purposes, a curve corresponding to the same amount of users each requiring 1Mbps is also given. As the SNR per subcarrier increases, the performance difference between the two cases is reduced because more QoS constraints can be met using SCSl. Also, the actual value of the capacity gain factor decreases as the power grows. In Appendix B, we show that as the SNR approaches infinity, the value of the capacity gain factor will be equal to one. In general the figures show that the performance difference between the ICSl and SCSl based resource allocation schemes is small. This is attributed to the Lambert-W approach which optimally loads the subcarriers in a Rayleigh environment. Optimal loading of subcarriers will lead to an improved performance when the channel gains are distributed according to a different p.d.f (i.e Ricean). However, closed form expressions that relate the optimum goodput with the data rate need to be developed.

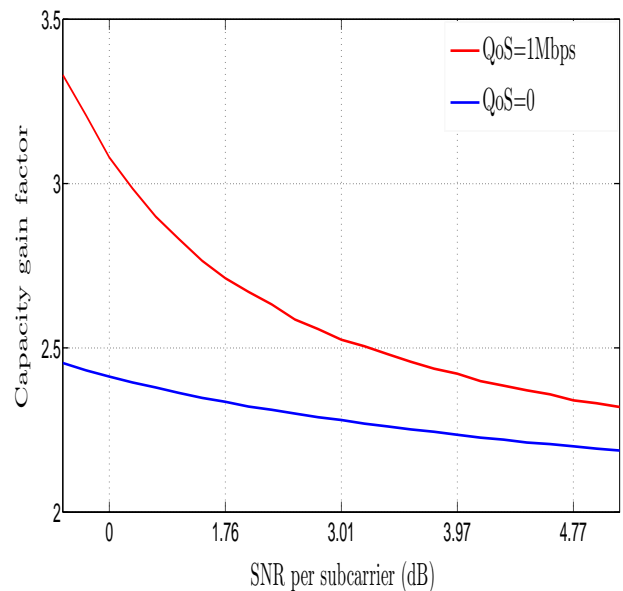


Fig. 5. Impact of SNR per subcarrier on the capacity gain factor

B. Impact of QoS constraint

The user QoS constraint in P1 plays an important role on the performance difference between the SCSl and ICSl based resource allocation schemes. Fig. 6 shows the variation of the capacity gain factor with the user QoS requirement. The transmit power equals 10mW (SNR per subcarrier is equal to 0dB). A close observation of this figure indicates that the value of this factor grows with the QoS constraint. As the user demands increase, the number of sub-carrier reallocation operations required to satisfy users whose instantaneous channel realizations are unavailable grows. This process has a negative impact on the optimum sum-goodput of the SCSl based scheme. Moreover, multiuser diversity has a strong effect on the results of Fig. 6. When the users' ICSl is known by the transmitter, it is easier for multiuser diversity to be

exploited. However, when SCSi is used to perform RRM, the benefits of multiuser diversity outweigh the drawbacks of sub-carrier reallocation only when the QoS constraint is low (i.e $< 0.1\text{Mbps}$ in our simulations). It is important to further investigate the significance of multiuser diversity on these results. In Fig. 7, we notice that when the user QoS requirement is equal to 0.1Mbps and the SCSi based RRM scheme is used, the overall system throughput increases with the number of users. However, when the user ICSI is unknown, it becomes increasingly difficult to exploit multiuser diversity as the QoS requirements grow. In this case, the effects of sub-carrier reallocation counteract multiuser diversity even when a relatively low number of active users are present in the cell. On the other hand, using ICSI based RRM enables multiuser diversity to be utilized much more efficiently when the QoS demands are high.

V. CONCLUSION

In this work, adaptive resource allocation has been performed for users whose instantaneous channel realizations are unavailable at the transmitter but known by the receiver. Sub-carriers were optimally loaded by using a relationship between the average SNR and the Lambert-W function. To further enhance the overall spectral efficiency, a well-known sub-optimal algorithm was extended. Using the proposed approach, numerical results showed that a significant number of user QoS requirements could be met using SCSi. However, an important loss in performance was observed when a performance comparison between the SCSi and ICSI based resource allocation scheme was made. This degradation was dependent on the number of active users present in the cell, the QoS constraint, and the transmit power.

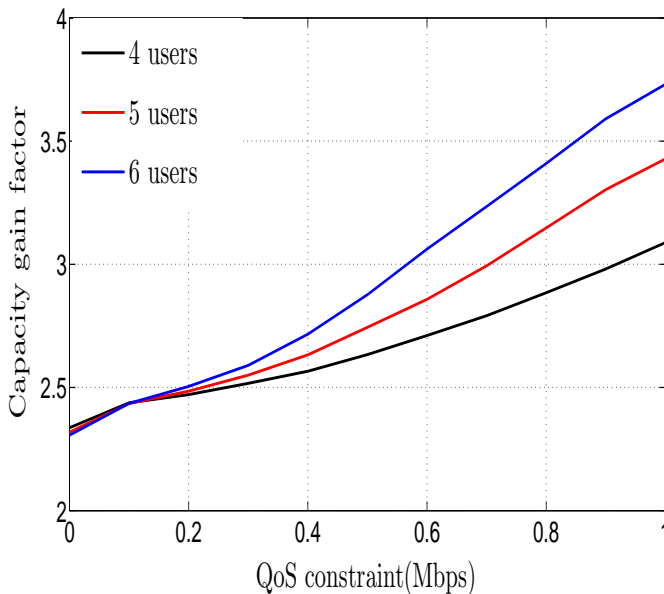


Fig. 6. Capacity gain factor dependence on QoS constraints

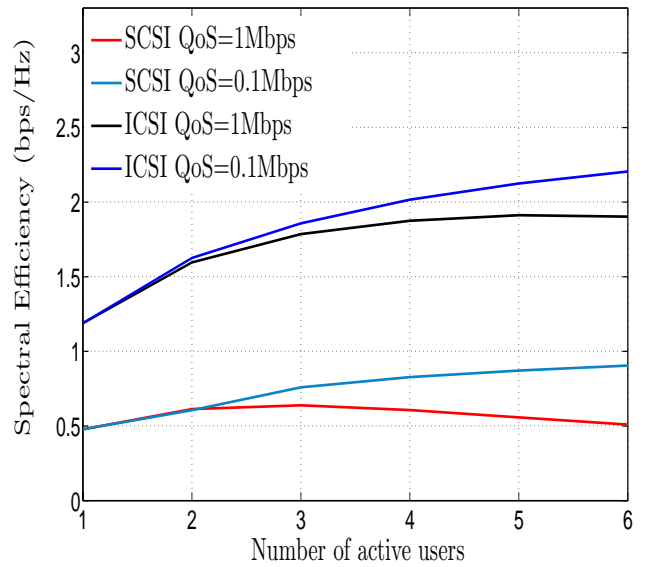


Fig. 7. Effect of QoS constraint on multiuser diversity

VI. APPENDIX A PROOF OF (4)

The goodput is written as

$$G(\rho) = \rho(\exp[-(\bar{\gamma}^{-1})(2^\rho - 1)]) \tag{8}$$

In order to find the value of ρ that yields the maximum values of G derivative of G with respect to ρ is set to zero. If we set $g(\rho) = -(\bar{\gamma}^{-1})(2^\rho - 1)$ this can be written as:

$$\frac{dG}{d\rho} = \exp(g(\rho)) + \rho \exp(g(\rho)) * \ln(2)g(\rho) = 0 \tag{9}$$

This reduces to

$$1 + \ln(2)\rho g(\rho) = 0 \tag{10}$$

By replacing $g(\rho)$ with its original value we obtain

$$\frac{\bar{\gamma}}{(2^\rho) \ln(2)\rho} = 1 \tag{11}$$

Using $2^\rho = \exp(\ln(2)\rho)$ this can be written as

$$\frac{\bar{\gamma}}{(\exp(\ln(2)\rho)) \ln(2)\rho} = 1 \tag{12}$$

By setting $y = \ln(2)\rho$ (12) can be written in the form $y \exp(y) = \bar{\gamma}$. By applying the Lambert W function we get $y = W(\bar{\gamma})$. Replacing with the original value of y will result in (4).

VII. APPENDIX B CALCULATION OF THE CAPACITY GAIN FACTOR LIMIT

In this appendix, we prove that when the SNR approaches infinity, the capacity gain factor becomes 1. After averaging over a large number of channel realizations, the values of $\bar{\gamma}$

and γ can be considered equal. The limit can therefore be written as:

$$\lim_{\gamma \rightarrow \infty} \exp \left[-(\gamma^{-1}) \left(2^{\frac{W(\gamma)}{\ln(2)}} - 1 \right) \right] \left(\frac{W(\gamma)}{\ln(2)} \right) \left(\frac{1}{\log_2(1 + \gamma)} \right)$$

Using the Lambert function identity, this can be written as:

$$\lim_{\gamma \rightarrow \infty} \exp \left[-\frac{\exp^{W(\gamma)} - 1}{\gamma} \right] \left(\frac{W(\gamma)}{\ln(\gamma)} \right) \left(\frac{\ln(\gamma)}{\ln(1 + \gamma)} \right)$$

Simple algebraic manipulations and application of Del'Hospital's rule to the second and third factor yield:

$$\lim_{\gamma \rightarrow \infty} \exp \left[-\frac{1}{W(\gamma)} - \frac{1}{\gamma} \right] \left(\frac{W(\gamma)}{1 + W(\gamma)} \right) \left(\frac{\gamma + 1}{\gamma} \right) = 1$$

REFERENCES

[1] Y. Zhang and K.B. Letaief, 'Multi-user Adaptive Sub-carrier and bit allocation with adaptive cell selection for OFDM systems', in *IEEE Trans. Wireless Commun.*, vol. 3, No. 5, pp. 1566-1575, September 2004.

[2] S. Pietrzyk, OFDMA for Broadband Wireless Access, Artech House, London, UK, 2006.

[3] B.Evans and I.B Wong, Resource Allocation in Multiuser Multicarrier Systems, Springer Science and Media, 2008.

[4] D.Kivanc and G.Liu, 'Computationally efficient bandwidth allocation and power control for OFDMA', in *IEEE Trans. Wireless Commun.*, vol.2, No 6, pp 1150-1158, November 2006.

[5] J.Jang and K.B.Lee, Transmit Power Adaptation for Multiuser OFDM Systems, in *IEEE Journal Selected Areas on Communications*, vol.21, No. 10, pp 171- 178, February 2003.

[6] E.Biglieri, J.Proakis, and S.Shamai, 'Fading Channels Information Theoretic and Communication Aspects' *Information Theory, IEEE Transactions on*, vol. 44, No 6, pp 1747-1758, October 1998.

[7] S. Stefanatos and N. Demetriou, 'Downlink OFDMA Resource Allocation under partial Channel State Information', in *Proc.IEEE ICC'09*, pp. 1-5, June 2009.

[8] W. Rhee and J.M. Cioffi, 'Increase in capacity of multi-user OFDM system using dynamic sub-channel allocation', in *Proc. IEEE Veh. Technol. Conf.*, pp. 1085-1089, Spring 2000.

[9] G.Sierksma, Linear and Integer Programming. New York: Marcel Dekker, 1996.

[10] G. Reklaitis, A. Ravindran, and K. M. Ragsdell, Engineering Optimization, Methods, and Applications. New York: Wiley, 1983.

Leonidas Sivridis is currently a Ph.D student at Swansea University, Swansea, U.K. He received his MSc degree in Communications and Radio Engineering from the Department of Electronic Engineering, Kings College London, London, U.K. His research interests include resource management in wireless networks and multiuser communications.

Dr. Xinheng (Henry) Wang is a senior lecturer in wireless communications at IAT. He graduated from Xian Jiaotong University with a BEng and an MSc degree in 1991 and 1994, respectively and obtained his PhD degree from Brunel University in 2001. He then worked as a post-doctoral research fellow at Brunel from June 2001. He joined Kingston University in 2003 as a senior research fellow and was promoted to a senior lecturer in June 2004. In September 2007 he joined the IAT to take up the senior lectureship. He is also a visiting professor at University of Electronic Science and Technology of China. His current research interests are wireless mesh and sensor networks, personal area networks, and their applications in healthcare.

Prof. Jinho Choi received his B.E. (magna cum laude) degree in electronics engineering in 1989 from Sogang University, Seoul, and his M.S.E. and Ph.D. degrees in electrical

engineering from Korea Advanced Institute of Science and Technology (KAIST), Daejeon, in 1991 and 1994, respectively. He is currently working with the Wireless Research Group within IAT. His research interests include wireless communications and array/statistical signal processing. He authored a book entitled Adaptive and Iterative Signal Processing in Communications (Cambridge University Press, 2006).

Understanding Static Inter-Cell Interference Coordination Mechanisms in LTE

Ashley Mills, David Lister, and Marina De Vos

Abstract—This work identifies the factors which determine the behaviour of static interference avoidance schemes: SINR distribution shift, MCS mapping, and proportional MCS usage. The work goes on to challenge the common assumption that it is “best” to give resources with a high reuse factor to those at the cell-edge, by showing for a fixed rate service class, that it is best to be greedy and give these resources to those at the cell-centre. The work is performed using monte-carlo simulations, only in the downlink direction, on a London scenario with realistic path loss and network data. All work is statistically quantified using appropriate tests.

Index Terms—LTE, Interference Coordination, Soft Frequency Reuse.

I. INTRODUCTION

THE next generation wireless technology, Long Term Evolution (LTE), has been designed to deliver higher spectral efficiency and increased cell-edge throughputs relative to HSPA [1]. It is expected that LTE will be deployed in a reuse one configuration, in which all frequency resources are available to use in each cell. Although LTE can operate at SINRs as low as -6.5dB [2], concern still persists over cell-edge performance.

This has led to the proposal of numerous inter-cell interference coordination mechanisms. A large number of these are dynamic in nature and usually assume communication between basestations [3]–[15]. These schemes have tended toward taking more and more cells into account, and it would appear that the industry is converging toward multi-cell processing with a centralised RAN architecture [16], [17].

Despite this progress and innovation, interest still persists in static schemes that it is assumed can be deployed within LTE without modification of the extant standards and without significant modification of extant equipment.

Static schemes usually fall into one of three broad categories: traditional hard frequency reuse, soft frequency reuse [18], and partial frequency reuse [19]. Notwithstanding variants and other techniques that do not fit the classification, this taxonomy will serve the argument advanced here.

A. Soft Frequency Reuse

Soft Frequency Reuse was proposed by Huawei in [18]; supplemented in [20]. This proposal is effectively reiterated by

Ashley Mills and David Lister are with Group R&D Technology, Vodafone Group Services Limited, The Connection, Newbury, Berkshire, RG142FN, UK

Marina De Vos is with The University of Bath, UK

Manuscript received April 14, 2011; revised May 1, 2011; accepted June 30, 2011

Ericsson in [21] and by LG Electronics in [19] although the latter augments the description with a priority based frequency planning scheme. Alcatel propose a method very similar to soft reuse in [22], albeit with a reuse factor higher than three at the cell edge. Semi-static variants of soft reuse are proposed in [23]. Soft frequency reuse is usually portrayed as depicted in Figure 1.

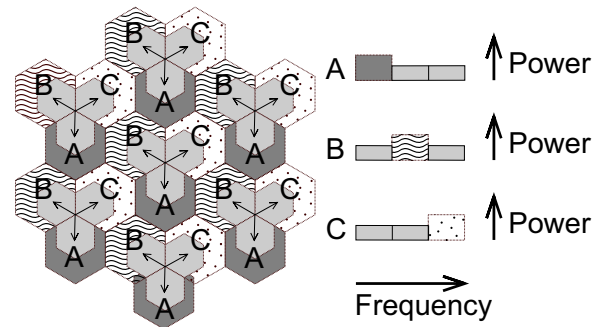


Fig. 1. Soft frequency reuse as conventionally presented

The left side of Figure 1 shows a hexagonal configuration of cells, colour coded and labelled according to a tessellating pattern to indicate which parts of the frequency band are allowed in each part of each cell. The right of the figure shows the frequency-power transmit profiles for each of the three types of cell that arise.

The general concept is that BSs transmit at reduced power over the whole transmission band, to create spatially separated cell centres that do not interfere with each other. At the cell edges, a boosted reuse three pattern is used so that received signals are orthogonal between otherwise interfering cell-edge UEs.

The mean cell throughput under soft reuse for the downlink is examined in [24]. It is claimed that 5th percentile throughput can be improved relative to reuse one in trade off for a reduction in total cell throughput by applying soft reuse. Since the work only examines the mean cell throughput, it provides no insight into the behaviour of more realistic schedulers.

Partial reuse differs from soft reuse in that the tessellated part of the spectrum is kept disjoint from the reused part of the spectrum [19].

B. Conflicting Results

Examining results on soft and partial reuse [14], [18], [22], [25]–[30] reveals some conflicting statements.

For example both [26] and [30] claim that partial reuse, relative to reuse one, gives improvements in throughput at the 5th percentile point, yet [29] concludes that “the basic partition-reuse scheme studied was not capable of improving the rate at the 5% CDF point”.

And [27] claims that soft reuse provides gains in both cell-edge *and* total throughput when compared with reuse one yet [28] concludes that “With the expected link performance no improvement can be found with static downlink reuse schemes.”. Furthermore [26] shows completely the opposite: losses in both cell-edge *and* total throughput for some scenarios.

The discussions in [29] and [28] go some way to explain, for their own results in isolation from others, why they turn out the way they do, yet no general explanation is proffered.

We contribute to this body of work in two ways: firstly we statistically quantify our results to provide confidence in them, something that none of the cited works do, and secondly: we explain clearly how different results can manifest from the application of the same or very similar schemes by identifying the principal factors involved and explaining their interactions (Section IV).

C. Challenging a common assumption

A common assumption in the works cited above, is that it is better to give the resources with a higher reuse factor to the UEs at the “cell-edge”. This is evidenced by the observation that none of the work suggests doing the opposite. And although in [31] a convincing mathematical argument is advanced as to why the cell edge may benefit *more* from interference coordination than the “cell-centre”, this says nothing of the trade-off in general.

Without strong empirical support, it is far from clear that giving the better resource to the cell-edge UEs is *always* the best scheduling strategy. And it must be observed that subbands with higher reuse factors offer improved SINR to *all* UEs, not just cell-edge UEs. So it isn’t clear apriori what the best scheduling strategy is for a given performance metric.

Against this backdrop we decided to examine scheduling strategies that favour high SINR UEs even when a soft reuse scheme has been applied, and were surprised to find, contrary to intuition, that a net gain in number of satisfied UEs could be obtained. This is explained with reference to the determinant factors identified in Section IV.

D. Document outline

The rest of this document is organised as follows. In Section II, the soft reuse terminology used here is defined. Experimental assumptions are explained in Section III. In Section IV, the factors complicit in causing static reuse results to differ are drawn out and explained through the medium of mean-rate experiments. In Section V, a feasible scenario is examined where favouring the cell-centre UEs gives a better outcome than favouring the cell-edge UEs. The implications of the presented results are discussed in Section VI and Section VII draws the work to a close with the conclusion.

1.3

TABLE I
RELATIVE TX POWER PER VRB ON THE ASB AND BSB.

Index	1	2	3	4	5	6	7	8	9	10
ASB TX	0	$\frac{1}{9}$	$\frac{2}{9}$	$\frac{3}{9}$	$\frac{4}{9}$	$\frac{5}{9}$	$\frac{6}{9}$	$\frac{7}{9}$	$\frac{8}{9}$	1
BSB TX	3	$\frac{25}{9}$	$\frac{23}{9}$	$\frac{21}{9}$	$\frac{19}{9}$	$\frac{17}{9}$	$\frac{15}{9}$	$\frac{13}{9}$	$\frac{11}{9}$	1

II. SOFT REUSE

A problem with the presentation in Figure 1 is that it confounds the physical aspects of soft frequency reuse with the virtual aspects of resource allocation by implying that the boosted resource *should* be given to the “cell edge” UEs.

Since this work looks at giving the boosted resource to the “cell-centre” UEs, soft reuse is presented neutrally as a tessellating pattern with a boosted part and an attenuated part, in the manner of Figure 2.

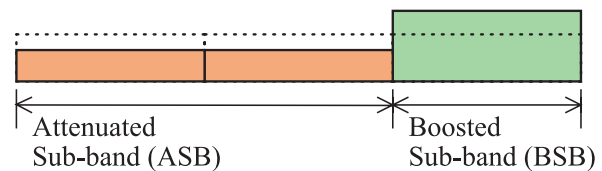


Fig. 2. Soft Frequency Reuse Configuration. The band is divided into attenuated and boosted regions. The scheduler decides which UEs are allocated to which regions.

The available bandwidth is partitioned into an Attenuated Sub Band (ASB) and a Boosted Sub Band (BSB) in the proportion of 2:1. The position of the BSB third in the overall band is changed on a per cell basis to create a tessellating pattern. The only difference from Figure-1 is that cell geography is not shown since we wish to avoid communicating apriori geographical biases on the usage of the ASB or BSB.

The relative transmit powers of the ASB and BSB determine how “soft” the overall reuse factor is. The power ratios shown in Table-I were examined in this work.

This range of soft reuse power ratios is bounded by two end points: reuse three at index 1, and reuse one at index 10. The points in between linearly interpolate across the space defined by these end points.

Observe that for Index 1, since the TX power on the ASB is 0, all UEs are assigned to the BSB. The BSB in this case uses 1/3rd of the total bandwidth at 3 times the transmit power.

In the following sections, the impact of applying each of these soft reuse power ratios is examined. Different scheduling strategies are considered to demonstrate the interaction between soft reuse power ratio and scheduling strategy. The cell performance is measured for each condition, to understand, if at all, where each soft reuse power ratio performs best.

III. EXPERIMENTAL METHODOLOGY

A. Overview

A realistic central London scenario is used to assess the gains of applying the static soft reuse power ratios shown in Table-I. The gains are measured in terms of scheduling

performance for two scheduling approaches: mean rate, and fixed rate.

B. LTE System Assumptions

The left of Figure 3 illustrates the essential components of a 10MHz LTE DL frame. In time, the frame consists of 10 subframes which each last 1ms. Half of a subframe is called a slot. In frequency, each subframe is split into 50 Virtual Resource Blocks (VRBs). Each VRB is comprised of a pair of physical resource blocks (PRBs). One VRB is the smallest unit of allocation in LTE [32]. Each PRB spans 12 subcarriers in frequency and 7 symbols in time (shorter cyclic prefix was used). Each element of a PRB is called a Resource Element (RE). An RE spans one subcarrier in frequency and one symbol in time. An RE has a frequency width of 15kHz and lasts approximately $70\mu\text{s}$.

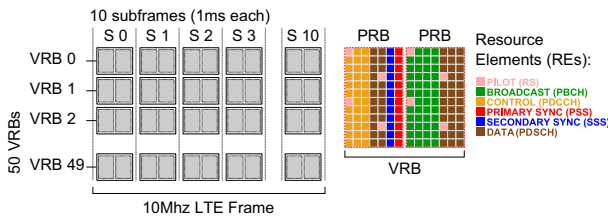


Fig. 3. The essential components of a DL LTE frame.

The right of the figure shows a VRB in detail, containing the RE types modelled here. Primary and secondary synchronisation, and broadcast channels, only occur on the three VRB either side of the central carrier. The former only occur in frames 0 and 5 and the latter only in frame 0. Their detailed action is not modelled: the channels only consume space that would otherwise be occupied by data REs. In the majority of the frame, only pilot, control, and data REs are present.

Pilot symbol positions and associated RSRP computation is modelled accurately according to [32]. Control channels are assumed to consume the first 3 symbols of every subframe, their action is not modelled, and they only consume space that would otherwise be occupied by data symbols. The average number of data REs per VRB was computed as 124.8720. This number is at the root of all throughput computations.

C. MCS Codeset

To map SINR to throughput, a lookup curve obtained from Vodafone Group [33] was used. Figure 4 shows the curve relative to the 3GPP reference curve which uses a single antenna (SISO) and assumes optimal switching between STBC and spatial multiplexing. The fading at the link level was based on the ITU Pedestrian B channel at 3km/h [34].

D. Deployment scenario

A realistic London scenario was used for all simulations. The data represents an area of central London. Antenna settings and terrain data reflect the actual network settings used in 2004 for the Vodafone UMTS macro deployment. Figure 5

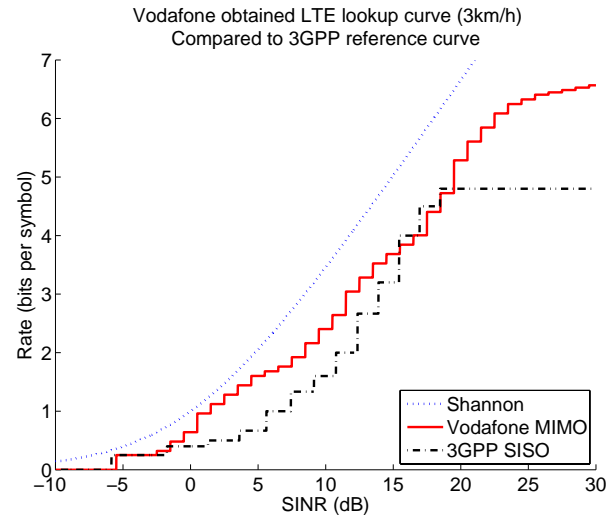


Fig. 4. SINR to MCS bitrate lookup curve used here in comparison to Shannon and a 3GPP reference curve.

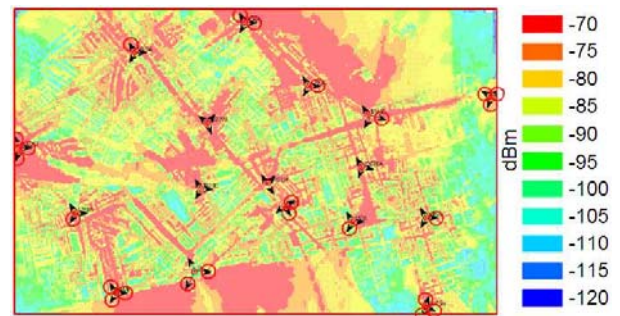


Fig. 5. Atoll predictions and antenna locations for the London scenario used in all simulations. Circled antennas were excluded from results collection.

shows the London area studied along with generated pathloss predictions.

Pathloss was calculated at a resolution of 10m^2 using the Pace3D ray tracing software module in Atoll [35]. Pace3D accurately models the effects of building penetration losses, reflection, and refraction effects and provides a realistic picture of the actual pathloss variation experienced in each cell. To mitigate border simulation affects, results were not collected for the circled cells in Figure 5.

In all experiments, each cell transmits continuously, so that the worst case interference scenario is represented.

IV. MEAN RESULTS

To generate mean cell results the following procedure was used:

```

ForEach ( Soft Reuse Power Ratio ) : Do
  ForEach ( Cell ) In ( Scenario ) : Do
    ForEach ( Square in Cell Area ) : Do
      A ← ASB Bitrate
      B ← BSB Bitrate
      C ← Mean: 2/3 * A + 1/3 * B
    Done
  Compute mean of A,B,C over Squares

```

Done

Compute mean of A,B,C over Cells
Record A,B,C for Soft Reuse Power Ratio

Done

In the first line, the transmit power profile is applied to the network. This means every cell transmits at exactly the power specified in the profile on each VRB. A full interference model is examined which means all cells are simultaneously transmitting on all VRBs. The algorithm then iterates over all cells in the scenario, and averages the measures A, B, and C for each cell at a resolution of $10m^2$. This is the meaning of “Square” in the algorithm. The algorithm ends by averaging the results across all cells.

Figure 6 plots the mean cell throughput as a function of soft reuse power ratio.

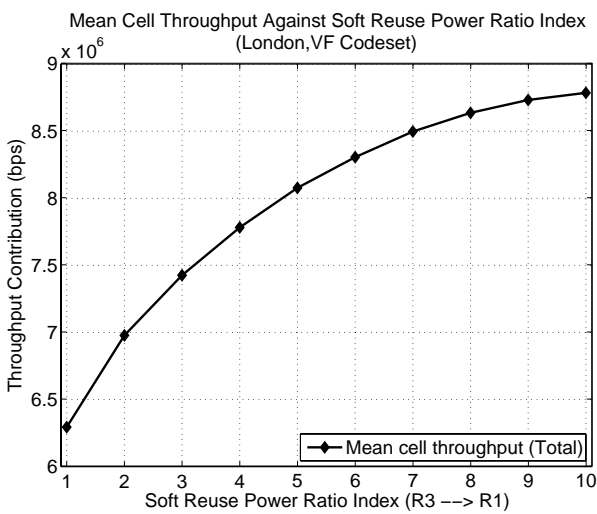


Fig. 6. Mean cell throughput

The general trend observed is a decline in throughput when moving away from reuse one toward reuse three. To compare the two extremes: mean throughput is $\approx 40\%$ greater under reuse one than it is under reuse three. This difference is significant with $p < 1 \times 10^7$ under a right tailed, unequal variance, ttest (Satterthwaites approximation was used to address the Behrens Fischer problem [36]).

It is desired to understand exactly why this result is observed. It is straightforward to examine the two end points: reuse three and reuse one. The question is why the reduction in bandwidth in the reuse three case is not “compensated”, to borrow terminology from [37], by the improved SINR conditions.

To see why, consider the SINR distributions under reuse three and reuse one, as illustrated in Figure 7.

The SINR distribution is right-shifted under reuse three compared to reuse one. For any monotonically increasing MCS lookup curve, improved SINR results in improved bitrate. Yet since bandwidth is reduced by a factor of three the effective bitrate observed will be reduced by a factor of three. For a given UE to benefit, it must thus obtain more than a factor three improvement in bitrate.

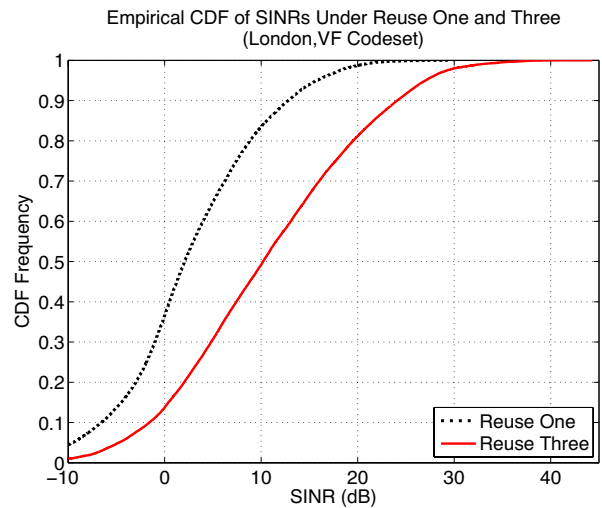


Fig. 7. Cell SINR CDFs under reuse three and reuse one.

Figure 8 illustrates which parts of the cell obtain such an improvement when switching from reuse one to reuse three and which do not. The figure plots the effective bitrate under reuse three, for sets of UEs defined by MCS index under reuse one. To make this clear, consider MCS index 10. The reuse one rate plotted is simply the rate for that MCS scheme. The reuse three rate, is the effective mean bitrate of all UEs under reuse three, that under reuse one were served by MCS index 10. A way to think of this is that each MCS serves an area of the cell under reuse one, and the plot shows how the mean bitrate changes over each MCS-area when switching to reuse three.

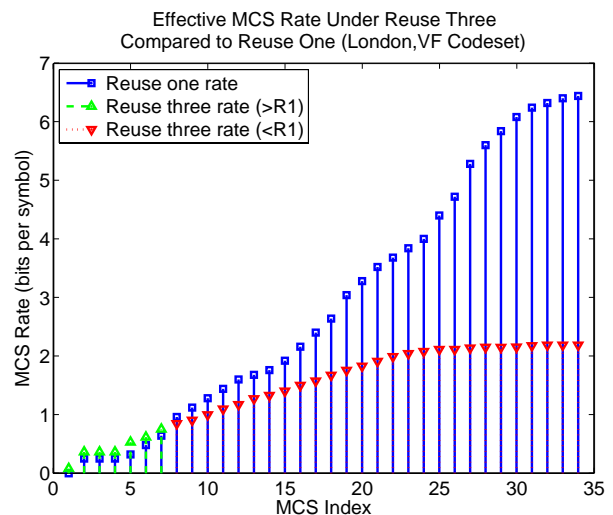


Fig. 8. Effective change in bitrate index when switching from reuse one to reuse three.

The points labelled with up arrows are those which result in an effective bitrate improvement and those labelled with down arrows an effective bitrate loss. As can be seen, some parts of the cell, namely those defined by low index MCS schemes, do benefit from switching to reuse three. It follows that the

mean cell result is determined by the relative proportional use of each MCS scheme. Figure 9 plots the relative proportional use of each MCS scheme under reuse one.

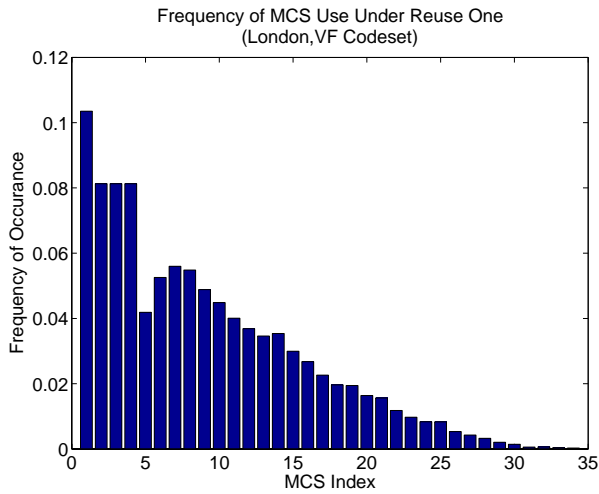


Fig. 9. Frequency of MCS use under reuse one.

When the MCS distribution shown in Figure 9 is considered against the effective bitrate changes shown in Figure 8, the outcome is that approximately 50% of the UEs gain from switching to reuse three, and approximately 50% do not gain. When reuse three wins out, a mean improvement of ≈ 0.13 bits per symbol is obtained, whereas when reuse one wins out, a mean improvement of ≈ 1.88 bits per symbol is obtained. The overall result is that reuse one wins out when the whole cell is taken into account, as was illustrated in Figure 6. It should now be clear that the mean cell result is determined by three items:

- 1) The change in SINR distribution brought about by the coordination of interference.
- 2) How this corresponds to a change in MCS schemes used due to the gradient of the MCS lookup curve.
- 3) The relative proportional use of each MCS scheme before coordination.

Clearly then, these items are critical, and anything that changes them can change the outcome of the competition between reuse three and reuse one, or in general reuse one and some other interference scheme such as soft reuse that improves SINR. From this it follows that scheduling policy plays a crucial role in determining whether a given interference coordination scheme brings about a benefit or not. The scheduler decides which UEs receive resources, and thus modifies the relative proportional use of MCS schemes, which is the third item above.

For schedulers which bias the resource allocation to low SINR UEs, or for cells which have a very large percentage of low SINR UEs, there is likely to be a benefit from statically applied soft reuse schemes. In other cases, there will not be. However, the exact scheduling strategy and exact UE distribution will determine the overall result and should be examined on a case by case basis.

To summarise: in the mean, no net benefit is obtained

from the application of any soft reuse scheme tested. The reason for this has been clearly explained in terms of the interaction between SINR distributions, MCS lookup curve, and proportional use of MCS schemes.

In the next section soft reuse is applied to a fixed rate scheduler to get some idea how in practise, scheduling shifts the relative proportional use of MCS schemes, and whether or not this results in an overall benefit under soft reuse.

V. FIXED RATE RESULTS

In this section a semi-realistic scheduler is examined whose goal is to satisfy as many UEs as possible, where each UE has the same fixed bitrate target. The scheduler operates as described below:

```

ForEach (UE in Scheduling Order) : Do
  Allocate VRBs from the BSB Until :
    No VRBs remain
  OR UE is satisfied.
  Allocate VRBs from the ASB Until :
    No VRBs remain
  OR UE is satisfied.
  Update satisfied UE count accordingly
Done

```

The scheduler always allocates the best resource, the BSB, first. This means that the scheduling order is important. To investigate the impact of which UEs get preference for the BSB, three scheduling orders were considered:

- 1) Greedy - The UEs are scheduled according to wideband SINR in descending order from best to worst.
- 2) Random - The UEs are scheduled in random order.
- 3) Leftist - The UEs are scheduled according to wideband SINR in ascending order from worst to best.

Note that the third of these is the approach which is usually promoted in the literature (see for example [18], [26], [38], [39]), namely that the boosted part of the spectrum should be given to the "cell-edge" UEs.

The complete process for obtaining results, which is executed for each fixed rate target, and each scheduling strategy, is as follows:

```

ForEach (Soft Reuse Power Ratio) : Do
  ForEach ( Cell ) In ( Scenario ) : Do
    ForEach ( Random seed in 1 to 1000 ) : Do
      Drop 25 UEs at random
      Schedule the UEs
      Record number of satisfied UEs
    End
    Compute mean over all UE drops
  End
  Compute mean over all cells
End

```

Figure 10 plots the number of satisfied UEs, under the best soft reuse power ratio, for each bitrate target, and for each of the scheduling strategies.

The results are surprising and show that giving the BSB to the "cell-edge" UEs, actually results in the worst performance. It turns out that it is always best to be greedy and give the BSB to the best SINR UEs, at least for the scheduler examined. Note that the number of UEs satisfied never reaches

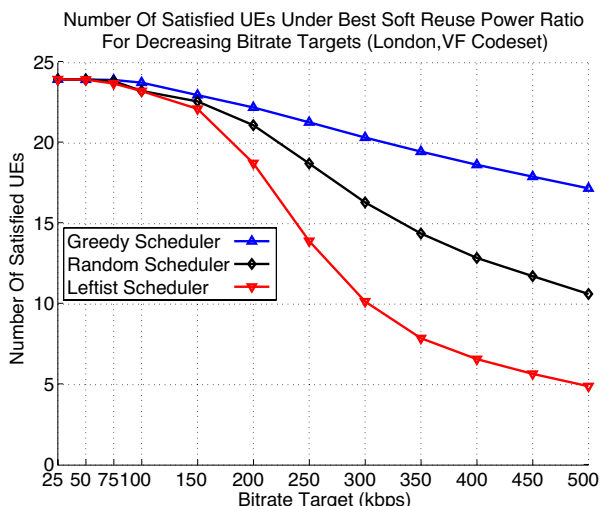


Fig. 10. Number of satisfied UEs under the best performing soft reuse power ratio, for each bitrate target.

the maximum 25, this is because the Monte Carlo simulation samples some areas which cannot receive any throughput under the MCS lookup curve used. In practise however, time dependent variation, and partial loading, should allow all UEs to be satisfied for reasonable bitrate targets.

Figure 10 plots the number of satisfied UEs under the best soft reuse power ratio for each fixed rate target. It does not specify which soft reuse power ratio is best for each fixed rate target. For the greedy scheduler, the only scheduler of interest given the above results, the answer is as follows: for bitrate targets 500 down to 200, reuse one satisfies the greatest number of UEs, and for bitrate targets 150 and below, reuse three satisfies the greatest number of UEs.

Thus, no intermediate soft reuse scheme ever does better than either reuse one or reuse three in this scheduling scenario. Given that either reuse one or reuse three satisfies the greatest number of UEs, Figure 11 plots the ratio of the number UEs satisfied under reuse three, to the number satisfied under reuse one.

When 25 UEs are trying to get 500kbps each, the system is overloaded, and in this case reuse one satisfies upto 10% more UEs than reuse three. For the lower load and saturation states, reuse three satisfies upto 4% more UEs than reuse one. The former gain comes about because the greedy scheduler prioritises UEs with a high MCS which benefit *most* from having the full resource available to them. The latter gain comes about because reuse three is able to serve UEs which cannot be served under reuse one due to the cut-off point in throughput caused by the lookup curve. In practise this gain is likely to be diminished because time-dependent fading will periodically bring cut-off UEs into service.

Furthermore, given the results of Section IV, it will be observed that any reuse three gain will come at the cost of reduced mean rate, and will only be apparent for low bitrate targets. Thus it is unlikely in practise that any significant gain in fixed rate satisfaction would be observed from the application of soft-reuse in the general case.

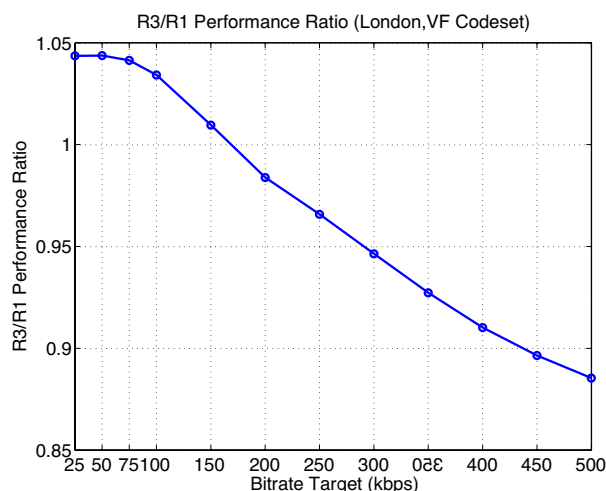


Fig. 11. Ratio of satisfied UEs under reuse three to satisfied UEs under reuse one, for each bitrate target.

VI. DISCUSSION

A. Summary

The conditions under which soft reuse can be expected to benefit have been clearly enumerated: SINR distribution shift under ICIC, SINR to MCS mapping, and proportional usage of each MCS scheme before and after ICIC. In addition, the intuitive notion that the “cell-edge” UEs should receive the boosted part of the spectrum has been demonstrated false in the case of a fixed bitrate service class presented.

B. Scope of results

It may be argued that the results presented here are too specific, and that they “overfit” the particular London scenario examined. Given this possibility, the experiments presented were repeated for a 57 cell hexagonal environment and repeated again for the 3GPP codeset shown in Figure 4.

In the hexagonal case, there are greater benefits from coordination, but overall the mean rate still favours reuse one, and the fixed rate scheduling outcome shows the same trends described here. Using the 3GPP codeset, the only differences observed are expected lower throughputs, but no diversion from the trends. In summary, there are no qualitative differences in the results or the implications of the results. Note however that the degradation observed when switching from hexagons to the London scenario is likely to be even greater for femtocells and highly irregular networks. This is because the spatial orthogonality on which static reuse schemes depend, will be eroded.

C. Contributions of this paper

The novel contributions of this work are threefold:

- The primary factors which manifest static reuse results are illustrated through a simple example. These are: SINR distribution shift under ICIC, SINR to MCS mapping, and proportional usage of each MCS before and after ICIC due to user distribution and scheduling strategy. Different

scheduling strategies may manifest fundamentally different outcomes for a given ICIC approach.

- Simulations are performed for a realistic London deployment, and all results are quantified statistically. This is in contrast to former work cited.
- The assumption that the cell-edge UEs should be assigned the best resources, implied by former work, is challenged and demonstrated false for the traffic class examined.

VII. CONCLUSION

We propose examining results in terms of relative MCS improvement curves *given* the scheduler examined as we have done here, rather than solely in terms of CDF shifts due to the soft reuse scheme applied. The former approach captures the important interactions between UE distribution, scheduling strategy, and MCS codeset, whereas the latter only reflects the SINR change independent of these.

The notion that it is better to give “cell-edge” UEs the resources having a high reuse factor has been demonstrated false in the case examined here.

REFERENCES

- [1] “3GPP TR 25.913, V9.0.0: Requirements for Evolved UTRA (E-UTRA) and Evolved UTRAN (E-UTRAN),” 2009.
- [2] “3GPP TS 36.942 - V8.2.0 - Evolved Universal Terrestrial Radio Access (E-UTRA); Radio Frequency (RF) system scenarios,” May 2009.
- [3] Mahmudur Rahman and Halim Yanikomeroglu and William Wong, “Interference Avoidance with Dynamic Inter-Cell Coordination for Downlink LTE System,” in *WCNC'09: Proceedings of the 2009 IEEE conference on Wireless Communications & Networking Conference*. Piscataway, NJ, USA: IEEE Press, 2009, pp. 1238–1243.
- [4] Alexander L. Stolyar and Harish Viswanathan, “Self-organizing Dynamic Fractional Frequency Reuse for Best-Effort Traffic Through Distributed Inter-cell Coordination,” in *INFOCOM 2008. The 27th Conference on Computer Communications. IEEE*, April 2008, pp. 691–699.
- [5] W. Wu, M. Gitlits, and T. Sakurai, “Dynamic resource allocation with inter-cell interference coordination for 3GPP LTE,” *Microwave Conference, 2008. APMC 2008. Asia-Pacific*, pp. 1–4, dec. 2008.
- [6] Zhifeng Tao et al and Toshiyuki Kuze, “Dynamic Inter-cell Interference Coordination (ICIC) and Signaling,” 2008.
- [7] X. Zhang, C. He, L. Jiang, and J. Xu, “Inter-cell interference coordination based on softer frequency reuse in ofdma cellular systems,” jun. 2008, pp. 270–275.
- [8] R. Chang, Z. Tao, J. Zhang, and C.-C. Kuo, “Multicell ofdma downlink resource allocation using a graphic framework,” *Vehicular Technology, IEEE Transactions on*, vol. 58, no. 7, pp. 3494–3507, sep. 2009.
- [9] N. Himayat, S. Talwar, A. Rao, and R. Soni, “Interference management for 4g cellular standards [wimax/lte update],” *Communications Magazine, IEEE*, vol. 48, no. 8, pp. 86–92, aug. 2010.
- [10] Ericsson, “R1-074444: On Inter-cell Coordination Schemes without/with Traffic Load Indication,” *3GPP TSG-RAN WG1 Meeting #50, Shanghai, China, October 2007*.
- [11] Marc C. Necker, “Scheduling Constraints and Interference Graph Properties for Graph-based Interference Coordination in Cellular OFDMA Networks,” vol. 14, no. 4, pp. 539–550, 2009.
- [12] M. Necker, “Towards Frequency Reuse 1 Cellular FDM/TDM Systems,” in *Proceedings of the 9th ACM/IEEE International Symposium on Modeling, Analysis and Simulation of Wireless and Mobile Systems (MSWiM 2006)*, October 2006.
- [13] M. C. Necker, “Integrated scheduling and interference coordination in cellular ofdma networks,” sep. 2007, pp. 559–566.
- [14] F. Xiangning, C. Si, and Z. Xiaodong, “An Inter-Cell Interference Coordination Technique Based on Users Ratio and Multi-Level Frequency Allocations,” in *Wireless Communications, Networking and Mobile Computing (WiCom 2007)*, September 2007, pp. 799–802.
- [15] Gabor Fodor and Chrysostomos Koutsimanis and Andrs Rcz and Norbert Reider and Arne Simonsson and Walter Muller, “Inter-cell Interference Coordination in OFDMA Networks and in the 3GPP Long Term Evolution System,” *Journal of Communications*, vol. 4, no. 7, pp. 445–453, August 2009.
- [16] Gary Boudreau and John Panicker and Ning Guo and Rui Chang and Neng Wang and Sophie Vrzic, “Interference Coordination and Cancellation for 4G Networks,” *IEEE Communications Magazine*, vol. 47, no. 4, April 2009.
- [17] China Mobile Research Institute, “C-RAN: The Road Towards Green RAN. White Paper. Version 1.0.0.” April 2010.
- [18] Huawei, “3GPP TSG RAN WG1 Meeting #41, R1-050507 - Soft Frequency Reuse Scheme for UTRAN LTE,” 2005.
- [19] Siemens, “3GPP TSG RAN WG1 Meeting #41, R1-050476: Evolved UTRA uplink scheduling and frequency reuse,” 2005.
- [20] Huawei, “3GPP TSG RAN WG1 Meeting Ad Hoc Meeting, R1-050629 - Inter-cell Interference Mitigation.doc,” 2005.
- [21] Ericsson, “3GPP TSG RAN WG1 Meeting #42, R1-050764 - Inter-cell Interference Handling for E-UTRA,” 2005.
- [22] Alcatel, “3GPP TSG RAN WG1 Adhoc Meeting, R1-050593 - Interference coordination for evolved UTRA uplink access,” 2005.
- [23] T. Instruments, “R1-051059: Inter-Cell Interference Mitigation for E-UTRA,” October 2005.
- [24] Nokia, “3GPP TSG RAN WG1 Meeting #44, R1-060291: OFDMA Downlink Inter-cell Inteferece mitigation,” 2006.
- [25] N. D. Ericsson, “TSG-RAN WG1 meeting #44, R1-060586 - Downlink and uplink inter-cell interference co-ordination/avoidance - impact on the specifications,” 2006.
- [26] Mohammad Abaii et al., “IST-4-027756. WINNER II D4.7.2 v1.0. Interference avoidance concepts.”
- [27] Texas Instruments, “3GPP TSG RAN WG1 Meeting #44, R1-060368 - Performance of Inter-Cell Inteferece Mitigation with Semi-Static Frequency Planning for EUTRA Downlink.txt,” 2006.
- [28] Ericsson, “R1-061374: Downlink inter-cell interference coordination/avoidance evaluation of frequency reuse,” May 2006.
- [29] IPWireless, “3GPP RAN WG1 Ad Hoc Meeting, R1-050652 - Attaining the Cell Edge Performance Requirements for the LTE Downlink,” 2005.
- [30] Siemens, “3GPP RAN WG1 Ad Hoc Meeting, R1-060135 - Interference Mitigation by Partial Frequency Reuse,” 2006.
- [31] Raymond Kwan and Cyril Leung, “A Survey of Scheduling and Interference Mitigation in LTE. Article ID 273486,” *Journal of Electrical and Computer Engineering*, vol. 2010.
- [32] “3GPP TS 36.211 - V8.7.0 - Evolved Universal Terrestrial Radio Access (E-UTRA); Physical Channels and Modulation,” May 2009.
- [33] “Vodafone Group Plc. Homepage. Accessed 28.09.10,” http://www.vodafone.com/hub_page.html.
- [34] I. Corporation, “3GPP TRG1-01-0030, Further Results on CPICH Interference Cancellation as A Means for Increasing DL Capacity.”
- [35] “Atoll Overview. Forsk website. Accessed 10/04/10,” <http://www.forsk.com/web/EN/11-atoll-overview.php>.
- [36] B D Hall and R Willink, “Does “Welch-Satterthwaite” make a good uncertainty estimate?” *Metrologica*, vol. 38, no. 1, 2001.
- [37] Andras Racz and Norbert Reider and Gabor Fodor, “On the Impact of Inter-Cell Interference in LTE,” in *Global Telecommunications Conference, 2008. IEEE GLOBECOM 2008. IEEE*, 2008, pp. 1–6.
- [38] Xiang Yikang, Luo Jijun, and Christian Hartmann, “Inter-cell Interference Mitigation through Flexible Resource Reuse in OFDMA based Communication Networks,” in *In proceedings of 13th European Wireless Conference (EW'07), Paris, France*, April 2007.
- [39] X. Xiang, F. Liu, and Y. Ji, “Simulation based performance evaluation of ICI mitigation schemes for broadband wireless access networks,” in *CNS '08: Proceedings of the 11th communications and networking simulation symposium*. New York, NY, USA: ACM, 2008, pp. 181–187.

Power-efficient Irregular Repeat-Accumulate Encoded BICM-ID for 16-ary Signal Constellations

Wei Kwang Han, Stephane Le Goff and Bayan Sharif
Newcastle University, Newcastle upon Tyne, United Kingdom
Email: weikwang.han@gmail.com, {stephane.le-goff, bayan.sharif}@ncl.ac.uk

Arafat Al-Dweik
Khalifa University of Science, Technology and Research, Sharjah, United Arab Emirates
Email: dweik@kustar.ac.ae

Abstract— The design of power-efficient forward error correction techniques over additive white Gaussian noise (AWGN) and frequency non-selective fading channels is considered in this work. The aim of this paper is to investigate the application of BICM with iterative demodulation and decoding (BICM-ID) system with irregular repeat-accumulate (IRA) codes to minimize the bit error rate (BER) and determine the most suitable constellation and mapping pairs for designing power-efficient BICM-ID systems over AWGN and Rayleigh fading channels using the concept of channel capacity limit. Simulation results have confirmed that a remarkable BER improvement can be achieved using the proposed design criterion. Based on the IRA-encoded BICM-ID technique considered, the BER improvement gained is exhibited either as an additional coding gain, error floor elimination, or both. The code components include the IRA codes, irregular low-density parity-check (LDPC) codes and convolutional codes (CC). The modulation technique considered is the widely-used 16-ary constellations with various bit mappings.

Index Terms— channel capacity, coded modulation, error correction codes, iterative decoding, OFDM, LTE

I. INTRODUCTION

Trellis-coded modulation (TCM) [1] achieves good performance over additive white Gaussian noise (AWGN) channel by maximizing the free Euclidean distance using set partitioning (SP). For fading channels, the TCM code performance is dominated by the minimum Hamming distance between the coded symbol sequences rather than the minimum Euclidean distance. As a consequence, a new approach called bit-interleaved coded modulation (BICM) was developed by Zehavi [2] to increase the time diversity of the coded modulation at the expense of reducing the free squared Euclidean distance (FED), resulting in degradation over AWGN

channels [2], [3]. BICM is a spectrally efficient coded modulation technique and it is well-suited for bandwidth efficient transmission over fading channels. The optimum receiver of the BICM is composed of a joint demapper and decoder. However, due to the high complexity of the optimum receiver, a low complexity receiver can be constructed when the demapping and decoding are decoupled. BICM with iterative demodulation and decoding (BICM-ID) achieves a turbo-like performance using 8-PSK and 16-QAM modulation over both AWGN and fading channels [4]-[6].

The optimised selection of the channel code and mapping leads to near capacity performance [7]. The selection process includes combinations of Gray mapping with powerful channel codes [7], [8] such as turbo codes [9], low-density parity-check (LDPC) codes or repeat-accumulate (RA) codes [10], and combinations of non-Gray mapping with less powerful channel codes [8] such as the simple convolutional codes (CC). For turbo codes, it is well-known that the 16-QAM combined with Gray mapping are very well-matched for BICM schemes [7], [11]. However, some constellations have been reported to outperform the 16-QAM over both AWGN and fading channels [12], [13]. Hence, these constellations can be used to design BICM-ID schemes. Motivated by the performance improvement gained by combining turbo codes with BICM schemes, this paper investigates the application of irregular RA (IRA) codes in BICM-ID systems to improve the error performance [14], [15]. The encoding efficiency of LDPC codes is quadratic in the block length since encoding requires multiplication by the generator matrix which is not sparse. On the other hand, the generator matrix for IRA codes is sparse. Similar to RA codes, IRA codes can be represented as a class of "turbo-like" codes and a class of LDPC codes. The aim of this paper is to investigate the application of BICM-ID system with IRA codes and determine the most suitable combinations of 16-ary constellations and mappings for designing power-efficient BICM-ID systems for AWGN and Rayleigh fading channels.

Manuscript received September 09, 2010; revised April 27, 2011; accepted June 25, 2011.

The BICM and BICM-ID schemes can be designed by employing any two-dimensional constellation. In this paper, we consider the design criterion of finding the best signal constellation and mapping pairs to construct power-efficient BICM and BICM-ID schemes, over AWGN and fading channels, by using the concept of channel capacity limit. The capacity limit of BICM for various 16-ary signal constellations is then evaluated. It is worthwhile to note that the channel capacity of a BICM system is defined regardless the channel code used and the existence of iterative decoding [16]. The idea of evaluating capacity limits to find the best signal constellation and mapping pair comes from the fact that power-efficient BICM and BICM-ID schemes usually employ state-of-the-art codes, and are thus capable of achieving near-capacity performance. For illustrating the obtained results, the BER performance of BICM and BICM-ID systems using various signal constellation and mapping pairs with other selected error-correcting codes influencing the error performance of BICM and BICM-ID schemes is investigated via computer simulations.

The rest of the paper is organised as follows. Section II provides a background of the generic structure of BICM-ID and the IRA codes. Section III provides a design criterion for choosing the best parameters for BICM-ID schemes by evaluating capacity limits of various 16-ary constellation-mapping pairs to determine the optimum pair. Section IV is devoted for computer simulation results obtained for several BICM and BICM-ID schemes comprised of selected error-correcting codes with various signal constellations and mappings. Section V describes combination of BICM and OFDM in the context of 4G standards. Finally, Section VI concludes the paper.

II. OVERVIEW OF BICM-ID AND IRA CODES

A. BICM-ID with soft-decision feedback

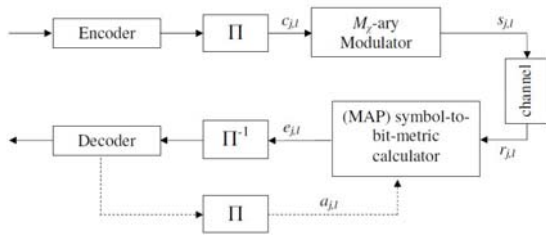


Figure 1. Structure of a BICM-ID transmission system. The dashed arrows represent iterations between RA decoder and the symbol-to-bit metric calculator.

A BICM-ID transmission system can be modelled as an interleaved concatenation of an encoder and a symbol mapper as shown in Fig. 1. Consider a 2^{m_b} -ary modulation represented by a two-dimensional signal constellation χ where $|\chi| = 2^{m_b} = M_\chi$. Let $\mathbf{c}_j = \{c_{j,1}, \dots, c_{j,m_b}\} \in \{0,1\}^{m_b}$, $1 \leq j \leq N/m_b$, denote a set of m_b bits at the modulator input, N denotes the length of the codeword, $c_{j,1}$ is the most significant bit (MSB), and c_{j,m_b} is the least significant bit (LSB). A bit-reliability mapping [17] is employed where the systematic bits of a codeword are mapped to the more significant bits of the signal constellation and the parity-

check bits are mapped to the less significant bits. In this paper, both AWGN and Rayleigh fading channel models are considered. The received complex symbol is $r_j = h_j s_j + n_j$, where n_j is a Gaussian noise sample with zero mean and variance $\sigma^2 = N_0/2$, N_0 being the one-sided power spectral density of white Gaussian noise and h_j is the complex time-invariant fading gain whose fading coefficients are normally distributed with zero mean and variance 1/2. It is worthy to note that $h_j = 1$ for AWGN channels. In this paper, perfect channel state (CSI) is assumed. For Rayleigh fading channels, the fading coefficients are normally distributed with zero mean and variance 1/2. At the receiver side, the channel outputs and the *a priori* log-likelihood ratios (LLRs) $a_{j,l}$ obtained from the decoder feedback are processed by the demapper to obtain the extrinsic LLRs $e_{j,l}$ for $l = 1, \dots, m_b$. The *a priori* and extrinsic LLRs are defined as,

$$a_{j,l} = \ln \left[\frac{P(c_{j,l} = 1)}{P(c_{j,l} = 0)} \right], \quad (1)$$

$$e_{j,l} = \ln \left[\frac{\sum_{s_j \in \chi^1} \exp \left\{ -\frac{(r_j - h_j s_j)^2}{N_0} + \sum_{i=1, \neq l}^{m_b} s_{j,i} a_{j,i} \right\}}{\sum_{s_j \in \chi^0} \exp \left\{ -\frac{(r_j - h_j s_j)^2}{N_0} + \sum_{i=1, \neq l}^{m_b} s_{j,i} a_{j,i} \right\}} \right], \quad (2)$$

where χ^t denotes the signals $s_j \in \chi$ whose labels have the value $t \in \{0, 1\}$. There is no feedback from the decoder to the demapper during the initial demapping, hence the *a priori* LLRs $a_{j,l}$ are set to zero. For subsequent iterations, the extrinsic information from the decoder is fed back as *a priori* information at the demapper.

B. Systematic IRA codes

The selection of the channel coding scheme can improve the BER performance of BICM and BICM-ID systems. Error floors can be reduced or eliminated by employing turbo-like codes (LDPC, RA) instead of CC. In this section, we consider the construction of IRA codes. The idea of jointly iterative detection and decoding has been proposed in [18]-[20]. The encoding of IRA codes is achieved by randomly generating its parity check matrix using the simple bit-filling algorithm [21] without any optimisation performed to the degree distributions of the IRA codes.

A systematic IRA code can be considered as an LDPC code which can be represented using a parity-check matrix \mathbf{H} ,

$$\mathbf{H} = [\mathbf{H}_1 \ \mathbf{H}_2]. \quad (3)$$

As shown in Fig. 2, the matrix \mathbf{H}_1 is an $M \times K$ matrix with column weights q_1, \dots, q_K and row weights p_1, \dots, p_M , the matrix \mathbf{H}_2 is an $M \times M$ matrix. The location of the nonzero entries is determined by the interleaver. An example illustrating an IRA code of length 15 with a parity-check matrix as described by (3) and Tanner graph is depicted in Fig. 2.

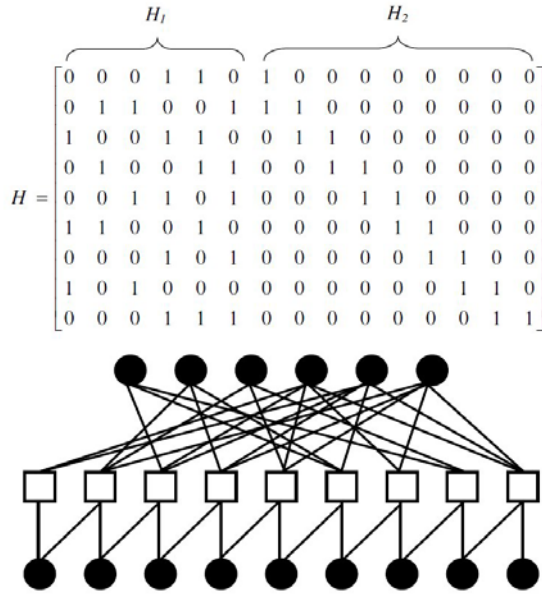


Figure 2. Parity-check matrix and Tanner graph representation of an IRA code of length 15 with $q=[3,3,3,5,5,5]$, $p=[2,3,3,3,3,2,2,3]$ and interleaver pattern $\Pi=[10,15,4,7,20,1,11,16,5,17,21,8,12,22,2,6,18,13,23,3,9,14,19,24]$.

For IRA codes, the variable node degree distribution in the code's Tanner graph is represented by $\nu(x) = \sum_i \nu_i x^{i-1}$ and the check node degree distribution is given by $\rho(x) = \sum_k \rho_k x^{k-1}$. The coefficient ν_i is the fraction of the Tanner graph edges connected to variable nodes of degree i . The row degrees are similarly represented by $\rho(x)$. Hence, the number of variable nodes and check nodes of degree i are given by

$$N_v(i) = N \left[\frac{\nu_i / i}{\sum_k \nu_k / k} \right], \quad (4)$$

$$N_c(i) = N \left[\frac{\rho_i / i}{\sum_k \rho_k / k} \right]. \quad (5)$$

To construct systematic IRA codes, there must be at least M nodes of degree-2 required by the accumulator. Moreover, short cycles involving only degree-2 variable nodes are avoided by setting $N_v(i) = M - 1$ [22]. Similar to IRA codes, parity-check matrix of an irregular LDPC (LDPC) code can be represented in the form of (3). The systematic generator matrix \mathbf{G} for the parity-check matrix from (3) of a systematic IRA code is represented by (6) where \mathbf{I} is the $K \times K$ identity matrix and \mathbf{P} is of dimension $K \times M$.

$$\mathbf{G} = [\mathbf{I} \mathbf{P}] = [\mathbf{H}_1^T \mathbf{H}_2^T]. \quad (6)$$

The decoding of IRA codes employs the message passing algorithm which is an efficient iterative decoding algorithm used also for the decoding of LDPC codes [23], [24]. The message passing algorithm comprises two stages which are the initialisation and iteration. Let M_n be defined as the set of check nodes connected to variable node n and let N_m be expressed as the set of variable nodes connected to check node m . $M_{n,m}$ represents the set

M_n , excluding check node m and $N_{m,n}$ describes the set N_m excluding variable node n . During the initialisation stage, each bit node computes its message defined in (7) and sends it to M_n .

$$\lambda_n^{[\tau=0]} = \ln \left[\frac{P(e_n | v_n = 1)}{P(e_n | v_n = 0)} \right] = L_c e_n, \quad 1 \leq n \leq N. \quad (7)$$

The symbols τ , e_n and v_n correspond to the decoding iteration number, the extrinsic LLRs from the demapper defined in (2) and systematic codeword, respectively. The channel reliability $L_c = 2\sqrt{E_c}/\sigma^2$ where E_c and σ^2 denote the energy per coded bit and the variance of the channel noise respectively. Each iteration has two different phases known as the check node update and variable node update which are described in (8) and (9), respectively.

$$\eta_{m,n}^{[\tau]} = -2 \tanh^{-1} \left[\prod_{j \in N_{m,n}} \tanh \left(-\frac{\lambda_j^{[\tau-1]} - \eta_{m,j}^{[\tau-1]}}{2} \right) \right], \quad (8)$$

$$\lambda_{n,m}^{[\tau]} = L_c e_n + \sum_{m \in M_{n,m}} \eta_{m,n}^{[\tau]}. \quad (9)$$

Equation (9) refers to the message that the bit node n sends to its check node m [25]. The intrinsic term $L_c e_n$ is determined by the measurement e_n influencing the bit c_n . The extrinsic term $\sum \eta_{m,n}^{[\tau]}$ is determined by the information given by all other observations and the code structure where $\eta_{m,n}$ is referred to as the message which is passed from the check node m to the bit node n during the τ -th iteration. These messages iterate among the variable nodes and check nodes to compute the *a posteriori* LLR for each variable node [4]. The LLR for each variable node is given by (10) where $\mathbf{E} = [e_1, e_2, \dots, e_N]$ is the received extrinsic LLRs from the demapper.

$$\lambda_{n,m} = \ln \left[\frac{P(v_n = 1 | E)}{P(v_n = 0 | E)} \right] = L_c e_n + \sum_{m \in M_{n,m}} \eta_{m,n}. \quad (10)$$

III. CONSTELLATION-MAPPING PAIRS DESIGN CRITERION FOR BICM-ID SCHEMES

The selection of the best signal constellation and mapping pairs for BICM-ID schemes can be achieved based on the concept of channel capacity limit which is a computationally efficient technique. The 16-ary signal constellations are focused because they are widely used in many standards and practical systems such as WLAN, DVB, DAB, WiMAX, and coherent optical communication systems. The 16-ary constellations considered are the rectangular 16-QAM, optimum, (1, 5, 10) and (5, 11) which have been found to be the most power-efficient constellations for coded and uncoded systems over AWGN and fading channels [7], [11]-[13]. The exact locations of the signal points in (1, 5, 10) and (5, 11) are reported in [13]. Since the channel code and the mapping should be well-matched to achieve near capacity performance, various types of mappings are considered in this paper. This includes the Gray, Schreckenbach (Schrec), modified set partitioning (MSP)

and maximum squared Euclidean weight (MSEW). The Schreckenbach mappings optimised for AWGN and Rayleigh fading channels are represented by $M16^a$ and $M16^c$, respectively and are obtained using the binary searching algorithm (BSA) [26]. However, for the 16-ary non-square constellations, some of these mappings are not applicable due to the structure of such constellations.

Mapping by set partitioning was originally proposed for TCM systems, hence it might not lead to optimum results for BICM-ID. It is shown in [6], [27] that the improvement of error performance for a BICM-ID scheme with SP mapping is not significant. As a result, quasi-Gray, quasi-MSEW and quasi-MSEW mappings are used which are as close as possible to their respective mappings. The best combinations of rectangular and non-rectangular 16-ary signal constellations with mappings (Fig. 3) for error-correcting codes considered in this paper are selected based on the BICM capacity limit, which is discussed in the next paragraph.

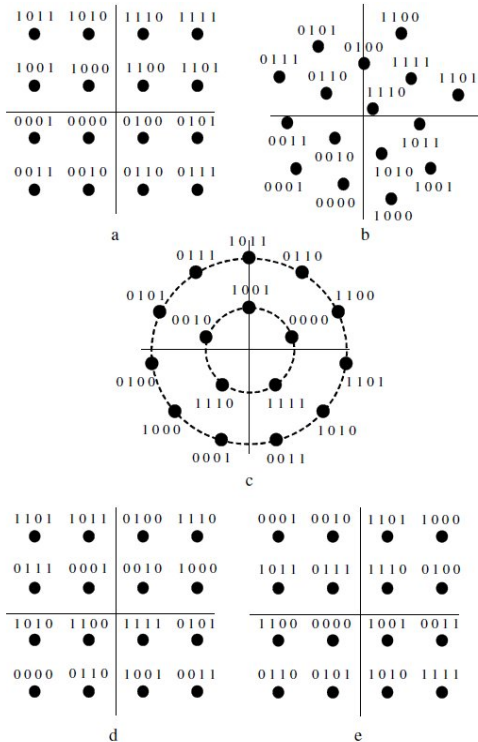


Figure 3. Optimal combinations of 16-ary signal constellations with mappings considered in this work. (a) 16-QAM signal constellation with Gray mapping, (b) optimum signal constellation with quasi-Gray mapping, (c) (5,11) signal constellation with quasi-MSEW mapping, (d) 16-QAM signal constellation with $M16^a$ mapping, (e) 16-QAM signal constellation with $M16^c$ mapping.

The expression of the BICM capacity limit over AWGN channels is evaluated to determine the most suitable constellation-mapping pairs. Consider a two-dimensional constellation χ of size $|\chi| = 2^{m_b}$. Based on the general results reported in [3], we can demonstrate that, under the constraint of uniform-input distribution and assuming ideal bit-by-bit interleaving, the capacity C of a BICM system using 2^{m_b} -ary constellation is expressed over AWGN channels as

$$C = m_b - \sum_{i=1}^{m_b} E_{c_j, r_j} \left[\log_2 \left[\frac{\sum_{z_j \in \chi} P(r_j | z_j)}{\sum_{z_j \in \chi_{i,c_j,i}} P(r_j | z_j)} \right] \right], \quad (11)$$

where $P(r_j|z_j)$ denotes the transition probability density function of the AWGN channel, E_{c_j, r_j} denotes the expectations with respect to c_j and r_j , and $\chi_{i,c_j,i}$ designates the subset of all the signals $z_j \in \chi$ whose labels have the value $c_{j,i} \in \{0, 1\}$ in position i . The capacity is expressed in information bits per channel use (bit/channel use) here, where each channel use corresponds to the transmission of a complex signal $z_j \in \chi$. Assuming an AWGN channel and performing some minor modifications, we finally obtain

$$C = E_{c_j, r_j} \left[m_b - \log_2 \frac{\left(\sum_{z_j \in \chi} \exp \left(-\frac{d_{r_j, z_j}^2}{2\sigma^2} \right) \right)^{m_b}}{\prod_{i=1}^{m_b} \sum_{z_j \in \chi_{i,c_j,i}} \exp \left(-\frac{d_{r_j, z_j}^2}{2\sigma^2} \right)} \right]. \quad (12)$$

where d_{r_j, z_j} is the Euclidean distance between the signals r_j and z_j . A general expression for representing the BICM capacity C for both AWGN and Rayleigh fading channel is given by

$$C = E_{c_j, r_j} \left[m_b - \log_2 \frac{\left(\sum_{z_j \in \chi} \exp \left(-\frac{(r_j - h_j \cdot z_j)^2}{2\sigma^2} \right) \right)^{m_b}}{\prod_{i=1}^{m_b} \sum_{z_j \in \chi_{i,c_j,i}} \exp \left(-\frac{(r_j - h_j \cdot z_j)^2}{2\sigma^2} \right)} \right]. \quad (13)$$

Moreover, (13) is used to evaluate the capacity when the mapping method is taken into consideration.

The capacity of a BICM is defined regardless of the channel code used as well as the presence of iterative demodulation and decoding [16]. Hence, the capacity for both BICM and BICM-ID can be defined using (13) for any mapping method. It is well known that for both turbo-like codes such as IRA codes and irregular LDPC (ILDPC), the sparse random parity check matrices were employed to establish promising distance properties. Both turbo-like codes have good minimum distance and possess a very small average number of nearest neighbour codewords (provided that the girth is greater than 4 [25]). The girth is known as the length of the smallest cycle in a Tanner graph. That is why the turbo-like codes achieve excellent BER performance at low SNR. Hence, in order to design a power-efficient BICM and BICM-ID schemes at moderate BERs, a modulation scheme optimised for operation at low SNR should be employed. The optimisation by Gray mapping, mainly consisting of minimizing the average number of nearest neighbours of the modulation, shows a profound impact on the error performance of BICM [7] and BICM-ID [28] schemes. Hence, for the case of powerful channel codes

such as IRA codes, combined with Gray or quasi-Gray mapping is required to obtain high coding gain through iterative demodulation and decoding. To determine the optimal combination of 16-ary signal constellations with various Gray and quasi-Gray mappings for powerful channel codes, the BICM capacity C defined in (13) is evaluated for both AWGN and Rayleigh fading channels.

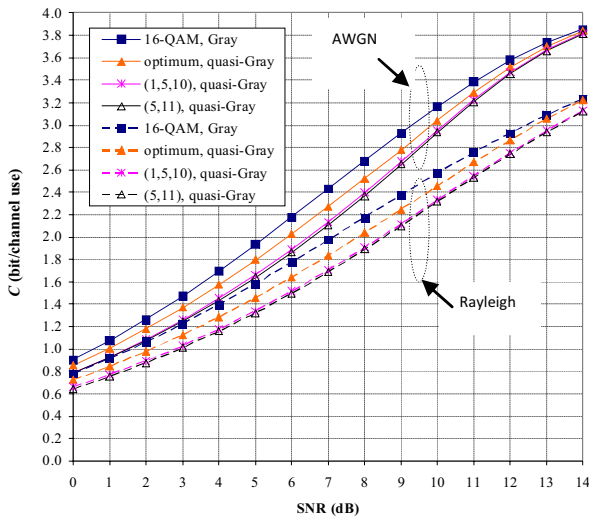


Figure 4. BICM capacity C versus SNR for different 16-ary signal constellations sets with Gray or quasi-Gray mappings over both the AWGN and Rayleigh fading channels for SNR ranging from 0 to 14 dB.

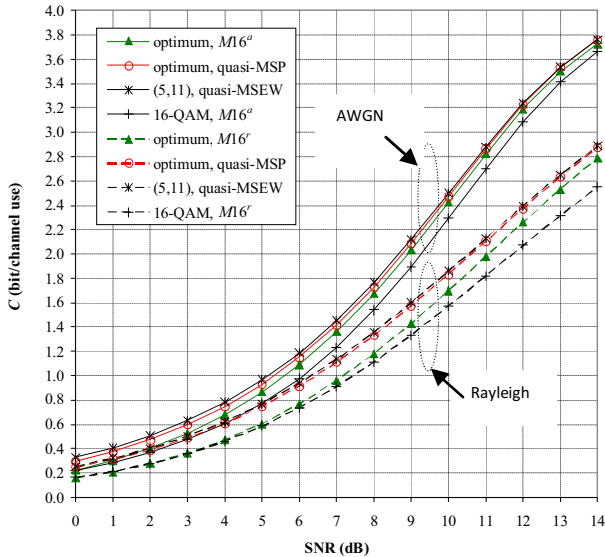


Figure 5. BICM capacity C versus SNR for different 16-ary signal constellations sets with non-Gray mappings over both the AWGN and Rayleigh fading channels for SNR ranging from 0 to 14 dB.

Fig. 4 shows the BICM capacity C versus SNR for various 16-ary signal constellations with Gray or quasi-Gray mappings over AWGN and Rayleigh fading channels. The SNR is defined as E_s/N_0 , where E_s is the average energy per symbol. By utilising Fig. 4, the capacity limit of BICM scheme for a required spectral efficiency ($S_{eff} = 2\text{-bit/s/Hz}$) can be attained for both AWGN and Rayleigh fading channels. Table I shows the

capacity limits or SNRs required to achieve error-free communications with a BICM scheme using various 16-ary signal constellations over AWGN and Rayleigh fading channels by employing Gray or quasi-Gray mappings. From Fig. 4, it can be noted that the best performance is achieved by the combination of rectangular 16-QAM signal constellation with Gray mapping over the entire SNR range considered for both AWGN and Rayleigh fading channels. For each of the non-Gray mappings, the best 16-ary signal constellation is selected and compared among the non-Gray mappings as shown in Fig. 5 for both AWGN and Rayleigh fading channels. From Table II, it is observed that for the case of non-Gray mappings, the combination of (5,11) signal constellation with quasi-MSEW mapping provides the best performance.

TABLE I.
CAPACITY LIMIT OF 2-BIT/S/Hz BICM FOR DIFFERENT 16-ARY SIGNAL CONSTELLATION SETS WITH GRAY OR QUASI-GRAY MAPPINGS.

Channel	Signal Constellations	Mapping Scheme	E_s/N_0 (dB)	E_p/N_0 (dB)
AWGN	16-QAM	Gray	5.26	2.25
AWGN	optimum	quasi-Gray	5.84	2.83
AWGN	(1,5,10)	quasi-Gray	6.45	3.44
AWGN	(5,11)	quasi-Gray	6.57	3.56
Rayleigh	16-QAM	Gray	7.06	4.05
Rayleigh	optimum	quasi-Gray	7.78	4.77
Rayleigh	(1,5,10)	quasi-Gray	8.41	5.40
Rayleigh	(5,11)	quasi-Gray	8.45	5.44

TABLE II.
CAPACITY LIMIT OF 2-BIT/S/Hz BICM FOR DIFFERENT 16-ARY SIGNAL CONSTELLATION SETS WITH NON-GRAY MAPPINGS.

Channel	Signal Constellations	Mapping Scheme	E_s/N_0 (dB)	E_p/N_0 (dB)
AWGN	optimum	$M16^a$	8.91	5.90
AWGN	optimum	quasi-MSP	8.77	5.76
AWGN	(5,11)	quasi-MSEW	8.67	5.66
AWGN	16-QAM	$M16^a$	9.28	6.27
Rayleigh	optimum	$M16^r$	11.08	8.07
Rayleigh	optimum	quasi-MSP	10.62	7.61
Rayleigh	(5,11)	quasi-MSEW	10.51	7.50
Rayleigh	16-QAM	$M16^r$	11.73	8.72

IV. SIMULATION RESULTS AND DISCUSSIONS

All the computer simulations consider the same codes having rate $R = 1/2$ and information block length $K = 2000$ bits. An interleaver block size of 4000 bits is used. The fading channels considered in this paper are frequency non-selective and frequency selective Rayleigh fading channels. The channel state information (CSI) is assumed to be known perfectly at the receiver side. A maximum of 10 iterations are performed between the decoder and demapper during iterative demodulation and decoding. For decoders using the message passing algorithm, a maximum of 100 decoding iterations are performed. The BER performance is investigated for

several 2-bit/s/Hz coded modulation schemes using optimal combinations of 16-ary constellations with various mappings. Table III presents the types of channel codes, signal constellations and mappings used in the simulations. The parameters d_v and d_c in Table III correspond to the variable node and check node degrees, respectively. The channel codes considered in this work are IRA codes, ILDPC codes and CC. Both IRA and ILDPC codes are constructed free of 4-cycles using the bit-filling algorithm. It is worthwhile to note that in the context of this paper, we use RA codes to represent an extended class of LDPC codes [22], thus the encoding complexity of both IRA and ILDPC codes are low. The irregular LDPC code for the simulations listed in Table III has weight-2 columns in its parity-check matrix, which is prone to error floors even for BPSK over AWGN channels. Hence, the error floors occurring in the simulations is due to the LDPC code itself. CC are constructed from a 4-state recursive systematic convolutional (RSC) codes with generator polynomials (7,5). Similar to turbo codes, BICM-ID can be added to RA/LDPC encoded BICM to achieve additional coding gain [6]. The effects of signal constellation and mapping combination from Fig. 3 on the BER performance for several BICMs and BICM-IDs are shown in Figs. 6 to 13. Each combination set of signal constellation and mapping is denoted by a different condition. A total of five conditions are provided in Table IV.

TABLE III. PARAMETERS CONSIDERED FOR THE SIMULATIONS. THE CODEWORD AND INTERLEAVER BLOCK SIZES USED FOR ALL CHANNEL CODES ARE 4000 BITS FOR $R = 1/2$. NOTE THAT THE NOTATION 'N/A' IN THE TABLE INDICATES THAT THE CC IS NOT DEFINED USING d_v AND d_c .

Channel	Codes	d_v	d_c	Signal Constellations	Mapping Scheme
AWGN/Ray	ILDPC	2,3	4,5	16-QAM	Gray
AWGN/Ray	ILDPC	2,3	4,5	optimum	quasi-Gray
AWGN/Ray	IRA	2,3,4,5,7,8	5,6	16-QAM	Gray
AWGN/Ray	IRA	2,3,4,5,7,8	5,6	optimum	quasi-Gray
AWGN	CC	N/A	N/A	16-QAM	$M16^a$
Ray	CC	N/A	N/A	16-QAM	$M16^c$
AWGN/Ray	CC	N/A	N/A	(5,11)	quasi-MSEW

TABLE IV. COMBINATIONS OF 16-ARY SIGNAL CONSTELLATIONS WITH DIFFERENT TYPES OF MAPPINGS FOR BOTH AWGN AND RAYLEIGH FADING CHANNELS.

Channel	Signal Constellations	Mapping Scheme	Condition
AWGN/Ray	16-QAM	Gray	A
AWGN/Ray	optimum	quasi-Gray	B
AWGN	16-QAM	$M16^a$	C
Ray	16-QAM	$M16^c$	D
AWGN/Ray	(5,11)	quasi-MSEW	E

The decoding algorithms employed by all the codes considered in this work are the message passing algorithm and BCJR algorithm. The BCJR algorithm is

also known as a message passing algorithm [29]. On the other hand, the encoding complexity of IRA codes and ILDPC codes are lower than some LDPC codes, which make them good alternatives for some LDPC codes. Both IRA codes and ILDPC codes have comparatively low encoding complexity as CC, but the coding gain achieved at BER of 10^{-5} using CC is much lower in comparison with IRA codes and ILDPC codes. Both IRA codes and ILDPC codes give comparable performance with IRA codes achieving the overall best performance at a BER of 10^{-5} over both AWGN and fading channels.

A. Performance of BICM/BICM-ID Schemes over AWGN Channels

In Fig. 6, for the case of rectangular 16-QAM signal constellation, it can be seen that IRA codes with condition A provide the best BER performance using BICM and BICM-ID systems. Moreover, pertaining to condition A, the performance gain with feedback is small for both IRA and ILDPC codes as the BICM-ID and BICM schemes give comparable BER performance using the same type of iterative decodable codes at a BER of 10^{-5} . In Fig. 6, for BICM-ID schemes, IRA codes (with condition A) outperform ILDPC codes (with condition A) and CC (with condition C) by approximately 0.3 dB and 0.81 dB, at a BER of 10^{-5} .

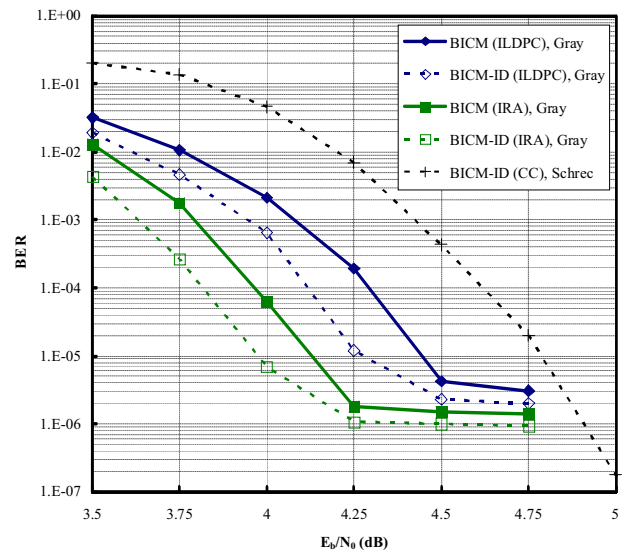


Figure 6. Performance comparison over AWGN channels among 2-bit/s/Hz BICM/BICM-ID schemes using channel codes and selected optimal combinations of rectangular 16-QAM signal constellations with mappings.

The non-rectangular 16-ary signal constellations with BICM schemes employing IRA and ILDPC codes with condition B provide comparable performance at a BER of 10^{-5} as depicted in Fig. 7. In addition, by considering condition B, the performance gain with feedback is moderate for both IRA and ILDPC codes. The BER performance gains between BICM-ID and BICM schemes using the same channel codes with condition B are approximately 0.88 dB and 1.18 dB for both IRA and ILDPC codes respectively, at a BER of 10^{-5} . Unlike the case of 16-QAM signal constellation, BICM-ID schemes using CC with condition E provide a comparable

performance to that of IRA and ILDPC codes with condition B.

The effects of rectangular and non-rectangular 16-ary constellations on BICM and BICM-ID schemes are shown in Figs. 8 and 9. For BICM schemes employing iterative decodable codes such as IRA and ILDPC codes, rectangular 16-QAM achieves a better BER performance than non-rectangular 16-ary constellations and IRA codes provide the best performance. For BICM-ID schemes, both rectangular and non-rectangular 16-ary constellations give comparable performance using IRA and ILDPC codes with IRA codes giving the best marginal BER performance, at a BER of 10^{-5} . Moreover, for 16-QAM signal constellation over AWGN channels as depicted in Fig. 6, the performance gain is minimal with iterative demodulation and decoding. However, error floors were lowered with iterative demodulation and decoding over the same AWGN channels by using powerful turbo-like codes and non-rectangular 16-ary signal constellations as shown in Fig. 7. Furthermore, it can be seen that BICM-ID employing IRA codes with 16-QAM and Gray mapping performs best over AWGN channels for spectral efficiency of 2-bit/s/Hz at low SNR as shown in Fig. 9. These results agree with those provided by Tables 1 and 2. The channel capacity limit for 2 bit/s/Hz 16-QAM BICM on AWGN channels is 2.25 dB. At a BER of 10^{-5} , the gap between the capacity and the performance of BICM-ID employing IRA codes with 16-QAM Gray mapping is 1.72 dB for AWGN channels.

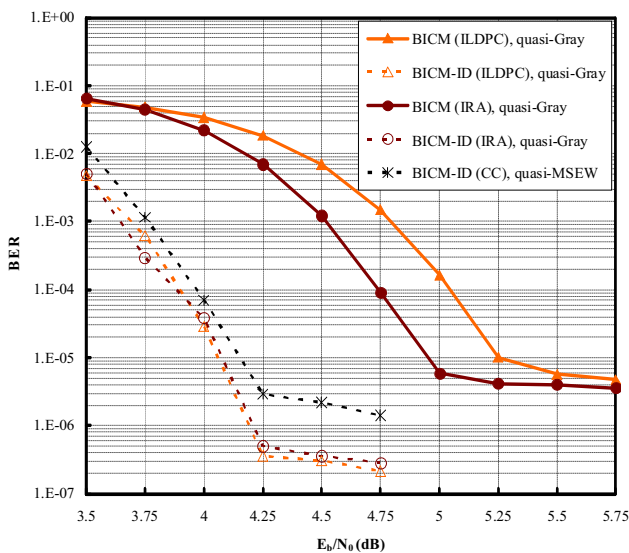


Figure 7. Performance comparison over AWGN channels among 2-bit/s/Hz BICM/BICM-ID schemes using channel codes and selected optimal combinations of non-rectangular 16-ary signal constellations with mappings. Both ILDPC and IRA codes employ optimum constellation while CC uses (5,11) constellation.

The effect of channel codes on BICM-ID schemes is shown in Fig. 9. For BICM-ID employing rectangular 16-ary signal constellations, IRA codes outperform CC at a BER of 10^{-5} . In addition, for BICM-ID employing non-rectangular 16-ary signal constellations, turbo-like codes such as IRA codes consistently perform better than CC, at

a BER of 10^{-5} . Overall, computer simulation results indicated that, at a BER of 10^{-5} , the best performance for BICM-ID scheme in AWGN channels is provided by IRA codes employing rectangular signal constellation with Gray mapping.

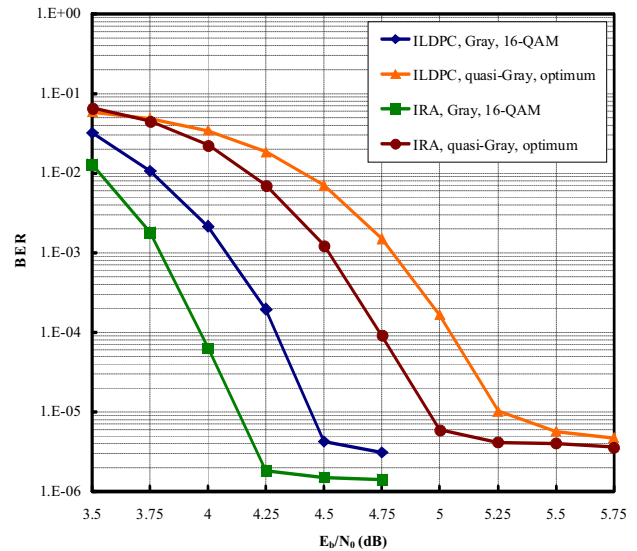


Figure 8. Performance comparison over AWGN channels among 2-bit/s/Hz BICM schemes using channel codes and selected optimal combinations of rectangular and non-rectangular 16-ary signal constellations with mappings.

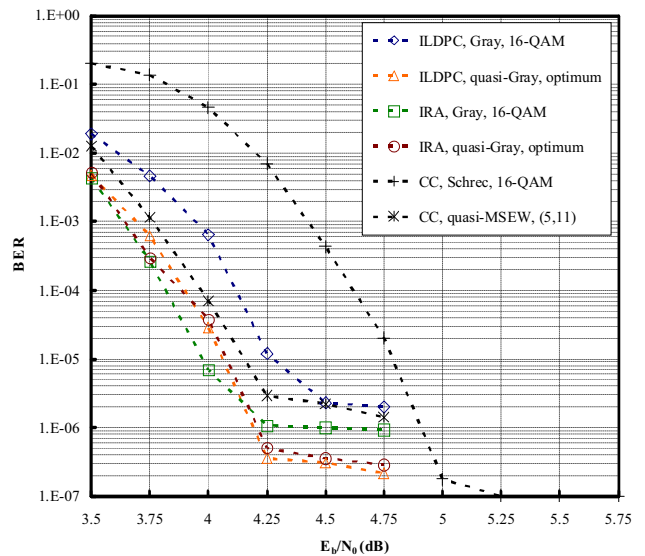


Figure 9. Performance comparison over AWGN channels among 2-bit/s/Hz BICM-ID schemes using channel codes and selected optimal combinations of rectangular and non-rectangular 16-ary signal constellations with mappings.

It is interesting to note that for BICM-ID schemes, CC with condition E achieves a comparable BER performance with both IRA and ILDPC codes. For BICM-ID schemes employing CC, nonrectangular 16-ary signal constellation (condition E) has approximately 0.63 dB performance gain over 16-QAM constellation (condition C) as depicted in Fig. 9. Error-floor occurs at BER level below 10^{-5} as shown in Fig. 8. Table V summarises the SNR required at $BER = 10^{-5}$ for various channel codes considered and their best combinations of signal constellations and mappings in AWGN channels.

TABLE V.

SIGNAL-TO-NOISE RATIO COMPARISON (SNR) AT BER = 10⁻⁵ BETWEEN SEVERAL 2-BIT/S/Hz 16-ARY BICM-ID SCHEMES. NOTE THAT THE NOTATION 'N/A' IN THE TABLE INDICATES THAT THE SNR REQUIRED FOR BER = 10⁻⁵ IS OUT OF THE CONSIDERED SNR RANGE.

Channel	Codes	Signal Constellations	Mapping Scheme	E _b /N ₀ (dB)
AWGN	IRA	16-QAM	Gray	3.97
AWGN	ILDPC	optimum	quasi-Gray	4.06
AWGN	CC	(5,11)	quasi-MSEW	4.15
Rayleigh	IRA	16-QAM	Gray	5.83
Rayleigh	ILDPC	16-QAM	Gray	5.93
Rayleigh	CC	(5,11)	quasi-MSEW	N/A

B. Performance of BICM/BICM-ID Schemes over Rayleigh Fading Channels

The influence of rectangular and non-rectangular 16-ary constellations with optimised mappings are shown in Figs. 10 and 11. In Fig. 10, IRA codes with rectangular 16-QAM constellation consistently provide the best coding gain in both BICM and BICM-ID systems at BER of 10⁻⁴, which agrees with the results obtained for the AWGN channel. Moreover, BICM-ID schemes employing IRA and ILDPC codes with non-rectangular 16-ary constellations provide comparable performance at a BER of 10⁻⁴. The BER performance of rectangular and non-rectangular constellations are evaluated and presented in Figs. 12 and 13 for BICM and BICM-ID schemes, respectively. It is observed that for the case of BICM schemes using iterative decodable codes, condition A outperforms condition B. Moreover, in BICM schemes, it can be seen that for both conditions A and B, IRA codes achieve a marginal performance gain over ILDPC codes at a BER of 10⁻⁴ as shown in Fig. 12. For the case of BICM-ID schemes using iterative decodable codes considered in this paper, the performance gain with feedback is moderate for both rectangular and non-rectangular constellations at a BER of 10⁻⁴ as depicted in Fig. 13. Moreover, similar to AWGN channels, 16-QAM constellation consistently outperforms the non-rectangular 16-ary constellations over Rayleigh fading channels for BICM-ID schemes using iterative decodable codes. In addition, for BICM-ID schemes using channel codes considered in this work, the BER performance gives comparable results at low SNR. In Rayleigh fading channels, BICM-ID employing IRA codes with 16-QAM and Gray mapping consistently performs best for spectral efficiency of 2-bit/s/Hz at low SNR. The channel capacity limits for 2-bit/s/Hz 16-QAM BICM on Rayleigh fading channels are approximately 4 dB. The gap between the capacity and the performance of BICM-ID employing IRA codes with 16-QAM Gray mapping is 1.83 dB for Rayleigh fading channels, at a BER of 10⁻⁵.

Similarly, the effect of channel codes on BICM-ID schemes is shown in Fig. 13 for Rayleigh fading channels. For BICM-ID employing rectangular 16-ary signal constellations, IRA codes achieves a better performance gain than CC at a BER of 10⁻⁵. For BICM-ID employing nonrectangular 16-ary signal constellations, IRA codes consistently outperform CC at

a BER of 10⁻⁵. Computer simulation results show that BICM-ID scheme employing IRA codes with optimal combination of rectangular signal constellation and Gray mapping offers the best performance in Rayleigh fading channels at a BER of 10⁻⁵.

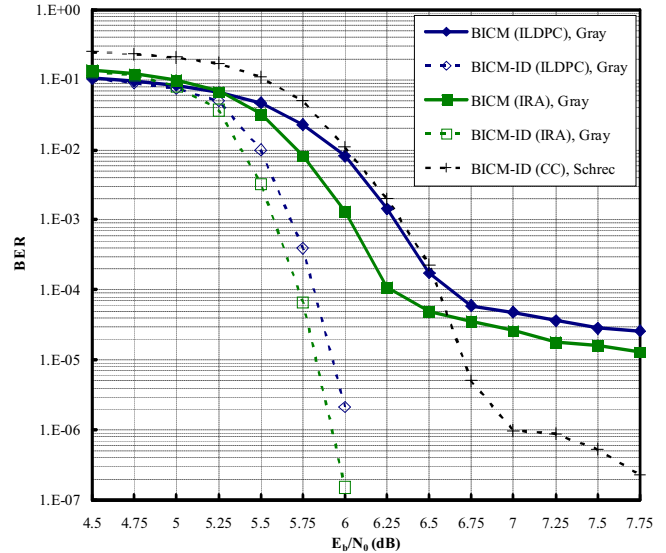


Figure 10. Performance comparison over Rayleigh fading channels among 2-bit/s/Hz BICM/BICM-ID schemes using channel codes and selected optimal combinations of rectangular 16-QAM signal constellations with mappings.

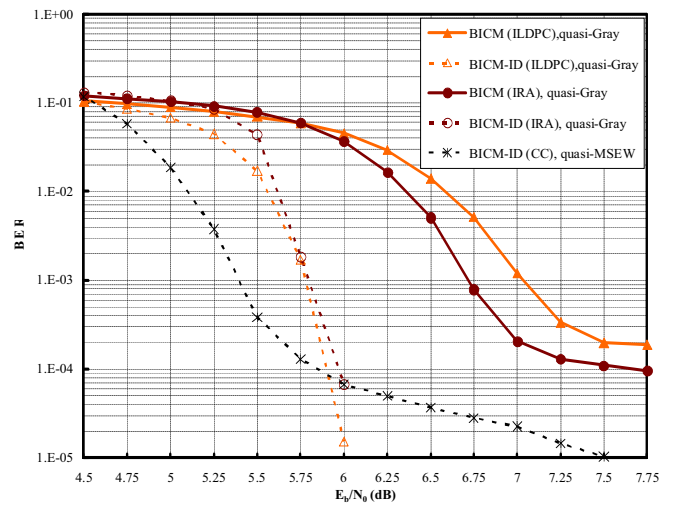


Figure 11. Performance comparison over Rayleigh fading channels among 2-bit/s/Hz BICM/BICM-ID schemes using channel codes and selected optimal combinations of non-rectangular 16-ary signal constellations with mappings. Both ILDPC and IRA codes employ optimum constellation while CC uses (5,11) constellation.

In addition, for Rayleigh fading channels, errors floors are eliminated with iterative demodulation and decoding for turbo-like codes in both rectangular and non-rectangular 16-ary constellations as depicted in Figs 10 and 11. In Fig. 13, it can be seen that although BICM-ID scheme using CC (with condition E) experiences an early convergence than IRA codes (with condition A); it suffers a large error floor. The same observation as AWGN channels is noted for BICM-ID employing CC over Rayleigh fading channels; non-rectangular

constellation (condition E) has a performance improvement over rectangular constellation (condition D) by approximately 0.7 dB, at a BER of 10^{-4} . BICM-ID schemes using IRA codes with 16-QAM signal constellation and Gray mapping provide the best performance over Rayleigh fading channels, at BER level below 10^{-5} . Again, all results agree with those reported in Tables I and II.

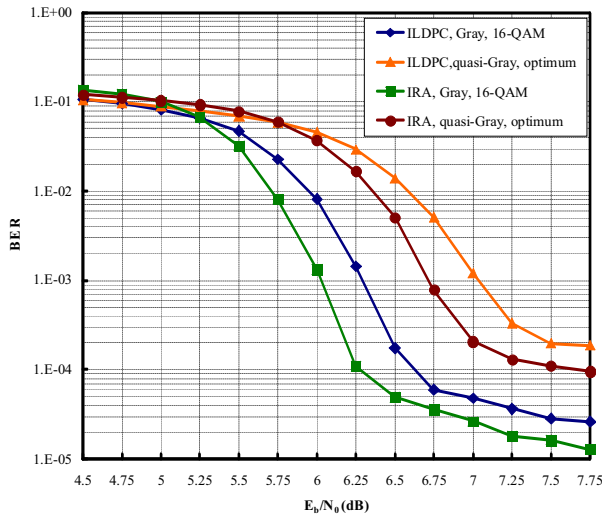


Figure 12. Performance comparison over Rayleigh fading channels among 2-bit/s/Hz BICM schemes using channel codes and selected optimal combinations of rectangular and non-rectangular 16-ary signal constellations with mappings.

Figs. 9 and 13 show that with iterative demodulation and decoding, convolutional coded BICM with condition E provides comparable performance to that of turbo or LDPC/RA coded modulation over both AWGN and Rayleigh fading channels for moderate block size. This agrees with [27].

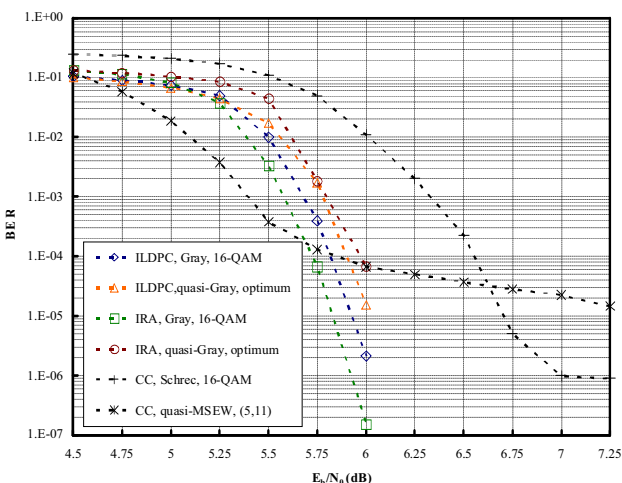


Figure 13. Performance comparison over Rayleigh fading channels among 2-bit/s/Hz BICM-ID schemes using channel codes and selected optimal combinations of rectangular and non-rectangular 16-ary signal constellations with mappings.

However as the codeword size increases to a very large value, turbo or LDPC/RA coded systems will be better [30] since the convolutional coded BICM with iterative

demodulation and decoding does not have any interleaving gain as codeword size increases to a large value. Error-floor effects occurring at BER level below 10^{-3} can be noticed as shown in Fig. 12. Similarly, Table V summarises the SNR required at BER = 10^{-5} for various channel codes considered and their best combinations of signal constellations and mappings in Rayleigh fading channels.

V. BICM AND 4G

BICM is currently the most popular coded modulation for both fading and non-fading channels. BICM is a promising method to achieve high spectral efficiency over wireless communication links. BICM has been adopted in many commercial systems such as wireless and wired broadband access networks, 3G and 4G telephony, ultra-wideband (UWB) transceivers, as well as DVB, imposing itself as the de facto standard for current wireless telecommunications systems. BICM is expected to form the basis of future communication standards [31]-[35].

The combination of Orthogonal Frequency Division Multiplexing (OFDM) and BICM can be found in many standards such as IEEE 802.11 WLAN, IEEE 802.16 WiMAX, UMTS Long Term Evolution (LTE) and 4th generation mobile communication systems. Both LTE and WiMAX 4G technologies uses OFDM as the modulation scheme. In this section, single-input single-output (SISO) wireless systems are considered. The same simulation parameters and conditions are extended to BICM-ID-OFDM system. Fig. 14 depicts the BER performance of BICM-ID-OFDM scheme for two types of channel codes (IRA, CC) over quasi-static frequency-selective Rayleigh fading channels. It can be observed that powerful channel codes (IRA) achieve significant performance improvement as compared to the less powerful channel codes (CC), at a BER of 10^{-5} . It is worthy to note that for BICM-ID-OFDM (IRA), no errors were observed for E_b/N_0 greater than 16 dB within 10^7 simulated information bits.

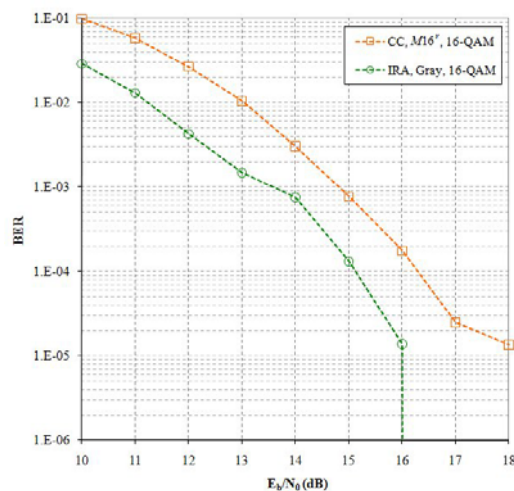


Figure 14. Performance comparison over frequency selective Rayleigh fading channels among 2-bit/s/Hz BICM-ID-OFDM schemes using channel codes considered (IRA, CC) and 16-QAM with mappings.

VI. CONCLUSION

Applications of BICM and BICM-ID systems with selected error-correcting codes and optimised combinations of 16-ary constellations with mappings to improve the error performance over AWGN and Rayleigh fading channels are considered in this paper. The BICM capacity for various 16-ary constellations has also been evaluated to determine the optimised signal constellation and mapping pair when combined with powerful error-correcting codes such as IRA codes. It has been shown that for the case of 16-ary constellations, the most attractive signal set for IRA codes is rectangular 16-QAM signal constellation with Gray mapping. Moreover, simulation results have demonstrated that the coding gains and error floors are remarkably affected by the selection of the signal constellation and bit mapping. The optimised selection of the such parameters can be used to avoid the severe performance degradation that is obtained when error floors occur. The powerful combinations of BICM-ID, OFDM and channel codes (turbo codes, LDPC codes, CC) are widely adopted in 3G/4G Wireless Systems.

ACKNOWLEDGMENT

The authors wish to thank the anonymous reviewers for their careful reading and valuable comments which greatly improved the presentation of the paper.

REFERENCES

- [1] G. Ungerboeck, "Channel coding with multilevel-phase signals," *IEEE Trans. Inform. Theory* vol. 28, no. 1, pp. 56-67, Jan. 1982.
- [2] E. Zehavi, "8-PSK trellis codes for Rayleigh channel," *IEEE Trans. Commun.*, vol. 40, no. 5, pp. 873-884, May 1992.
- [3] G. Caire, G. Taricco, E. Biglieri, "Bit-interleaved coded modulation," *IEEE Trans. Inform. Theory*, vol. 44, no. 3, pp. 927-946, May 1998.
- [4] X. Li, J. A. Ritcey, "Bit-interleaved coded modulation with iterative decoding using soft feedback," *Electronics Letters*, vol. 34, no. 10, pp. 942-943, Mar. 1998.
- [5] X. Li, A. Chindapol, J. A. Ritcey, "Bit-interleaved coded modulation with iterative decoding and 8PSK signalling," *IEEE Trans. Commun.*, vol. 50, no. 8, pp. 1250-1257, Aug. 2002.
- [6] A. Chinadapol, J. A. Ritcey, "Design, analysis, and performance evaluation for BICM-ID with square QAM constellations in Rayleigh-fading channels," *IEEE J. on Selected Areas in Commun.*, vol. 19, no. 5, pp. 944-957, May 2001.
- [7] S. Le Goff, "Signal constellations for bit-interleaved coded modulation," *IEEE Trans. Inform. Theory*, vol. 49, no. 1, pp. 307-313, Jan. 2003.
- [8] F. Schreckenbach, G. Bauch, "Bit-interleaved coded irregular modulation," *European Transactions on Telecommunications*, vol. 17, no. 2, pp. 269-282, Feb. 2006.
- [9] C. Berrou, A. Glavieux, P. Thitimajshima, "Near Shannon limit error-correcting coding and decoding: turbo-codes," in *IEEE Int. Conf. Commun. (ICC)*, Geneva, Switzerland, pp. 1064-1070, 1993.
- [10] W. K. Han, S. Le Goff, B. Sharif, "Systematic repeat accumulate codes for bit-interleaved coded modulation with iterative demapping over AWGN and Rayleigh fading channels," in *IEEE 3rd Int. Symp. on Wireless Pervasive Computing (ISWPC)*, Santorini, Greece, pp. 152-155, 2008.
- [11] S. Le Goff, "Bandwidth-efficient turbo coding over Rayleigh fading channels," *Int. Journal of Communication Systems*, vol. 15, no. 7, pp. 621-633, Jul. 2002.
- [12] G. J. Foschini, R. D. Gitlin, S. B. Weinstein, "Optimization of two-dimensional signal constellations in the presence of Gaussian noise," *IEEE Trans. Commun.*, vol. 22, no. 1, pp. 28-38, Jan. 1974.
- [13] X. Dong, N. C. Beaulieu, P. H. Wittke, "Signaling constellations for fading channels," *IEEE Trans. Commun.*, vol. 47, no. 5, pp. 703-714, May 1999.
- [14] S. J. Johnson, S. R. Weller, "Constructions for irregular repeat-accumulate codes," in *Proc. IEEE Int. Symp. Inform. Theory (ISIT)*, Adelaide, Australia, pp. 179-183, 2005.
- [15] S. J. Johnson, S. R. Weller, "Practical Interleavers for Systematic Repeat-Accumulate Codes," in *IEEE 63rd Vehicular Technology Conference (VTC-Spring)*, Melbourne, Australia, pp. 1358-1362, 2006.
- [16] T. M. Cover, J. A. Thomas, *Elements of Information Theory 2nd edition*, Hoboken, NJ: Wiley InterScience, 2006.
- [17] Y. Li, W. E. Ryan, "Bit-reliability mapping in ldpc-coded modulation systems," *IEEE Communications Letter*, vol. 9, no. 1, pp. 1-3, Jan. 2005.
- [18] S. ten Brink, G. Kramer, "Design of repeat-accumulate codes for iterative detection and decoding," *IEEE Trans. Commun.*, vol. 51, no. 11, pp. 2764-2772, Nov. 2003.
- [19] S. ten Brink, G. Kramer, A. Ashikhmin, "Design of low-density parity-check codes for modulation and detection," *IEEE Trans. Commun.*, vol. 52, no. 4, pp. 670-678, Apr. 2004.
- [20] A. Ashikhmin, S. ten Brink, G. Kramer, "Extrinsic information transfer functions: Model and erasure channel properties," *IEEE Trans. Inform. Theory*, vol. 50, no. 11, pp. 2657-2673, Nov. 2004.
- [21] J. Campello, D. S. Modha, S. Rajagopalan, "Designing LDPC codes using bit-filling," in *IEEE Int. Conf. Commun. (ICC)*, Saint Petersburg, Russia, pp. 55-59, 2001.
- [22] M. Yang, W. E. Ryan, Y. Li, "Design of efficiently encodable moderate-length high-rate irregular LDPC codes," *IEEE Trans. Commun.*, vol. 52, no. 4, pp. 564-571, Apr. 2004.
- [23] R. G. Gallager, *Low-Density Parity-Check Codes*, Cambridge, MA: MIT Press, 1963.
- [24] D. J. C. Mackay, R. M. Neal, "Near Shannon limit performance of low-density parity-check codes," *Electronics Letters*, vol. 32, no. 18, pp. 1645-1646, Aug. 1996.
- [25] T. K. Moon, *Correction Coding: Mathematical Methods and Algorithms*, Hoboken, NJ: John Wiley and Sons, 2005.
- [26] F. Schreckenbach, N. Gortz, J. Hagenauer, G. Bauch, "Optimization of symbol mappings for bit-interleaved coded modulation with iterative decoding," *IEEE Communications Letters*, vol. 7, no. 12, pp. 593-595, Dec. 2003.
- [27] J. Tan, G. L. Stuber, "Analysis and design of symbol mappers for iteratively decoded BICM," *IEEE Trans. Wireless Commun.*, vol. 4, no. 2, pp. 662-672, Mar. 2005.
- [28] C. A. Nour, C. Douillard, "Performance improvement using turbo coded BICM-ID with 16-QAM over Gaussian

and flat fading Rayleigh channels," *IST Mobile and Wireless Communications Summit*, Dresden, Germany, 1-4, 2005.

- [29] A. Abbasfar, *Turbo-like Codes: Design for High-Speed Decoding (1st edn.)*, Springer, 2007.
- [30] D. J. C. Mackay, "Good error-correcting codes based on very sparse matrices," *IEEE Trans. Inform. Theory*, vol. 45, no. 2, pp. 399-431, Mar. 1999.
- [31] R. Ghaffar, R. Knoop, "Interference Suppression for Next Generation Wireless Systems," in *69th IEEE Vehicular Technology Conference (VTC-Spring)*, Barcelona, Spain, pp. 1-5, 2009.
- [32] H. Luders, A. Minwegen, P. Vary, "Low Complexity Coding and Modulation for UMTS LTE: BICM-ID with Repetition Coding," in *14th International OFDM-Workshop 2009 (InOWo'09)*, Hamburg, Germany, 2009.
- [33] R. Ghaffar, R. Knoop, "Fractional Frequency Reuse and Interference Suppression for OFDMA Networks," in *8th Int. Symp. on Modeling and Optimization in Mobile, Ad Hoc and Wireless Networks (WiOpt)*, Avignon, France, pp. 273-277, 2010.
- [34] A. Nasri, R. Schober, L. Lampe, "Performance Evaluation of BICM-OFDM Systems Impaired by UWB Interference," in *IEEE Int. Conf. Commn. 2008 (ICC'08)*, Beijing, China, pp. 3616-3621, 2008.
- [35] S. Stiglmayr, M. Bossert, E. Costa, "Adaptive Coding and Modulation in OFDM Systems using BICM and Rate-Compatible Punctured Codes," *European Wireless*, Paris, France, 2007.



Wei Kwang Han received the B.Eng. degree in Electrical and Electronic Engineering from Nanyang Technological University, Singapore in 2003. He received both the M.Sc. degree in Communications and Signal Processing and Ph.D. degree in Electrical, Electronic and Computer Engineering from Newcastle

University, UK, in 2005 and 2009, respectively. His research interests include coded modulation, information theory, iterative receiver algorithms, error correction coding, diversity techniques, OFDM, LTE-Advanced and 4G wireless communications. Dr. Han is a member of the Institution of Engineering and Technology (MIET).



Stephane Le Goff received the BSc, MSc, and PhD degrees, all in electrical engineering, from the University of Western Brittany, Brest, Brittany, France, in 1990, 1991, and 1995, respectively. From 1995 to 1997, he worked as a teacher at the Institut Supérieur d'Electronique de Bretagne in

Brest. During 1999-2003, Dr. Le Goff was an Assistant Professor at the Emirates Telecommunications Corporation (Etisalat) College of Engineering, UAE. In 2003, he joined the Department of Physics and Electronics at the University of Waikato, Hamilton, New Zealand as a Senior Lecturer in Electronics. Since March 2005, he has been a Lecturer in the School of Electrical, Electronic, and Computer Engineering at Newcastle University, UK. Dr. Le Goff also held visiting positions at the Eastern Mediterranean University, Cyprus, during the Academic Year 1998-1999 and at the Sultan Qaboos University, Oman, from September to December 2004. His research interests include information theory, channel coding, and wireless communication systems.



Bayan Sharif is Professor of Digital Communications and Head of the School of Electrical, Electronic and Computer Engineering. He received the bachelor and doctorate degrees from Queens University of Belfast and Ulster University, N. Ireland, in 1984 and 1988, respectively. He then held a Research Fellowship at Queens

University of Belfast before he was appointed as Lecturer at Newcastle University in 1990, and then as Senior Lecturer and Professor in Digital Communications in 1999 and 2000, respectively. Prof. Sharif has research interests in digital communications with a focus on wireless receiver structures and optimisation of wireless networks. He has published over 200 journal and conference papers, and held UK and EU research grants in digital communications, underwater acoustics and signal processing worth over 3M. He is a Chartered Engineer and Fellow of the IEE.



Arafat Al-Dweik received the B.A. degree in Telecommunication Engineering from Yarmouk University, Jordan, in 1994, the M.S.E.E degree in 1998; and the Ph.D. in Electrical Engineering in 2001 from Cleveland State University, Cleveland, Ohio, USA. He joined Efficient Channel Coding Incorporated, Ohio, USA, in

1999-2001 where he was a Research and Development Engineer working on advanced modulation and synchronization techniques. He is currently an Associate Professor at the Communications Engineering Department, Etisalat University of Engineering, UAE. His research interests include synchronization techniques, OFDM technology, modeling and simulation of communication systems, error control coding, and frequency hopping spread spectrum systems. Dr. Al-Dweik is an IEEE senior member, member of Tau Beta Pi, and Eta Kappa Nu. He received several awards and scholarships including Fulbright scholarship in 1997-1999.

Dedicated-Relay vs. User Cooperation in Time-Duplexed Multiaccess Networks

Lalitha Sankar, *Member, IEEE*, Gerhard Kramer, *Fellow, IEEE*, and Narayan B. Mandayam, *Fellow, IEEE*

Abstract—The performance of *user cooperation* that results when users forward packets for each other in a multiaccess network is compared to that of *dedicated-relay cooperation* which results from using a dedicated wireless relay when the users do not cooperate. Using the total transmit and processing power consumed at all nodes as a cost metric, the outage probabilities achieved by dynamic decode-and-forward (DDF) and amplify-and-forward (AF) are compared for the two networks. A geometry-inclusive high signal-to-noise ratio (SNR) outage analysis in conjunction with area-averaged numerical simulations shows that in a K -user time-duplexed multiaccess network, user and dedicated-relay cooperation achieve a maximum diversity per user of K and 2, respectively, under both DDF and AF. However, when accounting for energy costs of processing and communication, dedicated-relay cooperation can be more energy efficient than user cooperation, i.e., dedicated-relay cooperation achieves *coding (SNR) gains*, particularly in the low SNR regime, that override the diversity advantage of user cooperation.

I. INTRODUCTION

Cooperation results when nodes in a network share their power and bandwidth resources to mutually enhance their transmissions and receptions. Cooperation can be induced in several ways. We compare two approaches to inducing cooperation in a multiaccess channel (MAC) comprised of K sources (users) and one destination. In the first approach, we allow source nodes to forward data for each other and in the second approach, we introduce a dedicated wireless relay node to forward data from the sources assuming cooperation between the source nodes is either undesirable or impossible. We refer to networks employing the former approach as *user cooperative (UC) networks* and those employing the latter as *dedicated-relay cooperative (RC) networks*. Our motivation for this terminology is that although users act as relays for one another in the UC network, they are primarily interested in transmitting their own data, while in contrast, the dedicated-relay node in the RC network is dedicated to relaying packets for the sources.

The work of L. Sankar and N. B. Mandayam was supported in part by the National Science Foundation under Grant No. 0429724. The work of G. Kramer was partially supported by the Board of Trustees of the University of Illinois Subaward No. 04-217 under NSF Grant No. CCR-0325673 and by the Army Research Office under the ARO grant W911NF-06-1-0182. The material in this paper was presented in part at the IEEE International Symposium on Information Theory, Adelaide, Australia, Sep. 2005; and at the 45th Annual Allerton Conference on Communications, Control, and Computing, Monticello, IL, Sep. 2007. L. Sankar is with Princeton University. G. Kramer was with Bell Labs, Alcatel-Lucent, Murray Hill, NJ, and with USC, Los Angeles, CA. He is now with the Technische Universität München, Germany. N. B. Mandayam is with the WINLAB, Rutgers University. Manuscript received February 15, 2011; revised May 15, 2011; accepted June 15, 2011.

There are important differences between UC and RC networks that are not easy to analyze from a communication-theoretic point of view. For example, in UC networks one likely needs economic incentives to induce cooperation amongst users. On the other hand, RC networks incur relay infrastructure costs. While incentives and infrastructure costs are important issues, we use the total transmit and processing power consumed as a cost metric for our comparisons. To this end, ignoring technology-dependent limitations on processing, we model the processing power as a function of the transmission rate, and thereby the transmit signal-to-noise ratio (SNR). We also introduce *processing scale factors* to characterize the ratio of the power costs of processing relative to that for transmission. While the processing (power and chip density) costs for encoding and decoding are complex functions of the specific communication and computing technologies used, the scale factors allow us to parametrize and study the impact of such processing costs.

We motivate the need for this analysis with examples of processing and transmission costs for wireless devices serving three different applications. Consider a Motorola RAZR GSM mobile phone. This device has a maximum transmit power constraint of 1 (2) W in the 900 (1900) MHz band. With a 3.7 V battery rated at 740 mAh it has a capacity of almost 10 kJ of energy resulting in an average talk time of 4 hours. On the other hand, consider the 802.11 wireless local area network (WLAN) interface. An Atheros whitepaper [1] found that typical WLAN interfaces consume 2 to 8 W for active communications. In contrast, the transmit power for this device in the range of 20 to 100 mW is only a small fraction of the processing costs. Finally, consider low-power sensor devices such as the Berkeley motes. The authors in [2] model the energy cost per bit for a reliable 1 Mbps link over a distance d and path-loss exponent α by a transmitter cost of $\mathcal{E}_{tx} = \mathcal{E}_t + \mathcal{E}_{pa}d^\alpha$ where $\mathcal{E}_t = 0.36$ J/MB is the energy dissipated in the transmitter electronics and $\mathcal{E}_{pa} = 8 \times 10^{-5}$ J/m²/MB scales the required transmit energy per bit. Accounting for the signal processing costs at the receiver as $\mathcal{E}_{rx} = 1.08$ J/MB, they show that for distances less than the transition distance of $d = \sqrt{\mathcal{E}_t/\mathcal{E}_{pa}} = 67$ m, processing energy cost dominates transmission cost and vice-versa. In general, the ratio of processing to transmission power depends on both the device functionality (long distance vs. local links) and the application (high vs. low rate) supported. Thus, accounting for both the transmit and processing power (energy) costs in our comparisons allows us to identify the processing factor regimes where cooperation is energy efficient.

We consider single-antenna half-duplex nodes and constrain

all transmitting nodes in both networks to time-duplex their transmissions. Thus, in the RC network each source cooperates with the dedicated relay over two-hops where in the first hop the source transmits while the dedicated relay listens and in the second hop both the source and the dedicated relay transmit. For the UC network, for $K > 2$ we consider the cooperative schemes of *two-hop*, where the set of users cooperating with any source transmit in the second hop, and *multi-hop*, where the cooperating users transmit sequentially in time. We assume that transmitters in both networks do not have transmit channel state information (CSI). Under this assumption, we develop geometry-inclusive upper and lower bounds on the outage probabilities of each network for the cooperative strategies of *dynamic* decode-and-forward (DDF) [3] and *amplify-and-forward* (AF). This allows us to compare the outage performance of each cooperative strategy for the two networks via both the diversity gain and a *coding (SNR) gain* [4]. Our approach of accounting for the power involved in data processing and transmission enables us to compare the outage performance of the two types of cooperative networks despite differences in the total number of nodes and cooperative strategies.

For single-antenna nodes, the maximum DDF and AF diversity for two-hop relaying is 2 [3] and our geometry-inclusive analysis demonstrates the same. For the two-hop UC network, we show that, if relay selection is allowed, AF achieves a maximum diversity of 2 for all $K \geq 2$. For the same network, we also show here that, except for a *clustered* geometry where the maximum diversity approaches K , DDF also achieves a maximum diversity of 2. On the other hand, when users cooperate using a K -hop scheme, our bounding analysis agrees with the earlier diversity-multiplexing results that both DDF [3] and AF [4] achieve a maximum diversity of K .

The coding gains achieved are in general a function of the transmission parameters and network geometry. In an effort to generalize such results, we present an *area-averaged* numerical comparison. Specifically, we consider a sector of a circular area with the destination at the center, a fixed dedicated-relay position, and the users randomly distributed in the sector which models wireless LAN, cellular, and sensor networks. Our results are summarized by the following observations: i) user cooperation can achieve higher diversity gains than dedicated-relay cooperation but at the expense of increased complexity and ii) dedicated-relay cooperation can achieve larger coding gains when we account for the energy costs of cooperation, thus diminishing the effect of the diversity gains achieved by user cooperation.

This paper is organized as follows. In Section II, we present the network and channel models and develop a power-based cost metric. In Section III, we present outage approximations for DDF and AF strategies for both networks. In Section IV, we present the numerical results. We conclude in Section V.

II. CHANNEL AND NETWORK MODELS

A. Network Model

Our networks consist of K users (source nodes) numbered $1, 2, \dots, K$ and a destination node d . In the absence of any

form of cooperation, this network is modeled as a K -user multiple access channel (MAC). For the RC network there is one additional node, the dedicated-relay node r . We impose a *half-duplex* constraint on every node, i.e., each node can be in one of two modes, *listen (L)* or *transmit (T)*. We write $\mathcal{K} = \{1, 2, \dots, K\}$ for the set of users and $\mathcal{T} = \mathcal{K} \cup \{r\}$ for the set of transmitters in the RC network. Let $X_{k,i}$ be the transmitted signal (channel input) at node k at time i , $i = 1, 2, \dots, n$. We model the wireless multiaccess links under study as additive Gaussian noise channels with fading. For such channels, the received signal (channel output) at node m at time i is

$$Y_{m,i} = \begin{cases} \left(\sum_{k \neq m} H_{m,k,i} X_{k,i} \right) + Z_{m,i} & M_{m,i} = L \\ 0 & M_{m,i} = T \end{cases} \quad (1)$$

where the $Z_{m,i}$ are independent, proper, complex, zero-mean, unit variance Gaussian noise random variables, $M_{m,i}$ is the half-duplex mode at node m , and $H_{m,k,i}$ is the complex fading gain between transmitter k and receiver m at time i . Note that for both networks as well as the MAC, $M_{d,i} = L$, for all i . Further, for the RC network and the MAC, since the sources do not cooperate, and hence do not listen, we have $M_{k,i} = T$, for all i and for all $k \in \mathcal{K}$. We assume that the transmitted signals in both networks are constrained in power as

$$\sum_{i=1}^n E \left[|X_{k,i}|^2 \right] \leq nP_k, \quad k \in \mathcal{T} \quad (2)$$

where P_k is the average power constraint at transmitter k . Throughout the sequel we assume that all transmitters use independent Gaussian codebooks with asymptotically large codelengths and the total transmission bandwidth is unity. We also assume that due to lack of transmit CSI, the transmitters do not vary power as a function of channel states. Further, we assume that the modes $M_{k,i}$ are made available to all nodes. We will clarify our motivation for this assumption in the sequel. Finally, we use the usual notation for entropy and mutual information [5] and take all logarithms to the base 2 so that our rate units are bits/channel use. We write random variables (e.g. H_k) with uppercase letters and their realizations (e.g. h_k) with the corresponding lowercase letters and use the notation $C(x) = \log(1+x)$ where the logarithm is to the base 2. Finally, throughout the sequel we use the words “user” and “source” interchangeably.

B. RC Network

The RC network has $K + 1$ inputs $X_{k,i}$, $k \in \mathcal{T}$, and two outputs $Y_{r,i}$ and $Y_{d,i}$ [6], [7]. We consider a time-duplexed dedicated-relay cooperative (TD-RC) model where each source transmits over the channel for a period $T_P = 1/K$ of the total time. Further, the transmission period of source k , for all k , is sub-divided into two slots such that the dedicated relay listens in first slot and transmits in the second slot. We denote the time fractions of the first and second slots as θ_k and $\bar{\theta}_k = 1 - \theta_k$, respectively, for user k and note that the duration θ_k of the dedicated relay mode M_r can be different for different k . The time-duplexed two-hop scheme for the RC network is illustrated in Fig. 1(a) for

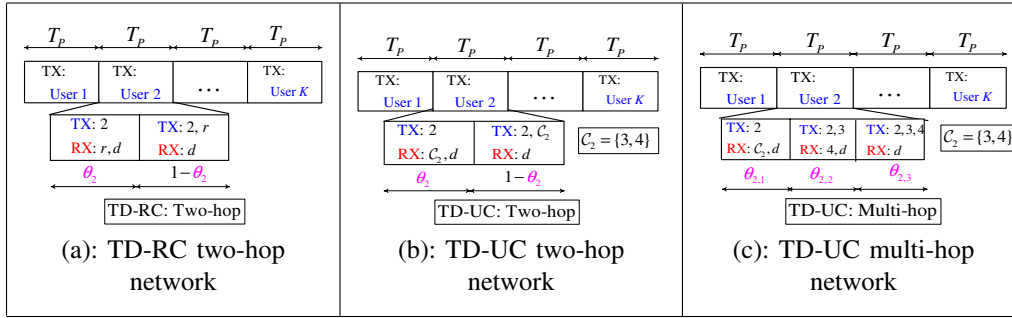


Fig. 1. Time-duplexed transmission schemes for the user cooperative and relay cooperative MACs.

user 2. Time-duplexing simplifies the analysis for each user to that of a single-source relay channel in each period T_P . We assume that the dedicated relay uses negligible resources to communicate its mode transition to the destination. We also assume that, due to the lack of transmit CSI, the transmitters use all available power for transmission subject to (2) in every channel use. Thus, in the k^{th} time period, for all k , user k and the dedicated-relay transmit at power $\bar{P}_k = KP_k$ and $\bar{P}_r = P_r/\bar{\theta}_k$, respectively, where $\theta_k = 1 - \bar{\theta}_k$. Finally, throughout the analysis we assume that P_r is proportional to P_k .

C. UC Network

In a user cooperative (UC) network, there is a combinatorial explosion in the number of ways one can duplex K sources over their half-duplex states. We present two transmission schemes which allow each user to be aided by up to $K - 1$ other users. In both schemes the users time-duplex their transmissions, thereby resulting in time-duplexed user cooperation (TD-UC); the two schemes differ in the manner the period T_P is further sub-divided between the transmitting and the cooperating users.

We first consider a *two-hop scheme* such that the period over which user k , for all k , transmits is sub-divided into two slots. In the first slot only user k transmits while in the second slot both user k and the set $C_k \subseteq \mathcal{K} \setminus \{k\}$ of users that cooperate with user k transmit. This is shown in Fig. 1(b) for user 2 and $C_2 = \{3, 4\}$. We remark that this scheme has the same number of hops as the TD-RC network except now user k can be aided by more than one user in C_k . We write θ_k and $1 - \theta_k$ to denote the time fractions associated with the first and second slots of user k .

We also consider a *multi-hop scheme* where the total transmission time for source k is divided into L_k slots, $1 \leq L_k \leq K$, where $L_k = |C_k| + 1$. Specifically, in each time-slot, except the first slot where only user k transmits, one additional user cooperates in the transmission until all L_k users transmit in slot L_k . When the cooperating users decode their received signals, we assume that the users are ordered in the sense that the new user that cooperates in the l^{th} time fraction is the first user that can decode the message when the l cooperating users are transmitting. We denote the l^{th} time fraction for user k as $\theta_{k,l}$, $l = 1, 2, \dots, L$ (see Fig. 1(c) for user 2 with $C_2 = \{3, 4\}$). We henceforth refer to the two schemes as two-hop TD-UC and multi-hop TD-UC.

User k transmits at power

$$\bar{P}_k = P_k \cdot K / (N_k + 1) \tag{3}$$

where $N_k \leq K - 1$ is the total number of users whose messages are forwarded by user k . For the two-hop scheme, in those sub-slots where user k acts as a cooperating node, its transmission power in (3) is scaled by the appropriate $\bar{\theta}_k$. For the multi-hop scheme, let $\pi_k(\cdot)$ be a permutation on C_k such that user $\pi_k(l)$ begins its transmissions in the fraction $\theta_{k,l}$, for all $l = 2, 3, \dots, L_k$, and $\pi_k(1) = k$. When user k acts as a cooperating node for user j , $j \neq k$, such that $\pi_j(l) = k$ for some $l > 1$, its power \bar{P}_k in (3) is scaled by the total fraction for which it transmits for user j , i.e., $\sum_{m=l}^{L_j} \theta_{j,m}$. Recall that the modes $M_{k,i}$ are available at all nodes; so we assume that a cooperating node or a dedicated relay uses negligible resources to communicate its transition from one mode to another to the destination and to other cooperating nodes. For AF we assume equal length slots and consider symbol-based two-hop and multi-hop schemes.

It is in general not possible to know *a priori* the number of users N_k whose messages are forwarded by user k . A decentralized scheme is to have all users forward packets for each other. Alternatively, for low mobility environments, the set C_k for user k can be chosen as the set of proximal users (see, for e.g., [8], [9] and the references therein).

D. Cost Metric: Total Power

We use the total power consumed by all the nodes as a cost metric for comparisons. We model the total power to account for both transmission and processing power costs motivated by the observation that wireless devices operate at different regimes of transmission and processing power requirements which in turn can affect their cooperative (processing and forwarding) capabilities. For instance, in addition to its transmit power a node also consumes processing power to encode and decode its signals. Furthermore, a node that relays consumes additional power in encoding and decoding packets for other nodes. We model these costs by defining encoding and decoding variables η_k and δ_k , respectively, and write the power required to process the transmissions of node j at node k as

$$P_{k,j}^{proc} = P_{k,0}^{proc} + (\eta_k I_k^{enc}(j) + \delta_k I_k^{dec}(j)) \cdot f(R_j) \tag{4}$$

for all $k \in \mathcal{T}, j \in \mathcal{K}$

where $P_{k,j}^{proc}$ is the power required by node k to cooperate with user j , $I_k^{enc}(j)$ and $I_k^{dec}(j)$ are indicator functions that are set to 1 if node k encodes and decodes, respectively, for user j , $P_{k,0}^{proc}$ is the minimum processing power at node k which is in general device and protocol dependent, and $f(R_j)$ is a function of the transmission rate R_j in bits/sec at user j (see also [10, (3)-(6)]). For example, a relay node that uses DDF consumes power for overhead, encoding, and decoding costs while a relay node using AF only has overhead costs. The unitless variables η_k and δ_k quantify the ratio of processing to transmission power at user k to encode and decode a bit, respectively. For example, $\eta \ll 1$ and $\delta \ll 1$ for cellular devices in which transmission costs dominate, $\eta \gg 1$ and $\delta \gg 1$ for the wireless LAN cards for which processing costs dominate, and η and δ are determined by the operational parameters for sensor-like devices. In general, the processing cost function f depends on the encoding and decoding schemes used as well as the device functionality. For simplicity, we choose f as

$$f(R_k) = R_k \quad \text{for all } k. \quad (5)$$

This choice fits the scenario where processing power is proportional to device throughput. Finally, we assume that the destination in typical multiaccess networks such as cellular or many-to-one sensor networks has access to an unlimited energy source and ignore its processing costs. We write the total power consumed on average (over all channel uses) at node k , $k \in \mathcal{T}$, as

$$P_{k,tot} = \begin{cases} P_k + P_{k,k}^{proc} + \sum_{j \in \mathcal{K}, j \neq k} I_k(j) P_{k,j}^{proc} & k \in \mathcal{K} \\ P_k + P_{k,k}^{proc} + \sum_{j \in \mathcal{K}} I_k(j) P_{k,j}^{proc} & k = r \end{cases} \quad (6)$$

where $I_k(j)$ is an indicator function that takes the value 1 if node k cooperates with node j . For user k , the first $P_{k,k}^{proc}$ term in (6) accounts for the power used to process its own message while the second summation term accounts for the power node k incurs in cooperating with all other source nodes. Note that at high SNR, i.e., high P_k for all k , the dominating term in (6) is P_k since $P_{k,k}^{proc}$ is usually a constant and R_j increases logarithmically in P_j , for all $k, j \in \mathcal{K}$. The total power consumed by all transmitting nodes in each network is given as

$$P_{tot} = \sum_{k \in \mathcal{A}} P_{k,tot}, \quad \mathcal{A} = \begin{cases} \mathcal{K} & \text{TD-MAC or TD-UC} \\ \mathcal{T} & \text{TD-RC} \end{cases} \quad (7)$$

E. Fading Models

We model the fading gains as $H_{m,k,i} = A_{m,k,i} / d_{m,k}^{\gamma/2}$ where $d_{m,k}$ is the distance between the m^{th} receiver and the k^{th} source, γ is the path-loss exponent, and the $A_{m,k,i}$ are jointly independent identically distributed (i.i.d.) zero-mean, unit variance, proper, complex Gaussian random variables. We assume that the fading gain $H_{m,k,i}$ is known only at receiver m . We also assume that $H_{m,k,i}$ remains constant over a coherence interval and changes independently from one coherence interval to another. Further, the coherence interval is

assumed large enough to apply information-theoretic quantities such as mutual information. Finally, we also assume that the fading gains are independent of each other and independent of the transmitted signals $X_{k,i}$, for all $k \in \mathcal{T}$ and i .

III. GEOMETRY-INCLUSIVE OUTAGE ANALYSIS

We first compare the outage performance of the UC and RC networks via a limiting analysis in SNR of the outage probabilities achieved by DDF. We later do the same for both networks for AF. In [4], Laneman develops bounds on the DF and AF outage probabilities for a relay channel where the source and the relay transmit on orthogonal channels to the destination. In [3], the authors introduce a DDF strategy for a half-duplex relay channel where the relay remains in the *listen* mode until it successfully decodes its received signal. Furthermore, the authors show that for both two-hop and multi-hop relay channels, DDF achieves the diversity-multiplexing tradeoff (DMT) performance [11] of an equivalent MIMO channel for small multiplexing gains.

In an effort to quantify both the diversity and the effect of geometry, we present geometry-inclusive upper and lower bounds on the DDF and AF outage probabilities for the TD-RC and the TD-UC networks. We summarize the results here and develop the detailed analyses in the Appendices. Under DDF, a cooperating node (resp. dedicated-relay) in the TD-UC (resp. TD-RC) network can indicate its mode change following successful decoding via a one bit feedback signal that is assumed available to all nodes. This in turn allows user k , for all k , to determine the order of its cooperating DDF users in the multi-hop TD-UC network. For the multi-hop TD-UC network, the difference $\theta_{k,l} - \theta_{k,j}$ for two cooperating users $l, j \in \mathcal{C}_k$ may be smaller than the symbol time in which case user k could choose arbitrarily between the two users. On the other hand, for an AF-based multi-hop TD-UC network, the node order could be determined *a priori* based on the proximity of sources.

A. Dynamic-Decode-and-Forward

1) *TD-RC*: In general, obtaining a closed form expression for the outage probability of each user is not straightforward. Suppose that $P_r = \lambda \bar{P}_k$ for some constant λ and recall that $\bar{P}_r = P_r / \bar{\theta}_k$. In Appendix II, we develop upper and lower bounds on the DDF outage probability $P_o^{(k)}$ of user k transmitting at a fixed rate R_k , for all k , as (see (36))

$$P_{o,2 \times 1} \leq P_o^{(k)} \leq \left[\frac{(2^{R_k/\bar{\theta}_k^*} - 1)^2 \bar{\theta}_k^*}{(2^{R_k} - 1)^2} + \frac{2d_{r,k}^{\gamma} (2^{R_k/\theta_k^*} - 1)^2}{d_{d,r}^{\gamma} (2^{R_k} - 1)^2} \right] \cdot \frac{(2^R - 1)^2 d_{d,k}^{\gamma} d_{d,r}^{\gamma}}{2\lambda (\bar{P}_k)^2} + O\left((\bar{P}_k)^{-3}\right) \quad (8)$$

where $P_{o,2 \times 1}$ is the outage probability of a 2×1 distributed MIMO channel whose i^{th} transmit antenna is at a distance $d_{d,i}$, $i = k, r$, from the destination and $\theta_k^* \in (0, 1)$ is a fraction chosen to upper bound $P_o^{(k)}$. The notation $O(x)$ in (8) means that there is a positive constant M and a real number x_0 such

that the $O(x)$ term is upper bounded by $M|x|$ for all $x \geq x_0$. In Appendix II, we show that

$$P_{o,2 \times 1} = (2^{R_k} - 1)^2 d_{d,k}^\gamma d_{d,r}^\gamma / 2\lambda (\bar{P}_k)^2 + O\left((\bar{P}_k)^{-3}\right). \quad (9)$$

Thus, from (8) and (9) we see that for a fixed rate transmission, the maximum diversity (negative exponent of \bar{P}_k) achieved by DDF is 2, as predicted by the DMT analysis for DDF in [3, Theorem 4]. Comparing (8) and (9), we further see that the bracketed expressions on the right side of the inequality in (8) upper bounds the coding gains by which $P_o^{(k)}$ differs from the MIMO lower bounds.

2) *TD-UC – Two-Hop*: The outage analysis for the two-hop TD-RC network can be extended to the two-hop TD-UC network with the observation that θ_k is now determined by the cooperating user that takes the longest to decode. In Appendix II, for sufficiently large power P_k , we bound $P_o^{(k)}$ as (see (38) and (43))

$$P_{o,L_k \times 1} \leq P_o^{(k)} \leq K_2 \cdot \frac{(2^{R_k} - 1)^{L_k} \prod_{j \in \mathcal{S}_k} d_{d,j}^\gamma}{(L_k!) (\bar{P}_k)^{L_k} \prod_{j \in \mathcal{S}_k} \lambda_j} + O\left((\bar{P}_k)^{-L_k-1}\right) \quad (10)$$

where $\lambda_j = \bar{P}_j / \bar{P}_k$ for all $j \in \mathcal{S}_k = \mathcal{C}_k \cup \{k\}$, $\theta_k^* \in (0, 1)$, $P_{o,L_k \times 1}$ is the outage probability of a $L_k \times 1$ distributed MIMO channel whose i^{th} transmit antenna is at a distance $d_{d,i}$, $i = 1, 2, \dots, L_k$, from the destination such that

$$P_{o,L_k \times 1} = \frac{(2^{R_k} - 1)^{L_k}}{(L_k!) (\bar{P}_k)^{L_k}} \prod_{j \in \mathcal{S}_k} \frac{d_{d,j}^\gamma}{\lambda_j} + O\left((\bar{P}_k)^{-L_k-1}\right) \quad (11)$$

and

$$K_2 = \left[\frac{(2^{R_k/\bar{\theta}_k^*} - 1)^{L_k} (\bar{\theta}_k^*)^{L_k-1}}{(2^{R_k} - 1)^{L_k}} + \frac{(2^{R_k/\theta_k^*} - 1)^2 \left(\sum_{j \in \mathcal{C}_k} d_{d,j}^\gamma\right) (L_k!) (\bar{P}_k)^{L_k-2}}{(2^{R_k} - 1)^{L_k} \left(\prod_{j \in \mathcal{C}_k} d_{d,j}^\gamma / \lambda_j\right)} \right]. \quad (12)$$

Note that for $L_k = 2$, our analysis simplifies to the outage analysis for the TD-RC network. For $L_k > 2$, comparing (10) and the two terms in square brackets in (12), one obtains a lower bound on the diversity from the first and second terms in (12) as L_k and 2, respectively. In fact, the first term dominates only when

$$\left(\sum_{j \in \mathcal{C}_k} d_{d,j}^\gamma\right) \leq \frac{(2^{R_k/\bar{\theta}_k^*} - 1)^{L_k-2}}{(L_k!) (\bar{P}_k)^{L_k-2}} \cdot \frac{\left(\prod_{j \in \mathcal{S}_k} d_{d,j}^\gamma / \lambda_j\right)}{d_{d,k}^\gamma}. \quad (13)$$

For a given P_k , for all k , achieving the maximum diversity L_k requires that user k and its cooperating users in \mathcal{C}_k are clustered close enough to satisfy (13). Thus, the maximum DDF diversity for a two-hop cooperative network does not exceed that of TD-RC except when user k and its cooperating users are *clustered*, i.e., the inter-node distances satisfy (13). We illustrate this distance-dependent behavior in Section IV.

3) *TD-UC – Multi-Hop*: Recall that $\pi_k(\cdot)$ is a permutation on \mathcal{C}_k such that user $\pi_k(l)$ begins its transmissions in the fraction $\Theta_{k,l}$, for all $l = 2, 3, \dots, L_k$, and $\pi_k(1) = k$. Unlike the two-hop case where Θ_k is dictated by the node with the worst receive SNR, the fraction $\Theta_{k,l}$, for $l = 1, 2, \dots, L_k - 1$, is the smallest fraction that ensures that at least one cooperating node, denoted as $\pi_k(l+1)$, decodes the message from user k . In general, developing closed form expressions for $P_o^{(k)}$ is not straightforward. In Appendix III, we lower bound $P_o^{(k)}$ by the MIMO outage probability, $P_{o,L_k \times 1}$ and use the CDF of $\Theta_{k,l}$, for all l , to upper bound $P_o^{(k)}$ for any $0 < \theta_{k,l}^* < 1$, for all l , as (see (56))

$$P_o^{(k)} \leq \frac{(2^{R_k} - 1)^{L_k}}{(L_k!) (\bar{P}_k)^{L_k}} \left(\prod_{j=1}^{L_k} \frac{d_{d,\pi_k(j)}^\gamma}{\lambda_{\pi_k(j)}} \right) \cdot [K_c + K_d] + O\left((\bar{P}_k)^{-L_k-1}\right) \quad (14)$$

where the constants K_c and K_d are given by (57) in Appendix III. Our analysis shows that DDF achieves a maximum diversity of L_k for a L_k -hop TD-UC network.

B. Amplify-and-Forward

A cooperating node or a dedicated relay can amplify its received signal and forward it to the destination; the resulting AF strategy is appropriate for nodes with limited processing capabilities. We present the outage bounds for two-hop TD-RC and TD-UC and L_k -hop TD-UC networks. We assume $\theta_k = 1/2$ and $\theta_{k,l} = 1/L_k$, $l = 1, 2, \dots, L_k$, for the two-hop and L_k -hop schemes, respectively.

1) *TD-RC and TD-UC – Two-hop*: We first consider a two-hop AF protocol where only user k transmits in the first fraction and both user k and its cooperating users (TD-UC) or dedicated relay (TD-RC) transmit in the second fraction. User k transmits with a different codebook in the first and second fractions. The other users transmit $X_{l,2} = c_l Y_{l,1}$ where $X_{l,2}$ represents a symbol in the second time fraction, c_l is a complex constant, and $Y_{l,1}$ represents a symbol in the first time fraction. The outage analysis for the two-hop TD-RC network, i.e., $|\mathcal{C}_k| = 1$, is the same as that developed for the half-duplex relay channel in [12]. For the TD-UC two-hop network, i.e., $L_k \geq 2$, in which all $L_k - 1$ cooperating nodes amplify and forward their received signals in the second fraction, the destination receives a signal from user k in the first fraction and receives a sum of signals from user k and the amplified signals from the $L_k - 1$ cooperating users. The resulting outage $P_o^{(k)}$ is given as

$$P_o^{(k)} = \Pr\left(\frac{1}{2}C(G) < R_k\right) \quad (15)$$

where

$$G = |H_{d,k}|^2 \bar{P}_k \left(1 + \frac{1}{c_s^2}\right) + \frac{\bar{P}_k}{c_s^2} \left| \sum_{j \in \mathcal{C}_k} c_j H_{d,j} H_{j,k} \right|^2, \quad (16)$$

the pre-log factor of 1/2 is a result of $\theta_k = 1/2$, $|c_j| = (2\bar{P}_j / |H_{j,k}|^2 \bar{P}_k + 1)^{1/2}$, and $c_s^2 = 1 + \sum_{j \in \mathcal{C}_k} |c_j H_{d,j}|^2$.

We can lower bound $P_o^{(k)}$ by the outage probability of a $L_k \times 1$ MIMO channel where all the relaying antennas transmit the same signal, i.e.,

$$P_o^{(k)} \geq \Pr \left(C \left(|H_{d,k}|^2 \bar{P}_k + \bar{P}_k \left| \sum_{j \in \mathcal{C}_k} H_{d,j} \right|^2 \right) < R_k \right) \quad (17)$$

$$= \frac{(2^{R_k} - 1)^2 d_{d,k}^\gamma}{2 (\bar{P}_k)^2 \left(\sum_{j \in \mathcal{C}_k} 1/d_{d,j}^\gamma \right)} + O \left((\bar{P}_k)^{-3} \right). \quad (18)$$

Thus, the maximum diversity of two-hop AF is bounded by 2. Further, since AF achieves a maximum diversity of 2 with one cooperating node or dedicated relay [4], allowing selection of one cooperating node with the smallest outage allows us to achieve diversity 2. Finally, using the fact that $P_o^{(k)}$ for a non-orthogonal relay channel is at most that of the orthogonal relay channel, we bound $P_o^{(k)}$ using the bound developed for the orthogonal case in [4] as

$$P_o^{(k)} \leq \frac{(2^{2R_k} - 1)^2 d_{d,k}^\gamma \max_{j \in \mathcal{C}_k} (d_{j,k}^\gamma + d_{d,j}^\gamma)}{2 (\bar{P}_k)^2}. \quad (19)$$

Thus, the maximum diversity achievable by a two-hop AF scheme is at most 2 and is independent of the number of cooperating users in \mathcal{C}_k .

2) *TD-UC – Multi-hop*: We consider an L_k -hop cooperative AF protocol where only user k and user $\pi_k(l)$, $l = 1, 2, \dots, L_k$, transmit in the l^{th} fraction, i.e., user $\pi_k(l)$ forwards in the fraction $\theta_{k,l}$ a scaled version of the signal it receives from user k in the first fraction. User k transmits with a different codebook in each fraction. Note that $\pi_k(1) = k$ and $\theta_{k,l} = 1/L_k$ for all l . We write the received signal, $Y_{d,l}$, at the destination in the l^{th} fraction as

$$Y_{d,l} = \begin{cases} H_{d,k} X_{k,l} + Z_{d,l} & l = 1 \\ H_{d,k} X_{k,l} + H_{d,\pi_k(l)} X_{\pi_k(l),l} + Z'_{d,l} & l = 2, \dots, L_k \end{cases} \quad (20)$$

where the signal transmitted by user $\pi_k(l)$ in the l^{th} fraction is $X_{\pi_k(l),l} = c_{\pi_k(l)} Y_{\pi_k(l),1}$ such that $c_{\pi_k(l)}$ is as given for the two-hop case earlier with $\mathcal{C}_k = \{\pi_k(l)\}$. We can write (20) compactly as $\underline{Y}_d = \mathbf{H} \underline{X}_k + \underline{Z}$, where the L_k entries of \underline{Y}_d and \underline{X}_k are related by (20) and \mathbf{H} is the resulting channel gains matrix. The destination decodes after collecting the received signals from all L_k fractions. Choosing $X_{k,l}$, for all l , as independent Gaussian signals, we have $P_o^{(k)} = \Pr \left(\log \left| I + \bar{P}_k \mathbf{H} \mathbf{H}^\dagger \right| < L_k R_k \right)$ where \mathbf{H}^\dagger is the conjugate transpose of \mathbf{H} . We lower bound $P_o^{(k)}$ with the outage probability of a $L_k \times 1$ MIMO channel in (11). On the other hand, one can upper bound $P_o^{(k)}$ by the outage probability of an orthogonal AF protocol in which user k and its cooperating users transmit on orthogonal channels, i.e., only user $\pi_k(l)$ transmits in the fraction $\theta_{k,l}$, as developed in [4]. Thus, we have

$$P_{out} \leq \frac{(2^{L_k R_k} - 1)^{L_k} d_{d,k}^\gamma \prod_{j \in \mathcal{C}_k} (d_{d,j}^\gamma + d_{j,k}^\gamma)}{L_k! (\bar{P}_k)^{L_k}}. \quad (21)$$

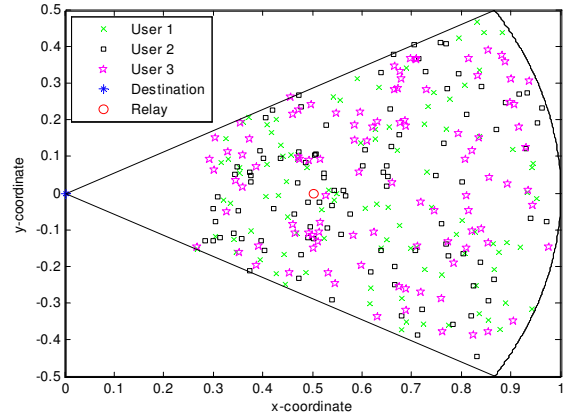


Fig. 2. Sector of a circle with the destination at the origin and 100 randomly chosen locations for a three-user MAC.

Comparing (11) and (21), we see that the L_k -hop AF scheme can achieve a maximum diversity of L_k in the high SNR regime at the expense of user k repeating the signal L_k times.

IV. ILLUSTRATION OF RESULTS

We consider a planar geometry with the users distributed randomly in a sector of a circle of unit radius and angle $\pi/3$. We place the destination at the center of the circle and place the dedicated relay at $(0.5, 0)$ as shown in Fig. 2. The K users are distributed randomly over the sector excluding an area of radius 0.3 around the destination. We consider 100 such random placements and for each such random placement, we compute the outage probabilities P_{out} for the TD-RC, the TD-UC, and the TD-MAC network as an average over the outages of all the time-duplexed users in each network. Finally, we also average P_{out} over the 100 random node placements. We consider a three-user MAC. We assume that all three users have the same transmit power constraint, i.e., $P_k = P_1$ for all k . For the dedicated relay we choose $P_r = f_r \cdot P_1$ where $f_r \in \{0.5, 1\}$. We set the path loss exponent $\gamma = 4$ and the processing factors $\eta_k = \delta_k = \eta$ for all k . We plot P_{out} as a function of P_{tot} for $\eta = 0.01, 0.5$, and 1 thereby modeling three different regimes of processing to transmit power ratios. We consider a symmetric transmission rate, i.e., all users transmit at $R = 0.25$ bits/channel use. We first plot P_{out} as a function of the transmit SNR P_1 in dB obtained by normalizing P_1 by the unit variance noise. We also plot P_{out} as a function of P_{tot} in dB where P_{tot} is given by (6) and (7). For user cooperation, we plot the outage for both the two-hop and three-hop schemes.

A. Outage Probability: DDF

We compare the DDF outage probability in Figs. 3 and 4. The plots validate our analytical results that DDF does not achieve the maximum diversity gains of 3 for the two hop TD-UC network (denoted Coop. 2-hop in plots). For the three-hop TD-UC network (denoted Coop. 3-hop), the slope of P_{out} approaches 3. Further, relative to DDF performance for the TD-RC network, DDF for this 3-hop TD-UC network achieves

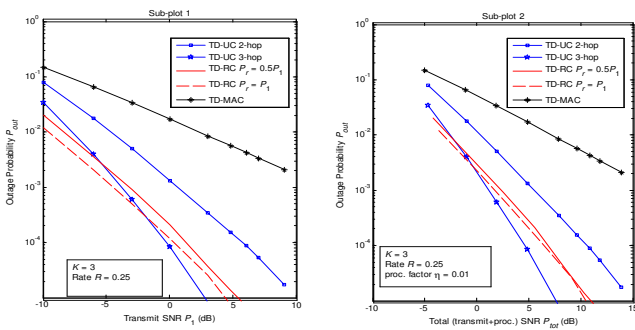


Fig. 3. DDF P_{out} vs. P_1 (sub-plot 1) and vs. P_{tot} (sub-plot 2) for $\eta = 0.01$ and $K = 3$.

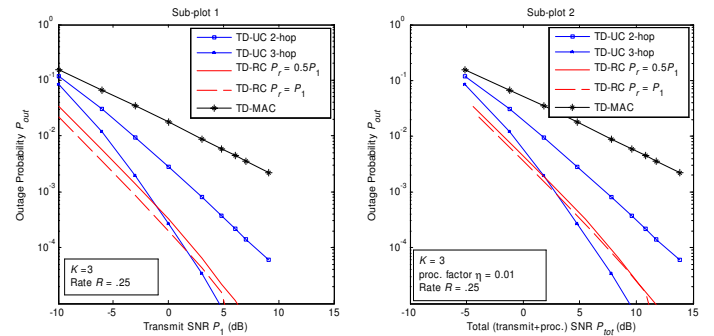


Fig. 5. AF P_{out} vs. P_1 (sub-plot 1) and vs. P_{tot} (sub-plot 2) for $\eta = 1$ (sub-plot 2) and $K = 3$.

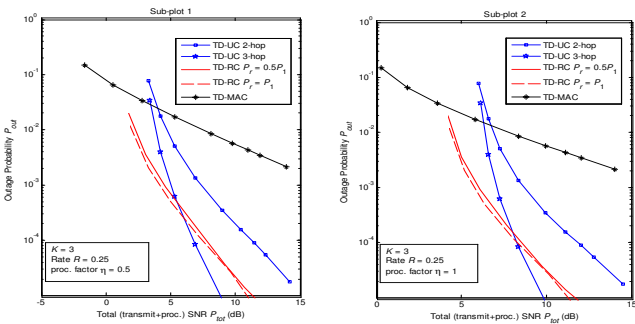


Fig. 4. DDF P_{out} vs. P_{tot} (dB) for $\eta = 0.5$ (sub-plot 1) and $\eta = 1$ (sub-plot 2) for $K = 3$.

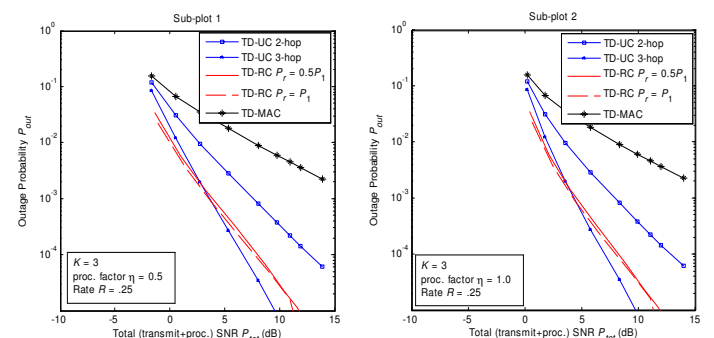


Fig. 6. AF P_{out} vs. P_{tot} for $\eta = 0.5$ (sub-plot 1) and $\eta = 1$ (sub-plot 2) and $K = 3$.

coding gains only as the SNR increases. This difference persists when the energy costs of cooperation are accounted for in sub-plot 2 and Fig. 4 by plotting P_{out} as a function of P_{tot} . This difference in SNR gains between UC and RC is due to the fact that UC increases spatial diversity at the expense of requiring users to consume power for cooperative transmissions. Observe that with increasing η , the outage curves are translated to the right. In fact, for a fixed R , the processing costs increase with increasing η , and thus, we expect the SNR gains from cooperation to diminish relative to TD-MAC, particularly in lower SNR regimes.

B. Outage Probability: AF

In Figs. 5 and 6 we plot the two user AF outage probability for all three networks. As predicted, both TD-RC and TD-UC networks achieve a maximum diversity of 2 for the two-hop scheme. The TD-UC three-hop scheme has a maximum diversity approaching 3. However, it achieves coding gains relative to the TD-RC network only as the SNR increases. These gains are a result of the model chosen for front-end processing and amplification costs, and thus, the total processing power will scale proportionate to the number of users that a node relays for. Observe that AF outperforms DDF for large processing factors η because AF requires little processing.

The numerical analysis can be extended to arbitrary dedicated relay positions. In general, the choice of the dedicated-relay position is a tradeoff between cooperating with as many

users as possible and being, on average, closer to the users than the destination is. Placing the dedicated relay at the symmetric location $(0.5, 0)$ seems to be a reasonable tradeoff.

V. CONCLUDING REMARKS

We compared the outage performance of user and dedicated-relay cooperation in a time-duplexed multiaccess network using the total transmit and processing power as a cost metric. We presented geometry-inclusive upper and lower bounds on the outage probability of DDF and AF to facilitate comparisons of diversity and coding gains achieved by the two cooperative approaches. Using area-averaged numerical results that account for the costs of cooperation, we demonstrated that the TD-RC network achieves SNR gains that diminish the diversity advantage of the TD-UC network.

In conclusion, we see that user cooperation is desirable only if the processing costs associated with achieving the maximum diversity gains are not prohibitive, i.e., in the regime where user cooperation achieves positive coding gains relative to the dedicated-relay cooperative and non-cooperative networks. The simple processing cost model presented here captures the effect of transmit rate on processing power. One can also tailor this model to explicitly include delay, complexity, and device-specific processing costs.

APPENDIX I
DISTRIBUTION OF WEIGHTED SUM OF EXPONENTIAL
RANDOM VARIABLES

Consider a collection of i.i.d. unit mean exponential random variables E_l , $l = 1, 2, \dots, L$. We denote a weighted sum of E_l , for all l , as $H = \sum_{l=1}^L c_l E_l$ where $c_l > 0$ and $c_m \neq c_k$ for all l and $m \neq k$. The following lemma summarizes the probability distribution of H [13, p. 11].

Lemma 1: The random variable H has a distribution given as

$$p_H(h) = \begin{cases} \sum_{l=1}^L \frac{c_l}{c_l} e^{-h/c_l} & h \geq 0 \\ 0 & \text{otherwise} \end{cases} \quad (22)$$

where the constants C_l , for all l , are

$$C_l = \begin{cases} 1 & L = 1 \\ \frac{(-c_l)^{L-1}}{\prod_{j=1, j \neq l}^L (c_j - c_l)} & L > 1. \end{cases} \quad (23)$$

The cumulative distribution function of H is

$$F_H(\eta) = \sum_{l=1}^L C_l (1 - e^{-\eta/c_l}) \quad (24)$$

and the first non-zero term in the Taylor series expansion of $F_H(\eta)$ about $\eta = 0$ is $\eta^L / \left(L! \prod_{l=1}^L c_l \right)$.

APPENDIX II
DDF OUTAGE BOUNDS

A. Two-Hop Relay Cooperative Network

For a DDF dedicated relay, the listen fraction is the random variable (see [3, (13), pp. 4157])

$$\Theta_k = \min \left(1, R_k / \log \left(1 + \frac{|A_{r,k}|^2 \bar{P}_k}{d_{r,k}^\gamma} \right) \right). \quad (25)$$

Θ_k is a mixed (discrete and continuous) random variable with a cumulative distribution function (CDF) given as

$$F_{\Theta_k}^{(r)}(\theta_k) = \begin{cases} 0 & \theta_k \leq 0 \\ \exp \left[-\frac{(2^{R_k/\theta_k} - 1) d_{r,k}^\gamma}{\bar{P}_k} \right] & 0 < \theta_k < 1 \\ 1 & \theta_k = 1. \end{cases} \quad (26)$$

The mutual information collected at the destination over both the *listen* and *transmit* fractions is (see [3, Appendix D]) $I_2^{DF} = \Theta_k G_1 + \bar{\Theta}_k G_2$ where $\bar{\Theta}_k = (1 - \Theta_k)$, $\bar{P}_k = K P_k$, $\bar{P}_r = P_r / \bar{\Theta}_k$, $G_1 = C(|H_{d,k}|^2 \bar{P}_k)$, and $G_2 = C(|H_{d,k}|^2 \bar{P}_k + |H_{d,r}|^2 \bar{P}_r)$. The outage probability for user k transmitting at a fixed rate R_k is then given as $P_o^{(k)} = \Pr(I_2^{DF} < R_k)$. From (25), $\Theta_k = 0$ only for $d_{r,k} = 0$, i.e., only when user k and the dedicated relay are co-located, and for this case $P_o^{(k)}$ simplifies to the 2×1 MIMO channel outage probability given by

$$P_{o,2 \times 1} = \frac{(2^{R_k} - 1)^2 d_{d,k}^\gamma d_{d,r}^\gamma}{2\lambda (\bar{P}_k)^2} + O\left((\bar{P}_k)^{-3}\right). \quad (27)$$

where we let P_r and \bar{P}_k scale such that $P_r / \bar{P}_k = \lambda$ is a positive constant. Using (24), we have $P_{o,2 \times 1}$ is a lower bound

on $P_o^{(k)}$ because $G_2 \geq G_1$. On the other hand, for any θ_k , $P_o^{(k)}(\theta_k)$ can be upper bounded as

$$P_o^{(k)}(\theta_k) \leq \Pr(\theta_k G_1 < R_k) = P_{o,1}^{(k)}(\theta_k), \text{ and} \quad (28a)$$

$$P_o^{(k)}(\theta_k) \leq \Pr(\bar{\theta}_k G_2 < R_k) = P_{o,2}^{(k)}(\theta_k) \quad (28b)$$

Thus, we have

$$P_o^{(k)} = \mathbb{E} P_o^{(k)}(\Theta_k) \leq \mathbb{E} \min(P_{o,1}^{(k)}(\Theta_k), P_{o,2}^{(k)}(\Theta_k)) = P_{UB}^{(k)} \quad (29)$$

Let $\eta = 2^{R_k/\bar{\theta}_k} - 1$, $c_1 = \bar{P}_k / d_{d,k}^\gamma$, and $c_2 = \bar{P}_r / d_{d,r}^\gamma$. From (23), we have $C_1 = c_1 / (c_1 - c_2)$ and $C_2 = c_2 / (c_2 - c_1)$. Using Lemma 1, we have

$$P_{o,1}^{(k)}(\theta_k) = \Pr\left(G_1 < \frac{R_k}{\theta_k}\right) = 1 - \exp\left[\frac{-(2^{R_k/\theta_k} - 1) d_{d,k}^\gamma}{\bar{P}_k}\right] \quad (30a)$$

$$\leq \frac{(2^{R_k/\theta_k} - 1) d_{d,k}^\gamma}{\bar{P}_k} \quad (30b)$$

$$P_{o,2}^{(k)}(\theta_k) = \Pr\left(G_2 < \frac{R_k}{\bar{\theta}_k}\right) = \sum_{l=1}^2 C_l (1 - e^{-\eta/c_l}) \quad (31a)$$

$$= \frac{(2^{R_k/\bar{\theta}_k} - 1)^2 \bar{\theta}_k d_{d,k}^\gamma d_{d,r}^\gamma}{2\lambda (\bar{P}_k)^2} + O\left((\bar{P}_k)^{-3}\right) \quad (31b)$$

where the bound in (31) follows from expanding and simplifying the exponential functions. From (31), we see that for a fixed \bar{P}_k and $d_{j,k}$ for all j, k , the minimum in (29) is dominated by $P_{o,2}^{(k)}(\theta_k)$ for small θ_k and by $P_{o,1}^{(k)}(\theta_k)$ as θ_k approaches 1. Finally, we have $P_{o,2 \times 1} = P_{o,2}^{(k)}(\theta_k = 0)$. In general, $P_{UB}^{(k)}$ is not easy to evaluate analytically. Since we are interested in the achievable diversity, we develop a bound on $P_{UB}^{(k)}$ for a fixed R_k . We have, for any θ_k^* , $0 < \theta_k^* < 1$,

$$P_{UB}^{(k)} = \int_0^1 P_{\Theta_k}(\theta_k) \min\left(P_{o,1}^{(k)}(\theta_k), P_{o,2}^{(k)}(\theta_k)\right) d\theta_k \quad (32)$$

$$\leq \int_0^{\theta_k^*} P_{\Theta_k}(\theta_k) P_{o,2}^{(k)}(\theta_k) d\theta_k \quad (33)$$

$$+ \int_{\theta_k^*}^1 P_{\Theta_k}(\theta_k) P_{o,1}^{(k)}(\theta_k) d\theta_k$$

$$\leq F_{\Theta_k}(\theta_k^*) P_{o,2}^{(k)}(\theta_k^*) + (1 - F_{\Theta_k}(\theta_k^*)) P_{o,1}^{(k)}(\theta_k^*) \quad (34)$$

$$\leq P_{o,2}^{(k)}(\theta_k^*) + \frac{(2^{R_k/\theta_k^*} - 1) d_{r,k}^\gamma}{\bar{P}_k} \cdot P_{o,1}^{(k)}(\theta_k^*) \quad (35)$$

$$\leq \left[\frac{(2^{R_k/\bar{\theta}_k^*} - 1)^2 \bar{\theta}_k^*}{(2^{R_k} - 1)^2} + \frac{2 d_{r,k}^\gamma (2^{R_k/\theta_k^*} - 1)^2 \lambda}{d_{d,r}^\gamma (2^{R_k} - 1)^2} \right]$$

$$\cdot \frac{(2^{R_k} - 1)^2 d_{d,k}^\gamma d_{d,r}^\gamma}{2\lambda (\bar{P}_k)^2} + O\left((\bar{P}_k)^{-3}\right) \quad (36)$$

where the equality in (33) holds when $P_{o,2}^{(k)}(\theta_k) < P_{o,1}^{(k)}(\theta_k)$ for $\theta_k < \theta_k^*$ and vice-versa, and (34) follows because $P_{o,1}^{(k)}(\theta_k)$ and $P_{o,2}^{(k)}(\theta_k)$ decrease and increase, respectively, with θ_k and (35) follows from using (26) to bound $1 - F_{\Theta_k}(\theta_k^*)$. Finally,

we note that for any fixed $0 < \theta_k^* < 1$, for fixed inter-node distances, the term in square brackets in (36) is a multiplicative constant separating the upper bound (36) and the lower bound (27) on $P_o^{(k)}$.

B. Two-hop User Cooperative Network

The above analysis extends to the two-hop TD-UC network. Recall that a DDF cooperating node remains in the *listen* mode until it successfully decodes its received signal from the source. Thus, for the two-hop TD-UC network, the *listen* fraction for each cooperating node j , for all $j \in \mathcal{C}_k$, is given by (25) with the substitution $r = j$. Further, since the *listen* fraction Θ_k is now the largest among all j , from (25) we have

$$\Theta_k = \min \left(1, \max_{j \in \mathcal{C}_k} \left\{ R_k / C \left(|A_{j,k}|^2 \bar{P}_k / d_{j,k}^\gamma \right) \right\} \right) \quad (37)$$

where the transmit power \bar{P}_k , for all $k \in \mathcal{K}$, satisfies (2) and is given by (3). Let $F_{\Theta_k}^{(j)}(\theta_k)$ be the CDF $F_{\Theta_k}^{(r)}(\theta_k)$ in (26) with the index r replaced by j . From the independence of $A_{j,k}$ for all $j \in \mathcal{C}_k$, the CDF of Θ_k is $F_{\Theta_k}(\theta_k) = \prod_{j \in \mathcal{C}_k} F_{\Theta_k}^{(j)}(\theta_k)$ which in turn is given by $F_{\Theta_k}^{(r)}(\theta_k)$ evaluated at $d_{r,k} = \sum_{j \in \mathcal{C}_k} d_{j,k}^\gamma$. The destination collects information from the transmissions of user k and all its cooperating nodes in \mathcal{C}_k over both the *transmit* and *listen* fractions. The resulting mutual information achieved by user k at the destination is (see [14]) $I_{2,DF}(\Theta_k) = \Theta_k G_1 + \bar{\Theta}_k G_2$ where $\bar{\Theta}_k = 1 - \Theta_k$, $G_1 = C(|H_{d,k}|^2 \bar{P}_k)$, and $G_2 = C(|H_{d,k}|^2 \bar{P}_k + \sum_{j \in \mathcal{C}_k} |H_{d,j}|^2 \bar{P}_j / \bar{\Theta}_k)$. The DDF outage probability for user k transmitting at a fixed rate R_k in a two-hop TD-UC network is thus given as $P_o^{(k)} = \Pr(I_{2,DF} < R_k)$. Analogously to the two-hop TD-RC analysis earlier, we can lower bound $P_o^{(k)}$ by the outage probability, $P_{o,L_k \times 1}$, of a $L_k \times 1$ distributed MIMO channel using (24), and scaling \bar{P}_j and \bar{P}_k such that $\bar{P}_j / \bar{P}_k = \lambda_j$ is a constant, for all j , as

$$P_{o,L_k \times 1} = \frac{(2^{R_k} - 1)^{L_k} d_{d,k}^\gamma}{(L_k!) (\bar{P}_k)^{L_k}} \cdot \left(\prod_{j \in \mathcal{S}_k} \frac{d_{d,j}^\gamma}{\lambda_j} \right) + O\left((\bar{P}_k)^{-L_k - 1}\right) \quad (38)$$

where we enumerate the $(L_k - 1)$ cooperative nodes in \mathcal{C}_k as $l = 2, 3, \dots, L_k$, and write $\mathcal{S}_k = \{k\} \cup \mathcal{C}_k$. Let $\eta = 2^{R_k/\theta_k} - 1$, $c_1 = \bar{P}_k / d_{d,k}^\gamma$, and $c_l = \bar{P}_l / d_{d,l}^\gamma \bar{\theta}_k$, $l = 2, 3, \dots, L_k$, where the $\bar{\theta}_k$ in c_l is due to the definition of \bar{P}_l in (3). The C_l , for all $l = 1, 2, \dots, L_k$, are given by (23). For a fixed R_k , we upper bound $P_o^{(k)}$ using (28) as

$$P_o^{(k)} = \mathbb{E} P_o^{(k)}(\Theta_k) \leq \mathbb{E} \min(P_{o,1}^{(k)}(\Theta_k), P_{o,2}^{(k)}(\Theta_k)) = P_{UB}^{(k)}. \quad (39)$$

We upper bound $P_{o,1}^{(k)}(\theta_k)$ using (30) and compute

$$P_{o,2}^{(k)}(\theta_k) = \frac{(2^{R_k/\bar{\theta}_k} - 1)^{L_k} (\bar{\theta}_k)^{L_k - 1}}{(L_k!) (\bar{P}_k)^{L_k}} \left(\prod_{j \in \mathcal{S}_k} \frac{d_{d,j}^\gamma}{\lambda_j} \right) + O\left((\bar{P}_k)^{-L_k - 1}\right). \quad (40)$$

Analogous to the steps in (32)-(36) for the TD-RC case, for any θ_k^* , $0 < \theta_k^* < 1$, we can upper bound $P_{UB}^{(k)}$ by

$$\begin{aligned} P_{UB}^{(k)} &\leq F_{\Theta_k}(\theta_k^*) P_{o,2}^{(k)}(\theta_k^*) + (1 - F_{\Theta_k}(\theta_k^*)) P_{o,1}^{(k)}(\theta_k^*) \quad (41) \\ &\leq P_{o,2}^{(k)}(\theta_k^*) + \frac{(2^{R_k/\theta_k^*} - 1) \left(\sum_{j \in \mathcal{C}_k} d_{j,k}^\gamma \right)}{\bar{P}_k} \cdot P_{o,1}^{(k)}(\theta_k^*) \quad (42) \end{aligned}$$

which simplifies to the expression

$$\begin{aligned} &\left[\frac{(2^{R_k/\bar{\theta}_k^*} - 1)^{L_k} (\bar{\theta}_k^*)^{L_k - 1}}{(2^{R_k} - 1)^{L_k}} + \right. \\ &\quad \left. \frac{(L_k!) \left(\sum_{j \in \mathcal{C}_k} d_{j,k}^\gamma \right) (\bar{P}_k)^{L_k - 2} (2^{R_k/\theta_k^*} - 1)^2}{\left(\prod_{j \in \mathcal{C}_k} d_{d,j}^\gamma / \lambda_j \right) (2^{R_k} - 1)^{L_k}} \right] \\ &\cdot \left[\frac{(2^{R_k} - 1)^{L_k}}{(L_k!) (\bar{P}_k)^{L_k}} \left(\prod_{j \in \mathcal{S}_k} \frac{d_{d,j}^\gamma}{\lambda_j} \right) \right] + O\left((\bar{P}_k)^{-L_k - 1}\right) \quad (43) \end{aligned}$$

APPENDIX III

MULTI-HOP COOPERATIVE NETWORK – DDF OUTAGE ANALYSIS

The DDF outage probability of user k transmitting at a fixed rate R_k in a multi-hop user cooperative network is $P_o^{(k)} = \Pr(I_{2,DF}^c < R_k)$ where $I_{2,DF}^c(\Theta_k) = \sum_{l=1}^{L_k} \Theta_{k,l} G_l$. The function G_l is given by

$$G_l = C \left(\sum_{j=1}^l |H_{d,\pi_k(j)}|^2 \frac{\bar{P}_{\pi_k(j)}}{\bar{\Theta}_{k,j}} \right) \quad l = 1, 2, \dots, L_k, \quad (44)$$

where \bar{P}_k is given by (3) and

$$\Theta_{k,l}^{sum} \triangleq \sum_{j=1}^{l-1} \Theta_{k,j}, \quad \text{for } l = 1, 2, \dots, L_k, \text{ and} \quad (45)$$

$$\bar{\Theta}_{k,l}^{sum} \triangleq 1 - \Theta_{k,l}^{sum} \quad (46)$$

with $\bar{\Theta}_{k,L_k}^{sum} = \Theta_{k,L_k}$ and $\Theta_{k,-1} = 0$ such that $\bar{\Theta}_{k,1}^{sum} = 1$. Recall that $\pi_k(\cdot)$ is a permutation on \mathcal{C}_k such that user $\pi_k(l)$ begins its transmissions in the fraction $\Theta_{k,l}$, for all $l = 2, 3, \dots, L_k$. Furthermore, $\pi_k(1) = k$ and we write $\pi_k(i:j) = \{\pi_k(i), \pi_k(i+1), \dots, \pi_k(j)\}$.

We write $\underline{\Theta}_k$ to denote a $(L_k - 1)$ -length random vector with entries $\Theta_{k,l}$, $l = 1, 2, \dots, L_k - 1$, and $\lambda_{\pi_k(j)} = \bar{P}_{\pi_k(j)} / \bar{P}_k$ for all $\pi_k(j) \in \mathcal{C}_k$. Further, we write $\underline{\Theta}_k^{(l)}$ to denote the vector of the first l entries of $\underline{\Theta}_k$. The fraction $\Theta_{k,l}$, $l = 1, 2, \dots, L_k - 1$, is the smallest value such that at least one new node, denoted as $\pi_k(l+1)$, decodes the message from user k . The analysis for this problem seems difficult; so we replace it by analyzing a simpler strategy where node $\pi_k(l+1)$ collects energy only in fraction $\Theta_{k,l}$ from the transmissions of user k as well as the users in $\pi_k(1:l)$. For this strategy, we have

$$\Theta_{k,l} = \min \left\{ \bar{\Theta}_{k,l}^{sum}, \min_{\pi_k(l+1) \in \mathcal{C}_k \setminus \pi_k(1:l)} f(\pi_k(l+1)) \right\} \quad (47)$$

where $f(\pi_k(l+1))$ is given by

$$C \left(\frac{R_k}{\sum_{m=1}^l |A_{\pi_k(l+1), \pi_k(m)}|^2 \bar{P}_{\pi_k(m)} / d_{\pi_k(l+1), \pi_k(m)}^\gamma} \right) \quad (48)$$

Applying Lemma 1, the CDF of $\Theta_{k,l}$ conditioned on $\underline{\Theta}_k^{l-1} = \underline{\theta}_k^{l-1}$ simplifies to

$$F_{\Theta_{k,l} | \underline{\Theta}_k^{l-1}}(\theta_{k,l} | \underline{\theta}_k^{l-1}) = \begin{cases} 0 & \theta_{k,l} \leq 0 \\ 1 - \tilde{F} & 0 < \theta_{k,l} < \bar{\theta}_{k,l}^{sum} \\ 1 & \theta_{k,l} = \bar{\theta}_{k,l}^{sum} \end{cases} \quad (49)$$

where

$$\tilde{F} = \prod_{j \in \mathcal{C}_k \setminus \pi_k(2:l)} \left[F_{H_{j,l}^{sum}}(2^{R_k/\theta_{k,l}} - 1) \right] \quad (50)$$

and from (47), $H_{j,l}^{sum} \triangleq \sum_{m=1}^l c_m |A_{j, \pi_k(m)}|^2$ with $c_m = \lambda_{\pi_k(m)} \bar{P}_k / d_{j, \pi_k(m)}^\gamma$ for all $m = 1, 2, \dots, l$, and $\bar{\theta}_{k,l}$ is given by (45). The dominant term of each $F_{H_{j,l}^{sum}}$ is proportional to $(\bar{P}_k)^{-l}$, and thus, the dominant term of $1 - F_{\Theta_{k,l} | \underline{\Theta}_k^{l-1}}$ is proportional to $(\bar{P}_k)^{-l(L_k-l)}$.

For a fixed R_k , we lower bound $P_o^{(k)}$ by the outage probability $P_{o,L_k \times 1}$ of a $L_k \times 1$ distributed MIMO channel in (38). Generalizing the analyses in Appendix II, we upper bound $P_o^{(k)}$ as

$$P_o^{(k)} \leq \mathbb{E} \min_{l \in \mathcal{K}} (P_{o,l}^{(k)}(\underline{\Theta}_k)) = P_{UB}^{(k)} \quad (51)$$

where we use Lemma 1 to write

$$P_{o,l}^{(k)}(\underline{\theta}_k) \triangleq \Pr \left(G_l < \frac{R_k}{\theta_{k,l}} \right) \quad (52)$$

$$= \frac{(2^{R_k/\theta_{k,l}} - 1)^l}{(l!) (\bar{P}_k)^l} \left(\prod_{j=1}^l \frac{d_{d, \pi_k(j)}^\gamma \bar{\theta}_{k,j}^{sum}}{\lambda_{\pi_k(j)}} \right) + O \left((\bar{P}_k)^{-l-1} \right). \quad (53)$$

The probability $P_{UB}^{(k)}$ is given as (see (45))

$$P_{UB}^{(k)} = \int_{\theta_{k,1}=0}^1 \dots \int_{\theta_{k,L_k-1}=0}^{\bar{\theta}_{k,L_k-1}^{sum}} P_{\underline{\Theta}_k}(\underline{\theta}_k) \min_{l \in \mathcal{K}} (P_{o,l}^{(k)}(\theta_{k,l})) d\theta_k. \quad (54)$$

For any $0 < \theta_{k,l}^* < \bar{\theta}_{k,l}^*$, $1 \leq l < L_k$, the integral in (54) over the $(L_k - 1)$ -dimensional hyper-cube can be written as a sum of 2^{L_k-1} integrals, each spanning $(L_k - 1)$ -dimensions, such that there are $\binom{L_k-1}{j}$ integrals for which j of the $(L_k - 1)$ $\theta_{k,l}$ parameters range from 0 to $\theta_{k,l}^*$, $j = 0, 1, \dots, L_k - 1$ while the remaining range from $\theta_{k,l}^*$ to 1. Thus, we upper bound $P_{UB}^{(k)}$ in (54) by

$$\int_0^{\theta_{k,1}^*} \int_0^{\bar{\theta}_{k,2}^{sum}} \dots \int_0^{\bar{\theta}_{k,L_k-1}^{sum}} P_{\underline{\Theta}_k}(\underline{\theta}_k) P_{o,L_k}^{(k)}(\underline{\theta}_k) d\theta_k + \int_{\theta_{k,1}^*}^1 \int_0^{\bar{\theta}_{k,2}^{sum}} \dots \int_0^{\bar{\theta}_{k,L_k-1}^{sum}} P_{\underline{\Theta}_k}(\underline{\theta}_k) P_{o,1}^{(k)}(\underline{\theta}_k) d\theta_k \quad (55)$$

where the dominant outage terms for $\theta_{k,1} \leq \theta_{k,1}^*$ and $\theta_{k,1} > \theta_{k,1}^*$ are bounded by $P_{o,L_k}^{(k)}(\underline{\theta}_k)$ and $P_{o,1}^{(k)}(\underline{\theta}_k)$, respectively. Furthermore, using the monotonic properties of $P_{o,l}^{(k)}$, the first

term in (55) is bounded by $P_{o,L_k}^{(k)}(\underline{\theta}_k^*)$ and the second term is bounded by $\left(1 - F_{\Theta_{k,1}}(\theta_{k,1}^*)\right) P_{o,1}^{(k)}(\underline{\theta}_k^*)$. From (49) and (52), using the fact that $P_{o,1}^{(k)}(\underline{\theta}_k^*)$ has the smallest absolute exponents of \bar{P}_k , namely 1, and $\left(1 - F_{\Theta_{k,1}}(\theta_{k,1}^*)\right) P_{o,1}^{(k)}(\underline{\theta}_k^*)$ scales as $(\bar{P}_k)^{-L_k}$, $P_{UB}^{(k)}$ can be upper bounded by

$$P_{o,L_k}^{(k)}(\underline{\theta}_k^*) + \left(1 - F_{\Theta_{k,1}}(\theta_{k,1}^*)\right) P_{o,1}^{(k)}(\underline{\theta}_k^*) \leq \frac{(2^{R_k} - 1)^{L_k}}{(L_k!) (\bar{P}_k)^{L_k}} \left(\prod_{j=1}^{L_k} \frac{d_{d, \pi_k(j)}^\gamma}{\lambda_{\pi_k(j)}} \right) [K_c + K_d] + O \left((\bar{P}_k)^{-L_k-1} \right) \quad (56)$$

where $K_c = \frac{(2^{R_k/\theta_{k,L_k}^*} - 1)^{L_k} \left(\prod_{j=1}^{L_k} \bar{\theta}_{k,j}^{sum} \right)^*}{(2^{R_k} - 1)^{L_k}}$, and

$$K_d = \frac{(2^{R_k/\theta_{k,1}^*} - 1)^{L_k} (L_k!)}{(2^{R_k} - 1)^{L_k}} \cdot \prod_{j=2}^{L_k} \frac{d_{\pi_k(j), \pi_k(1)}^\gamma}{\lambda_{\pi_k(j)}}. \quad (57)$$

Combining (56) and (38), the maximum achievable diversity is L_k .

REFERENCES

- [1] Atheros Communications, "Power consumption and energy efficiency comparisons of wlan products," www.atheros.com/pt/whitepapers/atheros_power_whitepaper.pdf.
- [2] W. Heinzelman, A. Chandrakasan, and H. Balakrishnan, "Energy-efficient communication protocols for wireless microsensor networks," in *Proc. 33rd Hawaii Intl. Conf. Systems and Sciences*, Maui, HA, Jan. 2000, pp. 1–10.
- [3] K. Azarian, H. El Gamal, and P. Schniter, "On the achievable diversity-multiplexing tradeoff in half-duplex cooperative channels," *IEEE Trans. Inform. Theory*, vol. 51, no. 12, pp. 4152–4172, Dec. 2005.
- [4] J. N. Laneman, "Network coding gain of cooperative diversity," in *Proc. IEEE Military Comm. Conf. (MILCOM)*, Monterey, CA, Nov 2004, pp. 3714–3722.
- [5] T. M. Cover and J. A. Thomas, *Elements of Information Theory*. New York: Wiley, 1991.
- [6] G. Kramer, H. Gastpar, and P. Gupta, "Cooperative strategies and capacity theorems for relay networks," *IEEE Trans. Inform. Theory*, vol. 51, no. 9, pp. 3027–3063, Sept. 2005.
- [7] L. Sankaranarayanan, G. Kramer, and N. B. Mandayam, "Cooperation vs. hierarchy: An information-theoretic comparison," in *Proc. IEEE Int. Symp. Inf. Theory*, Adelaide, Australia, Sept. 2005, pp. 411–415.
- [8] A. Nosratinia and T. E. Hunter, "Grouping and partner selection in cooperative wireless networks," *IEEE JSAC Cooperative Communications and Networking*, vol. 25, no. 2, pp. 369–378, Feb. 2007.
- [9] S. Kadloor and R. Adve, "Relay selection and power allocation in cooperative cellular networks," Mar. 2009, arxiv.org e-print 0903.2426.
- [10] M. Bhardwaj, T. Garnett, and A. P. Chandrakasan, "Upper bounds on the lifetime of sensor networks," in *Proc. 2001 IEEE Intl. Conf. Commun.*, Helsinki, Finland, June 2001.
- [11] L. Zheng and D. N. C. Tse, "Diversity and multiplexing: A fundamental tradeoff in multiple-antenna channels," *IEEE Trans. Inform. Theory*, vol. 49, no. 5, pp. 1073–1096, May 2003.
- [12] R. U. Nabar, H. Bölcskei, and F. W. Kneubühler, "Fading relay channels: Performance limits and space-time signal design," *IEEE JSAC*, vol. 22, no. 6, pp. 1099–1109, Aug. 2004.
- [13] D. R. Cox, *Renewal Theory*. London: Methuen's Monographs on Applied Probability and Statistics, 1967.
- [14] G. Kramer, "Models and theory for relay channels with receive constraints," in *42nd Annual Allerton Conf. on Commun., Control, and Computing*, Monticello, IL, Sept. 2004.

Green Communications: A Call for Power Efficient Wireless Systems

An He, Ashwin Amanna, Thomas Tsou, Xuetao Chen, Dinesh Datla, Joseph Gaeddert, Timothy R. Newman, S.M. Shajedul Hasan, Haris I. Volos, Jeffery H. Reed, and Tamal Bose
Bradley Department of Electrical and Computer Engineering, Virginia Tech, Blacksburg, VA, USA
Email: ahe@vt.edu

Abstract—Telecommunication usage has skyrocketed in recent years and will continue to grow as developing world reaches to wireless as the communication medium of choice. The telecommunications world is only now addressing the significant environmental impact it is creating as well as the incredible cost on power usage. This realization has led to a push towards Green Communications that strives for improving energy efficiency as well as energy independence of telecommunications. A survey of existing metrics for energy efficiency is discussed with specific adaptations for a communication centric viewpoint. This paper reviews recent energy efficient advances made at specific point within the communications cycle such as components, network operation and topology, and incorporating renewable and alternative energy into base stations. We further survey several holistic approaches that illustrate the dependencies between layers of the communications stack and operation/deployment. These approaches include cross layer design, cognitive radio, and wireless distributed computing.

Index Terms—green communications, wireless, energy efficiency, metrics

I. INTRODUCTION

The intersection of two undeniable trends, the escalating energy costs and the meteoric growth in communications usage, creates an urgent need to address the development of energy efficient communications. The cellular network is the largest factor contributing to the mobile industry's environmental impact [1] with the emissions from the telecommunications business sector estimated at between 0.5% [2] and 1% of the entire world's carbon footprint [3]. While this may sound paltry, the true seriousness of the issue is more apparent from the perspective of energy costs. In some telecommunications markets, energy-related costs account for as much as half of a mobile operator's operating expenses [4, 5]. The expectation that energy costs may rise three fold over the next seven years is great cause for concern [2].

Recently, the term 'Green Communications' has been marketed and sloganized as a solution to addressing the growing cost and environmental impact of telecommunications. However, there is a lack of explicit energy efficiency definitions and metrics for wireless telecommunications to provide a sound foundation for assessing overall improvement and quantifying Green Communications.

Fig. 1 highlights the relative power consumption of various components and operational aspects of a base station (BS) [6]. In this figure, the total power consumption of signal processing & control unit (30%) and RF conversion & power amplifier (70%) is used as the normalization baseline. From this figure, the top three power consuming components are feeder network, RF conversion & amplification, and climate control (e.g., air conditioning).

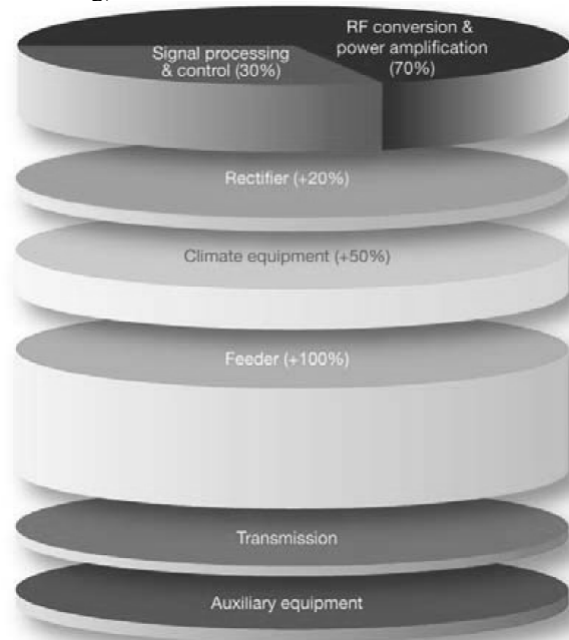


Figure 1. Energy consumption at a typical macro BS (normalized) [6].

Several hurdles must be overcome in order to significantly improve energy efficiency in communications. The current design paradigm focuses on separation between individual levels within the network protocol stack. Additionally, deployment, operations, and

Manuscript received January 31, 2011; revised May 9, 2011; accepted June 24, 2011.

A. He, A. Amanna, T. Tsou, X. Chen, D. Datla, J. Gaeddert, T. R. Newman, S.M. Hasan, H. I. Volos, J. H. Reed, T. Bose are with Wireless @ Virginia Tech, Virginia Tech, Blacksburg, VA 24061, USA (e-mail: {ahe, aamanna, tsou, chenxt, ddatla, joseph.gaeddert, trnewman, reedih, tbose}@vt.edu).

peripheral elements such as air conditioning and fuel transportation are further disconnected from the original component and system design cycle. This compartmentalized thinking severely limits truly transformational benefits. Currently, most advancements in energy efficient communications focus on a narrowly defined aspect of the communications cycle such as power amplifiers or incorporating renewable energy sources. This paper contends that energy efficient communications must be analyzed from an overall holistic system perspective rather than at singular levels.

In this paper, we strive to add a level of formalization to the term Green Communications and address fundamental hurdles to realizing overall improvements. Specifically, we survey and contrast existing definitions and metrics in energy efficiency and their applications towards communications. We collate advancements in energy efficiency from different layers within the communications cycle to provide a perspective of the current state of energy efficiency research and operations. Finally, we introduce solutions that incorporate interaction across multiple layers of the network stack and different aspects of the communications cycle. This paradigm ties together energy efficient strategies from different layers.

The remainder of this paper is organized as follows: Section II highlights current energy usage and costs associated with telecommunications and places these statistics into perspective by comparing to other aspects of our daily life. Section III reviews and discusses existing metrics for power and energy efficiency and identifies requirements for telecommunications specific metrics. Section IV presents advancements in energy efficiency in communications at specific levels within the communications stack and lifecycle. Section V discusses solutions that are not burdened by the status quo of existing separation among layers. Finally, the paper is summarized in Section VI.

II. THE NEED FOR GREEN COMMUNICATIONS

Information and communications technology usage has grown at a staggering rate worldwide with an estimated 6 billion subscriptions in 2010 [7]. Every year, 120,000 new BS's are deployed serving 400 million new mobile subscribers around the world [8]. Fig. 2 illustrates the growth pattern for mobile cellular subscriptions between 2000 and 2010 [7]. The developing regions are increasingly turning to wireless as a leap frog technology bypassing fixed infrastructure and the mobile subscription increases for a factor of ten. From 2000 till 2010, the mobile subscription in developed regions increases by about 200%, whereas that in developing regions increases by about 1300%. Statistics also show that in 2000 about 40% of all mobile subscriptions were attributed to the developing world and in 2009 this percentage grew to about 70% [9].

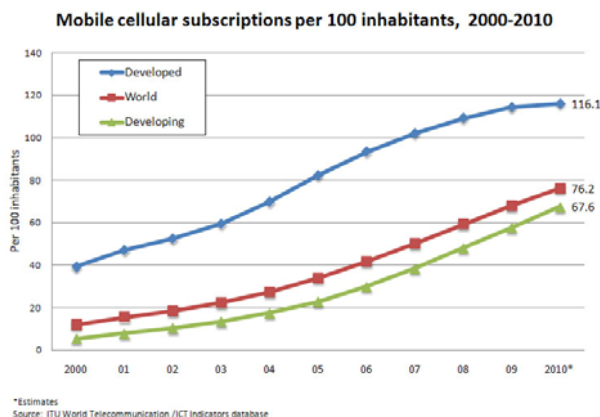


Figure 2. Mobile Cellular Subscriptions [7].

Mobile communications growth in developing countries may have a more alarming effect on carbon usage and energy costs due to the use of inefficient energy sources. Remote sites prevalent in developing regions often rely on inefficient diesel generators for power, expanding communication's carbon footprint at an even higher rate. A low power urban cell site requires 3kW of power (70-80kWh of energy for a 24-hour operation) and generates an estimated 11 tons of carbon dioxide [10]. Many rural base stations utilize significantly more power due to the larger coverage area required from each site.

At the same time, rising fuel costs are stifling service providers with energy expenditures accounting for as much as half of a mobile operator's operating expenses [4, 5]. With the strong business need to meet the rising costs, reduction of CO2 emission is becoming a dream for operators. Operators, such as Vodafone, have set goals to reduce their carbon footprint only to realize that their energy consumption has risen up by 23% [1]. In addition, the growing interest of telecom regulatory bodies on environmental and energy sustainability issues is yet another driving force for the green communication movement [11]. Table I compiled from [1], places the energy usage of cellular systems within the context of carbon footprint.

TABLE I. ENERGY USE OF TELECOMMUNICATIONS IN CONTEXT

Market	No. of Cell Sites	Energy Cost (/MWh)	Annual Operating Cost (M)	Carbon Footprint (annual CO ₂ Emission)
USA	50,000	\$ 54	\$ 150	1.8 million tons
Europe	25,000	\$ 114	\$ 100-130	0.58 million tons ~121,000 midsize cars

III. DEFINING GREEN COMMUNICATIONS

Significant variance exists in the definition of Green Communications in the telecommunications community

and it is most often a marketing term. Carbon footprint is often considered a metric of 'greenness', however telecommunications' effect on CO₂ emissions is currently under 1%. Perhaps reducing energy cost rather than CO₂ maybe a more applicable metric for wireless communications.

We define Green Communications as striving to reduce energy costs while still maintaining Quality of Service (QoS) in terms of coverage needs, capacity and user needs. When comparing system designs and improvements in energy efficient components the reduction of green house gases alone is not adequate. The QoS must be considered in tandem with energy efficiency. A difficult yet maybe the most important task related to green communications is quantifying the efficiency of the alternative approaches. How can the improvements of such a broad effort be interpreted in a way that accurately reflects the savings achieved? The popular metrics covered shortly primarily focus on measuring power consumption of the system. While power consumption is certainly a major factor in reducing the carbon footprint of system operations, we also suggest metrics that take into account energy consumption. In many cases, the terms power and energy are incorrectly used interchangeably.

The information technology (IT) industry has taken a leadership role in improving energy efficiency in the information communications technology (ICT) ecosystem. The Green Grid association of IT professionals has published efficiency metrics for data centers [12] and solicited proposals for enhanced metrics [13]. The initial report proposed the metric Power Usage Efficiency (PUE) and its reciprocal, Datacenter Efficiency (DCE) to enable operators to quickly assess energy efficiency of power hungry data centers. The PUE represents a data center's total power consumption divided by the power used only by the servers, storage systems and network equipment, as:

$$PUE = \frac{\text{Total Facility Power}}{\text{IT Equipment Power}} \quad (1)$$

A PUE rating of 1 means that all of the power for the data center is being used for the computational infrastructure and no power is being used on the non-computational infrastructure such as the air-conditioning systems. While this metric is a popular starting point, the focus is narrow and only reveals a small portion of the whole picture. The primary disadvantage is that it does not represent the efficiency of the computational equipment. Specifically for communications systems, the efficiency of the computational equipment plays a large role in energy consumption of the system.

An alternate method, perhaps more appropriate for telecommunications, strives to quantify the computational energy efficiency of a system. In this method, the ratio of energy consumption of the communications system relative to the performance of the computational system is calculated.

This may sound like an intuitive solution; however, quantifying the performance of communication is much more difficult than quantifying the performance of hardware. Typically in server farms or data centers, the performance of the hardware is measured by observing the processor utilization. For example, a typical server will consume between 60% and 70% of its total power when running at low levels of processor utilization. Increasing the processor utilization has a minimal impact on the power consumption; however, it affects the ratio of energy consumption to processor utilization significantly, thus increasing computational energy efficiency. The challenge, when applying this metric to communication systems, is how to properly quantify the performance.

In communication systems, performance comes in many different flavors. At the lowest level, the Bit Error Rate (BER) is a frequently used quantitative measure of the link. The good-put or application-level throughput measures the amount of usable bits that are received by the application. As a more strictly wireless level metric, the spectral efficiency refers to the information rate that can be transmitted over a given bandwidth, and is typically expressed as bits per second per hertz. These physical layer metrics provide an extremely low-level and detailed view of the performance of a communications system.

From a more practical and commercial focused view, an interesting metric for the cellular industry is the power utilization with respect to the number of calls or users during a specific block of time.

$$PUE_{(t_1, t_2)} = \frac{\text{Total Facility Power}}{\text{Total Number of Users}} \quad (2)$$

This metric provides insight for carrier to evaluate overall economic tradeoffs in cost, coverage and cellular site planning and management.

The telecommunications industry is addressing metrics and standards related to energy efficiency specifically for cellular hardware components [14]. For example, Verizon's Networks and Building Systems (NEBS) compliance requirements are driving the development of new metrics for evaluating energy efficiency in telecommunications systems. Their updated technical purchasing requirements define the minimum energy efficiency requirements for the purchase of new telecommunications equipments [15]. The Telecommunications Equipment Energy Efficiency Rating (TEEER) has been used by Verizon to quantify the energy efficiency of products [16]. The TEEER is defined for different types of equipments. Some sample definitions are shown in Table II, where the total power consumption P_{Total} is modeled as a weighted sum of power consumption of the equipment at different modes (full rate, P_{max} , half rate P_{50} and sleep/idle mode P_{sleep}). The weights are presumably determined statistically.

$$P_{Total} = 0.35P_{max} + 0.4P_{50} + 0.25P_{sleep} \quad (3)$$

TABLE II. VERIZON TEEER FORMULAS [16]

Equipment Type	TEEER Formula	
Transport / Gateway	$-\log\left(\frac{P_{Total}}{Throughput}\right)$	(4)
Switch / Router	$-\log\left(\frac{P_{Total}}{Forwarding\ Capacity}\right)$	(5)
Media Gateway	$-\log\left(\frac{P_{Total}}{Throughput}\right)$	(6)
Access	$\left(\frac{Access\ Lines}{P_{Total}}\right) + 1$	(7)
Power	$\left(\frac{Total\ output\ power}{Total\ input\ power}\right) \times 10$	(8)
Power Amplifier (Wireless)	$\left(\frac{Total\ RF\ Output\ Power}{Total\ Input\ Power}\right) \times 10$	(9)

From the above TEEER definition, we can see that the larger the TEEER is, the more power efficient the equipment is. The calculation of TEEER is straightforward. For example, for a router with the following specs $Forwardingcapacity = 160Gbps$, $P_{max} = 4320W$, $P_{50} = 3000W$, and $P_{sleep} = 1500W$, its total power consumption can be calculated using (3) as $P_{Total} = 3087W$. Then, the TEEER can be calculated using (5) as $TEEER = 7.71$.

While Verizon’s TEEER metric focuses on the company specific purchasing decisions, the Alliance for Telecommunications Industry Solutions (ATIS) has published industry wide standards on general requirements [17], transport equipment [18], and server equipment [19] and is developing standards for routers, power rectifiers, and wireless access equipment. The Telecommunications Energy Efficiency Ratio (TEER) for network-element efficiency is introduced in the standards. Similar to the TEEER definitions, the standards are specific to equipment type, network location, and classification. Table III summarizes some performance metrics used in the standards.

TABLE III. SUMMARY OF ATIS ENERGY PERFORMANCE METRICS

Metric	Focus	Description
Power Usage Effectiveness (PUE)	Computational infrastructure power efficiency	Total facility power consumption per total equipment power consumption
Datacenter Efficiency (DCE)	Computational infrastructure power efficiency	Reciprocal of PUE
Bit Communications Energy Efficiency (BCEE)	Overall communications throughput energy efficiency	
Energy Spectral Efficiency (ESE)	Information capacity efficiency in the frequency domain	
Base Station User Energy Efficiency	Efficiency for overall hardware and communications systems	
Telecommunications Equipment Energy Efficiency Rating (TEEER)	Networks and Building Systems Compliance Purchasing Requirements	Minimum energy efficiency specifications for components for meeting purchasing requirements
Telecommunications Energy Efficiency Ratio (TEER)	Quantifies Network-element Efficiency	Specific to equipment type, network location and classification

IV. ADVANCES AT SPECIFIC POINTS IN THE COMMUNICATIONS LIFECYCLE

Researchers are addressing the need for improving energy efficiency at individual levels within the protocol stack as well as through system architecture, operational management and physical elements. This section reviews some advancements roughly defined within an elemental area of the communications cycle (shown in Fig. 3) such as the radio component, the network operation and topology, and the integration of renewable energy sources.

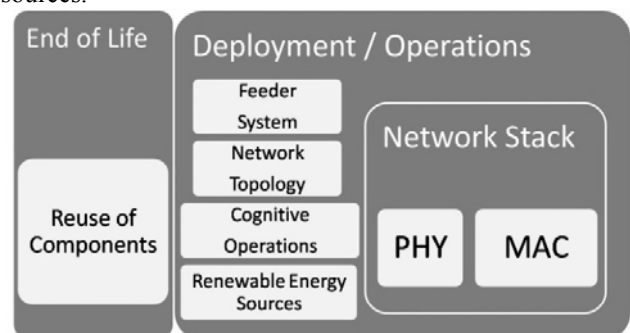


Figure 3. Communications Life Cycle.

A. Radio Component – Power Amplifier

A BS usually consists of three major components: the baseband unit, the radio and the feeder network. Among these elements, the radio accounts for around 80% of a BS' energy needs, 50% of which is consumed by the power amplifier (PA) [20-21]. Similarly, in a handheld mobile station (MS), the wireless modem consumes most of the power. The PA in the modem dominates even for computing intensive applications, such as, video conference [23].

For this reason, much emphasis has been focused on increasing PA efficiency while maintaining linearity and broadening the operating bandwidth. The PA enhances the input signal to a required output power level by converting DC power to RF AC power. However, this conversion is lossy. The characteristics of the input signal (e.g., modulation scheme) affect the PA efficiency. Non-constant magnitude modulation schemes with better spectrum efficiency have a strict linearity requirement, which usually requires a large back-off from the PA's saturation point. For example, OFDM has been exploited in many emerging wireless standards, such as, WiFi, WiMAX, and LTE, to achieve higher data rate. Its high peak to average power ratio (PAPR) is a big challenge in the PA design since large back-off is required to maintain linearity. This leads to low efficiency as the PA efficiency is maximal at its peak envelope power (PEP) and drops as its output power decreases. The improvement in PA efficiency has been achieved through new PA architecture, material, and digital signal processing algorithms.

The use of high efficiency nonlinear switch-mode PA in different PA structures, such as the Doherty [24] and the out-phasing [25, 26] structures, improves its efficiency, and its linearity. For example, a multi-stage Doherty PA has shown a theoretical efficiency of 70% for Rayleigh distributed envelope signals [27]. More recently, a high power (190W PEP), 32% efficient LDMOS (lateral double-diffused metal-oxide semiconductors) Doherty PA with a more compact load network than that of a conventional Doherty PA was designed for base stations [28]. Dynamic voltage scaling and envelope tracking are two additional techniques to increase RF PA efficiency [37].

The high frequencies in wireless systems and switch-mode architectures are pushing research in the material science of transistor technology. Currently, the LDMOS technology dominates the market. However, high electron mobility transistors (HEMT's) utilizing Aluminum Gallium Nitride (AlGaN) show potential in providing higher output power as it is able to work under higher temperature and higher voltage [29-31].

Moreover, digital signal processing techniques are exploited to reduce the nonlinear effects caused by efficiency enhancement techniques [32-35]. PAPR reduction techniques, such as, clipping, windowing, interleaving, elective mapping, and polar transmission, help increase the PA efficiency for OFDM signals [36].

There are other efficiency enhancement techniques. Multi-carrier base station technology, such as GSM

Quadruple Transceiver Technology using 6 carriers, can reduce maximum consumption of the PA by up to 30% [21].

B. Network Operation and Topology

Since the BS is the main power consuming component in a cellular network, a lot of efforts have been devoted to develop green BS. For example, Huawei's green GSM Base Transceiver Station (BTS) efforts address energy efficiency at several layers [38]. At the PA level, the Doherty-based technology is used to improve PA efficiency from 33% to 45%. Operation software with TRX shutdown technologies reduced static power consumption by 60%. Multi-density radio transceivers enabled a single module to support up to six carrier frequencies. This led to smaller and lighter base stations that require less cooling and auxiliary equipment.

The relative location between an antenna and radio has significant impact on energy efficiency. Traditionally, all radio equipment has been located in an enclosure at the ground level with connection to antennas through feeder cables, which could produce over 50% of loss into the system [6, 21]. Modular BS designs that locate RF transmitter closer to the antenna reduce the cable loss and maintain the same QoS at lower transmit power [39].

Topology specific design perspectives and improved planning methodologies improve power efficiency by reducing the number of sites. The smaller and more agile BS's dovetail to a distributed BS architecture, which can replace larger and more power-hungry macro BS's. Actual deployments of these more agile base stations have achieved more than a 40% power savings without affecting overall output signal power [38]. Other techniques such as transmit diversity and higher receive sensitivities can also yield power savings [21]. In addition, game theoretic principles have been used for analyzing the energy efficiency in CDMA networks [40].

Femtocell and picocell technologies have potential to reduce overall power usage while still optimizing capacity and service. A fundamental pathway to improving cellular capacity is to reduce the distance between an MS and a BS. Femtocells connect miniaturized, lower power BS's to wired backhubs such as home digital subscriber lines (DSL) or cable modems and radiate very low power compared to a full size BS. At the meantime, they can achieve improved capacity in large scale deployment [41]. Simulations have shown that joint deployment of macro BS's with publicly accessible residential picocells can reduce energy consumption up to 60% [42]. Initial research has predicted 102 million users worldwide using more than 32 million femtocells by 2011. However, early mass deployment has been delayed at least a year due to the current economic crisis [43]. While femtocells create a pathway to high capacity under low power usage, many research issues arise with regards to distributed frequency management [44, 45], Femtocell/macrocell interference [46], handover, self optimizing networks [47], security, and backhaul data load balancing.

Fluctuations in cellular usage are often spatially and temporally correlated. For example, during evening rush

hour usage is high and decreases later in the night while also decreasing geographically around business districts in the evenings and weekends. BTS equipment can learn from these patterns and turn off or decrease the number of transmitting antennas and hence, reduce power consumption [39]. In addition, due to the diversity at different users, spectrum can be dynamically allocated to different users so that the overall power budget is minimized. To explore the channel fluctuation, it requires coordinated management of BS's to maintain desired capacity and customer QoS.

The green initiative also impacts the standardization process. For example, in the recently 3GPP LTE-Advanced standard release, a study item on potential solutions to energy saving has been proposed [48]. This study item includes the following use cases: intra-eNB energy saving, inter-eNB energy saving, and inter-RAT energy saving. Both user accessibility and backward compatibility are required in the evaluation of solutions. In addition, it is required that the solutions should not impact the Uu physical layer and increase the user equipment (UE) power consumption.

C. Incorporation of Alternative Energy

Several cellular operators are experimenting with the use of alternative energy sources such as fuel cells, wind, and solar for BS operation. These alternative energy sources can provide an energy efficient alternative to 'dirtier' and more expensive fuel sources such as diesel and strive towards energy independence. In addition to the cost of the fuel itself, energy can be saved from minimizing the transportation and storage of the fuel, especially for remote sites. Similarly, energy harvesting techniques such as solar, thermal, optical and kinetic energy (vibration and biochemical) [49] can replace or complement batteries in mobile handsets.

While traditional radio design is based on consistently available power supply, green radios are expected to maintain the same QoS even when the power supply stochastically varies in space and time, thereby experiencing outages not only in the channel but also in the system itself. The design objectives also differ from extending the system lifetime to maximizing the system availability. Additionally, the overall network design should include redundant energy sources and neighboring BS's should be able to compensate for BS's that go down due to insufficient power.

In Namibia, the Mobile Telecommunications Limited (MTC) of Namibia, the GSMA Development Fund, and Motorola initiated a 90 day trial in 2007 to evaluate the use of solar and wind as a feasible cost-effective energy source for a cellular base station [50]. This trial utilized a 6kW wind turbine and 28kW solar panels combined with battery capable of supporting 60 hours of operation. The system provided an average of 198kW of power per week which was 10kWh more than necessary for regular operations. MTC calculated a return on investment of 3 years and reduction of approximately 4,850kg of CO₂ annually compared to a typical electrical grid installation. Additional reduction of 649.25kg CO₂ annually could be achieved by eliminating the diesel generators.

A startup company, on the request of Ericsson, has developed a BS that runs on wind and solar power [51]. Currently, over 40,000 BS's operate in Africa with most running on diesel power consuming almost 20,000 liters of diesel per year per BS. According to the manufacturer, Flexenclosure, the cost of running a diesel base station exceeds \$30,000 per year. Potentially, \$120,000 to \$150,000 in operation cost can be saved over a five-year period using the alternative energy.

In addition to the above areas where power efficiency improvement can lead to great overall power reduction, power efficiency improvement of any other individual element in the wireless network will also lead to power reduction. Nowadays, many of the research results have seen their adoption in actual product design. And the benefit achieved using the new technologies stimulates and accelerates further research on improving power efficiency of elements in the network.

V. HOLISTIC SOLUTIONS

Simply combining the power efficiency improvement technologies developed for single element might not lead to optimal power reduction. Instead, a holistic strategy that explores the synergy between various technologies may optimize overall power performance. This section presents a couple of approaches under this strategy, including cross-layer design method, cognitive approach, and radio coordination approach.

A. Cross Layer Design for Power Efficiencies

Communication networks have traditionally followed a layered architecture where specific functional are completely separate. This modular architecture simplifies overall design and development. On the other hand, a cross-layer design method can obtain performance gains by designing protocols with interaction between different layers [52]. Energy efficiency and security are examples of aspects that could benefit from a cross-layer design strategy that ties the PHY layer to the MAC layer or other networking functions.

Cross-layer design for resource allocation has been applied to 3G networks for optimizing radio resource allocation with a BER constraint [53]. The information exchange across protocol layers shows better performance especially with heterogeneous data and video services. QoS and capacity are evaluated outside the protocol stack, while energy efficiency is measured within the PHY layer. Various QoS constraints are studied with the goal of minimizing energy consumption [54].

QoS metrics such as average conditional expectation of delay is typically correlated with channel gain. If delay is constrained to a fixed level across all channel gains then average power can be minimized subject to a specific delay constraint. By imposing this tighter delay constraint, power savings can be achieved through cross-layer design and source-channel coding as opposed to the typical power control methodology [55].

B. Cognitive Radio for Power Optimizaion

Cognitive Radio (CR) is a relatively new research area in communications that incorporates environment observation, decision making and learning, and radio reconfiguration to improve the performance of communication systems [56, 57]. CR springboards off of the successful adoption of software radio platforms and has shown promise in military [58] and public safety [59] domains. The concept of cognitive systems has great promise towards Green Communications. Leveraging the advancements in the capability of environment observation, realizable learning and decision making algorithms can be applied in a cellular network. Environment observation includes traditional RF metrics such as signal to noise ratio (SNR), channel occupancy as well as application QoS requirement. Additionally, observing the power usage of base stations and manipulating interaction with the underlying electrical system has significant potential to contributing towards a smart grid capable of more balanced energy delivery.

Leveraging advances in emerging CR technologies, we have proposed a power optimization framework using CR, as shown in Fig. 4, to dynamically implement favorable trade-offs in radio parameters to minimize power consumption for the required QoS for a particular application and radio environment [60]. In this framework, the solid lines with arrows and the blocks in solid boundaries are existing components in conventional wireless communication devices. The dashed lines with arrows and the cognitive engine (CE) block are new components enabling CR capability in conventional systems. The bidirectional dashed lines between the CE and various building blocks enable the CE to learn the characteristics and the capabilities of the building blocks and control/configure the blocks based on its decision for different application and environment.

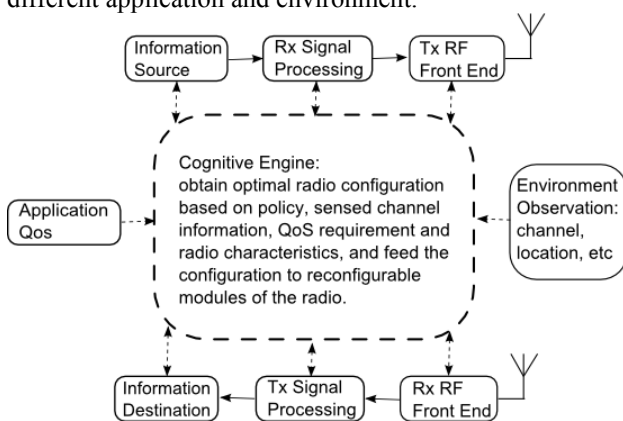


Figure 4. Cognitive Radio Framework for Power Optimization [60].

A general active process starts with CE receiving a service request along with the QoS requirement, it then queries the radio platform for platform capabilities and characteristics and environment information. The CE uses the obtain information to determine a favorable radio configuration that satisfies the application QoS and optimizes some radio performance metrics. For green

communications purpose, these performance metrics can include power consumption.

This framework can be applied to radio systems with different technologies. For example, for a conventional single input single output system, two levels of operation, adaptive transmission with component knowledge and adaptive transmission with component adaptation, have shown significant energy savings (up to 75%) compared to conventional adaptive transmission [60, 61]. This work has been extended to multiple input multiple output (MIMO) systems [62]. Conventionally, various power and bit allocation schemes were proposed to tradeoff total radiated power and capacity. Leveraging the knowledge on the platform (component) characteristics learned by the CR, system power consumption, instead of radiated power, can be minimized for given target rate. Simulation results show up to 75% of power savings for a 4 by 4 MIMO system using Class A PA's.

In addition to hardware power consumption, resource consumption of digital signal processing can also play a significant role in system power consumption. [63] investigates the use of real-time resource monitoring to reduce the computational complexity of the baseband processor. Specifically [63] demonstrates by minimally sacrificing physical layer system performance, computational complexity can be significantly reduced without compromising the QoS of the application. Supervised intelligent heuristic-based learning algorithms are used to achieve this resource management. These learning algorithms optimize energy and processing efficiencies in dynamic spectrum environments using software-level feedback of the radio's active resource consumption.

C. Coordinated Approach to Improving Efficiency

In a wireless network, while each node might have a selfish goal of improving performance in capacity, QoS or power, the needs of the overall system must be balanced with the goals of each node. In addition, each node is also a power hungry citizen of the overall power grid network. Coordinated management and load balancing among nodes underneath an overall smart grid has positive impact on energy consumption without adversely affecting QoS and capacity. Recent developments in wired distributed computing theory [64, 65] provide initial models for its application to wireless networks and the interaction between different nodes and between the entire telecommunication network and the electrical grid network.

It is challenging to apply similar concepts in a wireless environment due to disruptive characteristics of the wireless channels, such as varying channel conditions, a shared medium, and drastically different power-costs of communication. The Wireless Distributed Computing (WDC) system design tradeoffs involve cross-system interaction between the computation subsystem (or application layer where the computing process is executed) and the communication subsystem (or underlying networking, radio access and physical layers). Consequently, new methodologies have been proposed to as performance in terms of range, power efficiency and

scalability is greatly influenced by the underlying radio environment [66]. The new methodologies try to develop protocols, service architecture, resource allocation and computational load balancing, and power consumption minimization algorithms.

A group of collaborating radios offers several benefits over a lone radio, such as: (1) enabling lower power consumption per node and, under certain conditions, lower power consumption for the whole network; (2) allowing matching between power demand and supply; (3) meeting high computing and latency requirements by leveraging the computing resources in the network; and (4) simplifying small form factor node designs with lower computing and power resources per node.

Minimizing energy consumption in WDC networks through optimal computational workload allocation has been discussed in [67]. In a WSC network the communication subsystems connect the computation subsystems on various nodes through wireless links, disseminate the computational workload, pass inter-process messages, and collect processing results. For example, in a broadcast network, a master node distributes its computational load among several slave nodes. The slave nodes process their share of the workload and return the results to the master node. The master node then fuses the results from participating slave nodes.

In WDC, the savings in computational power consumption are partially negated by the overhead of communication power consumption. In addition, the improvement in the computational power savings with an increase in the number of collaborating nodes is countered by an increase in the overhead of power consumption for communication between the nodes. Thus, as shown in Fig. 5 [66], a breaking point may exist, beyond which WDC is not power efficient as compared to on-board processing.

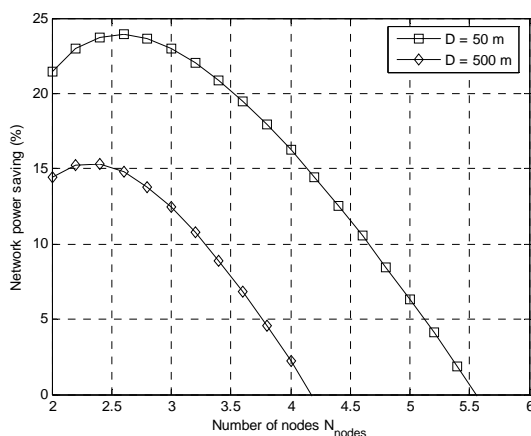


Figure 5. Network power savings achieved by distributed computing for various network sizes and network ranges [66].

A similar idea, called Coordinated Multipoint Transmission (CoMP), has been recently proposed in the 3GPP LTE-Advance standardization process [68]. This technology coordinates transmission among multiple cells

and reduces the interference from other cells thus reduces the power required to maintain certain QoS.

VI. CONCLUSIONS

There is no doubt that the explosive growth in voice and data usage and the rising energy costs are leading to significant impact in the carbon emission and the operation expense. In this paper, we present some initial efforts in Green Communications to compensate these effects. A few efficiency definitions that can be used to evaluate different approaches are discussed first. We then review the existing developments within singular aspect of the communication life cycle, including network components, network operation and topology, and integration of alternative energy in the network. Finally, we present several holistic approaches that incorporate multiple aspects in the communication life cycle. These approaches include cross-layer design, cognitive radio approach, and wireless distributed computing solution.

As we can see from the existing work, researchers are creating novel solutions to the energy problem faced by the wireless industry by employing and combining existing technologies developed for related issues in wireless domain as well as in other domains. As the advancements in designing power efficient network components, a framework, which is aware of the capabilities and characteristics of each component, can further optimize the network operation for various goals given the application QoS requirement and operation environment. For this scenario we think a cognitive radio based framework can be of great help. This is reflected in the development of emerging wireless standards. For example, the new universal mobile telecommunications system (UMTS) proposals advocate self-configuring and self-organizing wireless networks [69]. The self-organizing networks can automatically optimize wireless network operation, e.g., potentially reducing power consumption given QoS requirements and channel conditions. A cognitive radio based solution is favorable through online learning and monitoring of network operation, integration of learned knowledge about network operation in network optimization, and dynamic reconfiguration of network to improve network efficiency.

As we move down the path to greener communications, we will identify new useful technologies developed in related areas. The capability of integrating new technologies into an existing system becomes crucial in developing a future-proof green communication solution. The success of this green endeavor depends on the synergy gained from the cooperation of researchers from many disciplines, some of which may seem to be quite remote from today's review point.

ACKNOWLEDGMENT

The authors wish to thank Wireless@VT affiliates, Office of Naval Research (ONR), National Science Foundation (NSF), and Intel Corporation. Any opinions,

findings, and conclusions or recommendations expressed in this paper are those of the authors and do not necessarily reflect the views of Wireless@VT affiliates, ONR, NSF, and Intel.

REFERENCES

- [1] C. Lamour, "Energy Consumption of Mobile Networks," in *The Basestation e-Newsletter*, 2008.
- [2] G. Fettweis and E. Zimmerman, "ICT Energy Consumption – Trends and Challenges," in *The 11th International Symposium on Wireless Personal Multimedia Communications*, Lapland, Finland, 2008.
- [3] "How green is your network?" *The Economist*, Dec 4th 2008.
- [4] Ericsson. "Green Power to Bring Mobile Telephony to Billions of People," Available: <http://www.thefreelibrary.com/Green+Power+to+Bring+Mobile+Telephony+to+Billions+of+People.-a0190611482>, 2008.
- [5] "Core 5 – Green Radio: Programme Objectives and Overview," Mobile VCE.
- [6] Ericsson, "Sustainable Energy Use in Mobile Communications – White paper," 2007.
- [7] ITU, "Market Information and Statistics," International Telecommunications Union, Available: <http://www.itu.int/ITU-D/ict/statistics/>, 2010.
- [8] H. Sistik, "Green-tech base stations cut diesel usage by 80 percent," in *CNET News Green Tech*, ed, 2008.
- [9] "Measuring the Information Society – The ICT Development Index," International Telecommunications Union, 2010.
- [10] J. Walko. "Green Issues Challenge Basestation Power," *EE Times Europe*. Available: <http://eetimes.eu/showArticle.jhtml?articleID=201807401>, 2007
- [11] P. Jarich, "Green Telecom: More than Just Marketing?," *GLG News*. Available: <http://www.glggroup.com/News/-Green--Telecom--More-than-Just-Marketing--21960.html>, 2008.
- [12] C. Belady, et al., "Green Grid Data Center Power Efficiency Metrics: PUE and DCIE," *The Green Grid*, 2008.
- [13] J. Haas, et al. "Proxy Proposals for Measuring Data Center Productivity," *The Green Grid*, 2009.
- [14] R. Grigonis, "ATIS Announces Three New Energy Efficiency Standards for Telecom," *Green News*. Available: <http://green.tmcnet.com/topics/green/articles/52647-at-is-announces-three-new-energy-efficiency-standards-telecom.htm>, 2009.
- [15] "Verizon NEBS Compliance: Energy Efficiency Requirements for Telecommunications Equipment," Verizon VZ.TPR.9205, 2008.
- [16] "Verizon NEBS Compliance: TEEER Metric Quantification," Verizon VZ.TPR.9207, 2009.
- [17] "Energy Efficiency for Telecommunication Equipment: Methodology for Measurement and Reporting – General Requirements," Alliance for Telecommunications Industry Solutions (ATIS) ATIS-0600015.2009.
- [18] "Energy Efficiency for Telecommunication Equipment: Methodology for Measurement and Reporting – Server Requirements," Alliance for Telecommunications Industry Solutions (ATIS) ATIS-0600015.01.2009.
- [19] "Energy Efficiency for Telecommunication Equipment: Methodology for Measurement and Reporting – Transport Requirements," Alliance for Telecommunications Industry Solutions (ATIS) ATIS-0600015.02.2009.
- [20] "Green Base Station – The Benefits of Going Green," *Mobile Europe*. Available: http://www.mobileeurope.co.uk/features/113824/Green_base_station_-_The_benefits_of_going_green.html, 2008.
- [21] Huawei, "Improving energy efficiency, Lower CO2 emission and TCO," 2009.
- [22] C. Anderson, et al., "Mobile Media and Applications, From Concept to Cash: Successful Service Creation and Launch," Wiley, 2006.
- [23] F. Fitzek and F. Reichert, Eds., "Mobile Phone Programming and its Application to Wireless Networking," Springer, 2007.
- [24] W. H. Doherty, "A New High Efficiency Power Amplifier for Modulated Waves," *Proceedings of the IRE*, Vol. 24, No. 9, Sep. 1936, pp. 1163-1182.
- [25] H. Chireix, "High power outphasing modulation," *Proc. IRE*, vol. 23, pp. 1370-1392, Nov. 1935.
- [26] L. F. Gaudernack, "A phase-opposition system of amplitude modulation," *Proc. IRE*, vol. 26, pp. 983-1008, Aug. 1938.
- [27] F. H. Raab, "Efficiency of Doherty RF Power-Amplifier Systems," *Broadcasting, IEEE Transactions on*, vol. BC-33, pp. 77-83, 1987.
- [28] S. Kwon, "Inverted Load network for high power Doherty amplifier," *IEEE Microwave Magazine*, vol. 10, February 2009.
- [29] B. Berglund, et al., "High Efficiency Power Amplifiers," *Ericsson Review*, no. 3, 2006.
- [30] H. Sano, et al., "A 40W GaN HEMT Doherty Power Amplifier with 48% Efficiency for WiMAX Applications," in *Compound Semiconductor Integrated Circuit Symposium, 2007. CSIC 2007. IEEE*, 2007, pp. 1-4.
- [31] D. Schemetzer and S. Long, "A GaN HEMT Class F Amplifier at 2 GHz with >80% PAE," *IEEE Journal of Solid-State Circuits*, vol. 42, pp. 2130-2136, 2007.
- [32] J. K. Cavers, "Amplifier linearization using a digital predistorter with fast adaptation and low memory requirements," *Vehicular Technology, IEEE Transactions on*, vol. 39, pp. 374-382, 1990.
- [33] L. Larson, et al., "Device and circuit approaches for improved wireless communications transmitters," *Personal Communications, IEEE*, vol. 6, pp. 18-23, 1999.
- [34] P. Garcia, et al., "An adaptive digital method of imbalances cancellation in LINC transmitters," *IEEE Trans. On Vehicular Technology*, vol. 54, pp. 879-886, May 2005.
- [35] X. Chen, et al., "A high efficiency outphasing transmitter structure for wireless communications," presented at the IEEE 13th DSP/SPE workshop, Marco Island, FL, 2009.
- [36] S. H. Han and J. H. Lee, "An overview of peak-to-average power ratio reduction techniques for multicarrier transmission," *Wireless Communications, IEEE*, vol. 12, no. 2, pp. 56-65, 2005.
- [37] T. Haynes, "Designing energy-smart 3G base stations," *RF Design*. Available: <http://rfdesign.com/mag/708RDFD1.pdf>, 2007.
- [38] J. Zhou, et al., "China Mobile In Action," *How to Operate*, 2008.
- [39] J. T. Louhi, "Energy efficiency of modern cellular base stations," in *Telecommunications Energy Conference, 2007. INTELEC 2007. 29th International*, 2007, pp. 475-476.
- [40] S. M. Betz and H. V. Poor, "Energy Efficient Communications in CDMA Networks: A Game Theoretic

- Analysis Considering Operating Costs,” *Signal Processing, IEEE Transactions on*, vol. 56, pp. 5181-5190, 2008.
- [41] V. Chandrasekhar, *et al.*, “Femtocell networks: a survey,” *Communications Magazine, IEEE*, vol. 46, pp. 59-67, 2008.
- [42] H. Claussen, *et al.*, “Effects of joint macrocell and residential picocell deployment on the network energy efficiency,” in *Personal, Indoor and Mobile Radio Communications, 2008. PIMRC 2008. IEEE 19th International Symposium on*, 2008, pp. 1-6.
- [43] C. Gallen. “102 Million Femtocell Access Users by 2011,” Available: <http://www.abiresearch.com/abiprdisplay.jsp?pressid=709>, 2006.
- [44] D. Lopez-Perez, *et al.*, “Interference avoidance and dynamic frequency planning for WiMAX femtocells networks,” in *Communication Systems, 2008. ICCS 2008. 11th IEEE Singapore International Conference on*, 2008, pp. 1579-1584.
- [45] L. T. W. Ho and H. Claussen, “Effects of User-Deployed, Co-Channel Femtocells on the Call Drop Probability in a Residential Scenario,” in *Personal, Indoor and Mobile Radio Communications, 2007. PIMRC 2007. IEEE 18th International Symposium on*, 2007, pp. 1-5.
- [46] V. Chandrasekhar and J. G. Andrews, “Uplink Capacity and Interference Avoidance for Two-Tier Cellular Networks,” in *Global Telecommunications Conference, 2007. GLOBECOM '07. IEEE*, 2007, pp. 3322-3326.
- [47] H. Claussen, *et al.*, “Self-optimization of coverage for femtocell deployments,” in *Wireless Telecommunications Symposium, 2008. WTS 2008*, 2008, pp. 278-285.
- [48] 3rd Generation Partnership Project, “Potential solutions for energy saving for E-UTRAN (release 10),” *Technical Specification Group Radio Access Network, Evolved Universal Terrestrial Radio Access Network (E-UTRAN)*, Feb. 2011
- [49] A. Kansal, *et al.*, “Performance Aware Tasking for Environmentally Powered Sensor Networks,” in *Joint International Conference on Measurement and modeling of computer systems*, 2004, pp. 223-234.
- [50] J. Rowley and D. Haig-Thomas, “Unwiring the Planet - Wireless Communications and Climate Change,” in *ITU International Symposiums ICT's and Climate Change*, London, UK, 2008.
- [51] H. Sistik. “Green-tech base stations cut diesel usage by 80 percent,” Available: http://news.cnet.com/8301-11128_3-9912124-54.html?tag=mncol:title, 2008.
- [52] V. Sriastava and M. Motani, “Cross-Layer Design and Optimization in Wireless Networks,” in *Cognitive Networks: Towards Self-Aware Networks*, Q. H. Mahmoud, Ed., John Wiley & Sons, 2007.
- [53] J. Hai, *et al.*, “Cross-layer design for resource allocation in 3G wireless networks and beyond,” *Communications Magazine, IEEE*, vol. 43, pp. 120-126, 2005.
- [54] W. Eberle, *et al.*, “From myth to methodology: cross-layer design for energy-efficient wireless communication,” presented at the Proceedings of the 42nd annual conference on Design automation, Anaheim, California, USA, 2005.
- [55] S. Cui and A. Goldsmith, “Cross-layer Design in Energy-constrained Networks Using Cooperative MIMO Techniques,” *EURASIP Journal on Applied Signal Processing, Special Issue on Advances in Signal Processing-based Cross-layer Designs*, Vol. 86, No. 8, pp. 1804-1814, August 2006.
- [56] J. Mitolla, “Cognitive Radio – An Integrated Agent Architecture for Software Defined Radio,” Teleinformatics, Royal Institute of Technology (KTH), 2000.
- [57] S. Haykin, “Cognitive Radio: Brain Empowered Wireless Communications,” *IEEE Journal on Selected Areas in Communications*, vol. 23, 2005.
- [58] I. F. Akyildiz, *et al.*, “NeXt generation/dynamic spectrum access/cognitive radio wireless networks: A survey,” *Computer Networks*, vol. 50, 2006.
- [59] B. Le, *et al.*, “A Public Safety Cognitive Radio Node,” *2007 SDR Forum Technical Conference*, Denver, CO, 2007.
- [60] A. He, *et al.*, “Minimizing Energy Consumption Using Cognitive Radio,” in *Performance, Computing and Communications Conference, 2008. IPCCC 2008. IEEE International*, 2008, pp. 372-377.
- [61] A. He, *et al.*, “Energy consumption minimization for mobile and wireless devices – a cognitive approach,” *IEEE Transactions on Consumer Electronics*, vol. 56, no. 3, pp. 1814-1821, Aug. 2010.
- [62] A. He, *et al.*, “Power consumption minimization for MIMO systems – a cognitive radio approach,” *IEEE Journal on Selected Areas in Communications*, Feb. 2011.
- [63] J. Gaedert, “Facilitating Wireless Communications through Intelligent Resource Management on Software-Defined Radios in Dynamic Spectrum Environments” PhD dissertation, *Virginia Tech*, Jan. 2011.
- [64] M. Goff, “Network Distributed Computing: Fitscapes and Fallacies,” Prentice Hall PTR, 2004.
- [65] W. Jai and W. Zhou, “Distributed Network Systems,” Springer, New York, 2005.
- [66] D. Datla, *et al.*, “Power Efficiency in Wireless Network Distributed Computing,” in *IEEE Vehicle Technology Fall Conference Anchorage*, 2009.
- [67] X. Chen *et al.*, “The Impact of Channel Variations on Wireless Distributed Computing Networks”, in *Proceedings of the 28th IEEE Conference on Global Telecommunications*, Honolulu, HI, 2009
- [68] 3rd Generation Partnership Project, “LTE-Advanced feasibility studies in RAN WG4 (release 9),” *Technical Specification Group Radio Access Network, Evolved Universal Terrestrial Radio Access Network (E-UTRAN)*, June 2010
- [69] 3rd Generation Partnership Project, “Self-configuring and self-optimizing network use cases and solutions (release 9),” *Technical Specification Group Radio Access Network, Evolved Universal Terrestrial Radio Access Network (E-UTRAN)*, Sept. 2009



An He received his Ph.D. degree in electrical engineering in 2011 with the Bradley Department of Electrical and Computer Engineering, Virginia Tech, Blacksburg, VA.

He is currently Sr. Systems Engineer with Qualcomm, San Jose, CA. He was a Research Intern with Telcordia in 2010 and a Graduate Technical Intern with Intel

in 2007. His research interests include cognitive radio, software-defined radio, radio power consumption optimization, radio resource management, artificial intelligence, signal detection and classification, and MIMO and OFDM systems.



Ashwin Amanna received a BS in electrical engineering from University of California, Davis in 1991 and a MS in electrical engineering from Virginia Tech, Blacksburg, VA, in 1994. Currently, he is a PhD Candidate at Virginia Tech with a focus in Cognitive Radio decision making/learning and testing/evaluation.

He is Senior Research Associate with the Wireless@Virginia Tech research center. He is Co-Director of a National Security Center of Academic Excellence. He is principal investigator for a Federal Railway Administration project developing a Cognitive Radio for railway applications. Additionally, he serves as Business Development Manager for Wireless@VT fostering opportunities for research partnerships.



Thomas Y. Tsou received his B.S. degree in computer engineering from the University of Illinois at Urbana-Champaign in 2002. He is currently pursuing a Ph.D. in electrical engineering at Virginia Tech, Blacksburg, VA and involved in open source software-defined radio platforms for cellular networks.

His research interests include wireless standards, reconfigurable devices, and security.



Xuetao Chen received his B.S. and M.S. in electrical engineering from Wuhan University, China, in 2001 and 2004, respectively. Currently, he is pursuing a Ph.D. degree in electrical engineering at Virginia Tech, Blacksburg, VA.

His research interests include cognitive radio, wireless distributed computing networks, high efficiency power amplifier design.



Dinesh Datla is currently pursuing his Ph.D degree in the Bradley Department of Electrical and Computer Engineering at Virginia Tech, Blacksburg, VA, USA. He received his M. S. in electrical engineering from the University of Kansas, Lawrence, KS, USA in 2007 and B.E. in electronics and communications from the University of Madras, Chennai, India in 2004.

His current research interests include wireless distributed computing, software defined radio networks, cognitive radios and dynamic spectrum access radios.



Joseph Gaeddert was born in Albuquerque, NM, on July 22, 1980. He received the B.S. degree in electrical engineering in 2002 from the University of Kentucky, Lexington, and the M.S. degree and Ph.D. degree in electrical engineering from Virginia Tech, Blacksburg, VA in 2005 and 2011, respectively.

His research interests concern the reduction of receiver complexity in reconfigurable radio platforms and the parametric estimation of synchronizers in the context of filterbank multicarrier transmission schemes.



Timothy R. Newman received the Ph.D. degree in electrical engineering from the University of Kansas, Lawrence, in 2008.

He joined Wireless @ Virginia Tech, Bradley Department of Electrical and Computer Engineering, Virginia Polytechnic Institute and State University, Blacksburg, as a Postdoctoral Research Fellow and primarily focuses on researching cognitive radio network security issues. His other research interests include software-defined radio, dynamic spectrum access protocols, high-speed networking, and general wireless security issues.

Dr. Newman is currently a Cochair of the International Radio Security Services application programming interface (API) task group within the Wireless Innovation Forum, where he works with a collection of international researchers to create an openly available security API for tactical radios.



S.M. Hasan received his BS degree from the Bangladesh University of Engineering and Technology, MS degree from the University of Tennessee, Knoxville, TN, and PhD from the Virginia Tech, Blacksburg, VA all in electrical engineering in 2002, 2005 and 2009, respectively.

He is currently a Research Scientist with the Bradley Department of Electrical and Computer Engineering at the Virginia Tech, Blacksburg, VA. His research interests are in the RF front end, software radio and cognitive radio areas.

Dr. Hasan was the Recipient of the 2007 William Bazy Fellowship from the Microwave Journal. He was also the Recipient of the first prize of the IEEE Myron Zucker Student Design Award in 2001.



Haris I. Volos received his B.S. degree from the Old Dominion University, Norfolk, VA, and his M.S. and PhD degrees from Virginia Tech, Blacksburg, VA in electrical engineering in 2006 and 2010, respectively.

He is currently a Postdoctoral Associate with the Bradley Department of Electrical and Computer Engineering at Virginia Tech, Blacksburg, VA. His research interests include channel modeling, software-defined radios, cognitive radio, smart grid, and wireless distributed computing.

Dr. Volos is a recipient of the 2011 Paul E. Torgersen research excellence award and the 2010 Fred W. Ellersick MILCOM award for the best paper presented in the unclassified technical program.



Jeffrey H. Reed received the B.S.E.E., M.S.E.E., and Ph.D. degrees from the University of California, Davis, in 1979, 1980, and 1987, respectively.

He is the Willis G. Worcester Professor in the Bradley Department of Electrical and Computer Engineering. He currently serves as Director of Wireless

@ Virginia Tech, one of the largest and most comprehensive university wireless research groups in the US and is the Interim Director of the Ted and Karyn Hume Center for National Security and Technology. Since joining Virginia Tech in 1992, Dr. Reed has been PI or co-PI of approximately 100 projects covering areas such as software radio, cognitive radio, ultra wideband, and channel modeling. He is cofounder of CRT Wireless, a company that is developing cognitive radio techniques for commercial and military systems and has served on the advisory boards of numerous companies. He is the author of three books and over 200 journal and conference papers. Dr. Reed has two books scheduled for publication later year in the areas of cellular communications and software defined and cognitive radio.

Dr. Reed is a Fellow of the IEEE for contributions to software radio and communications signal processing and for leadership in engineering education and is a past recipient of the College of Engineering Award for Excellence in research.



Tamal Bose received the Ph.D. degree in electrical engineering from Southern Illinois University in 1988.

After a faculty position at the University of Colorado, he joined Utah State University in 2000, where he served as the Department Head and Professor of Electrical and Computer Engineering from 2003-2007. Currently, he is

Professor in the Bradley Department of Electrical and Computer Engineering at Virginia Tech, Blacksburg, VA. He is the Associate Director of Wireless@VT and Director of the NSF center site WICAT@VT. He is author of the text *Digital Signal and Image Processing*, John Wiley, 2004, and coauthor of *Basic Simulation Models of Phase Tracking Devices Using MATLAB*, Morgan & Claypool Publishers, 2010. He is also the author or co-author of over 150 technical papers. His research interests include signal classification for cognitive radios, channel equalization, adaptive filtering algorithms, and nonlinear effects in digital filters.

Dr. Bose served as the Associate Editor for the IEEE Transactions on Signal Processing from 1992 to 1996. He is currently on the editorial board of the IEICE Transactions on Fundamentals of Electronics, Communications and Computer Sciences (Japan) and Research Letters in Signal Processing. He also served on the organizing committees of several international conferences and workshops. He is an IEEE EAC program evaluator and a member of the DSP Technical Committee for the IEEE Circuits and Systems society.

Call for Papers and Special Issues

Aims and Scope.

Journal of Communications (JCM) is a scholarly peer-reviewed international scientific journal published monthly, focusing on theories, systems, methods, algorithms and applications in communications. It provide a high profile, leading edge forum for academic researchers, industrial professionals, engineers, consultants, managers, educators and policy makers working in the field to contribute and disseminate innovative new work on communications.

JCM invites original, previously unpublished, research, survey and tutorial papers, plus case studies and short research notes, on both applied and theoretical aspects of communications. These areas include, but are not limited to, the following topics:

- Signal Processing for Communications
- Multimedia Processing and Communications
- Communication QoS and Performance Modeling
- Cross-layer Design and Optimization
- Communication and Information Theory
- Communication Software and Services
- Protocol and Algorithms for Communications
- Wireless Communications and Networking
- Wireless Ad-hoc and Sensor Networking
- Broadband Wireless Access
- Cooperative Communications and Networking
- Optical Communications and Networking
- Broadband Networking and Protocols
- Internet Services, Systems and Applications
- P2P Communications and Networking
- Pervasive Computing and Grid Networking
- Communication Network Security
- Cognitive Radio Communications and Networking
- Hardware Architecture for Communications and Networking
- Parallel and Distributed Computing
- Satellite and Space Communications
- Emerging Communication Technology and Standards

Special Issue Guidelines

Special issues feature specifically aimed and targeted topics of interest contributed by authors responding to a particular Call for Papers or by invitation, edited by guest editor(s). We encourage you to submit proposals for creating special issues in areas that are of interest to the Journal. Preference will be given to proposals that cover some unique aspect of the technology and ones that include subjects that are timely and useful to the readers of the Journal. A Special Issue is typically made of 8 to 12 papers, with each paper 8 to 12 pages of length, and the papers include:

- A Guest Editorial;
- 2-3 Invited Survey papers from world well-known scientists in the specific area;
- 6-10 Research papers reflecting the latest advances in the specific area.

The following information should be included as part of the proposal:

- Proposed title for the Special Issue
- An initial version of Call for Papers with specific topics covered in the Special Issue
- Name, contact, position, affiliation, and biography of the Guest Editor(s)
- Tentative time-table for the call for papers and reviews
- Potential authors and topics for the Invited Survey papers
- List of potential reviewers
- Plans for advertising the Call for Paper and attracting high-quality paper submissions

If a proposal is accepted, the guest editor will be responsible for:

- Submitting a final "Call for Papers" to be included on the Journal's Web site.
- Distribution of the Call for Papers broadly to various mailing lists and sites.
- Leading a fair and strict review process for the paper submissions, collecting 2-3 reviews for each paper before the final decision making. Authors should be informed the Author Instructions.
- Providing JCM the completed and approved final versions of the papers formatted in the Journal's style, together with all authors' contact information.
- Writing a one- or two-page introductory editorial to be published in the Special Issue.

In the Guest Editor Team building process, it is highly recommended that a world well-known scientist (e.g., IEEE or ACM Fellow) in the area is involved in this effort to promote the visibility of the Special Issue in the society. On the other hand, it is suggested to consider the geographic coverage of the team. Due to conflict-of-interest, the Guest Editors are not encouraged to submit their own papers to the Special Issue.

Recommended Papers from an International Conference

JCM accept recommendations from well-known International conferences. The conference organizer can recommend the best papers (top 5% of the accepted papers) to be considered in either JCM regular issue or a JCM special issue. A fast-track review process would be conducted by a JCM Editor for these recommended papers and the final decisions are made based on the review feedback.

The following information should be included as part of the proposal:

- The name of the conference/workshop, and the URL of the event
- A brief description of the event, including: number of submitted and accepted papers, and number of attendees. If these numbers are not yet available, please refer to previous events. First time conference would NOT be considered.
- Tentative time-table for the paper submission.

If a proposal is accepted, the conference organizer needs to submit the following items at a later stage:

- The list of the best papers (top 5% of the accepted papers) for recommendation
- The submitted conference paper draft and review feedbacks

If a conference contributes more than 5 papers that are finally accepted by JCM, the organizer would be invited to serve as a Guest Co-Editor of a JCM annual Special Issue, "SI on the Latest Advances in Communications and Networking", and these accepted papers would be included in the same Special Issue. Otherwise, the accepted papers would be published in JCM regular issues.

More information is available on the web site at <http://www.academypublisher.com/jcm/>.